

Max-Planck-Institut für Astrophysik

Analysis of Light Curves of Type Ia Supernovae

Gertrud Contardo

Vollständiger Abdruck der von der Fakultät für Physik der Technischen Universität München
zur Erlangung des akademischen Grades eines
Doktors der Naturwissenschaften
genehmigten Dissertation.

Vorsitzender: Univ.-Prof. Dr. F. von Feilitzsch

Prüfer der Dissertation:

1. Hon.-Prof. Dr. W. Hillebrandt
 2. Univ.-Prof. Dr. M. Drees

Die Dissertation wurde am 09.04.2001 bei der Technischen Universität München eingereicht und durch die Fakultät für Physik am 28.05.2001 angenommen.

Contents

1	Introduction	7
2	Type Ia Supernovae	9
2.1	What are Type Ia Supernovae (SNe Ia)?	9
2.2	Light Curve Width-Luminosity Relation	10
2.3	High Redshift SNe and their Use as Distance Indicators	15
3	Observational Data	19
3.1	Light Curve Data	19
3.2	Reddening	19
3.3	Distances	19
4	Fitting Routine	23
4.1	Method	23
4.2	Error Estimates with Monte Carlo Techniques	28
4.3	Epochs of Maxima	31
4.4	Rise Times	33
5	Bolometric Light Curves	37
5.1	Method and Uncertainties	37
5.1.1	Correction for Missing Pass Bands	38
5.1.2	Uncertainties	40
5.1.3	Comparison with Spectra	41
5.1.4	SN 1998bu and the Contribution of <i>JHK</i> to the Bolometric Light Curve	42
5.2	Shape of the Bolometric Light Curves	45
5.2.1	Peak Light Curve Shape	45
5.2.2	Secondary Bump	47
5.3	Derived Quantities from the Bolometric Light Curves	49
5.3.1	Radioactive Decay and γ -ray Escape	49
5.3.2	Nickel Mass	51
5.3.3	γ -ray Escape and the Total Mass of SNe Ia	54
6	Conclusions	57
A	Catalogue	59
A.1	Introduction	59
A.2	Annotations to Individual SNe	61

A.3 Fit Parameters	65
A.4 Light Curve Parameters	78
A.5 <i>UBVRI</i> Light Curves	94
Bibliography	155
Abstract/Zusammenfassung	161

List of Figures

2.1	The decline of SN 1997cj with HST (Garnavich et al. 1998).	9
2.2	<i>BVRI</i> evolution of bright SNe Ia (Suntzeff 1996).	11
2.3	Illustration of the decline parameter Δm_{15} and $t_{1/2}$	12
2.4	Phillips relation (Phillips et al. 1999).	15
2.5	Hubble diagram for high and low redshift SNe (Riess et al. 1998).	16
4.1	Fit of Equation 4.1 to the <i>R</i> photometry of SN 1992bc.	24
4.2	Fit of Equation 4.1 to the observed <i>I</i> data of SN 1992bc.	25
4.3	The distribution of the time of t_{\max} and m_{\max} from Monte Carlo simulations.	29
4.4	Distribution of the 10 fit parameters.	30
4.5	Times of the filter maxima from <i>U</i> to <i>I</i> and of the bolometric luminosity.	32
4.6	The distribution of the rise time parameter in <i>B</i> and <i>R</i> for SN 1994D.	34
4.7	Comparison of different derivations of the <i>B</i> band rise time of SN 1994D.	35
5.1	Bolometric light curves for some well observed SNe.	38
5.2	Correction factors for missing pass bands and residuals for substituting individual pass band observations.	39
5.3	Constructing the bolometric light curves before and after fitting filter light curves.	42
5.4	<i>UBVIJHK</i> light curves of SN 1998bu.	43
5.5	The <i>UBVIJHK</i> light curve of SN 1998bu compared with the <i>UBVRI</i> light curve.	44
5.6	Fraction of <i>UBVIJHK</i> -flux observed in <i>UBVRI</i> and in the pass bands.	45
5.7	Rise to and decline from maximum in bolometric light curves.	47
5.8	First derivative of the bolometric light curve function of SN 1992bc.	48
5.9	Extrema of the first derivative versus the position of the secondary maximum in <i>I</i> and versus $t_{+1/2}$	49
5.10	Epoch of the extrema of the first derivative versus L_{\max}	50
5.11	Radioactive decay and γ -ray deposition.	51
5.12	Variation of the amount of ^{56}Ni dependent on the rise time t_{rise}	52
5.13	Fit of the γ -ray escape to the observed bolometric luminosity.	55
5.14	Fiducial time t_0 versus amount of ^{56}Ni	56
A.1-A.60	<i>UBVRI</i> light curves of SN 1989B to SN 1998de.	94

List of Tables

3.1	Light curve data, color excess and distance modulus.	21
4.1	Range of parameters as in- and output of the fitting routine.	27
4.2	Times of peak relative to the <i>B</i> maximum.	31
4.3	Comparison of rise times.	36
5.1	Parameters describing the light curve shape of the bolometric light curve. . .	46
5.2	Gamma escape fit parameters.	53
A.1	Fit parameters.	65
A.2	Light curve parameters.	78

Chapter 1

Introduction

Supernovae have been known as some of the most spectacular phenomena on the sky ever since they have first been observed. Over the last decade, supernovae gained even more attention, since a subclass – Type Ia Supernovae (SNe Ia) – proved to be a reliable distance estimator. Due to their enormous brightness, these supernovae can be seen out to very large distances, allowing measurements of fundamental cosmological parameters, as described in the introduction to the field of Type Ia SNe given in Chapter 2.

However, despite of their heavy use, our knowledge about the progenitors and the detailed explosion mechanism of supernovae is still quite limited. The deductions for cosmology thus fully rely on empirical relations found for the light curves of SNe Ia, which lack a detailed explanation by theory at this point.

One way to make progress in this situation is to make a strong effort to investigate and analyze the observations in ever more detail. In Chapter 4, an analytic model for the light curve analysis is introduced which follows this strategy. It avoids a-priori assumptions commonly made and uses fits to observational data to objectively evaluate light curve parameters. Therefore, this model is ideally suited to explore the variety among individual SNe Ia and to provide an independent way to look for correlations among parameters of the supernova light curves. A catalogue of light curve parameters obtained with this method is given in Appendix A. This catalogue is a rich tool for the systematic analysis of SNe Ia light curves and was derived using published light curve data described in Chapter 3.

A different approach for putting the empirical relations on a firmer basis is to try to directly connect theory with observations. Bolometric light curves (Chapter 5) form an important link between the explosion models and the radiation transport calculations for SNe Ia ejecta. Using simple theoretical modeling, a number of physical parameters of the supernovae can be derived from the bolometric light curves directly.

Chapter 2

Type Ia Supernovae

2.1 What are Type Ia Supernovae (SNe Ia)?

Supernovae are exploding stars which are characterized by a fast and enormous increase in brightness within a few weeks followed by a fading away during several months. This fading of the SN light (SN 1997cj, a high redshift supernova, as an example) can be seen in Figure 2.1 (Garnavich et al. 1998). Although supernovae are rare events in a single galaxy, systematic SN searches are successful in finding a fair number of SNe. (For a recent review of observations of Type Ia Supernovae see Leibundgut (2000).)

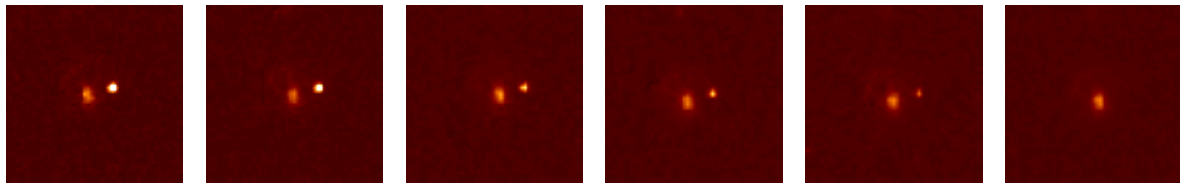


Figure 2.1: The decline of SN 1997cj observed with HST: adapted from Garnavich et al. (1998).

In the 1940s it was noticed (Minkowski 1941) that there are at least two different kinds of SNe; supernovae without hydrogen features in their spectra have been categorized as of Type I, those with hydrogen as of Type II. With a growing number and improved quality of observations, the class of Type I SNe had to be subdivided in those with a strong Si II absorption feature (SNe Ia) and those without (SNe Ib and Ic), SNe Ib having prominent He I and SNe Ic neither Si II nor He I features (for more information about SN spectra see Fillipenko (1997)). This classification scheme originally being an observational separation according to spectral features has proven to identify physically distinct objects: Type Ia SNe are thermonuclear explosions of low mass stars. All other supernova explosions (Type II and Ib/c) are due to the collapse of massive stars. Type Ia SNe are found also in elliptical galaxies without recent star formation whereas the other types are not.

Although there is consensus about SNe Ia being thermonuclear explosions of low mass stars, it is still unclear, what leads to these thermonuclear explosions and how the explosion mechanism can be described. (For a review on models of SNe Ia see e.g. Hillebrandt & Niemeyer (2000).)

One possible scenario for the progenitor system is a single carbon-oxygen white dwarf in a tight binary with a stellar companion. When matter is accreted from the companion onto the white dwarf with a rate within a narrow range, the Chandrasekhar mass might be reached, where the degeneracy pressure of the electrons is not able to support the star against gravity. The star collapses.

If the accretion rate is too low, the envelope of the star explodes. This phenomenon is called nova and the explosions blow away more matter than has been accreted, making it impossible to reach the critical mass. If the accretion rate is too high, steady quiet hydrogen burning or the build up of a hydrogen rich envelope is possible, which contradicts the fact, that there are no hydrogen features seen in the spectra of SNe Ia.

Another ignition scenario is a helium layer built up on top of the carbon-oxygen white dwarf. It can ignite and propagate a burning front into the white dwarf.

The compression and heating during the collapse of the star leads to the incineration of the white dwarf and a lot of energy can be gained from burning to the iron-peak and intermediate mass elements (such as Ca, Si, S, Ne, Mg). The star explodes and disrupts the progenitor system.

Other models exist in which the companion is another compact object, a white dwarf or neutron star. After merging a compact object with more than the Chandrasekhar mass can form, which also collapses. But these models have problems in reproducing the observed homogeneity of the luminosity at maximum light as the total mass of the two progenitors can vary significantly and so do the burning conditions.

The ejecta of the supernova are rich in heavy elements, especially ^{56}Ni , which powers the light curve of the supernova during several months with its radioactive decay. Without the input from the radioactive decay, the adiabatic expansion would cool down the debris to invisibility within a short time.

In favor of the exploding white dwarf scenario is that there have been no neutron stars found in historical SNe Ia, the appearance of SNe Ia is very homogeneous and the assumption of a few tenths of a solar mass of ^{56}Ni fits well the observed light curve and the observed spectra. The different scenarios, however, are not easily distinguishable as they cause only small differences in the observed quantities. Therefore, observations in many wavelength regions and at early epochs are needed. For example the rise times depend on the ejecta opacity and the distribution of ^{56}Ni and thus on the carbon to oxygen ratio. Observing the early light curve thus can give hints on the progenitor, the explosion physics, and the radiation transport.

SNe Ia show a tremendous homogeneity in their light curves. This has made them very useful for distance estimation, as they can be used as “standard candles”. But careful inspection of high quality data has proven that there are differences. This is shown in the compilation of SN light curves in Figure 2.2 (taken from Suntzeff 1996).

2.2 Light Curve Width-Luminosity Relation

It has been found that the absolute magnitude (for explanations see box on page 11) of SNe Ia is related to the width of the light curve. Earlier versions of such light curve shape vs. luminosity relations had been proposed already in the 1970s, but could not be supported by the available data. After acquiring a lot of high quality data in the early 1990s, the breakthrough came with the Phillips relation (Phillips 1993) in which a linear relationship between the

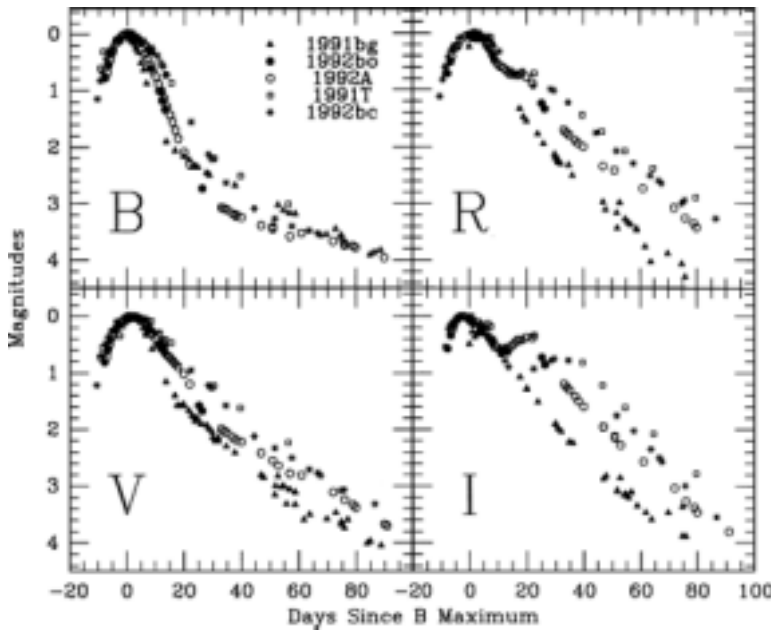


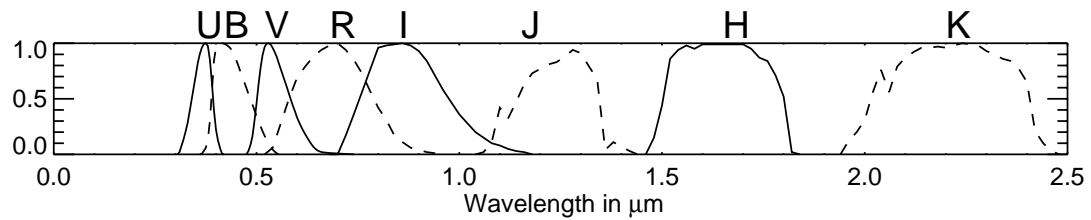
Figure 2.2: *BV* (left panel) and *RI* (right panel) evolution of bright SNe Ia. From Suntzeff (1996). The light curves are normalized to the maximum luminosity and to the epoch of maximum light in *B*.

Magnitudes and the distance modulus

The absolute magnitude M of an astrophysical object gives its intrinsic brightness in a logarithmic scale. It is defined as $M = \text{const.} - 2.5 \log L$, with L being the luminosity in erg/sec and the constant defined such that some normalization requirements are fulfilled and it corresponds to the apparent magnitude m of an object at a distance of 1 pc (1 pc (parsec) = 3.086×10^{16} m) after further corrections for reddening and redshift have been taken into account. The apparent flux is not only diminished (the apparent magnitude increased) by the distance modulus, but also by reddening through interstellar dust (see box on page 13) and cosmological redshift (which originates from the expansion of the Universe and shifts the flux to longer wavelengths. The flux in a particular filter can be diminished or enhanced, depending on the flux which is shifted into its wavelength range.): $m = M - \mu + RE(B-V) + k_{\text{corr}}$. The distance modulus is the logarithm of the ratios of apparent to absolute luminosities, equal to the difference of absolute magnitude to apparent magnitude. $\mu \equiv m - M = 5 \log r - 5$, where r , the luminosity distance, which is defined by the inverse square law, is measured in parsecs.

Broadband Filters

The light curves are observed typically in the broad-band optical filters following the Bessell (1990) system. The transmission efficiencies for the UBVIJHK filters versus wavelength are shown below.



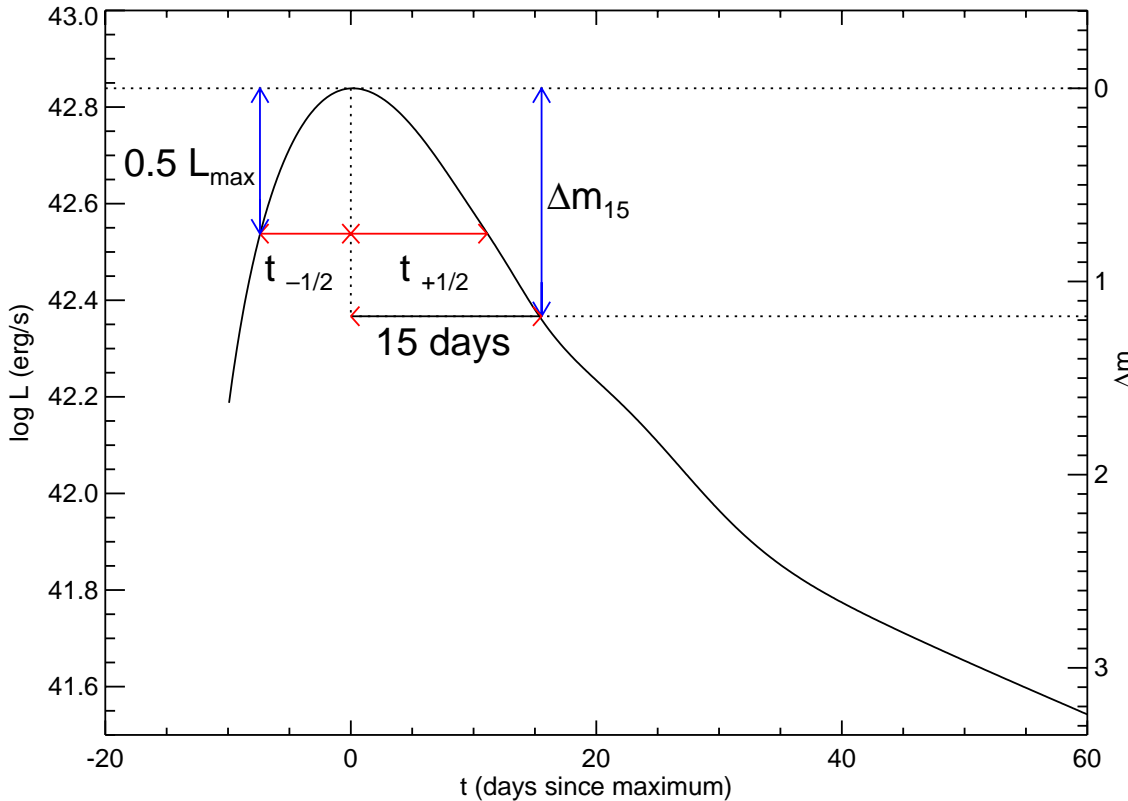


Figure 2.3: Illustration of the decline parameter Δm_{15} denoting the magnitude difference between maximum light and 15 days after and $t_{1/2}$. $t_{1/2}$ is the time it takes the SN to rise to ($t_{-1/2}$) and decline from ($t_{+1/2}$) maximum to half its luminosity. This parameter will be used for the analysis of bolometric light curves in Chapter 5.

linear decline parameter Δm_{15} and the absolute magnitude was found.

Figure 2.3 illustrates this parameter together with the half light width $t_{1/2}$ (the time it takes the SN to rise to and decline from maximum to half its luminosity), a light curve shape parameter which will be used for the analysis of bolometric light curves in Chapter 5.

Employing the observed correlation between light curve shape and luminosity improved the precision of distance estimates derived from SNe Ia significantly and allowed using SNe Ia for the determination of cosmological parameters. The success can be seen best in the Hubble diagram (see box on page 14), where the distribution around a straight line narrows significantly, when brightness corrections depending on this width luminosity relation are applied. For the luminosity correction mainly three different implementations are used:

The template-fitting method (Hamuy et al. 1996c): The decline rate parameter $\Delta m_{15}(B)$ and the magnitude at maximum are determined from the comparison of the goodness of fits of the photometric data to a set of template SN Ia light curves. These template light curves are chosen to span the full range of observed decline rates. The magnitude at maximum light is corrected to a standard value using a linear (now extended to a quadratic (Phillips et al. 1999)) relation between the decline rate and maximum lumi-

nosity gained from supernovae in the Hubble flow, which have also been corrected for extinction.

It is important to notice, that although this method often is referenced as the “ Δm_{15} method” the parameter is not determined directly from the magnitude difference of the first 15 days past maximum of the observations, but from the fit to pre- and post-maximum light data out to 40 days past maximum. Also the fit is done simultaneously in more than one filter band, depending on the availability of observations.

The stretch factor method (Perlmutter et al. 1997, 1999): It was found, that if the B light curves of SNe Ia are stretched or contracted in time, they overlay. This is used in the stretch factor method, where a template light curve is stretched to match the observed light curve. The width luminosity relation has been derived using the light curves of the Calán/Tololo supernovae.

The multicolor light curve shape method (MLCS, Riess et al. 1998): The third approach is a quadratic estimation algorithm to determine the relationship between the shape of the light curve and its peak luminosity. A training set of SNe in the Hubble flow is used to calibrate this method. And depending on the purpose of the brightness correction two or more filters are used to estimate the extinction due to the host galaxy of the SN.

Figure 2.4 shows the luminosity–width relation as Phillips et al. (1999) find it. In the left half of the figure the absolute magnitudes corrected only for Galactic reddening (see box on page 13) for their full sample in the Hubble flow is shown. In the right half 23 SNe in their sample are eliminated because of significant host galaxy reddening. A clear correlation and the need for a second order term can be seen.

Some SNe are peculiar and do not fit into this picture: e.g. SNe 1991T and 1991bg. They are not in Figure 2.4, because they are not in the Hubble flow. Not only do they show unusual

Reddening

Intervening dust in the host galaxy of the supernova and in our Galaxy is absorbing and scattering the light of the supernova. Therefore the light is reddened and dimmed. Comparing the colors of reddened and unreddened stars, the color excess $E(B-V) = (B-V) - (B-V)_0$ can be obtained.

From spectrophotometric measurements it was found, that the interstellar extinction A_λ is proportional to $1/\lambda$. In this work the conventional extinction law of Savage & Mathis (1979) is used for correcting the supernova light for interstellar extinction.

Galactic reddening

Reddening occurring in our Galaxy depends on the direction to the supernova. Used here are the dust maps of Schlegel et al. (1998), which are based on measuring the dust infrared emission with instruments on the IRAS and COBE satellites. Since the diffuse emission in the infrared is a direct measure of the column density of the interstellar dust, such a map can be used as a measure of extinction for extragalactic objects.

Host galaxy reddening

The light coming from a supernova can already be reddened in its host galaxy. For estimating the extinction by the host galaxy either the color at maximum or the color evolution of the supernova can be used (see explanation in Section 3.2). Furthermore the intensity of interstellar absorption bands is well correlated with the extinction measured by the color excess $E(B-V)$. The equivalent width of the Na I D line at the redshift of the host galaxy thus can be used for the reddening estimation.

spectral features, colors and belong to the brightest resp. faintest SNe Ia, but often they show up as outliers in relations.

What determines the light curve shape?

The light curve of a SN Ia is determined by a competition between three effects: the deposition of energy from radioactive decay, the adiabatic conversion of internal energy to kinetic energy of expansion, and the escape of internal energy as the observed light curve. The deposited energy stems from the γ -rays of the electron capture processes of ^{56}Ni and ^{56}Co and the kinetic energy of the positrons, which are generated in 19% of the ^{56}Co decay, and their annihilation γ -rays (this will be discussed in detail in Section 5.3.1).

The ^{56}Ni yield and the γ -ray escape fraction play the determining roles in the relation between the light curve's width and peak luminosity, whereas models are quite insensitive to the distribution of radioactivity and to the composition of non-radioactive material, within limits set by achieving the appropriate explosion energies and acceptable nucleosynthesis (Pinto & Eastman 2001).

The peak luminosity and the heating rate of the gas are determined by the amount of ^{56}Ni . The more ^{56}Ni is synthesized, the higher are the temperatures and the cooling is less efficient, a higher ionization being responsible for this. This leads to broader and brighter light curves.

If the efficiency of the γ -ray escape is increased, the evolution rate of the light curve is increased and the greater escape leads to narrower light curves. As SNe with synthesized ^{56}Ni extending to higher velocities or higher overall velocities have larger γ -ray escape fractions at a given time, they have narrower light curves. Models with higher ^{56}Ni yields tend to have their radioactivity distributed over a broader range in velocity, leading to larger escape fractions. This greater escape fraction acts to oppose the tendency for broader light curves resulting from higher temperatures. Thus these two effects are not independent. Pinto & Eastman (2001) have shown that they can reproduce the observed width luminosity relation with only varying the ^{56}Ni yield.

Analyzing the light curves of SNe Ia can yield insight in the progenitor system, the explosion mechanism, and the radiation transport. By comparing the kinetic energy as derived from line widths and the measured amount of ^{56}Ni it should be possible to derive global parameters of the explosion.

Hubble diagram and Hubble flow

The Hubble diagram shows distance vs. redshift. The law that recessional speed is proportional to distance for a homogeneous and isotropic Universe is called Hubble law. Galaxies moving away from us with a speed precisely following this law are said to follow the Hubble flow. Because the actual Universe is not precisely homogeneous, with lumpiness arising from clustering of galaxies and voids of empty space, the motions of nearby galaxies deviate somewhat from the Hubble flow. High redshift supernovae deviate from the straight line (Hubble law) because higher orders of the redshift dependence have to be taken into account.

In the case of supernovae the distance modulus can be measured, if the absolute magnitude is known. The absolute magnitude is derived from the apparent magnitude considering reddening and correcting with the width-luminosity relation. The redshift is measured from the shift of lines in the observed spectrum. Comparing the observational data with theoretical lines leads to a determination of cosmological parameters, its geometry and mass-energy content.

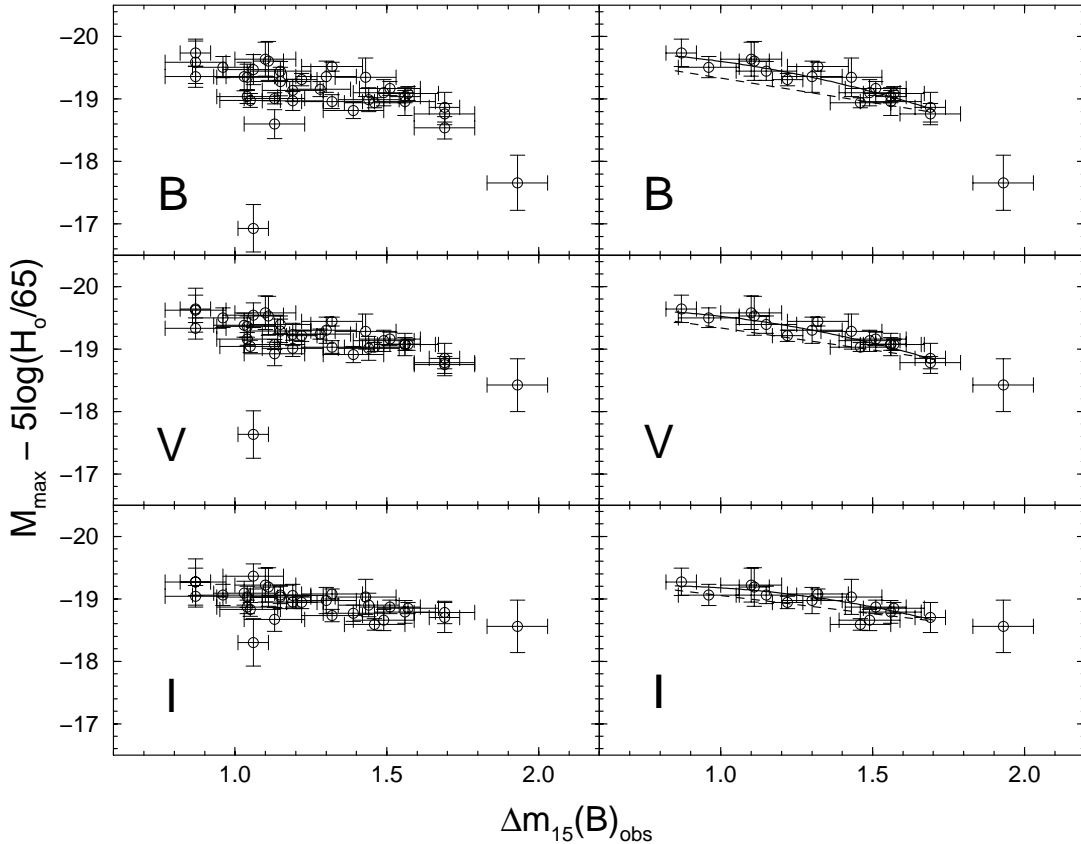


Figure 2.4: Figure from Phillips et al. (1999): Left: Absolute BVI magnitudes corrected only for Galactic reddening plotted vs. the decline rate parameter $\Delta m_{15}(B)$ for the full sample of 41 Calán/Tololo and CfA SNe Ia in the Hubble flow. Right: Same diagram after elimination of the 23 SNe in the sample for which they find significant host galaxy reddening. The dashed lines correspond to the linear fits given by Hamuy et al. (1996c).

2.3 High Redshift SNe and their Use as Distance Indicators

Assuming that SNe are standard candles (Branch & Tammann 1992) or that their maximum luminosity can be corrected with the luminosity width relation (see Section 2.2), the luminosity distance can be calculated. Together with the redshift of the SN, it can be put in the Hubble diagram (see box on page 14).

Two independent groups are searching for SNe at high redshifts ($0.5 \lesssim z \lesssim 1.2$) at the moment (Riess et al. 1998; Perlmutter et al. 1999). These redshifts are in the non-linear regions of the Hubble flow and allow to distinguish different cosmologies. Systematically surveying patches of the sky searching for SNe at high redshift together with pre-scheduled follow-up observations within large collaborations with access to the biggest telescopes made it possible to collect data of more than 100 high redshift supernovae up to now. The two groups use different methods to correct for the width luminosity relation, but still draw the same conclusions.

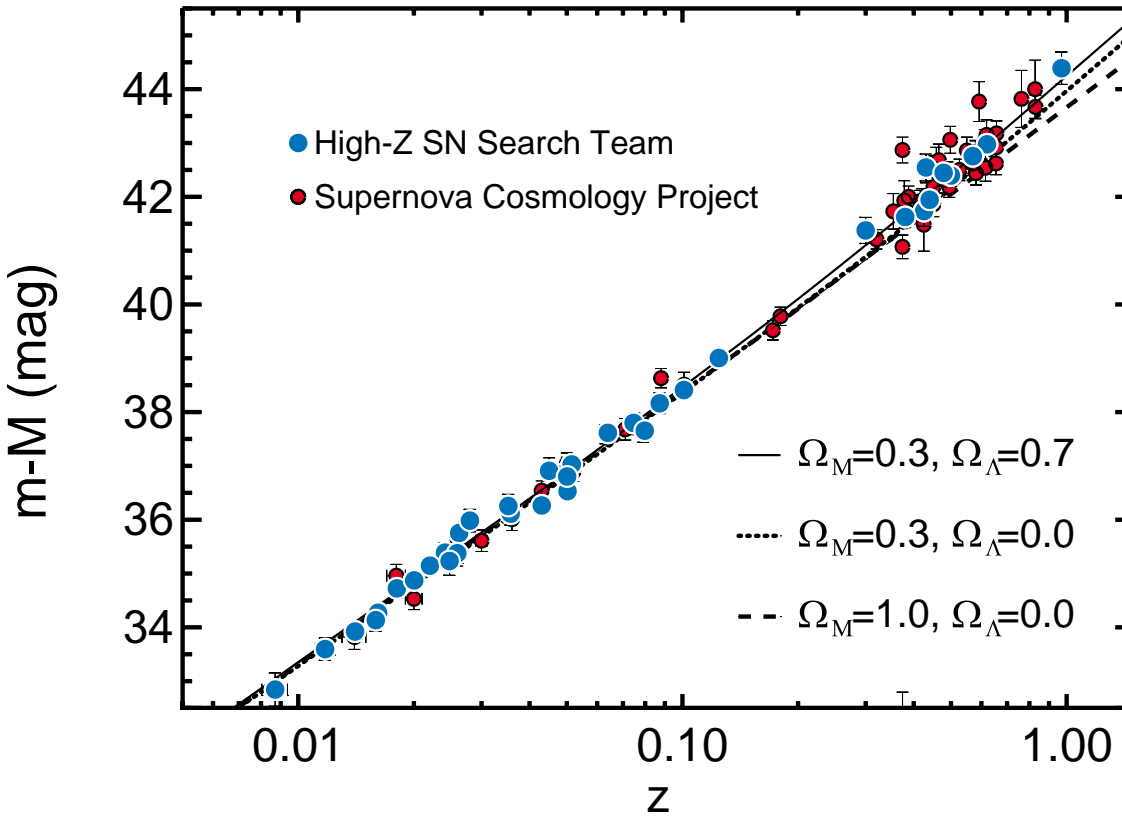


Figure 2.5: Hubble diagram for high and low redshift SNe (Riess et al. 1998) from both groups (symbols). The distance moduli are measured from the template-fitting method parameterized by $\Delta m_{15}(B)$ (Hamuy et al. 1996c). Overplotted are three cosmologies: “low” and “high” Ω_M with $\Omega_\Lambda = 0$ and the best fit for a flat cosmology, $\Omega_M = 0.3$ with $\Omega_\Lambda = 0.7$.

The determination of cosmological parameters (Riess et al. 1998; Perlmutter et al. 1999) has induced a vivid discussion in cosmology (for a review see Riess (2000)). The distant SNe are too dim for a matter dominated, flat or open Universe. This faintness can be interpreted as a greater than expected distance, resulting from an accelerating, ever expanding Universe. This result implies the existence of a new constituent of the Universe, either the cosmological constant or something else with similarly negative pressure capable of accelerating the expansion (“dark energy”).

Both groups take care of excluding systematic contaminations of the observations. The so-called Malmquist-bias (only detecting the brightest SNe), gravitational lensing and sample contamination have been tested, but none of these effects can make the data compatible with a decelerating Universe.

Extinction by interstellar dust and evolution of the intrinsic properties of SNe Ia or a change in the population of SNe Ia could bias the results.

Dust has a different signature than an accelerated Universe. Normal dust grains show

up not only as extinction but also as a color excess as it preferentially extinguishes bluer light. Both groups observe in at least two filters (restframe B and V). The color excess for the high redshift SNe is consistent with zero color excess in both samples. But even assuming a “worst-case” plausible color excess is not enough to disfavor an accelerating Universe. So called “grey” dust, which reddens less than normal dust, could extinguish enough light to again favor a non-accelerating Universe. If the grey dust is patchy like normal dust, it would increase the scatter of the observations further than by the measurement uncertainties, but this is not seen in the measurements. The other possibility would be uniformly distributed grey dust. If it is not perfectly grey, measurements in a wider wavelength range (restframe $UBVRI$) could measure it, observations are underway (Jha & the High-Z Supernova Search Team 2001). Also observations at higher redshift ($z > 1$) can distinguish dimming by dust and other systematic effects from the faintness because of cosmology. Whereas systematic effects can be assumed to grow with redshift, the most favored model at the moment has its biggest deviation from an empty Universe at a redshift around 1.

So far there is no indication that SNe Ia observed at high redshift are different from the low redshift sample, as their light curves and spectra show a strong similarity. But further observations especially in restframe U , where variations in the progenitors are predicted to lead to observable effects, might strengthen this assumption. Also observations in the IR are made to check, if SNe at high redshift show the secondary maximum seen in longer wavelength filters in the nearby sample.

Chapter 3

Observational Data

3.1 Light Curve Data

For this work published light curves of 60 SNe have been compiled. The references for these light curves and the availability of the filter light curves are listed in the second and third column of Table 3.1.

3.2 Reddening

Before constructing the bolometric light curves (Chapter 5) the filter light curves had to be dereddened. Reddening by dust affects the absolute luminosity as well as the spectral energy distribution.

The color excess due to Galactic reddening (Schlegel et al. 1998) is listed in the forth column in Table 3.1. To have a consistent data set, the values of Phillips et al. (1999) are used for the host galaxy dust extinction where available. They use information about the color at maximum and the fact, that the $B-V$ evolution during the period from 30 to 90 days after V maximum is remarkably similar for all events. The sixth column lists the color excess $E(B-V)$ (Phillips et al. 1999) and the seventh column gives the sum of the two color excesses.

For four SNe other sources for the color excess had to be used, as they are not included in the Phillips et al. (1999) sample: The color excess of SN 1996ab was estimated by Riess (2001) using the multicolor light curve shape method described in Section 2.2. For SN 1997br the value by Li et al. (1999) has been used. In the case of SN 1997cn Turatto et al. (1998) state that there is no absorption in the host galaxy. Modjaz et al. (2001) find for SN 1998de that there is no NaI absorption and the SN is in the outskirts of a lenticular galaxy, where no absorption is expected. The total color excesses of these SNe are given in column seven.

3.3 Distances

The distance to the SN is the major uncertainty in the calculation of the bolometric luminosity (see Section 5.1), but the distance scale just shifts the light curves and does not alter the light curve shape. As local SNe as well as SNe in the Hubble flow have been included in the analysis, different distance estimators had to be used (Column eight in Table 3.1 and reference in column nine). For an overview on techniques for measuring extragalactic distances

see Jacoby et al. (1992). To have as uniform as possible a set of distances, all distances have been converted to a distance scale of $H_0 = 65 \text{ km s}^{-1} \text{ Mpc}^{-1}$.

The distances for the SNe from the Riess et al. (1999c) sample are derived from the heliocentric velocities given in Riess et al. (1999c), which are converted to cosmic microwave background (CMB) velocities. Hamuy et al. (1996c) give already the heliocentric velocities to the host galaxies corrected to the cosmic microwave background frame.

For the nearby SNe Cepheid, Tully-Fisher, and SBF distances have been used. Calculating the distance with the method of the globular cluster luminosity function (Drenkhahn & Richtler 1999; Della Valle et al. 1998) for SNe 1994D and 1992A reveals the same values within the uncertainties.

In the columns seven to nine of Table 3.1 the distance modulus, the applied method and the reference are given.

Table 3.1: Light curve data and $E(B-V)$ and distance modulus for the SNe used in this work. The galactic reddening is taken from Schlegel et al. (1998), the host galaxy reddening is from Phillips et al. (1999).

SN	Ref.	$E(B-V)$	$E(B-V)$	$E(B-V)$	Distance	Method ¹
		Galactic	Host	Total	Modulus	& Ref.
SN 1989B	<i>UBVRI</i>	2	0.032	0.340	0.372	30.22 CH 3
SN 1990N	<i>UBVRI</i>	4	0.026	0.090	0.116	32.03 CH 5
SN 1990O	<i>BVRI</i>	6	0.093	0.020	0.113	35.74 HV 7
SN 1990T	<i>BVRI</i>	6	0.053	0.090	0.143	36.36 HV 7
SN 1990Y	<i>BVRI</i>	6	0.008	0.230	0.238	36.29 HV 7
SN 1990af	<i>BV</i>	6	0.035	0.040	0.075	36.85 HV 7
SN 1991S	<i>BVRI</i>	6	0.026	0.060	0.086	37.08 HV 7
SN 1991T	<i>UBVRI</i>	4	0.022	0.140	0.162	31.07 CG 8
SN 1991U	<i>BVRI</i>	6	0.062	0.110	0.172	35.91 HV 7
SN 1991ag	<i>BVRI</i>	6	0.062	0.070	0.132	34.02 HV 7
SN 1991bg	<i>BVRI</i>	9	0.040	0.030	0.070	31.26 SBF 10
SN 1992A	<i>BVRI</i>	11	0.017	0.000	0.017	31.34 CC 12
SN 1992J	<i>BVI</i>	6	0.057	0.030	0.087	36.65 HV 7
SN 1992K	<i>BVI</i>	6	0.101	0.000	0.101	33.56 HV 7
SN 1992P	<i>BVI</i>	6	0.021	0.070	0.091	35.44 HV 7
SN 1992ae	<i>BV</i>	6	0.036	0.120	0.156	37.73 HV 7
SN 1992ag	<i>BVI</i>	6	0.097	0.100	0.197	35.40 HV 7
SN 1992al	<i>BVRI</i>	6	0.034	0.010	0.044	34.08 HV 7
SN 1992aq	<i>BVI</i>	6	0.012	0.000	0.012	38.39 HV 7
SN 1992au	<i>BVI</i>	6	0.017	0.000	0.017	37.27 HV 7
SN 1992bc	<i>BVRI</i>	6	0.022	0.000	0.022	34.82 HV 7
SN 1992bg	<i>BVI</i>	6	0.185	0.010	0.195	36.10 HV 7
SN 1992bh	<i>BVI</i>	6	0.022	0.120	0.142	36.61 HV 7
SN 1992bk	<i>BVI</i>	6	0.015	0.010	0.025	37.17 HV 7
SN 1992bl	<i>BVI</i>	6	0.011	0.000	0.011	36.51 HV 7
SN 1992bo	<i>BVRI</i>	6	0.027	0.000	0.027	34.63 HV 7
SN 1992bp	<i>BVI</i>	6	0.069	0.000	0.069	37.85 HV 7
SN 1992br	<i>BV</i>	6	0.026	0.010	0.036	38.08 HV 7
SN 1992bs	<i>BV</i>	6	0.012	0.100	0.112	37.36 HV 7

continued on next page

1 – CH – Cepheids to host galaxy, HV – heliocentric velocity, CG – Cepheids to group, SBF – Surface brightness fluctuations, CC – Cepheids to cluster, TF – Tully-Fisher

2 – Wells et al. (1994)

3 – Saha et al. (1999)

4 – Lira et al. (1998)

5 – Saha et al. (1997)

6 – Hamuy et al. (1996a)

7 – Hamuy et al. (1996c)

8 – Fisher et al. (1999)

9 – Filippenko et al. (1992); Leibundgut et al. (1993); Turatto et al. (1996)

10 – Hamuy et al. (1996b) and references therein.

11 – Suntzeff (1996)

12 – Silbermann et al. (1999)

SN	Ref.		$E(B-V)$ Galactic	$E(B-V)$ Host	$E(B-V)$ Total	Distance Modulus	Method & Ref.
SN 1993B	<i>BVI</i>	6	0.079	0.120	0.199	37.60	HV 7
SN 1993H	<i>BVRI</i>	6	0.060	0.050	0.110	35.31	HV 7
SN 1993O	<i>BVI</i>	6	0.053	0.000	0.053	36.93	HV 7
SN 1993ac	<i>BVRI</i>	13	0.163	0.120	0.283	36.81	HV 13
SN 1993ae	<i>BVRI</i>	13	0.039	0.000	0.039	34.61	HV 13
SN 1993ag	<i>BVI</i>	6	0.112	0.070	0.182	36.85	HV 7
SN 1993ah	<i>BVI</i>	6	0.020	0.010	0.030	35.63	HV 7
SN 1994D	<i>UBVRI</i>	14	0.022	0.000	0.022	30.68	SBF 15
SN 1994M	<i>BVRI</i>	13	0.024	0.080	0.104	35.25	HV 13
SN 1994Q	<i>BVRI</i>	13	0.017	0.060	0.077	35.66	HV 13
SN 1994S	<i>BVRI</i>	13	0.021	0.000	0.021	34.37	HV 13
SN 1994T	<i>BVRI</i>	13	0.029	0.090	0.119	36.11	HV 13
SN 1994ae	<i>BVRI</i>	13	0.031	0.120	0.151	31.87	TF 16
SN 1995D	<i>BVRI</i>	17	0.058	0.040	0.098	32.71	HV 13
SN 1995E	<i>BVRI</i>	13	0.027	0.740	0.767	33.65	HV 13
SN 1995ac	<i>BVRI</i>	13	0.042	0.080	0.122	36.79	HV 13
SN 1995ak	<i>BVRI</i>	13	0.043	0.180	0.223	35.06	HV 13
SN 1995al	<i>BVRI</i>	13	0.014	0.150	0.164	32.18	HV 13
SN 1995bd	<i>BVRI</i>	13	0.495	0.150	0.645	34.30	HV 13
SN 1996C	<i>BVRI</i>	13	0.014	0.090	0.104	35.74	HV 13
SN 1996X	<i>BVRI</i>	13	0.069	0.010	0.079	32.78	HV 13
SN 1996Z	<i>BVR</i>	13	0.063	0.330	0.393	32.99	HV 13
SN 1996ab	<i>BV</i>	13	—	—	0.049 ¹⁸	38.86	HV 13
SN 1996ai	<i>BVRI</i>	13	0.014	1.440	1.454	31.31	HV 13
SN 1996bk	<i>BVRI</i>	13	0.018	0.190	0.208	32.62	HV 13
SN 1996bl	<i>BVRI</i>	13	0.105	0.080	0.185	36.05	HV 13
SN 1996bo	<i>BVRI</i>	13	0.078	0.280	0.358	34.38	HV 13
SN 1996bv	<i>BVRI</i>	13	0.105	0.210	0.315	34.45	HV 13
SN 1997br	<i>BVRI</i>	19	—	—	0.350 ¹⁹	32.32	HV 19
SN 1997cn	<i>UBVRI</i>	20	—	—	0.000 ²⁰	34.53	HV 20
SN 1998bu	<i>UBVRIJHK</i>	21	0.025	0.330	0.355	30.37	CH 22
SN 1998de	<i>BVRI</i>	23	—	—	0.060 ²³	34.32	HV 23

13 – Riess et al. (1999c)

14 – Richmond et al. (1995); Patat et al. (1996); Meikle et al. (1996); Smith et al. (2000)

15 – Tonry (1997)

16 – Riess et al. (1996b)

17 – Riess et al. (1999c); Sadakane et al. (1996)

18 – Riess (2001)

19 – Li et al. (1999)

20 – Turatto et al. (1998)

21 – Hernandez et al. (2000); Jha et al. (1999); Suntzeff et al. (1999); Munari et al. (1998)

22 – Tanvir et al. (1995)

23 – Modjaz et al. (2001)

Chapter 4

Fitting Routine

4.1 Method

To avoid assumptions made in template fitting methods the light curves are analyzed individually using a descriptive model (Vacca & Leibundgut 1996). For each supernova the observed light curve in each filter (in magnitudes, for an explanation see box on page 2.2) is fitted with an empirical model consisting of a Gaussian (for the peak phase) atop a linear decay (late-time decline), a second Gaussian (to model the secondary maximum in the V , R , and I band light curves), and an exponentially rising function (for the pre-maximum segment). The functional form of the fit is:

$$m = \frac{f_0 + \gamma(t - t_0) + g_0 \exp\left[\frac{-(t-t_0)^2}{2\sigma_0^2}\right] + g_1 \exp\left[\frac{-(t-t_1)^2}{2\sigma_1^2}\right]}{1 - \exp\left(\frac{\tau-t}{\theta}\right)}. \quad (4.1)$$

The first Gaussian and the decline are normalized to the phase t_0 , while the second Gaussian occurs at a later phase t_1 . The exponential cutoff function for the rise has a characteristic time θ and a separate phase zero-point τ . The amplitudes of the two Gaussians, g_0 and g_1 , as well as the intercept of the line, f_0 , the slope, γ , the phases t_0 and t_1 , and the widths, σ_0 and σ_1 , the characteristic rise time θ and its phase τ are free parameters in the fit. Each filter light curve is fitted individually and independently using a χ^2 -minimization procedure to determine the best-fit values of the parameters. Other parameters which characterize the shape of the light curve, such as the time of maximum brightness or Δm_{15} (see Figure 2.3 for an illustration), can then be derived from the best-fit model. Although the model is a completely empirical description of the general shape of SNe Ia light curves, it can be noted that theoretical models (Pinto & Eastman 2000) predict a Gaussian shape for the peak in models with constant opacity and ^{56}Ni buried well within the ejecta. Furthermore, the late decline of the SNe Ia flux, particularly in the B and V bands, often appears quasi-exponential. This justifies the linear decline in magnitude.

Figure 4.1 shows the example of the fit to the R light curve of SN 1992bc (photometry from Hamuy et al. 1996c). The various components of the fit are displayed. The exponential function (solid line) rises steeply to unity, modeling the rapid brightness increase of the supernova. The decline rate (dotted line) is set by the long tail beginning about 50 days past maximum. The first Gaussian (dashed line) fully describes the maximum phase, as further demonstrated in the inset. The second Gaussian (dashed-dotted line) reproduces

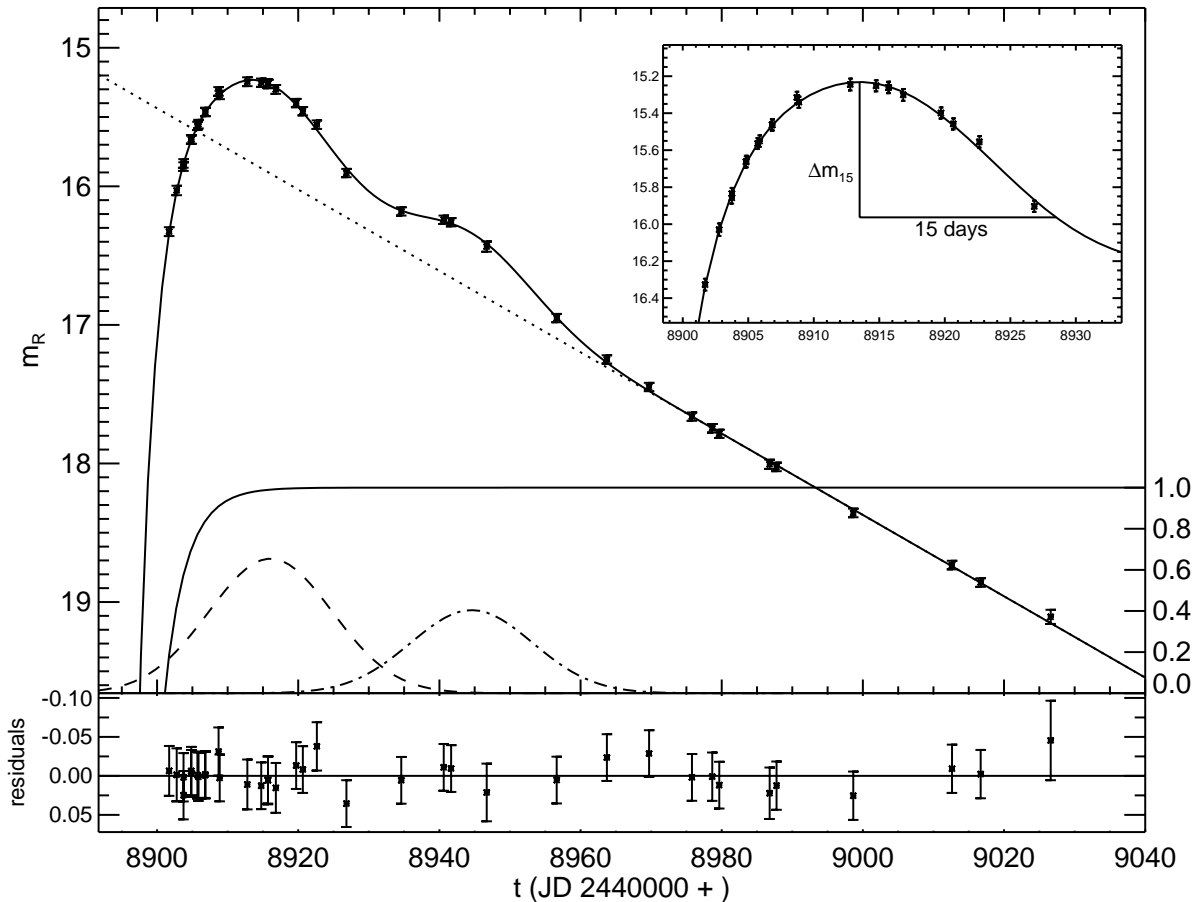


Figure 4.1: Fit of Equation 4.1 to the R photometry of SN 1992bc. The various components of the fit are displayed as the following: a linear (in magnitudes) decay (dotted line), an exponential rise factor (solid line) from 0 to 1 as indicated by the right ordinate, two Gaussians for the peak and the second maximum (dashed and dashed-dotted line) with the amplitude in magnitudes as indicated by the right ordinate. The inset shows the light curve around maximum light. Δm_{15} can be obtained easily because of the continuous representation of the data by the fit. The residuals from the fit are displayed in the bottom panel with the observational error bars.

the “bump” in the light curve. The bottom panel of Figure 4.1 displays the residuals of the fit with the observational error bars. It is clear that the function is an accurate, continuous description of the data. The small systematic undulations of the residuals indicate that the fit is not perfect and can be used to make detailed comparisons between individual supernovae. This model has been fitted to the filter light curves of 60 supernovae. These fits and the fit parameters are presented in Appendix A.

The fits provide objective measures of the magnitude (m_{\max}) and date (t_{\max}) of maximum, the extent of the peak phase, the amplitude and extent of the secondary peak, the late decline rate, and an estimate of the rise time. The accuracy of these parameters depends strongly on the number and quality of the observations in each phase. While in most

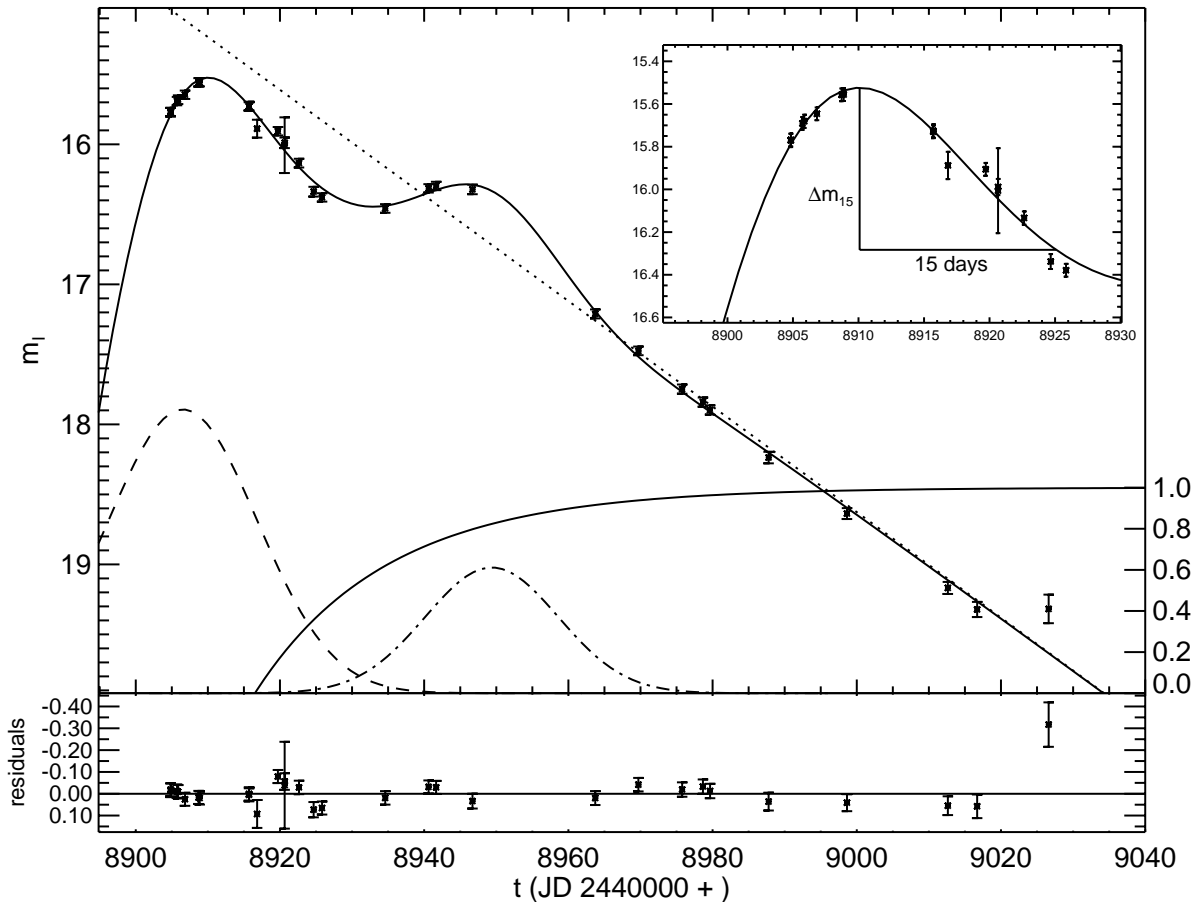


Figure 4.2: Fit of Equation 4.1 to the observed I data of SN 1992bc. The description of the lines is given in Figure 4.1.

cases the late decline can be derived fairly easily, the rise time is undetermined when no pre-maximum observations are available. It is possible to derive other light curve shape descriptions, such as Δm_{15} , for each filter objectively and independently without comparing it to templates.

Other functional forms could be imagined for the fit. However, the late decline and the steep rise can be assumed to have simple functional forms. Fitting polynomials or spline functions, for example, could not produce the transition to the linear decline as observed, but would simply transfer the undulations of the early phases to the late decline and fail to match the observed linear decline. Furthermore, such functions would not provide a small set of adjustable parameters which can be compared between different objects.

Nevertheless, the adopted functional form is not a perfect representation of all optical filter light curves. When fitting the I light curves of some SNe Ia it is found that the model has difficulties to match the observations with the same accuracy as in the other filters. This can be seen in Figure 4.2.

The slope of the I band light curve decline (dotted line) is so steep that the model can-

not reproduce the observed light curve. This steep slope causes the function to overshoot the observed values near the second maximum and the fitting program inverts the second Gaussian to produce the observed minimum in the light curve. If the fitting routine is constrained to fit only positive Gaussians (positive in flux, i.e. negative in magnitudes), the exponential rising function (solid line) is shifted to late times and depresses the linear decay (dotted line) before the second maximum; in addition the first Gaussian (dashed line) is enhanced and shifted to earlier times. This implies that, for the I band, the fit parameters describing the first Gaussian (i.e. its magnitude, its center and its standard deviation) cannot be used to characterize the first maximum, even if the light curve appears fitted well. In spite of this problem, the I band light curves of the SNe in the analyzed sample can all be reasonably well fitted with the model and the descriptive parameters derived from these fits are meaningful. This steep decline in the I band is a rather unexpected result. The physical explanation behind this behavior is that the I filter light curve is dominated by a rapidly decreasing flux component and significant flux redistribution takes place in the evolution. Similar results have been found by Suntzeff (1996) in the observations of SN 1992A and by Pinto & Eastman (2000) in theoretical models.

If there are no observations in the time range of one component of the fit, this can result in strange features of the fits. For example, the light curves of SN 1990N (see Figure A.2) suffer from two gaps in the observations, one being at the time where the secondary maximum is expected, which makes the fit overestimating the second maximum in the filter light curves by far. This has as a result that also the secondary bump in the bolometric light curve is inflated.

The applied method is a Levenberg–Marquardt algorithm (see Bevington & Robinson 1992; Press et al. 1992; Davis 1993) to minimize χ^2 for a nonlinear fit. This method combines the advantages of a gradient-search method with those of an expansion method. In gradient-search methods the parameters of the fit are changed simultaneously, so that the resultant direction of travel in parameter space is along the gradient of χ^2 . This makes it a fast method while far away from the minimum, but it loses efficiency as the search approaches a minimum, because the evaluation of the derivative involves taking differences between nearly equal numbers. Also it has a good chance to end up in long, flat valleys in the parameter space. The second ingredient to the Levenberg–Marquardt algorithm is the expansion method as soon as the approximation comes close enough to the minimum, that the deviations caused by the linearization do not introduce a big error. The Levenberg–Marquardt method has the advantage of being reasonably insensitive to the starting values of the parameters, it provides an estimate of the full error matrix and a better calculation of the diagonal errors.

Although the method is reasonably insensitive to the starting values in general, the multitude of 10 parameters can cause the fit to end up in a local minimum far away from reasonable parameters. Therefore the initial values of the parameters are varied within the ranges given in Table 4.1 and the output of the fit is checked, if the parameters are in the range of reasonable values. The resultant parameters of the fit have to be within the following ranges: f_0 has to be between -10 and 30 , 30 being an upper limit of apparent magnitude and -10 allowing also normalized ($m_{\max} = 0$) light curves to be fitted. The slope γ is required to be declining (> 0) and smaller than 1 mag/day. The two Gaussians have amplitudes $g_{0/1}$ between 0 and -8 magnitudes, standard deviations $\sigma_{0/1}$ between 0.5 and 50 days and times in the range of -20 to 20 or -20 to 50 days past the input value t_0^{ini} for $t_{0/1}$ respectively.

Table 4.1: Range of parameters as input in the fitting routine and for checking the output.

		initial range	final range
f_0	[mag]	10 … 20	–10 … 30
γ	[mag/day]	0.002 … 0.040	0 … 1
g_0	[mag]	–5.1 … 0.1	–8 … 0
t_0	[days]	$t_0^{\text{ini}} - 10 \dots t_0^{\text{ini}} + 10$	$t_0^{\text{ini}} - 20 \dots t_0^{\text{ini}} + 20$
σ_0	[mag]	0.1 … 30.1	0.5 … 50
g_1	[mag]	–5.1 … 0.1	–8 … 0
t_1	[days]	$t_0^{\text{ini}} + 12 \dots t_0^{\text{ini}} + 32$	$t_0^{\text{ini}} - 20 \dots t_0^{\text{ini}} + 50$
σ_1	[mag]	0.1 … 30.1	0.5 … 50
τ	[days]	$t_0^{\text{ini}} - 30 \dots t_0^{\text{ini}} - 10$	–100 … t_0
θ	[days]	1 … 10	1 … 20

The asymptotic value for the exponential rise has to be before t_0 , otherwise it would damp the light curve in an unacceptable way and past day –100 (to allow enough time for the rise even for normalized ($t_{\max} = 0$) light curves). A reasonable range for the steepness of the exponential rise is between 1 and 20 days.

10000 sets of initial parameters have been chosen and the number of accepted fits (according to the criteria above: the fit parameters resulting from the calculations is in the range of the last column of Table 4.1) averages to about 33% in B for the whole sample of 60 SNe; for the V band one gets 24%, for the R band 15% and 12% for I . But the standard deviations of these values can be of the same order and the rejection rate has a big variation in the supernova sample. For the U band no statistical statement can be made because of the small number of available light curves.

χ^2 of the non-rejected values is a continuous function and as 10000 iterations are taken, even with an rejection rate of 90% enough parameter sets are calculated to get this continuous representation of χ^2 (also of small χ^2 's). Also within the non-rejected parameter sets there are enough parameter sets with $\chi^2 < 10$. This does not hold for most I light curves, as for the I band the χ^2 distribution can be very broad as, as explained above, the minima of the χ^2 hypersurface are broad and numerous. The distribution of best χ^2 can be used as a measurement of reliability of the fit parameters. But as already stressed above, this doesn't mean that the fit itself was not reliable. The value of χ^2 also depends on the number of observations, therefore a small χ^2 can be the result of a strong determination of the fit because there are not many more observations than fit parameters.

To test the dependence of the fit on the number and distribution of data points artificial light curves were constructed. The fitted light curves of the B and I band of SN 1992bc were chosen as examples of light curves with and without a secondary bump. From these light curves 8, 16, 32, 64, 128, and 256 epochs have been chosen uniformly distributed within –10 and 92.3 days of B maximum. Normal distributed noise with $\sigma = 0.05$ mag has been added to the brightness and these newly-created data pairs are again fit with the fitting routine. This has been done for a sample of 10 light curves for each sampling of epochs given above. The variations in the fit parameters and derived parameters depending on the number of epochs show where the problem in the fitting method is posed. For the small number of 8 epochs randomly spaced in the range of more than 100 days the light curves can not be

reproduced. The fit parameters f_0 and γ , which enter the fit linearly, give approximately the same results from 32 datapoints upwards, whereas the fit parameters with non-linear dependence require more datapoints. The derived parameters, t_{\max} , m_{\max} , Δm_{15} show a fast convergence with number. But for example the Gaussians, which are described by 3 parameters, have to be determined by at least as many observations as parameters in the relevant time interval. This is not the case for only 16 datapoints (if they are spread over the whole interval of 100 days as calculated here). In practice there will be more observations around peak than in these calculations, where the late slope, which could be determined from 2 observations is overdetermined. The rise of the light curve is underdetermined in the majority of cases. This makes the fit parameters τ and θ and t_{rise} varying much from representation to representation. The tests described here have not been extensive enough to make quantitative statements about the fitting method in general, but in the next section the derivation of errors will be given for the fitting parameters as well as for the derived parameters.

4.2 Error Estimates with Monte Carlo Techniques

The fitting procedure provides an estimate of the goodness of fit, as well as the associated uncertainties on the fit parameters. Uncertainties on the derived quantities depend strongly on the quality and number of data points. If there are no data before 5 days prior to maximum, e.g., the rise time cannot be determined reliably.

The uncertainties of the derived parameters have been estimated using a Monte Carlo method (see Press et al. 1992). Synthetic data sets have been constructed with the same temporal sampling as the observed light curve. The magnitude at each point was computed from the best fit model, with the assumption of a Gaussian probability distribution whose width was given by the observational uncertainty. The standard deviations of the observed data points range from 0.03 to 0.14 magnitudes. In this manner, 1000 synthetic data sets were simulated. Each synthetic data set was fit and the frequency distribution for each model parameter was constructed. Two examples of the resulting distributions (the time of B maximum t_{\max} and the B magnitude at maximum m_{\max} for SN 1992bc) are shown as histograms in Figure 4.3. The value of the best fit and the mean of the distribution are displayed as vertical dotted and solid lines respectively. The differences between the mean and the best fit is less than 0.015 days for the time of maximum and less than 0.001 magnitudes for the peak brightness. In this example the skewness and kurtosis are negligible. Non-zero values of skewness and kurtosis provide an indication of the unreliability of the derived fit parameters (see e.g. Figure 4.6). The uncertainties for the light curve parameters given by the Monte Carlo simulations are shown in Table A.2.

Occasionally the standard deviations obtained for a fit parameter from the fitting procedure differed significantly from the values obtained from the Monte Carlo simulations. This arises because the standard deviations derived from the fit are calculated from the diagonal elements of the curvature matrix, while the standard deviations derived from the Monte Carlo simulations result from actual frequency distributions. Both standard deviations should be the same for a perfect light curve, i.e. well sampled data, where the brightness differs from the analytical shape of the light curve by only a small error. The code has been confirmed with this test (using artificial data points, which have been created from a set of fit parameters, equally spaced, enough of them (200), deviating only with a stan-

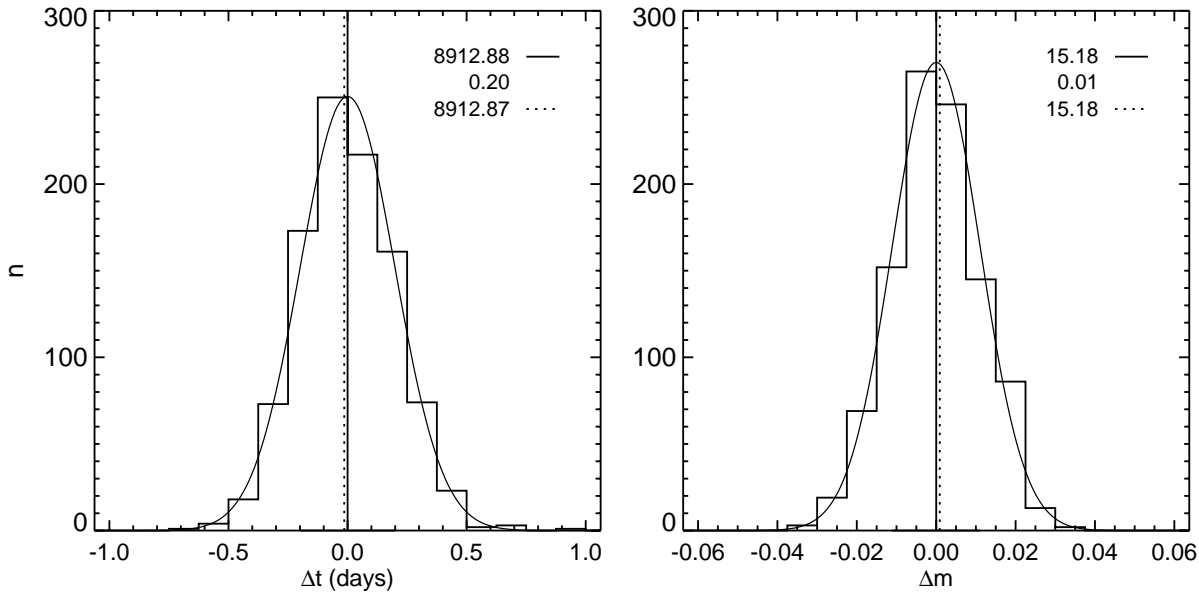


Figure 4.3: The distribution of the time of B maximum t_{\max} and the B magnitude at maximum m_{\max} for SN 1992bc as calculated from Monte Carlo simulations of 1000 synthetic data sets as described in the text. The standard deviation of the distribution together with the mean of the distribution (upper two values) and the value of the best fit (lower values) for the two derived parameters (vertical solid and dotted lines) are given in the upper right part of the plots. For comparison the plot shows also a Gaussian distribution with the same mean and standard deviation.

dard deviation of 0.001 from an analytical curve). In Figure 4.4 the distributions of the 10 fit parameters and of t_{\max} and m_{\max} , the time and magnitude at maximum light, are shown (histograms) together with the mean of the distribution (solid vertical line) and the input value (dotted). For comparison with a Gaussian distribution the normal distribution with the same mean and standard deviation is drawn. The mean of the distribution does not deviate significantly from the input value and the standard deviation of the distribution is very small in all cases.

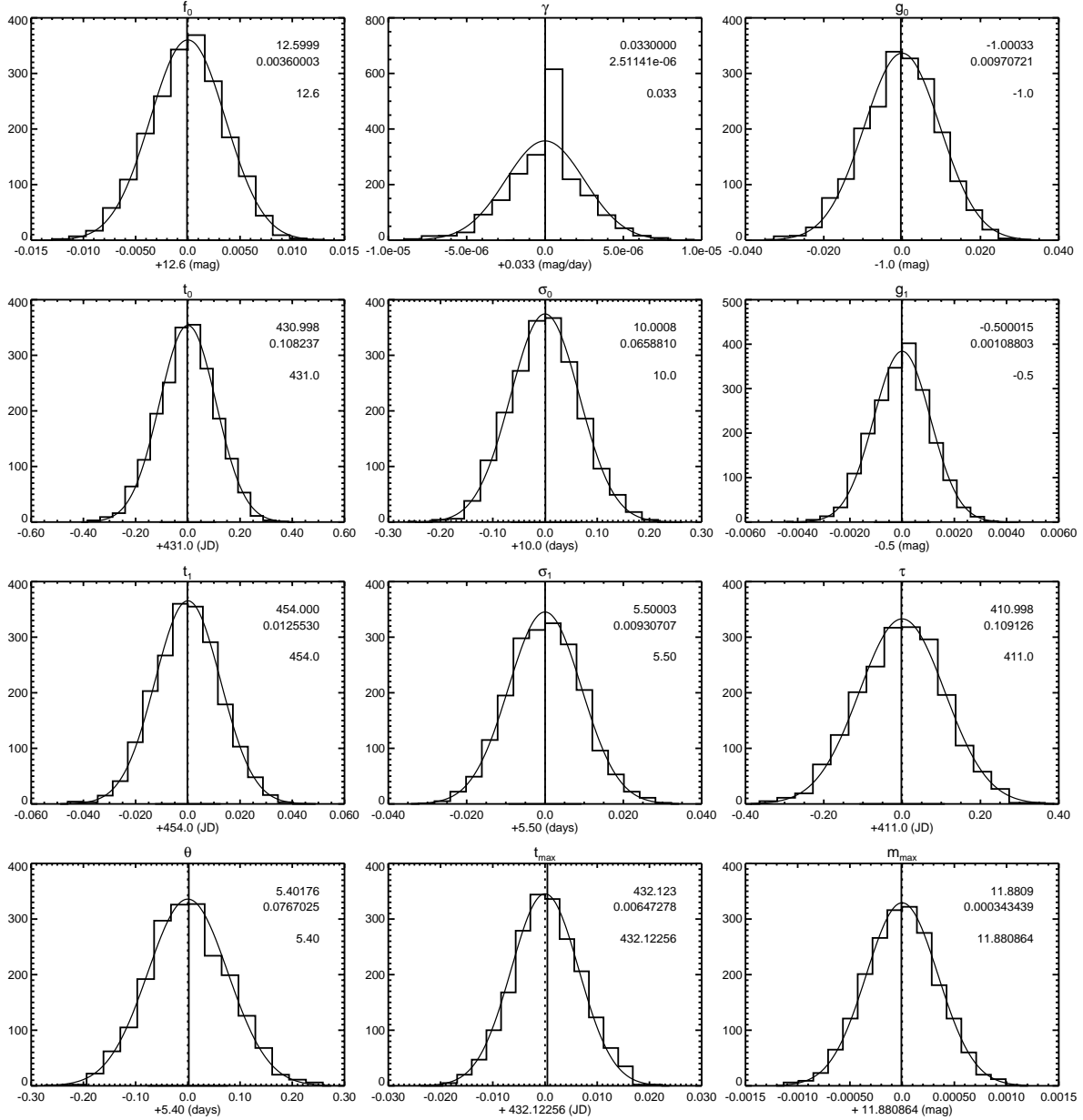


Figure 4.4: Distribution (histograms) of the 10 fit parameters and of t_{\max} and m_{\max} as calculated with the Monte Carlo simulations as described in the text. The vertical lines denote the input value (dotted) or the mean (solid) of the distribution. The mean and the standard deviation are printed in the upper right corner of the plots. Lower value: the input value, upper values: the mean and the standard deviation calculated from the distribution. The solid line shows a Gaussian distribution with the same mean and standard deviation as the distribution. The histograms can be described as a Gaussian very well. The mean never deviates significantly from the input value and the standard deviations are small.

4.3 Epochs of Maxima

For all 27 SNe Ia whose light curves were well-sampled around the peak (SNe 1989B, 1990N, 1990af, 1991T, 1991bg, 1992A, 1992al, 1992bc, 1992bh, 1992bo, 1992bp, 1993H, 1993O, 1993ag, 1994D, 1994S, 1994ae, 1995D, 1995E, 1995ac, 1995al, 1995bd, 1996X, 1996bo, 1997br, 1998bu, 1998de see Table 3.1) the epochs of individual filter maxima (see Table 4.2) and of the bolometric luminosity (see Chapter 5) have been determined.

Table 4.2: Times of peak (in days) relative to the B maximum in the supernova light curves.

SN	$t_U - t_B$	$t_V - t_B$	$t_R - t_B$	$t_I - t_B$	$t_{\text{bol}} - t_B$
SN 1989B	-1.45	2.54	0.37	—	0.44
SN 1990N	-1.49	0.64	0.27	-1.96	-0.96
SN 1990af	—	1.21	—	—	—
SN 1991T	-2.24	2.75	2.05	-0.47	-0.08
SN 1991bg	—	2.24	2.52	2.69	1.39
SN 1992A	—	2.37	1.78	-1.02	0.74
SN 1992al	—	0.80	2.75	3.06	—
SN 1992bc	—	0.08	0.63	-2.78	-0.16
SN 1992bh	—	1.65	—	—	—
SN 1992bo	—	0.60	0.98	-2.50	0.06
SN 1992bp	—	1.29	—	—	—
SN 1993H	—	1.83	0.72	—	0.45
SN 1993O	—	2.74	—	1.21	0.41
SN 1993ag	—	1.46	—	—	0.74
SN 1994D	-0.59	0.16	-0.73	-3.28	-0.37
SN 1994S	—	1.13	—	—	—
SN 1994ae	—	0.18	1.03	-2.92	-0.07
SN 1995D	—	0.85	1.04	-2.17	0.09
SN 1995E	—	1.01	2.13	-1.37	0.46
SN 1995ac	—	2.59	3.42	0.17	0.74
SN 1995al	—	0.68	-0.69	-2.36	0.09
SN 1995bd	—	2.13	3.92	-0.43	1.11
SN 1996X	—	0.68	2.14	-2.49	0.19
SN 1996bo	—	1.62	1.03	-0.92	0.29
SN 1997br	—	4.25	1.83	—	—
SN 1998bu	-1.89	1.95	2.34	-2.29	-0.14
SN 1998de	—	1.71	2.44	5.10	1.18

A general trend can be observed in Figure 4.5, which presents the time of the filter maxima relative to the epoch of the maximum in B . The U band appears to rise faster than the B band, although the limited number of objects (5 supernovae) precludes any definitive statements. The V light curve clearly peaks some time after the B maximum for all observed SNe Ia. This behavior is more or less expected from models of an expanding cooling atmosphere (Arnett 1982), as indicated by the lines in Figure 4.5. However, the behavior of the R

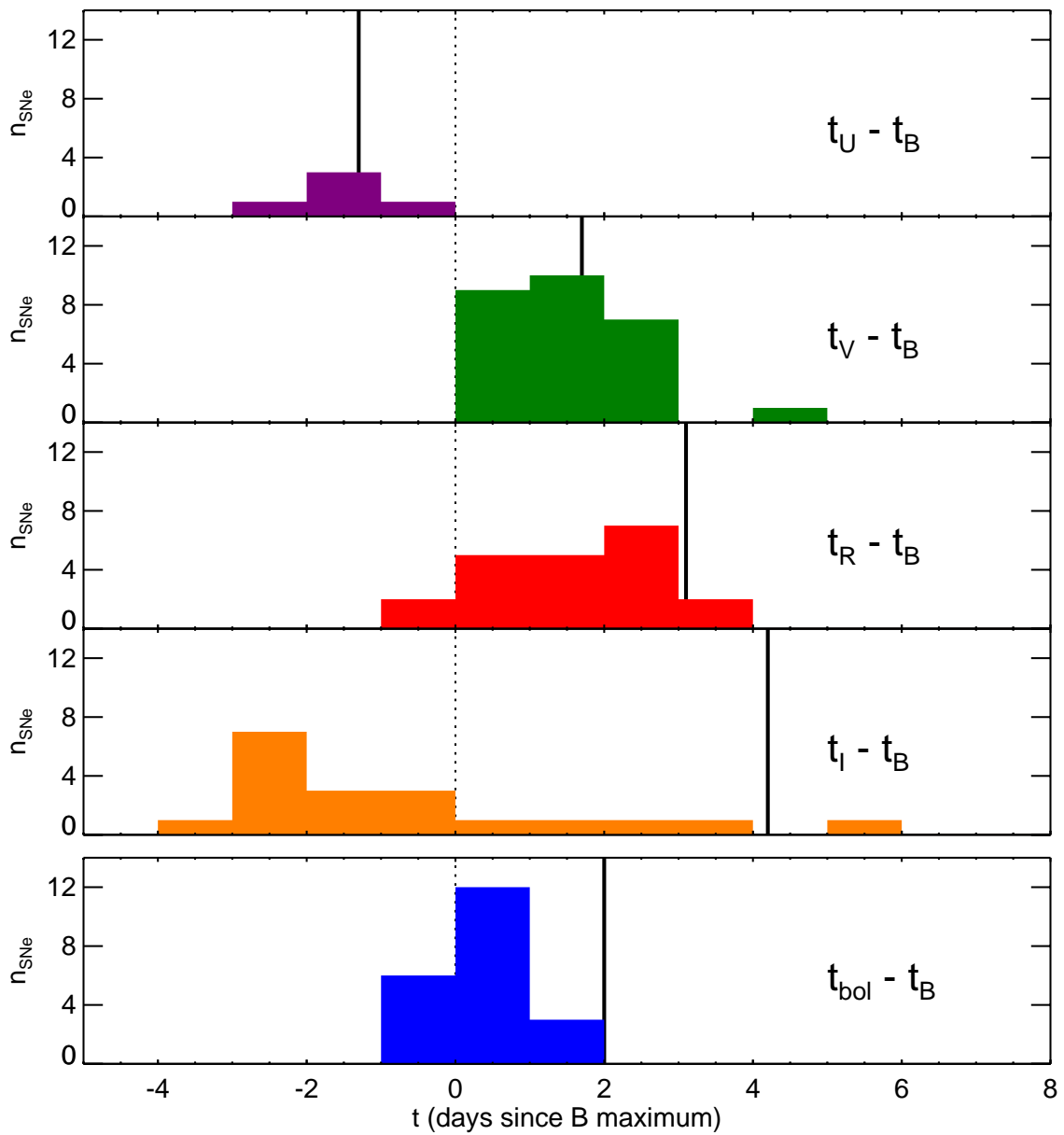


Figure 4.5: Histograms showing the times of the filter maxima from U to I and of the bolometric luminosity relative to the B maximum. The vertical lines show the time differences as expected for an expanding, adiabatic cooling sphere according to Arnett (1982).

and I band maxima does not agree with this simple model; for these bands, the light curve maxima are reached earlier than in a thermal model. The I histogram is very broad but for most objects the rise in I is clearly faster than in B . This trend is further continued in the JHK light curves which all peak before B (Elias et al. 1985; Leibundgut 1988; Meikle 2000; Meikle & Hernandez 2000). The early appearance of the peak in the infrared rules out the idea of an expanding, cooling sphere in the analyzed time range.

The SN with $t_V - t_B = 4.25$ is SN 1997br where there are no observations around maximum light for 6 days, making it difficult to determine the time and magnitude of the maximum. The calculated uncertainties nevertheless are small because the fit is determined by the amount of observations before and after peak.

The SN with $t_I - t_B = 5.10$ is SN 1998de which exhibits, like SN 1991bg, no secondary bump and is underluminous. Whereas for SN 1991bg the observations in B started after maximum, SN 1998de is well observed around maximum. Its I maximum is not only very late compared to B maximum, but also relative to V and R compared to SN 1991bg.

If the Spearman rank-order correlation coefficient (see e.g. Press et al. 1992, Chapter 14) for the epochs of maximum light is calculated, it can be seen, that earlier I and R maximum means later U maximum (only 4 SNe). The times of maximum in I and R as well as in I and V show a correlation (with the correlation coefficient being 0.75 at a high significance). So do the times of maximum in the bolometric and I light curve, whereas there is no correlation between the other bands.

4.4 Rise Times

As the high redshift data of SNe Ia have given evidence for an accelerating universe (Riess et al. 1998; Perlmutter et al. 1999) the calibrated standard candles have to be tested thoroughly, because evolution (if combined with a change in the peak luminosity of SNe Ia) might account for the observed faintness of high redshift SNe. One light curve parameter which is examined to check for systematic effects is the rise time, i.e. the time between explosion and maximum luminosity of the SN.

A first comparison of observations of nearby and high-z SNe (Riess et al. 1999a,b) has shown a 5.8σ difference between the rise times of the low redshift data and a preliminary analysis of high redshift data. The high redshift data have shorter rise times by 2.4 days. But a more thorough analysis of the data (Aldering et al. 2000) has shown, that the discrepancy with the low redshift rise times is about 2σ or less. The first analysis underestimated the uncertainties in both the low and high redshift sample. But even if the rise times at high and low redshift differ, this not necessarily implies a difference in peak magnitude, because the light curves of the SNe may differ only in the first few days after the explosion, if the conditions vary only near the outer part of the exploding white dwarf.

In the analysis of Riess et al. (1999b) the rise time was calculated in fitting a t^2 model (with t_r denoting the rise time and a scale factor α) to the premaximum part of the light curve:

$$L = \alpha(t + t_r)^2. \quad (4.2)$$

Shortly after explosion a SN Ia can be theoretically represented as an expanding fireball. A t^2 model can be justified under the conditions of uniform expansion and constant effective temperature from simple physics (see also Arnett 1982).

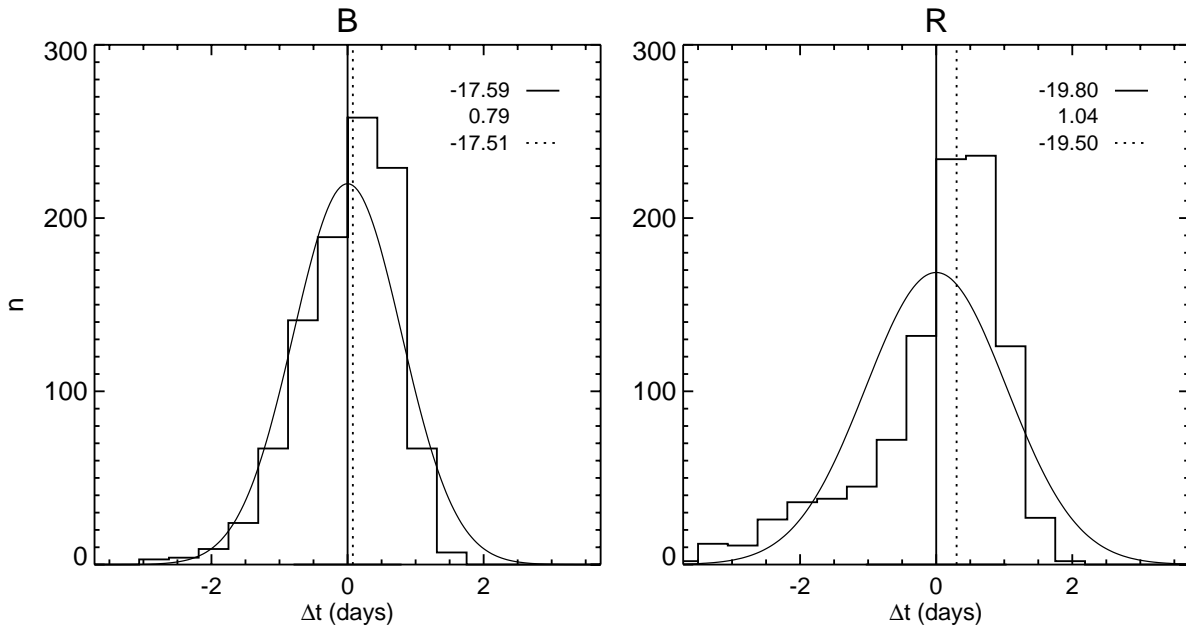


Figure 4.6: The distribution of the rise time parameter in B and R for SN 1994D as calculated from Monte Carlo simulations of 1000 synthetic data sets as described in Section 4.2.

Our approach to derive the rise time is different. With the method described above the rise time is defined as the time it takes for the SN to increase the magnitude from 30 mag below maximum to maximum brightness (this rise corresponds to the typical increase in luminosity from a white dwarf to a SN). As the rise of the SN light curve is fitted with an exponential function and as already described in Section 4.1 problems in fitting the too steep late decline together with the non availability of early light curve data makes the uncertainty of the rise time quite large. The exponential function also has to make the maximum non-symmetric. This behaviour can be seen in Figure 4.6 where the distribution of the rise time in B and R for SN 1994D as calculated from Monte Carlo simulations (see Section 4.2) are displayed as histograms. A Gaussian distribution with the same mean and standard deviation is plotted for comparison. Whereas the distribution of the B band rise time is quite narrow and symmetric, the distribution of the R band rise time is asymmetric. The late decline in the R band is much steeper than in B , which results in a stronger influence of the post-maximum data on the pre-maximum rise. Therefore the rise times calculated with the model described in this work are only reliable for a few SNe, where there are early pre-maximum observations and the post-maximum evolution does not require the exponentially rising function to adjust because of the fit past maximum.

The comparison of different derivations of the rise time of a Type Ia supernova is shown in Figure 4.7. The chosen example is the B light curve of SN 1994D. The diamonds are the data from Richmond et al. (1995), which were used for the determination of the rise time with the method described in Section 4.1 (solid line). The squares show the data Riess et al. (1999b) use for their estimation of the rise time. Doing the fit as they describe results in the dotted line. Including the Richmond et al. (1995) data till day -6 (asterisks) gives the dashed

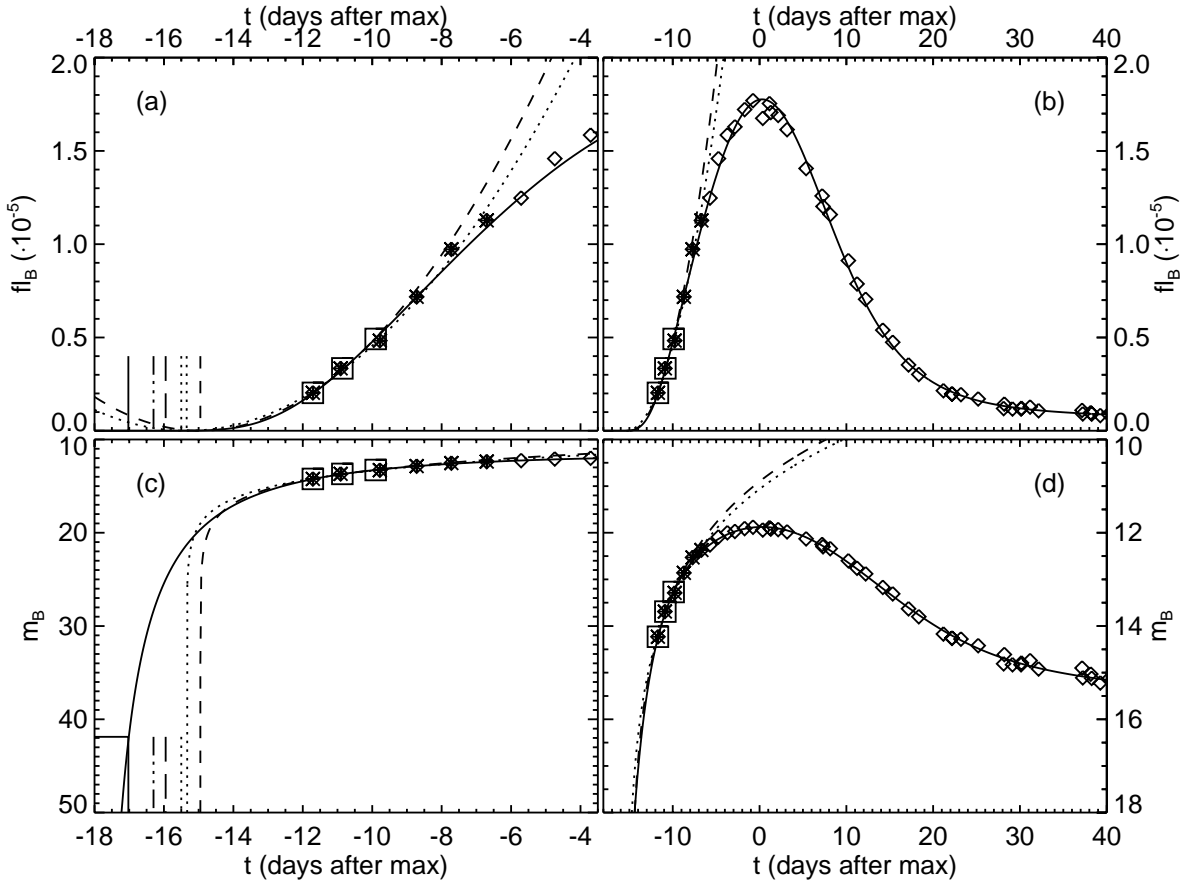


Figure 4.7: Comparison of different derivations of the B band rise time of the Type Ia supernova 1994D. The diamonds are the data from Richmond et al. (1995), which have been used for the determination of the rise time with the method described in Section 4.1 (solid line). The squares show the data Riess et al. (1999b) use for their estimation of the rise time. Doing the fit as they describe results in the dotted line. Including the Richmond et al. (1995) data till day -6 (asterisks) gives the dashed line. The quoted results of Riess et al. (1999b) are shown as vertical lines and are described in the text. (a) and (b) The premaximum rise and the light curve till day 40 is shown in flux units. (c) and (d) The light curve and fits in magnitudes. See detailed explanation in text.

line. The light curve is shown in flux units (upper row) and magnitudes (lower row). The differences in the two t^2 -fits clearly can be seen in (a) and (b). Including three more data points shifts the rise time by 0.4 days. The differences in the methods to derive the rise times can be seen best in units of magnitude (c). The t^2 -fits are approaching zero level flux at the rise time, whereas the exponential fit for the pre-maximum rise is rising much slower. As already mentioned above, the fit to the pre-maximum rise with the method described in this work is also affected by the post-maximum fit because the exponential rise also has to dim the exponential decline, if the slope is too steep. The definition of the rise time as the time it takes for the SN to increase the magnitude from 30 mag below maximum to maximum

Table 4.3: Comparison of rise times calculated with different methods: The rows labelled t^2 give the values calculated from the tables in Riess et al. (1999b), those labelled with “exp” were calculated with the model described in Section 4.1.

	SN 1990N		SN 1994D	
	B	V	B	V
t^2 MLCS	-22.06	-23.56	-16.30	-18.02
t^2 decline	-20.28	—	-15.95	—
t^2 direct	-21.4	—	-15.5	—
exp. fit	-18.59	-24.75	-17.31	-20.75
exp. fit including unfiltered data	-25.86	-28.51	—	—

brightness is shown as solid box in the lower left corner. For the t^2 -fit incorporating the data till day -6 extends the rise time by 0.4 days, which gets closer to the quoted results in Riess et al. (1999b). The vertical dotted line is the rise time they get for the direct fit to Equation 4.2, the long dashed and the dashed dotted vertical lines denote the rise times calculated from the fits in Riess et al. (1999b) with the decline rate and the multicolor light curve shape (MLCS) methods respectively. For the range of 6 magnitudes below maximum light (d) the differences in the methods are still small.

The two SNe both included in our sample and in Riess et al. (1999b), are SN 1990N and SN 1994D. In Table 4.3 the rise times of the B and V light curves of the SNe 1990N and 1994D are given. The rows labelled t^2 give the values calculated from the tables in Riess et al. (1999b) either using the MLCS or decline rate parameters or the direct fit they quote in their discussion section. Comparing these numbers to the rise times we get for the exponential fit (rows 4 and 5) it can be seen, that the rise time of SN 1990N is several days longer for the exponential fit, if the unfiltered observations published in Riess et al. (1999b) are included. If they are not included, the light curve fit for SN 1990N is steeper leading to a shorter rise time. As already shown in Figure 4.7 the exponential fit to the light curve of SN 1994D is slower than the t^2 fit; the rise times are about 1 day longer.

This comparison together with Figure 4.7 has shown the problems of determining the rise time with the analytical fit. Especially if the post-maximum decline requires the exponential rise to dim the light curve, the rise often is too slow, leading to an overestimation of the rise time.

Chapter 5

Bolometric Light Curves

5.1 Method and Uncertainties

The flux emitted by a SN Ia in the **UV**, **optical**, and **IR** wavelength range, the so-called “UVOIR bolometric flux”, traces the radiation converted from the radioactive decays of newly synthesized isotopes. As nearly 80% of the bolometric luminosity of a typical SN Ia is emitted in the range from 3000 to 10000 Å (Suntzeff 1996), the integrated flux in the *UBVRI* pass bands provides a reliable measure of the bolometric luminosity and therefore represents a physically meaningful quantity. This luminosity depends directly on the amount of nickel produced in the explosion, the energy deposition, and the γ -ray escape, but not on the exact wavelengths of the emitted photons.

The fits of the filter light curves in the *UBVRI* pass bands have been used to construct an optical bolometric light curve for the SNe in the sample of Table 3.1. For the analysis all objects with well-sampled light curves at least in three pass bands have been included. To calculate the absolute bolometric luminosities, one has to account for reddening and distance moduli; the adopted values were taken from the literature as described in Chapter 3 and listed in Table 3.1. A galactic extinction law has been employed, as justified by Riess et al. (1996a).

To calculate the total flux in the UVOIR region of the spectrum, the observed magnitude in every single pass band is converted to its corresponding flux at the effective wavelength. These fluxes are multiplied by the bandwidth of the filter and summed up to get the total flux. As there are gaps and overlaps between the filters, the flux had to be corrected for. Missing pass bands have been corrected afterwards (see Section 5.1.1) and no interpolation for missing pass bands has been used for the calculation of the bolometric flux.

The bolometric light curves of a subset of the SNe Ia are shown in Figure 5.1. Only the time range with all available filter photometry is plotted. The peak luminosities are clearly different for the objects in the sample, and these differences are larger than the uncertainties in the derivation. The most striking feature, however, is the varying strength of the secondary shoulder, which stems from the *R* and *I* light curves (see also Suntzeff (1996); for the detailed discussion of the shape of the bolometric light curves see Section 5.2).

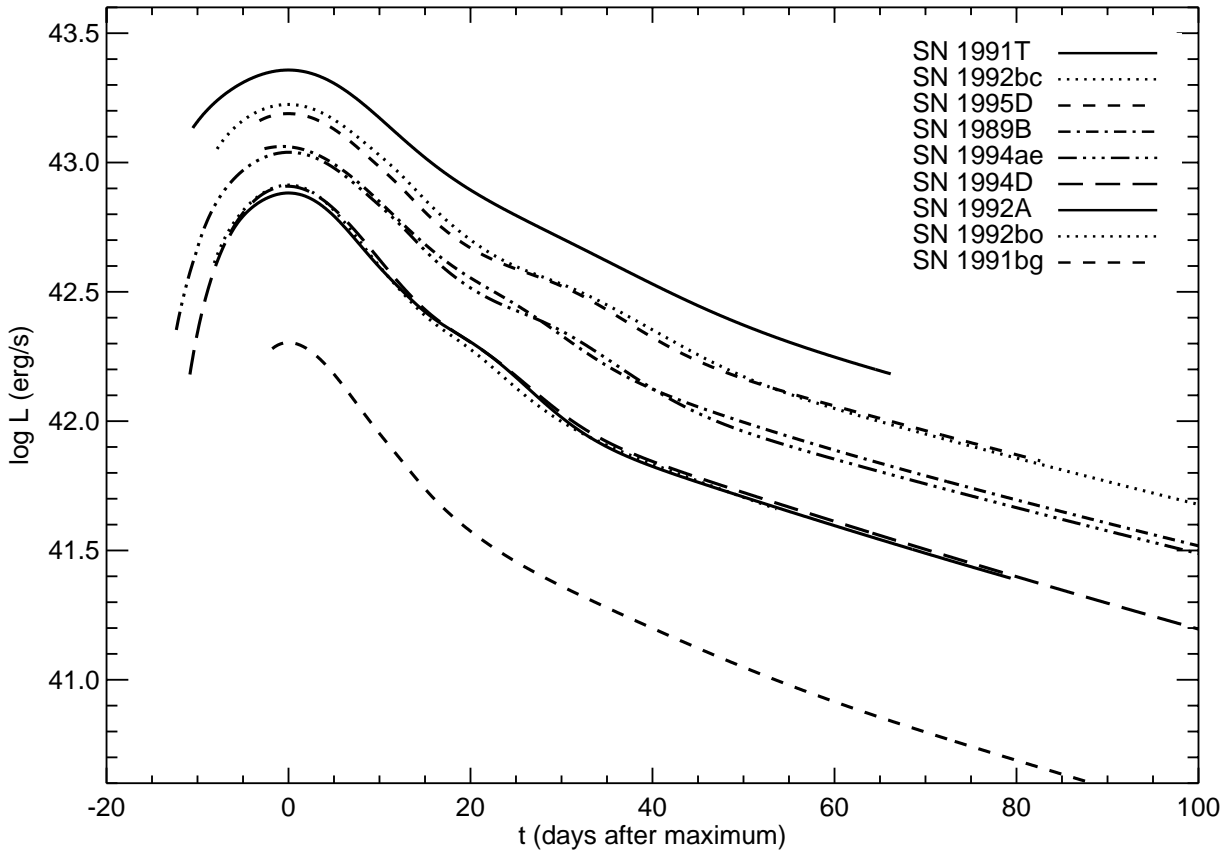


Figure 5.1: Bolometric light curves for some well observed SNe. Only the time range with the maximum number of filters for each supernova is displayed. The reddening and distance moduli have been taken from the literature as listed in Table 3.1 and corrections for missing *U* band are applied as described in Section 5.1.1.

5.1.1 Correction for Missing Pass Bands

Flux outside *UBVRI*:

In this analysis any flux outside the optical wavelength range has been neglected. In particular, contributions to the bolometric flux from the ultraviolet (below 3200 Å) and the infrared above 1 μm (*JHK*) regimes should be considered in the calculations of the bolometric flux. Using HST and IUE spectrophotometry for SN 1990N and SN 1992A, Suntzeff (1996) estimated the fraction of bolometric luminosity emitted in the UV. He found that the bolometric light curve is dominated by the optical flux; the flux in the UV below the optical window drops well below 10% before maximum. The *JHK* evolution was assumed to be similar to that presented by Elias et al. (1985); these pass bands add at most 10% at early times and no more than about 15% 80 days after maximum, but around 25% at the time of the secondary maximum in the IR. For example, examination of the data of SNe 1980N and 1981D (infrared data from Elias et al. (1981) and optical from Hamuy et al. (1991)) shows that not more than 6% of the total flux is emitted beyond *I* until 50 days past maximum, when the IR data stop.

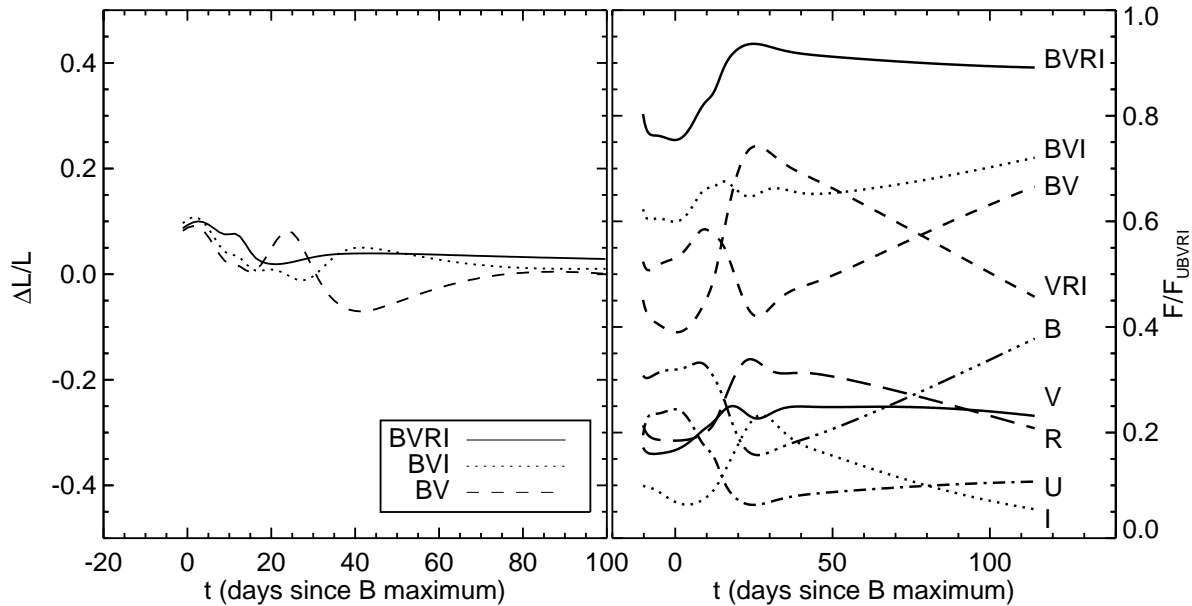


Figure 5.2: Left: Residuals for substituting individual pass band observations of SN 1989B by the corrections derived from SN 1994D. The errors never exceed 10% even when more than one filter is missing. Right: Correction factors for missing pass bands. The correction factors are obtained by comparing the flux in the pass bands with the total $UBVRI$ -flux.

In this work there is no correction applied for the flux outside $UBVRI$ unless stated explicitly (see Section 5.3 and Section 5.1.4).

Corrections for pass bands missing in the optical range

For missing pass bands between U and I one can infer corrections derived from those SNe Ia which have observations in all filters. Fig. 5.2 shows the correction factors obtained from SN 1994D. A cautionary note is appropriate here: SN 1994D displayed some unusual features, in particular a very blue color at maximum. To estimate the flux corrections the flux in each pass band was divided by the bolometric flux. Since the filter transmission curves do not continuously cover the spectrum (i.e., there are gaps between U and B as well as between B and V and overlaps between V and R , and R and I) the coaddition suffers from the interpolation between these pass bands.

An interesting result from Figure 5.2 is the nearly constant bolometric correction for the V filter. This filter has been used in the past as a surrogate for bolometric light curves (e.g. Cappellaro et al. 1997). The validity of this assumption is confirmed for phases between 30 and 110 days after B maximum where the overall variation is less than 3%.

In order to test the procedure, bolometric light curves for SNe Ia (SNe 1989B, 1990N, 1991T), which have the full wavelength coverage, have been calculated after purposely omitting one or more pass bands and applying the correction factors derived from SN 1994D. As Figure 5.2 demonstrates for SN 1989B, the error is less than 10% at all times even if more than one filter is missing, although the errors vary considerably during the peak and the secondary shoulder phases. These results give confidence that the bolometric light curves of

the SNe with missing U band can be corrected without incurring large errors.

5.1.2 Uncertainties

Effects of systematic differences in photometry sets on the bolometric light curves

Filter light curves from different observatories often show systematic differences of a few hundredths of a magnitude and up to more than 0.1 magnitude in the U band (Suntzeff et al. 1999). The blue cutoff of the U sensitivity function, for example, influences the transformation from the natural to the standard system. This has big effects for supernovae, which have nonstellar spectra. The effect such systematic errors might have on the bolometric light curves has been examined by artificially shifting individual filter light curves by 0.1 magnitudes and recomputing the bolometric light curves. In all cases the effect on the bolometric light curve is far less than the uncertainties in the distances and the extinction of the supernovae. Shifting the R or I light curve by 0.1 magnitude it was found that the bolometric luminosity changed by 2% at maximum and 5% 25 days later (approximately at second maximum). For typical systematic uncertainties of 0.03 magnitudes in all filters, a maximal error of 2 to 3% is incurred.

Also the bolometric light curve of SN 1994D was constructed for the individual data sets available (see references in Table 3.1). The difference never exceeds 4% out to 70 days after maximum even though the photometry in the individual filters differs up to 0.2 magnitudes in U , 0.1 mag in BRI and 0.05 mag in V .

Uncertainties introduced by external parameters

While uncertainties in the distance moduli will alter the absolute luminosities in each pass band (as well as the bolometric luminosity), the shape of the light curve is unaffected. As all distances used here are scaled to a Hubble constant of $H_0 = 65 \text{ km s}^{-1} \text{ Mpc}^{-1}$, the luminosity differences are influenced only by errors in the determination of the relative distance modulus.

Reddening, however, affects both the absolute luminosity and the light curve shape. The influence of extinction changes as a function of phase with the changing color of the supernova. A color excess of $E(B-V) = 0.05$ decreases the observed bolometric luminosity at $t = t_{\max}(\text{bol})$ by 15%, while near the time of the second maximum in the R and I light curves ($t = 20$ days) the observed bolometric luminosity is reduced by 12%. A stronger extinction of $E(B-V) = 0.35$ reduces the observed bolometric luminosity by 67% (56%) at $t = t_{\max}$ ($t = 20$ days).

The uncertainty in the reddening estimate introduces subtle additional effects. If $\delta E(B-V) = 0.02$ mag at low reddenings ($E(B-V) < 0.05$), an additional uncertainty of 5% in the bolometric luminosity is introduced. At higher reddening values ($E(B-V) = 0.3$), uncertainties of $\delta E(B-V) = 0.05$ and 0.10 produce changes of 15% and 31% in the bolometric luminosity, respectively.

The decline rate of the bolometric light curve decreases with increasing reddening due to the color evolution of the supernova and the selective absorption. For SN 1994D $\Delta m_{15}(\text{bol})$ would evolve linearly from 1.13 at hypothetical $E(B-V) = 0$ to 0.99 at $E(B-V) = 0.35$. The linearity breaks down at about $E(B-V) \approx 0.5$.

As described by Leibundgut (1988) the reddening depends on the intrinsic color of the observed object (Schmid-Kaler 1982). This implies that the color evolution influences the shape of the filter light curves (and not only the different proportions of the flux in the filters

and consequently the shape of the bolometric light curve). A typical color evolution of $B-V=0.7$ for SNe Ia in the first 15 days results in an increase of $\Delta m_{15}(B)$ by $0.2 \times E(B-V)$ simply due to the color dependence of the reddening. The increase of Δm_{15} for blue filters is larger than for the redder pass bands. This diminishes the effect of the color dependence on $\Delta m_{15}(\text{bol})$, which comes from the color evolution of the supernova and the selective absorption.

Uncertainties introduced by the method

The effect of fitting the light curves before constructing the bolometric light curves can be seen in Figure 5.3. The bolometric flux for SN 1992bc determined in this way is compared against the straight integration over the wavelengths of the filter observations. The symbols indicate the bolometric luminosity as calculated directly from the observations, asterisks for those epochs, when observations in 4 bands (*BVRI*) are available, squares for 3 bands (*BVR* or *BVI*), triangles for 2 bands (*BR* or *VR*) and diamonds for observations in one band only (*B* or *R*). The correction for missing bands is applied as described in Section 5.1.1. The dotted line is the bolometric luminosity calculated from the fits to the individual pass bands. The agreement between the two approaches is excellent and no differences can be observed. This also applies to the correction for the missing pass bands. Even when more than 2 pass bands are not observed, the corrected flux matches with the flux calculated from the fits.

Deviations can be found only for those parameters derived from the light curve, which extrapolate far from the observed epochs, e.g. the rise time.

The integration over wavelengths to calculate the bolometric light curve can be performed in different ways. A straight integration of the broad-band fluxes has to take into account the transmission of, and any overlaps and gaps between, filters. Several integration techniques have been tried, but it was found that for all interpolation methods, the bolometric flux has been reproduced to within 2% at any considered epoch. This has already been shown for SN 1987A by Suntzeff & Bouchet (1990). The chosen method in this work is to calculate the bolometric flux by summing the flux at the effective filter wavelength multiplied with the filter bandwidth.

5.1.3 Comparison with Spectra

To justify the applied procedure of constructing the bolometric light curves, the method has been tested by comparing the bolometric light curve with the flux calculated by the straight integration over the spectrum.

From the spectra of SNe 1990N (Leibundgut et al. 1991; Jeffery et al. 1992) and 1992A (Kirshner et al. 1993) the fluxes and magnitudes in the filter bands have been calculated. These magnitudes were then used to construct bolometric light curves with the method described above (see Section 5.1). Comparing the fluxes with those gained from direct integration over wavelength of the spectrum shows an accuracy of better than 10% for the spectra with good wavelength coverage from *U* to *I*. This gives us further confidence to use the method described above. The internal accuracy of the *UBVRI* flux can be very high, since the broad-band photometry is known to a few percent everywhere. However, the external accuracy is much lower than this due to the non-rectangular bandpasses of the filters and the non-stellar nature of the spectrum (Bouchet et al. 1991).

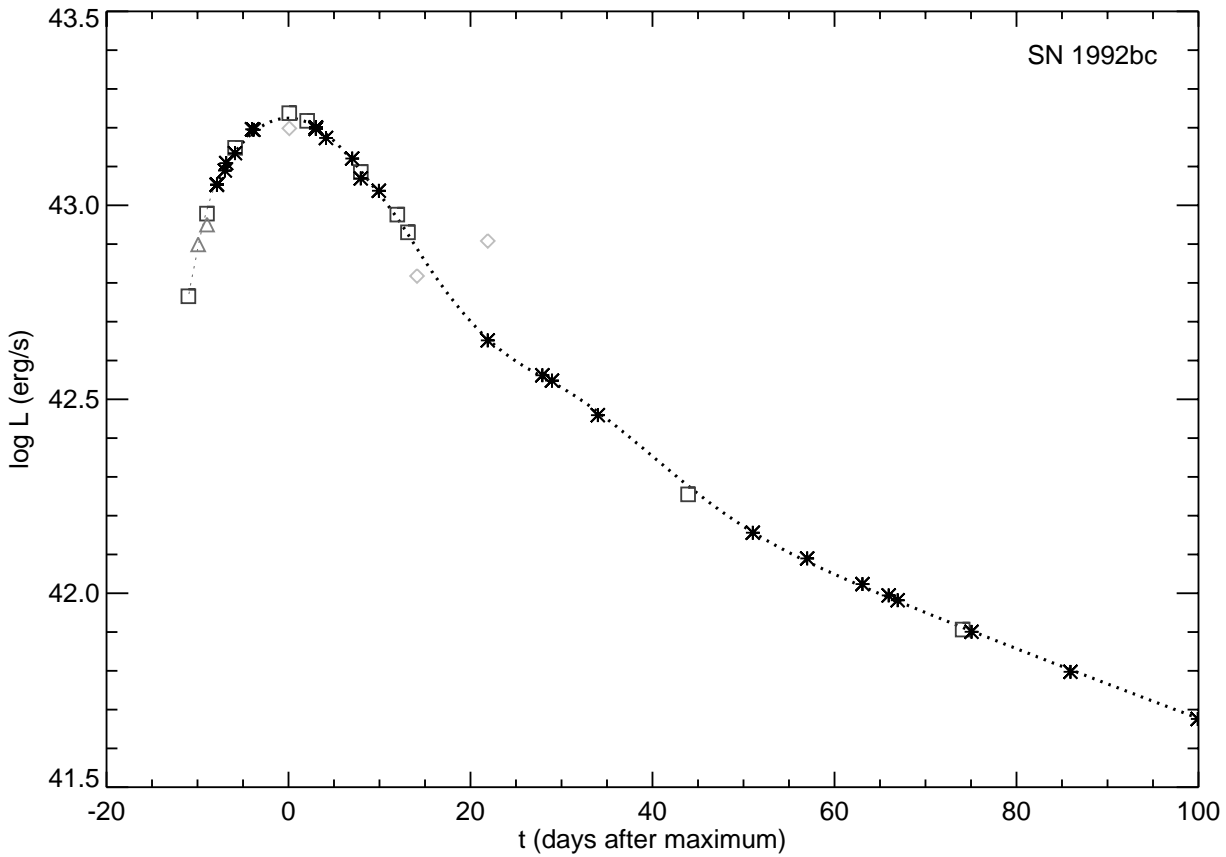


Figure 5.3: Constructing the bolometric light curves before and after fitting the filter light curves of SN 1992bc. The symbols indicate the bolometric luminosity as calculated directly from the observations, asterisks for those epochs, when observations in 4 bands are available, squares for 3 bands, triangles for 2 bands and diamonds for observations in one band only. The correction for missing bands is applied as described in Section 5.1.1. The dotted line is the bolometric luminosity calculated from the fits to the individual pass bands.

5.1.4 SN 1998bu and the Contribution of JHK to the Bolometric Light Curve

As for most SNe only *UBVRI* filter observations are available for the construction of the bolometric light curves, it is interesting to estimate the amount of flux which is missed in the infrared. Some SNe (1998bu, 1980N, 1981D) have excellent optical observations as well as infrared light curves (infrared data for SNe 1980N and 1981D from Elias et al. (1981, 1985) and optical from Hamuy et al. (1991), for SN 1998bu see Table 3.1).

SN 1998bu has been chosen to be shown here, because its IR light curve starts as early as 8.4 days before *B* maximum and has a fairly good coverage within the first season of observations in the IR as well as at optical wavelengths (see Figure 5.4). The observations of Hernandez et al. (2000), Jha et al. (1999), Suntzeff et al. (1999), and Munari et al. (1998) have been combined. For the distance modulus and reddening the values given in Table 3.1 have been adopted. In Figure 5.5 the *UBVRIJHK* light curve of SN 1998bu is plotted.

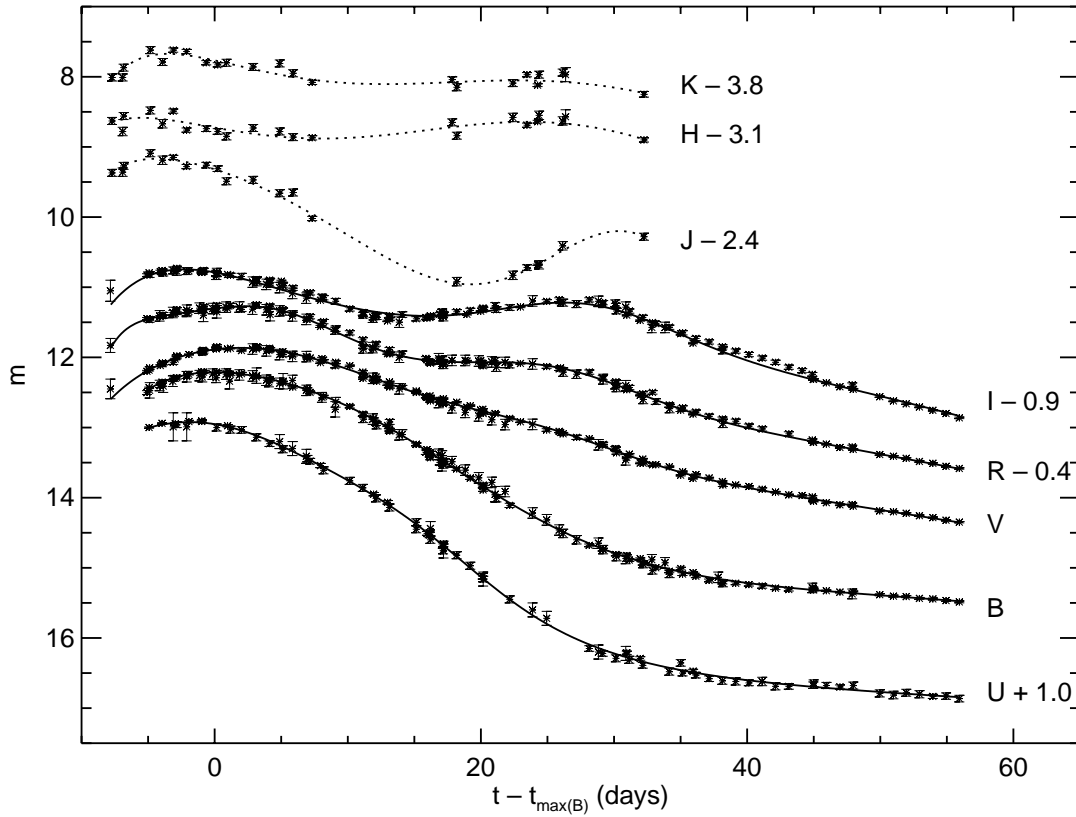


Figure 5.4: *UBVRJHK* light curves of SN 1998bu. The light curves have been shifted by the amount labelled. The solid lines show the fit of Equation 4.1 to the well sampled *UVRI* light curves. The fits to *JHK* suffer from the non availability of late time observations (dotted lines).

For the calculation of the bolometric light curve the light curves of the optical filters have been fitted with the method described in Chapter 4 to get a continuous representation of the observations also at the epochs of IR observations. The combination of optical and IR observations leads to the *UBVRJHK* light curve of SN 1998bu (crosses) and if those luminosities are fit, one gets the solid line for the *UBVRJHK* light curve. As the IR observations are sparsely sampled and stop after about 33 days past maximum, consequently the fit suffers from the non availability of the late decline. Also the secondary bump is not sampled till its end. Therefore the derived parameters of the *UBVRJHK* light curve have to be handled with care. Only the observations with full wavelength coverage have been taken into account. For comparison the *UVRI* light curve is shown as dotted line in Figure 5.5. The enhancement of the secondary bump and the shift of the time of maximum to about 0.5 days earlier caused by the inclusion of the IR data can be seen, too. The *JHK* light curves peak about 5 days earlier than in the *B* band (Hernandez et al. 2000). Although the contribution of the flux in the IR is not large around maximum light, it is enough to shift the time of maximum to earlier epochs.

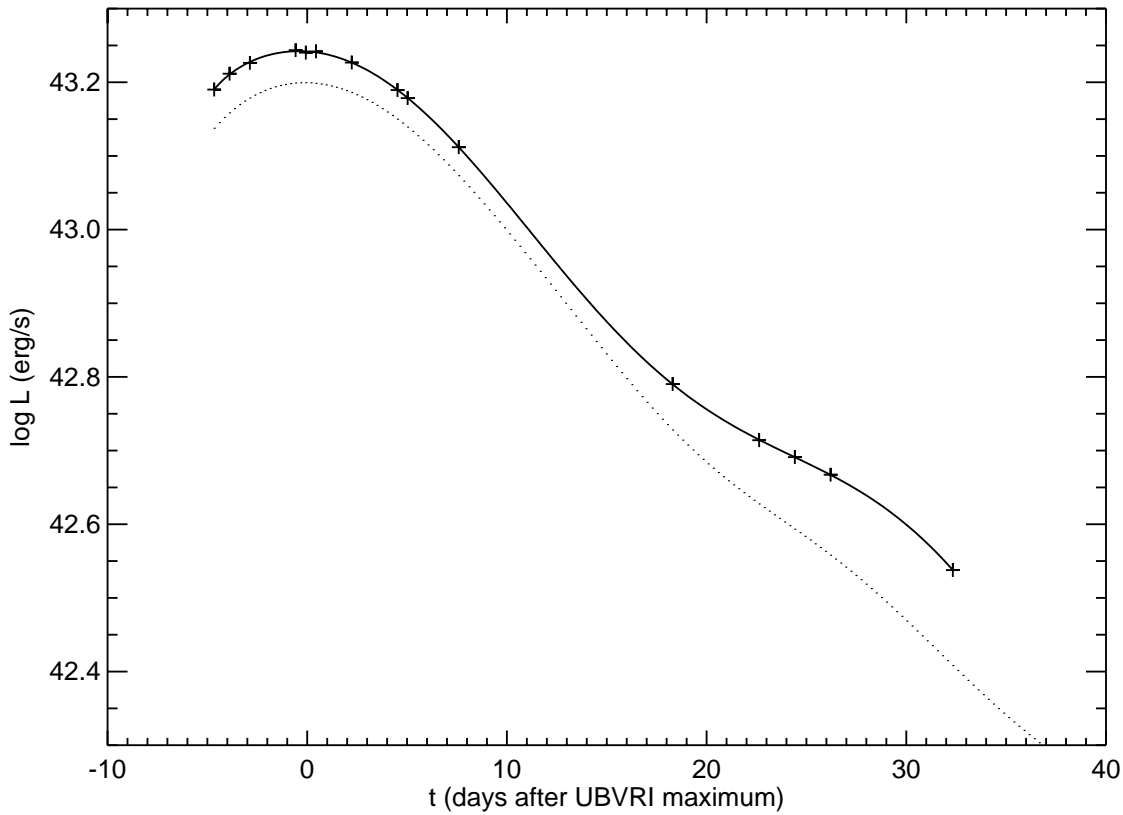


Figure 5.5: The $UBVRIJHK$ light curve of SN 1998bu (crosses) and fit (solid line) compared with the $UBVRI$ light curve (dotted). The enhancement of the secondary bump and the shift of the maximum to earlier times can be seen.

The contributions of the filter light curve to the total $UBVRIJHK$ -flux can be seen in Figure 5.6 (left panel), where the increase of the redder filters can be seen. In the right plot of Figure 5.6 the fraction of the $UBVRIJHK$ -flux which can be observed in $UBVRI$ is displayed. The triangles show the epochs of the IR observations and the dotted line is the fit to the $UBVRI$ luminosity divided by the $UBVRIJHK$ luminosity. The fraction of light in the infrared, which is missed because of limiting the integration to $UBVRI$, increases from about 10% around maximum to 25% 30 days after $UBVRI$ maximum, where the contribution of the longer wavelengths is biggest (see also Figure 5.2). This is in perfect concordance with the results of Section 5.1.1 where the JHK flux contribution of SNe 1980N and 1981D was estimated. With later data of SN 1998bu, which have been already observed but not yet published, the flux in the IR of SNe Ia can be determined. Only the high extinction which SN 1998bu suffers from is a major uncertainty in the determination of the flux distribution as well as of the bolometric light curve as described in Section 5.1.2.

One could estimate the flux in the IR from fitting a blackbody spectrum to the observed magnitudes in the optical wavelength range. The magnitude can be converted to the flux at the effective wavelength and then a blackbody spectrum is fitted. As spectra of SNe Ia

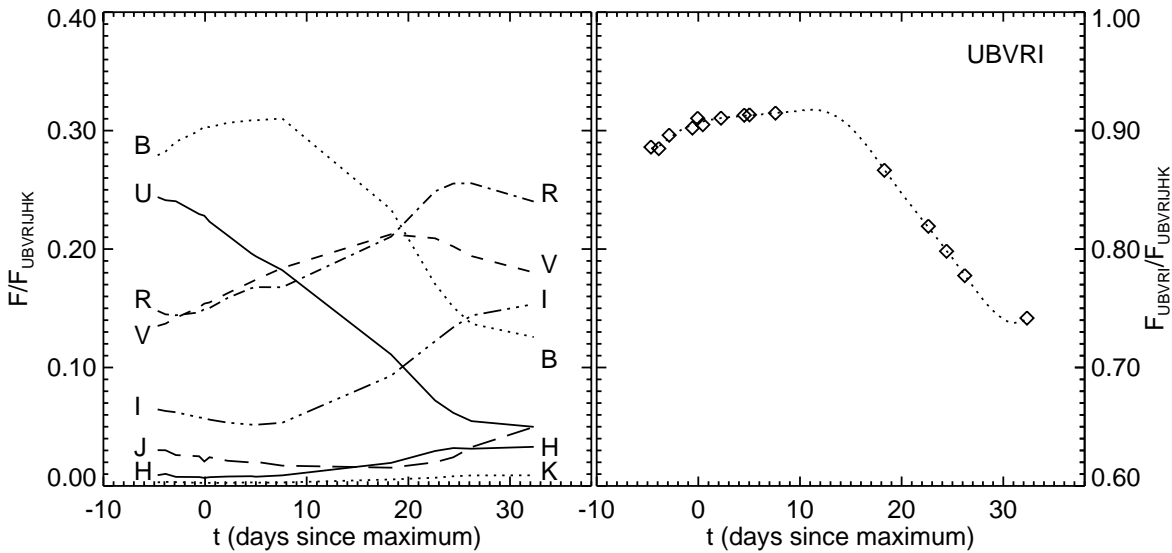


Figure 5.6: Left: Comparing the flux in the pass bands with the total $UBVRIJHK$ -flux. Right: Fraction of $UBVRJHK$ -flux observed in $UBVR$. The diamonds show the bolometric luminosities as calculated directly from the IR observations, the dotted line from the fits of the individual filter light curves.

can be hardly seen as blackbody spectra, this method is quite unpromising. For SN 1998bu there are JHK observations and the flux can be compared directly to the blackbody flux. Minimizing χ^2 in for optical wavelengths, the temperature of the blackbody is calculated. For high temperatures as before maximum, this approach leads to a reasonable estimation of the IR flux (about 15%), whereas at later times (around 30 days past maximum) the fit gets worse and the IR flux is estimated to be around 40% which is by far in excess of the 25% derived from the JHK magnitudes in the previous paragraph.

5.2 Shape of the Bolometric Light Curves

5.2.1 Peak Light Curve Shape

Inspection of Fig. 5.1 clearly shows the brighter SNe having wider primary peaks than the fainter SNe.

In order to quantify this statement the width of the bolometric light curve has been measured at half the peak luminosity (with $t_{-1/2}$ denoting the time it takes to rise and $t_{+1/2}$ to decline, see Tables 5.1 and A.2). For a descriptive illustration see Figure 2.3.

There are sufficient pre-maximum observations available for nine supernovae from which the full width of the peak can be reliably determined (SNe 1990N, 1991T, 1992A, 1992bc, 1992bo, 1994D, 1994ae, 1995bd, 1998de). In five cases the first observations were obtained below the half-maximum flux level; in the case of SN 1991T the bolometric light curve was extrapolated by about 1.5 days, for SN 1992A and SN 1992bc by about 2 days and for SN 1995bd by about 0.5 days. The bright SNe 1990N, 1991T, 1992bc and 1995bd show a peak width

Table 5.1: Parameters describing the light curve shape of the bolometric light curve: Width of the light curve at half the peak luminosity ($t_{-1/2}$ and $t_{+1/2}$), epoch of the maxima and the minimum of the first derivative (t_{\max}^{1std} , t_{\min}^{1std} and $t_{2\text{ndmax}}^{\text{1std}}$, see Section 5.2.2) and the secondary maximum in I ($t_{2\text{ndmax}}^I$) relative to bolometric maximum light.

SN	$t_{-1/2}$	$t_{+1/2}$	$t_{2\text{ndmax}}^I$	t_{\max}^{1std}	t_{\min}^{1std}	$t_{2\text{ndmax}}^{\text{1std}}$
(days relative to bolometric maximum)						
SN 1989B	—	12.6	—	9.8	—	—
SN 1990N	9.2	14.2	32.0	14.3	28.8	41.3
SN 1991T	11.6	13.7	22.2	11.3	28.5	35.7
SN 1991bg	—	8.9	—	8.8	—	—
SN 1992A	7.7	10.3	21.0	8.5	18.3	26.5
SN 1992bc	9.5	13.1	33.0	12.6	29.3	41.4
SN 1992bo	8.2	9.7	19.0	8.5	18.2	24.0
SN 1993H	—	10.0	15.5	9.1	—	—
SN 1993O	—	11.4	27.5	10.4	24.7	33.3
SN 1993ag	—	11.0	—	9.2	21.9	29.6
SN 1994D	7.9	10.3	21.4	9.0	20.3	27.0
SN 1994ae	9.3	12.7	29.2	11.8	26.3	37.4
SN 1995D	—	12.8	29.0	12.0	26.6	37.5
SN 1995E	—	12.3	26.3	11.8	24.4	32.1
SN 1995ac	—	13.8	25.3	13.2	25.6	34.2
SN 1995al	—	12.9	27.6	11.3	25.7	35.8
SN 1995bd	9.3	12.8	30.9	11.4	26.4	39.1
SN 1996X	—	11.3	24.7	10.5	22.4	30.5
SN 1996bo	—	11.5	24.0	10.4	21.4	29.8
SN 1998bu	—	13.0	26.3	12.4	23.8	31.8
SN 1998de	6.7	10.1	—	12.2	—	—

of 23 to 26 days, the intermediate SN 1994ae one of 22 days, while the fainter SN 1994D, SN 1992A, and SN 1992bo remained brighter than half their maximum luminosity for about 18 to 19 days and the subluminous SN 1998de only for about 17 days.

The pre-maximum rise $t_{-1/2}$ in the bolometric light curve is, in all cases, substantially faster than the decline $t_{+1/2}$ by between 20 to 30% or a time difference of between 1.5 to almost 5 days (Table 5.1).

The decline to half the supernova's peak luminosity $t_{+1/2}$ is available for 21 SNe (1989B, 1990N, 1991T, 1991bg, 1992A, 1992bc, 1992bo, 1993H, 1993O, 1993ag, 1994D, 1994ae, 1995D, 1995E, 1995ac, 1995al, 1995bd, 1996X, 1996bo, 1998bu, 1998de, see Table 5.1) and varies from 9 days to 14 days. A weak correlation between maximum brightness and half light width can be seen (Figure 5.7). For this analysis only SNe with sufficient coverage (rise: first observation not later than 3 days after $t_{\max} - t_{-1/2}$, decline: first observation before $t_{\max}(\text{bol})$) have been included. The half light time for the rise helps to characterize the rise to maximum light without extrapolating the light curve to epochs earlier than ever observed. As the rise to maximum is sensitive to the initial composition of the exploding white dwarf (Höflich et al. 1998) quantifying the rise part of the light curve is of importance for investigating

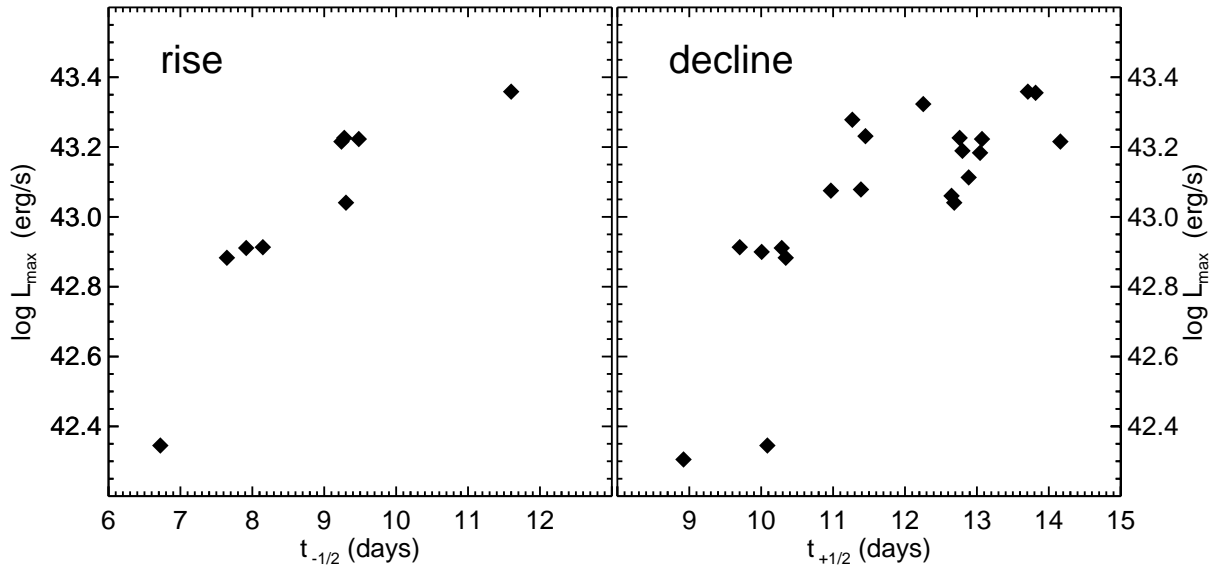


Figure 5.7: Rise to and decline from maximum in bolometric light curves. The time between maximum luminosity and half its value is plotted. Only SNe with sufficient coverage (rise: first observation not later than 3 days after $t_{\max} - t_{-1/2}$, decline: first observation before $t_{\max}(\text{bol})$) have been included.

possible environmental effects.

5.2.2 Secondary Bump

The second maximum which is observed in the R , I , and IR light curves still is visible as a deflection in the bolometric light curves (Suntzeff 1996). It is not possible in all cases to quantify this secondary bump with the parameters of the fitting function described in Chapter 4, because the fit parameters are not independent and even the pre-maximum exponential rise still can affect the light curve shape 20 to 40 days after maximum, especially in the R and I light curves as already mentioned in Section 4.1. This may result in damped or enhanced second Gaussians of Equation 4.1.

For that reason the first derivative of the fit is calculated:

$$\frac{dm}{dt} = \frac{\gamma - g_0(t - t_0) \exp\left[-\frac{(t-t_0)^2}{2\sigma_0^2}\right] \sigma_0^{-2} - g_1(t - t_1) \exp\left[-\frac{(t-t_1)^2}{2\sigma_1^2}\right] \sigma_1^{-2}}{\left[1 - \exp\left(\frac{\tau-t}{\theta}\right)\right]} - \frac{\left\{f_0 + \gamma(t - \sigma_0) + g_0 \exp\left[-\frac{(t-t_0)^2}{2\sigma_0^2}\right] + g_1 \exp\left[-\frac{(t-t_1)^2}{2\sigma_1^2}\right]\right\} \exp\left(\frac{\tau-t}{\theta}\right)}{\left[1 - \exp\left(\frac{\tau-t}{\theta}\right)\right]^2 \theta}. \quad (5.1)$$

Again the advantage of the model is that it is a continuous representation and a differentiable function. Almost all SNe with sufficient observational data show two maxima and one minimum in the first derivative (listed in Table 5.1).

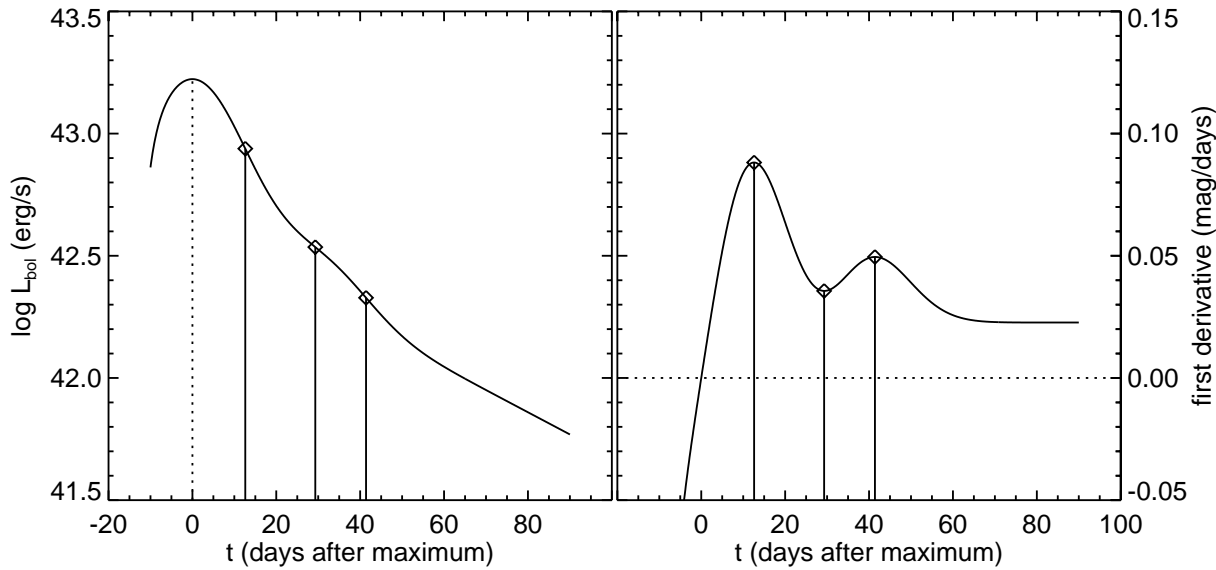


Figure 5.8: First derivative of the bolometric light curve function of SN 1992bc (Right) with the position of the minimum and maxima and the zero-crossing of the first derivative also shown in the bolometric light curve (Left). The vertical lines denote the epochs of the maxima and minima of the first derivative as well as of the light curve itself.

The first derivative of the bolometric light curve and the position of these maxima and of the minimum and the zero-crossing is shown in Figure 5.8 (Right) for SN 1992bc. The left panel shows the bolometric light curve for clarification, where the epochs of the minima and maxima of the first derivative are indicated as solid vertical lines just as the maximum is as a dotted line. After maximum light the slope of the light curve increases, reaches its maximum at 12.6 days (point of inflection¹) and gets flatter again, obtains its minimum value 29.3 days after maximum, getting steeper again with a second maximum slope at 41.4 days before finally settling down to a constant slope of about $0.025 \text{ mag day}^{-1}$ from 60 days on.

In Figure 5.9 the maxima and the minimum of the first derivative of the fit function are plotted versus the position of the secondary maximum in the I light curve (Left) and versus $t_{1/2}$ (Right). It shows that the second maximum in the I band is shortly after the minimum of the first derivative of the bolometric light curve (dotted line in Figure 5.9 (Left)). Also the maximum slope is reached within a few days after $t_{+1/2}$ (see Figure 5.9 (Right)).

Not in all cases the slope differs a lot in its extreme values, sometimes the minimum of the first derivative is very shallow with the slope at the second maximum being not much steeper. Therefore, the depth of the minimum is an indicator of the strength of the bump of the light curve. For example, the outlier in the left plot at $t_{2\text{ndmax}}^I = 23$ is SN 1991T which has a very weak secondary maximum in I . This also means, that the minimum of the first derivative is very shallow and thus uncertain. SN 1991T being an outlier has been tested by

¹Hamuy et al. (1996d) have calculated the inflection point for their template light curves in B . They found that it correlates with $\Delta m_{15}(B)$ as well as the bend of the light curve does with the time of the secondary maximum in I .

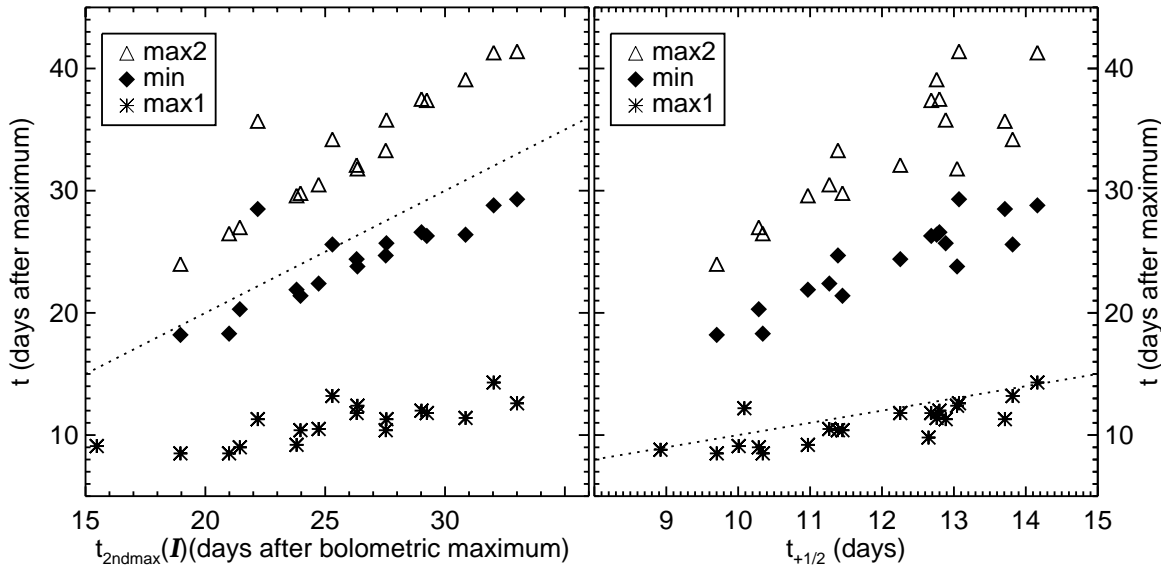


Figure 5.9: Left: Epochs of the maxima and the minimum of the first derivative of the bolometric light curve versus the position of the secondary maximum in the I light curve. Right: Epochs of the maxima and the minimum of the first derivative of the bolometric light curve versus $t_{+1/2}$. The dotted line indicates the time of the secondary maximum in the I and $t_{+1/2}$ respectively. The asterisks and triangles indicate the epochs of the maxima of the first derivative and the filled triangles the position of the minimum.

calculating the ratio of the difference between the first maximum and the minimum slope to the difference between the second maximum and the minimum slope:

$$s = \frac{\left| \frac{dm}{dt} \right|_{t_{\text{max}}^{\text{1stddev}}} - \left| \frac{dm}{dt} \right|_{t_{\text{min}}^{\text{1stddev}}} }{ \left| \frac{dm}{dt} \right|_{t_{\text{2ndmax}}^{\text{1stddev}}} - \left| \frac{dm}{dt} \right|_{t_{\text{min}}^{\text{1stddev}}} }.$$

Using this value to test, SN 1991T is more than 3σ away from the mean what clearly identifies it as an outlier.

As there is a correlation between $t_{1/2}$ and L_{max} (see Figure 5.7) it is not surprising that L_{max} and the epochs of the extrema of the first derivative are correlated, too. This is shown in Figure 5.10. The luminosity width relation also holds for the light curve shape at later times.

5.3 Derived Quantities from the Bolometric Light Curves

5.3.1 Radioactive Decay and γ -ray Escape

As already mentioned in Chapter 2, the deposited and in the optical wavelength range reradiated energy stems from the radioactive decay of ^{56}Ni synthesized in the explosion.

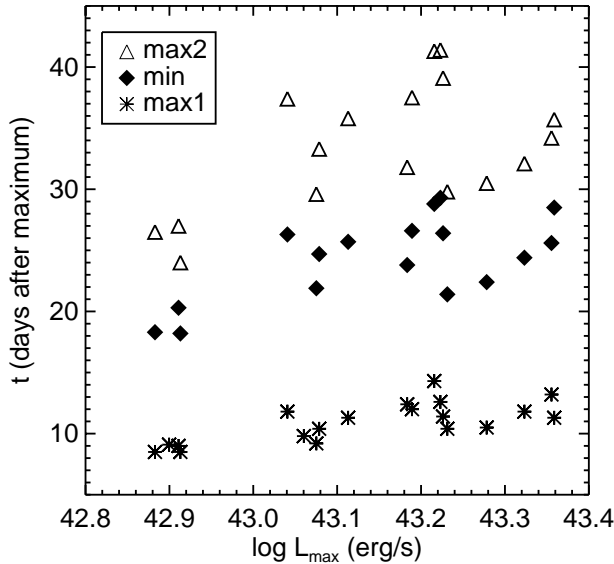


Figure 5.10: Epoch of the extrema of the first derivative of the bolometric light curve versus L_{\max} . The asterisks and triangles indicate the epochs of the maxima of the first derivative and the filled triangles the position of the minimum.

There is also observational evidence for the decay from ^{56}Ni to ^{56}Co to ^{56}Fe in SNe Ia (Kuchner et al. 1994), as the observed iron to cobalt flux ratio derived from spectral features evolves as expected when the $^{56}\text{Fe}/^{56}\text{Co}$ abundance ratio follows the ^{56}Ni to ^{56}Co to ^{56}Fe decay.

A compilation of the radioactive properties of ^{56}Ni and ^{56}Co can be found in Nadyozhin (1994). ^{56}Ni decays to ^{56}Co via electron capture with a half-life time of $T_{1/2} = 6.10$ days ($\lambda_{\text{Ni}} = \ln 2/T_{1/2} = 1/8.8$ days $^{-1}$) and a total energy emitted via gamma photons of $Q_{\text{Ni}\gamma} = 1.75$ MeV whereas $Q_{\text{Ni}\nu} = 0.41$ MeV is carried away by neutrinos. ^{56}Co transforms to the stable isotope ^{56}Fe with a half-life time of $T_{1/2} = 77.12$ days ($\lambda_{\text{Co}} = 1/111.3$ days $^{-1}$) in 81% via electron capture and in 19% via positron decay. The total energy emitted via gamma photons is $Q_{\text{Co}\gamma} = 3.61$ MeV, the total kinetic energy of the positrons is $Q_{\text{Co}e^+} = 0.12$ MeV and $Q_{\text{Co}\nu} = 0.84$ MeV are carried away by neutrinos.

As long as the energy input from ^{56}Ni decay plays a role, the optical depth for γ -rays is still very large, the ^{56}Ni γ -rays can not escape but thermalize. Also, for the epochs analyzed in this work, the positrons are completely trapped. At later times they can escape, depending on the geometry of magnetic fields (Ruiz-Lapuente & Spruit 1998; Milne et al. 1999). A fraction of $\exp(-\tau)$ γ -rays from the ^{56}Co decay can escape (Jeffery 2001), where τ is the mean of the effective γ -ray absorption opacity optical depth of the beam path, which is assumed to be location- and direction-independent in the optical thin limit with only one radioactive species.

This is summarized in the equation for the energy deposition of $N_{\text{Ni}0}$ ^{56}Ni atoms:

$$\begin{aligned} E_{\text{dep}} &= E_{\text{Ni}} + E_{\text{Co}e^+} + [1 - \exp(-\tau)] E_{\text{Co}\gamma} \\ &= \lambda_{\text{Ni}} N_{\text{Ni}0} \exp(-\lambda_{\text{Ni}} t) Q_{\text{Ni}\gamma} \\ &\quad + \lambda_{\text{Co}} N_{\text{Ni}0} \frac{\lambda_{\text{Ni}}}{\lambda_{\text{Ni}} - \lambda_{\text{Co}}} [\exp(-\lambda_{\text{Co}} t) - \exp(-\lambda_{\text{Ni}} t)] \{ Q_{\text{Co}e^+} + Q_{\text{Co}\gamma} [1 - \exp(-\tau)] \}. \end{aligned} \quad (5.2)$$

Figure 5.11 shows the energy deposition of the radioactive decay energy of a SN Ia with

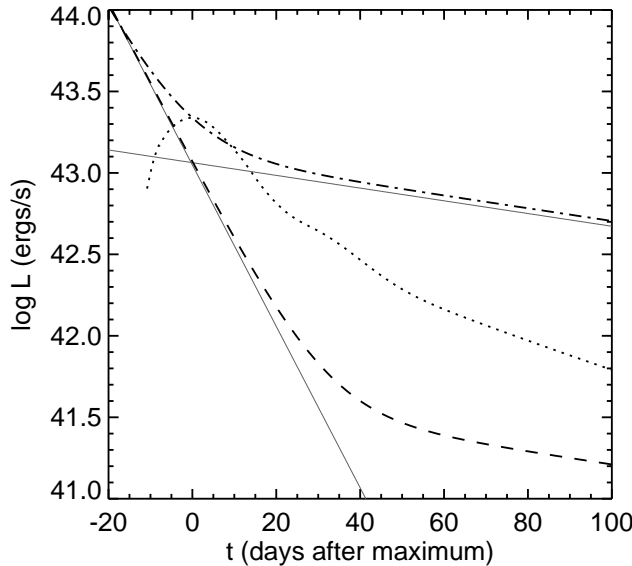


Figure 5.11: Radioactive decay and γ -ray deposition of a SN Ia with $1 M_{\odot}$ ^{56}Ni (light curve shape adopted from the bolometric light curve of SN 1992bc, shifted to a higher luminosity). A rise time of 17 days is assumed. The dashed-dotted line indicates the energy deposition with complete trapping of γ -rays and positrons, whereas the dashed line shows the energy deposition for γ -rays from the ^{56}Co decay escaping freely. The thin solid lines show the energy input from the ^{56}Ni and the ^{56}Co decay respectively.

$1 M_{\odot}$ ^{56}Ni (light curve shape adopted from the bolometric light curve of SN 1992bc, shifted to a higher luminosity). The dashed-dotted line indicates the energy deposition with complete trapping ($\tau = \infty$) of γ -rays and positrons, whereas the dashed line shows the energy deposition for γ -rays from the ^{56}Co decay escaping freely (the γ -rays from the ^{56}Ni decay and the positrons are completely trapped). The curve for complete trapping (dashed-dotted) approaches the energy input from the ^{56}Ni and the ^{56}Co decay respectively asymptotically (thin solid lines). In the case of free escape (dashed line) the line follows the ^{56}Ni decay longer because the only energy input from the ^{56}Co decay is from annihilating electron-positron pairs and the positron channel is taken only in 19% of the decays and, in addition, is less energetic.

5.3.2 Nickel Mass

Nickel mass derived from the bolometric luminosity at maximum light

Given the peak luminosity it is straight forward to derive the amount of ^{56}Ni , the so-called “nickel mass”, which powers the supernova emission. Arnett (1982) has shown, that the luminosity at peak was equal to the instantaneous energy deposition rate under the assumption of constant opacity both in space and time, a constant-density structure, and the requirement that the radial distribution of the energy deposition was identical to that of the thermal energy. Thus the luminosity at the maximum is directly related to the total amount of ^{56}Ni synthesized in the explosion (“Arnett’s law”: see Arnett 1982; Arnett et al. 1985; Pinto & Eastman 2000).

Pinto & Eastman (2000) have included more eigenmodes for the description of the shape of the energy density. The higher order modes describe variations of the energy density on smaller spatial scales. As these energy variations do not have far to go to diffuse out to smoother distributions, the power in these modes declines rapidly. If the energy depositon is uniform over the entire star, the higher order modes have to be taken into account, as

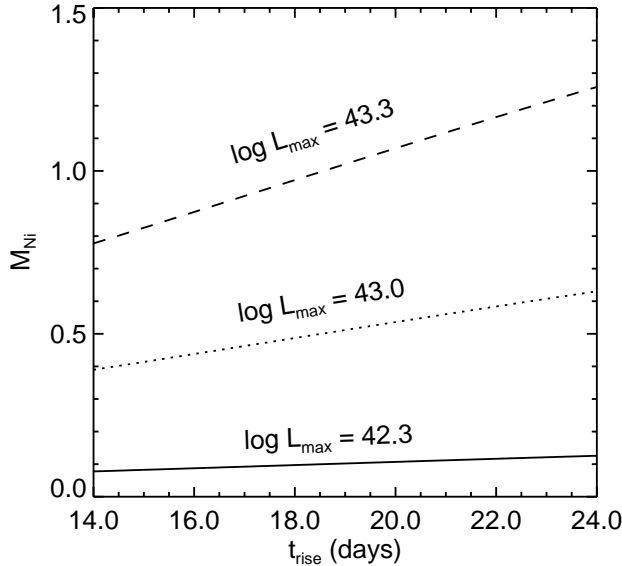


Figure 5.12: Variation of the amount of ^{56}Ni dependent on the rise time t_{rise} shown for three bolometric luminosities. The dependence has been calculated assuming Arnett's law and the ^{56}Ni to ^{56}Co to ^{56}Fe decay as described in the text.

the energy deposited near the surface suffers less from adiabatic decompression. The light curve peaks earlier and at a higher luminosity. But if ^{56}Ni does not extend beyond 85% of the radius, the distribution of the radioactivity has little effect on the light curve.

For the calculation of the ^{56}Ni mass the simple equation

$$L_{\text{max}} = 2.2 \pm 0.2 \times 10^{43} M_{\text{Ni}} \text{ erg s}^{-1} M_{\odot}^{-1} \quad (5.3)$$

of Arnett et al. (1985) has been used.

Since not all the emerging energy from the SNe Ia is sampled by *UBVRI*, but is restricted to the optical fluxes, the total luminosity is underestimated. As in Section 5.1.1 and 5.1.4 described, about 10% of the bolometric flux is not accounted by the optical filters near maximum light. We use this estimate as a lower limit of the bolometric flux. All masses thus had to be increased by a factor 1.1. The nickel masses are listed in Table 5.2.

Another uncertainty is the exact rise time, which is an important parameter in the calculation. Equation 5.3 corresponds to the energy deposition of Equation 5.2 with a rise time of about 17 days to the bolometric maximum and complete trapping of γ -rays. It is likely that there are significant differences in the rise times and this would alter the estimates for the Ni mass. A longer rise time would imply a larger nickel mass for a given measured luminosity. This is shown in Figure 5.12. Decreasing the rise time to 12 days yields only 70% M_{Ni} of the values given in Table 5.2. Such a short rise time is excluded for most of the SNe Ia, where observations as early as 14 days have been recorded (SN 1990N: Leibundgut et al. (1991), Lira et al. (1998), SN 1994D: Vacca & Leibundgut (1996)), but could still be feasible for SN 1991bg. For a more realistic range of 16 to 20 days between explosion and bolometric maximum the nickel mass would change by only $\pm 10\%$ from the values provided here. If the relation between the bolometric luminosity and $t_{-1/2}$ (Figure 5.7) is taken as a measurement of the dependence of the rise time on the bolometric luminosity, this trend would make the brighter SNe even more ^{56}Ni rich relative to less luminous SNe.

Table 5.2: Gamma escape fit parameters, M_{Ni} and t_0 . FWHM is the full width at half maximum of the 4700 Å feature due to Fe III forbidden lines and v_{mod} is the model velocity (Mazzali et al. 1998). The last column shows the root of Equation 5.7 with the fiducial values used by Jeffery (2001).

SN	M_{Ni} (M_{\odot})	t_0 (days)	FWHM (10^3 km/s)	v_{mod} (10^3 km/s)	$v_{\text{mod}} t_0$
SN 1989B	0.57	35.46	12.60	7.80	2.51
SN 1990N	0.82	—	15.40	9.65	—
SN 1991T	1.14	38.10	18.00	10.70	3.69
SN 1991bg	0.10	23.78	3.50	2.00	0.43
SN 1992A	0.38	28.87	14.80	9.30	2.43
SN 1992al	0.75	33.16	—	—	—
SN 1992bc	0.84	35.12	—	—	—
SN 1992bo	0.41	—	—	—	—
SN 1993H	0.40	25.43	—	—	—
SN 1993O	0.60	—	—	—	—
SN 1993ag	0.59	31.25	—	—	—
SN 1994D	0.41	27.90	15.30	9.60	2.43
SN 1994ae	0.55	34.56	14.60	9.20	2.88
SN 1995D	0.77	37.70	15.20	9.50	3.24
SN 1995E	1.05	34.17	—	—	—
SN 1995ac	1.13	—	—	—	—
SN 1995al	0.65	37.45	—	—	—
SN 1995bd	0.84	39.57	—	—	—
SN 1996X	0.95	—	15.00	9.40	—
SN 1996bo	0.85	—	—	—	—
SN 1998bu	0.76	—	—	—	—
SN 1998de	0.11	—	—	—	—

Clearly, the dominant uncertainty in the determination of the nickel mass stems from the uncertainties in the distances and the extinction corrections.

With the currently best available distances the SNe span a range of 2.5 in the ^{56}Ni mass (excluding SNe 1991bg and 1998de, which have about 1/10 of the ^{56}Ni mass of the brightest objects).

Comparison with other determinations of the ^{56}Ni masses

For a few of the supernovae, nickel masses have been measured by other methods.

As both the applied distance moduli (μ) and the values of the total absorption (A_{bol}) used from different authors vary the following equation has to be used to compare nickel masses:

$$M_{\text{Ni}} = M_{\text{Ni}}^* 10^{0.4(\mu - \mu^* + A_{\text{bol}} - A_{\text{bol}}^*)}. \quad (5.4)$$

For the total bolometric absorption $A_{\text{bol}} = -2.5 \log \frac{L_{\text{red}}}{L}$ (L_{red} and L being the reddened and dereddened bolometric luminosity) at the bolometric maximum the following dependence on $E(B-V)$ has been derived from the flux distribution of SN 1991T at maximum (valid for

$E(B-V)$ between 0 and 2):

$$A_{\text{bol}} = [3.55 - 0.57 E(B-V)] E(B-V). \quad (5.5)$$

SN 1991T has an upper limit for the radioactive nickel produced in the explosion of about $1 M_{\odot}$ based on the $1.644 \mu\text{m}$ Fe lines (Spyromilio et al. 1992). This value depends on the exact ionization structure of the supernova one year after explosion and a conservative range of 0.4 to $1 M_{\odot}$ had been derived. This is consistent with the estimate from the bolometric luminosity at maximum.

Bowers et al. (1997) have derived nickel masses for several SNe Ia in a similar way. Their best estimates for SN 1991T, SN 1994ae, and SN 1995D are all about half the value found here, when converted to their distances and extinctions (with Equation 5.4). However, they point out that their values should be increased by a factor of 1.2 to 1.7 to account for ionization states not included in their analysis. With this correction a fair agreement is found.

Cappellaro et al. (1997) derived masses from the late V light curves using a simple Monte Carlo code for the γ -ray and positron deposition to calculate the bolometric light curve. For the escape of the optical photons a grey opacity is assumed. M_{Ni} determines the absolute luminosity, and the total mass of the ejecta M_{ej} determines the optical depth for the radiation from the radioactive decay. Fitting both the light curve around maximum and the late decline results in a single set of these two parameters. There are four objects in common with our study: SN 1991bg, SN 1991T, SN 1992A, and SN 1994D. Adjusting the determinations to the same distances and re-normalizing to the SN 1991T ^{56}Ni mass found in this work, there is a general agreement, although there are differences at the $0.1 M_{\odot}$ level.

Nickel masses were also derived from the line profiles of [Fe II] and [Fe III] lines in the optical by Mazzali et al. (1998). These measurements depend critically on the ionization structure in the ejecta and had been normalized to a nickel mass of SN 1991T of $1 M_{\odot}$. They assume that the line width defines the volume of the ^{56}Ni sphere and that this translates directly into a ^{56}Ni mass. Thus the ^{56}Ni masses scale with v^3 . They find that SN 1986G has 0.3 times the mass of SN 1991T, SNe 1981B and 1992A have 0.4 – 0.5, and SNe 1990N and 1994D have 0.5 – 0.6, the very subluminous SN 1991bg has only 0.01 times the mass of SN 1991T. As this SN has a lower degree of ionization the investigated lines are not blended (the fractional abundance of the Fe III is smaller). When their masses are scaled to our measurements a reasonable agreement is found.

5.3.3 γ -ray Escape and the Total Mass of SNe Ia

The nickel mass is determined from the bolometric luminosity at maximum light (see Section 5.3.2), while the energy deposition can be calculated from the late decline of the bolometric light curve. A fit of Equation 5.2 to the observed bolometric luminosity (dotted line) at epochs later than 50 days past maximum (vertical dotted line), when thermalized photons can escape freely, is shown in Figure 5.13 (solid line). Like in Figure 5.11, the dashed-dotted line indicates the energy deposition with complete trapping ($\tau = \infty$) of γ -rays and positrons, and the dashed line shows the energy deposition for γ -rays from the ^{56}Co decay escaping freely (while the γ -rays from the ^{56}Ni decay and the positrons from the ^{56}Co decay are completely trapped).

The bolometric light curves have been corrected for missing pass bands, but they only have been used, if at least BVI are observed till day 70. The fit has been restricted to the

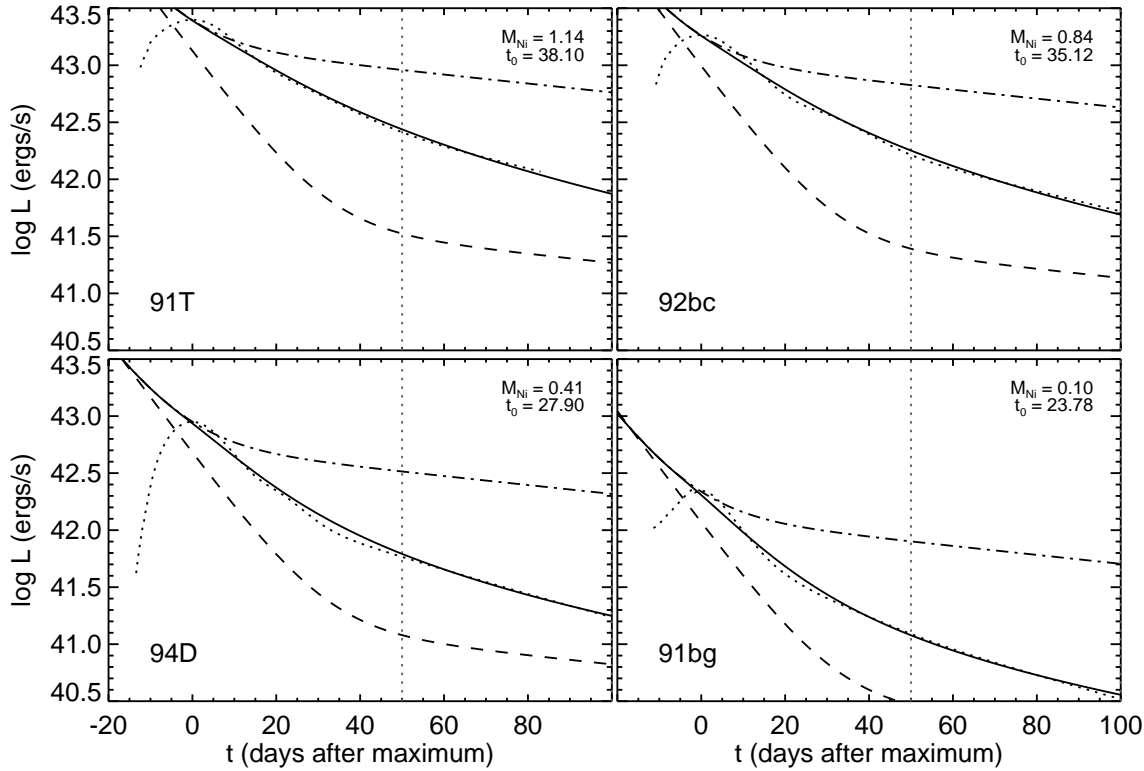


Figure 5.13: Fit of Equation 5.2 to the observed bolometric luminosity (solid line). The dashed and dashed dotted lines are the energy deposition for γ -rays and positrons from the radioactive decay with the γ -rays from the ^{56}Co decay escaping freely or completely trapped respectively.

time range from 50 to 100 days, as till day 50 the supernova ejecta is not optical thin and Equation 5.2 is not applicable.

Note that at these epochs basically all ^{56}Ni has decayed to ^{56}Co and contributes a negligible amount to the deposited energy. If there is only a single radioactive species, the mean optical depth $\bar{\tau}$ has a simple t^{-2} time dependence:

$$\bar{\tau} = \frac{t_0^2}{t^2}. \quad (5.6)$$

Following the discussion in Jeffery (2001) one gets for the fiducial time t_0 , i.e. roughly the time of transition between the optically thick and thin epochs:

$$t_0 = \sqrt{\frac{M \kappa q}{8\pi} \frac{1}{v_e}}. \quad (5.7)$$

q is a general form factor and describes the initial ^{56}Ni concentration. It is large for high concentration to the center (with a maximum value of 1), small for low concentration and

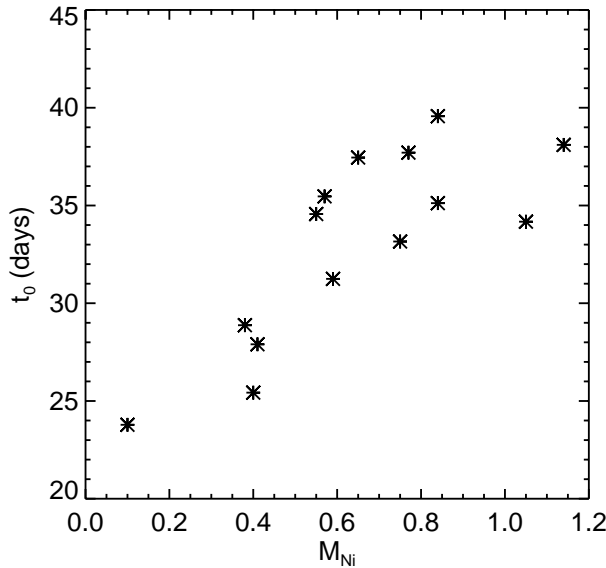


Figure 5.14: Fiducial time t_0 versus amount of ^{56}Ni .

$1/3$ for evenly spread ^{56}Ni . M is the total mass and κ a constant opacity. t_0 is independent of the distance, because it only depends on the shape of the light curve.

The range of t_0 together with the velocities obtained from Mazzali et al. (1998) show, that the physical parameters q , κ or/and M have to vary for the different SNe. If one assumes that the distribution of ^{56}Ni and κ is constant, the total mass has to differ by a factor of 2.4 (excluding SN 1991bg). To accomplish for a factor of 2.4 only with changing the concentration factor q , this parameter would have to change more than its expected range. ^{56}Ni is synthesized most where the density of the white dwarf is highest, making it most concentrated in the center. t_0 itself spans a range of a factor of 1.55 (see Table 5.2).

In Figure 5.14 the fiducial time t_0 is plotted versus the ^{56}Ni mass. A strong correlation can be seen.

Chapter 6

Conclusions

In this work, a new method (Vacca & Leibundgut 1996; Contardo et al. 2000) to analyze Type Ia supernova light curve data was extended and for the first time thoroughly applied.

It is a useful tool for uniform determination of light curve parameters. I estimated the error budget and applied our method to two specific questions to show the advantages and differences compared to other methods. Our method gives a continuous representation of the often too sparse observational data. This continuous representation can be used to derive important light curve parameters. Assumptions as in template fit methods are avoided, allowing the parameters to be derived more individually. An affluent collection of light curves and parameters is given in Appendix A. This catalogue will be a valuable base for further analysis.

By analyzing the epochs of maximum light in different wavelength regimes it has been demonstrated, that Type Ia supernovae do not act like an expanding cooling sphere. The determination of the rise time – the time it takes the supernova to reach maximum light – has shown differences and problems of our approach compared to other studies. The major disadvantage is that the fit of the rising part of the light curve might be influenced by the availability or absence of observations after maximum light.

The fits of the light curves in *UBVRI* have been used to construct optical bolometric light curves; the continuous representation of the light curve again being an advantage. The integrated flux in *UBVRI* provides a reliable measure of the bolometric luminosity and therefore represents a meaningful physical quantity. This quantity depends directly on the amount of nickel produced in the explosion, on the energy deposition, and on the γ -ray escape. The error budget has been investigated and the bolometric light curves constructed from the broadband filters have been compared with direct calculations from observed spectra. Using the early IR observations of SN 1998bu, the flux in the infrared can be estimated. The continuous form of the *UBVRI* light curves allows to calculate the bolometric flux *UBVR_{IJHK}* at the epochs of the IR observations. I analyzed the shape of the peak light curve and found a weak correlation between the maximum brightness and half light time for both rise and decline. The half light time for the rise may be used to characterize the rise to maximum light without the need to extrapolate the light curve to epochs earlier than observed. Compared to the rise time, I thus get a more reliable parameter for the region of the light curve, which is sensitive to the initial composition of the exploding white dwarf. The secondary bump which is seen in most red and infrared light curves is still visible in the bolometric light curves and can be quantified by the maxima and minima of the first derivative. I found a correlation between

the maximum luminosity and the epochs of the extrema of the first derivative. This shows that the luminosity width relation also holds for the light curve shape at later times.

The bolometric light curves can be used to derive further quantities. As the energy radiated in the optical wavelength range stems from the radioactive decay of ^{56}Ni synthesized in the explosion, the amount of ^{56}Ni can be calculated. Following Arnett's law – the luminosity at peak being equal to the instantaneous energy deposition rate – the amount of ^{56}Ni has been derived. These ^{56}Ni masses are consistent with other determinations. The γ -ray escape fraction can be determined by fitting theoretical curves to the bolometric light curves. Combining these results with other parameters derived from observations, it can be shown that the total mass, the distribution of ^{56}Ni and the opacity of the ejecta have to have different values throughout the sample of SNe analyzed in this work.

Appendix A

Catalogue

A.1 Introduction

Using published observations of Type Ia SNe (see Table 3.1), a catalogue of fit parameters (Table A.1) and light curve parameters (A.2) has been compiled. Figures A.1 to A.60 show the observations and fits.

In Table A.1 the fit parameters of all analyzed SN light curves are shown. The 10 fit parameters of Equation 4.1 described in Section 4.1, the time range of the fit and the reduced χ^2 are given. It has to be noted, that χ^2 depends on the adopted errors of the data points, which are taken from the published values. As a consequence, if χ^2 of SNe observed by different groups are compared, the smaller χ^2 not necessarily means the better fit. When for a single SN data sets of more than one group are considered, this may result in over/underestimating the weight of some observations in the fit. In a few cases (SN 1991bg, SN 1994D, SN 1997br) the errors had to be set to an reasonable value (0.1, 0.1, 0.03 mag), because of the non-availability of errors in at least one data set so as to result in a χ^2 of the order of 1. If the resulting χ^2 is much smaller than 1 the fit converges too fast and maybe not to the minimum χ^2 . But as all data points are set to the same error, the late data (less luminous and therefore more noisy) get too much weight if the errors have to be fixed to a single value.

For some SNe parts of the light curve are not well sampled with observations. Therefore, some fit parameters had to be fixed (printed in italics). The dashes signify the fits without exponential rise or second Gaussian respectively. The second Gaussian has not been fitted for the *U* and *B* light curves or if there were not enough observations. The bolometric light curves have all been fitted with two Gaussians and with errors chosen to be 0.01 regarding the fact that they were fitted to the bolometric light curves constructed from the fits in the filter light curves. Exceptions to this procedure are listed in Section A.2.

Table A.2 presents the light curve parameters which were derived from the fits shown in Table A.1 and Figures A.1 to A.60. The rise time t_{rise} is calculated from the fit as the time the SN takes to rise from 30 mag below maximum to maximum light, t_{\max} , m_{\max} , t_{\min} , m_{\min} , $t_{2\text{ndmax}}$, and $m_{2\text{ndmax}}$ are the epoch (in JD +2440000) and magnitude (in mag) at the first maximum, the minimum and the second maximum, as calculated from the fit respectively. The now classical decline parameter Δm_{15} is the difference in magnitude from maximum to 15 days later. The width of the light curve at half the peak luminosity is measured, $t_{-1/2}$ denoting the time (in days) it takes to rise and $t_{+1/2}$ to decline. Furthermore, the slope of the

late decline (in mag/day) between 50 and 80 days after maximum is shown. This slope is not necessarily the same as the fit parameter γ as especially in I the secondary Gaussian and even the exponential rise have still not negligible influence on the late light curve. Usually the late slope as calculated from the fitted light curve is bigger than γ . All these parameters are only shown, if the time range important for the parameter is covered by observations, e.g. if the SN is not observed at maximum, the peak magnitude and the epoch of maximum is not shown and Δm_{15} either.

For SNe 1989B, 1990N, 1990af, 1991T, 1991bg, 1992A, 1992al, 1992bc, 1992bg, 1992bo, 1992bp, 1993B, 1993H, 1993O, 1993ag, 1994D, 1994M, 1994S, 1994ae, 1995D, 1995E, 1995ac, 1995ak, 1995al, 1995bd, 1996C, 1996X, 1996bo, 1997br, 1998bu, 1998de the uncertainties are shown in the second row as given by the Monte Carlo simulations described in Section 4.2.

For both tables (Table A.1 and A.2), the bolometric luminosities have been converted to an arbitrary magnitude system to allow for the same treatment as the filter light curves (using a constant of 120):

$$m_{\text{bol}} = \text{const.} - 2.5 \log L_{\text{bol}}. \quad (\text{A.1})$$

As the zero points of the bolometric magnitude scale in the literature differ, the bolometric magnitude is replaced by Equation A.1 for simplicity. For the light curve shape the normalization does not matter and using the absolute fluxes is preferred for the comparison to models.

In Figures A.1 to A.60 the individual $UBVRI$ and bolometric light curves as well as the residuals of the data are shown. The dotted line represents the fit, the solid line indicates the time range over which the fit was restricted. The symbols are the data points. The left axis shows the observed apparent magnitudes and the right axis the magnitude below maximum light or (if no maximum magnitude could be calculated) relative to the observation with maximum flux. The time axis is relative to the B maximum.

For those filters where no fit could be achieved only the observations are shown. In the panels of the bolometric light curves the solid line shows the bolometric light curve constructed from the fits to the filter observations and corrected for missing filters within $UBVRI$ as described in Section 5.1. The dotted line is the extension also to epochs, when not the maximum number of filters (as written in column 2 of Table 3.1) is available. The bolometric flux as calculated from the observations is shown as asterisks only for epochs with simultaneous observations in all filters (compare to Figure 5.3).

In most cases the computation of the bolometric luminosity gives the same result no matter whether it was calculated from the fits to the filter light curves or directly from the observations. But the two values can differ significantly, if it was not possible to fit one or more of the filter light curves (e.g. SN 1991U, Figure A.9): The bolometric luminosities from the observations have been calculated from all available observations ($UBVRI$), but the fitted light curve is from fewer bands (B band only for SN 1991U). The bolometric luminosity from the fit (solid line) is the B band light curve corrected for missing pass bands as described in Section 5.1. As it has to be corrected for more bands than were available, the slope of the bolometric luminosity differs and is not reliable.

A.2 Annotations to Individual SNe

In the following the fits to the observations of the individual SNe are discussed. All bolometric light curves have been fitted with all 10 fit parameters, even if the filter light curves have not. The time range of the observations has been restricted to 150 days after maximum unless stated otherwise. The *U* and *B* light curves have been fitted with only one Gaussian. If some parameters have been fixed or the rise or the second Gaussian have not been fitted, it is mentioned in the discussion and can be seen in Table A.1 (dashes for not fitted parts of the light curve and italics for fixed values).

SN 1989B

UBV light curves have been calculated with no rise because of lack of pre-maximum data.

SN 1990N

As there is a big gap in the observations between JD 2448125 and 2448250 all fits had to include data until after 200 days past maximum (not shown) to fix the late decline. Also around the time where the second maximum is expected, there are no data. Those two gaps make it impossible to fit the *R* and *I* light curves. The secondary bump is by far overestimated. But there are early pre-maximum data which makes the fits reliable around maximum.

SN 1990O

There are no pre-maximum data, again a big gap between JD 2448160 and 2448350 and only about 10 observations. Therefore the fits had to be restricted in the number of parameters. All light curves have been fitted without rise and only *I* with a second Gaussian.

SN 1990T

There are no observations at maximum, but the *B* and *V* light curves can be used for the determination of the late slope and postmaximum data. There are not enough observations for fitting the second peak in *R* and *I* well. For *I* the width of the second Gaussian had to be fixed.

SN 1990Y

As there are no pre-maximum data, the rise has not been fitted. The *B* and *V* light curves

can be used for the late slope and for a continuous representation of the postmaximum data. As there are only 10 observations in *R*, the secondary peak is not reliable.

SN 1990af

There are *B* and *V* observations until 25 days after maximum. Even fitting the *V* light curve with only one Gaussian produces strange results (small bump 6 days after maximum).

SN 1991S

The *B* and *V* light curves are neither observed at maximum nor at late times.

SN 1991T

The rise times of *U* and *I* are not reliable because there are not enough pre-maximum observations.

SN 1991U

Only the *B* light curve could be fitted, but neither the maximum nor the late light curve is observed.

SN 1991ag

There are no observations at maximum light and there are not enough data in *V*, *I* and *R* for fitting the second Gaussian.

SN 1991bg

The maximum in *B* is not observed, but otherwise the light curves could be fitted without problems. As there are no errors given in the literature, a observational uncertainty of 0.1 mag has been assumed.

SN 1992A

The light curves could be fitted very well, but as in all well observed light curves with enough data, oscillations in the residuals especially in the *I* band can be seen. This indicates the imperfections of the adopted model.

SN 1992J

As there are not a lot of observations the light curves can not be fitted well.

SN 1992K

The maximum is not observed, but the late slope could be fitted well in *BV*. For the *I* fit there are not enough data, several parameters had to be fixed.

SN 1992P

There are no pre-maximum data and there is a gap after maximum. No second Gaussian could be fitted and in *I* there are not enough observations to get a good representation for the light curve at all.

SN 1992ae

In *B* and *V* the fit can give some hint for the light curve, but there are no observations at maximum light and at later times.

SN 1992ag

There are neither pre-maximum data nor late observations and the *B* observations are discrepant by 0.5 mag 30 days after maximum. Fitting a second Gaussian was not possible.

SN 1992al

No second Gaussian could be fitted in *V*, but otherwise the light curve fitting had no problem.

SN 1992aq

Because of the lack of observations at maximum and at late times, the light curves could not be fitted very well. Fitting a second Gaussian was not possible.

SN 1992au

The SN was not observed at maximum light and not for a long time. Again the light curves could not be fitted well.

SN 1992bc

SN 1992bc did not make trouble at all.

SN 1992bg

The observations in *I* are too sparse to be fitted well, but *B* and *V* give continuous representations within the observed epochs, even without fitting the second Gaussian in *V*.

SNe 1992bh, 1992bk and 1992bl

Again the second Gaussian in *V* could not be fitted because of the lack of late and pre-maximum data. The *I* light curves suffer from not enough observations.

SN 1992bo

There are not enough data in the time range of the second bump to fit a second Gaussian in *V*. This observational gap at the time of the second bump makes the secondary maximum in *R* and *I* uncertain.

SN 1992bp

The second Gaussian in *V* could not be fitted because of the lack of late and pre-maximum data. The *I* light curves suffer from not enough observations.

SN 1992br

There are not enough data to fit the second Gaussian in *V* and difficulties in the fit to *B* light curve because of the early end of the light curve due to the dimness of the SN.

SN 1992bs

The second Gaussian in *V* could not be fitted because of the lack of late and pre-maximum data. The *I* light curves suffer from not enough observations.

SN 1993B

The second Gaussian in *V* could not be fitted because there are not enough data.

SN 1993H

No second Gaussian could have been fitted in R because of a gap of observations around those epochs and no pre-maximum data which would fix the exponential rise.

SN 1993O

The exponential rise could not be fitted in I .

SN 1993ae

The maximum was not observed and the width of the second Gaussian had to be fixed in I and R because of a gap in the observations of about 20 days.

SN 1993ag

The I fit at maximum overestimates the light curve, but the exponential rise had to be included because of the steep late slope and the minimum (see discussion in Section 4.1). In V there are not enough data to fit a second Gaussian.

SN 1993ah

There are not enough observations for fitting all parameters and a gap of about 40 days.

SN 1994D

There was no problem in fitting the light curves, but again the undulations in the residuals can be seen. As observations by different observers with and without errorbars have been compiled, an observational uncertainty of 0.1 mag has been assumed.

SN 1994M

The second Gaussian in V is not very well sampled and therefore overestimated.

SN 1994Q

There were not enough data in V , R and I to fit the exponential rise and to get a good continuous representation of the observations.

SNe 1994S and 1994T

The light curves are sparsely sampled with no late observations.

SNe 1994ae and 1995D

There have been no problems fitting SN 1994ae and SN 1995D.

SN 1995E

The second Gaussian could not be fitted in V .

SN 1995ac

As there are no data later than 60 days after maximum, the width of the second Gaussian had to be fixed.

SN 1995ak

No exponential rise could be fitted, what is problematic in I , but there are not enough data for fitting 10 parameters.

SN 1995al

The light curve is sampled well for more than 100 days, but the V light curve is only fitted with one Gaussian.

SN 1995bd

The second Gaussians (with a fixed width in V) are determined mainly by a single observation.

SN 1996C

Although there are no pre-maximum data, R and I had to be fitted with exponential rise, I also with a fixed width of the second Gaussian.

SN 1996X

There have been no restrictions in the fit, but the pre-maximum observations do not constrain the fit well especially in R .

SN 1996Z

There are only a few observations with a big gap, which could be fitted with one Gaussian only.

SN 1996ab

The same applies for SN 1996ab, for B even the late slope had to be fixed.

SN 1996ai

There is a gap around the time of the secondary bump, which makes the secondary Gaussians very undetermined. In *I* the slope and the width of the second Gaussian has been fixed.

SN 1996bk

There are big gaps between the sparse observations. Fitting the light curves with only one Gaussian and without exponential rise (besides in *B*) has been tried.

SN 1996bl

SN 1996bl is lacking of early and late observations. This makes it impossible to fit a second Gaussian in *V*. In *R* and *I* the slope had to be fixed.

SN 1996bo

Again the slope had to be fixed in *V*, *R* and *I*.

SN 1996bv

The observations are very sparse; it was not possible to fit the exponential rise. In *I* this was necessary so three other parameters had to be fixed.

SN 1997br

I has not been observed at maximum hence the time of the first Gaussian had to be fixed and no exponential rise could be fitted. *B* has a gap in the observations at maximum light, which lets the fit overestimate the maximum brightness.

SN 1997cn

Only the *V* light curve could be fitted with only one Gaussian as in the other filters there are not enough late time data and the maximum is not observed.

SN 1998bu

For the *JHK* light curves (not included in Figure A.59, but shown in Figure 5.4), the slope had to be set to 0, because the light curves do not extend after the second maximum. As the error estimates of the two datasets disagree, the late fit in *I* is determined by the Suntzeff et al. (1999) data as they give smaller errors. The *U* and *B* light curves could be fitted better with a second Gaussian to account for the non-symmetry of the maximum.

SN 1998de

All light curves have been fitted without a second Gaussian.

A.3 Fit Parameters

Table A.1: Fit parameters.

f_0 (mag)	γ (mag/day)	g_0 (mag)	t_0 (JD)	σ_0 (days)	g_1 (mag)	t_1 (JD)	σ_1 (days)	τ (JD)	θ (days)	t_{start} (JD)	t_{end} (JD)	χ^2	Filter
89B													
13.92	0.0220	-1.03	7562.12	9.32	-1.11	7571.02	18.94	7534.69	8.89	7562.87	7694.97	2.27	bol
15.43	0.0168	-3.02	7564.59	13.17	—	—	—	—	—	7561.79	7695.53	2.21	U
15.05	0.0128	-2.66	7566.05	14.28	—	—	—	—	—	7561.83	7695.53	0.91	B
13.22	0.0237	-1.20	7570.03	11.10	-0.37	7591.03	7.08	—	—	7561.83	7695.53	1.24	V
12.58	0.0298	-0.68	7570.98	10.76	-0.42	7590.81	6.12	7464.57	15.53	7561.86	7695.53	0.62	R
11.48	0.0383	-1.49	7559.14	8.75	-0.81	7588.65	20.12	7528.45	18.39	7562.81	7695.53	0.91	I
90N													
14.32	0.0148	-4.97	8064.81	28.11	-0.86	8117.29	6.77	8052.74	14.16	8071.59	8213.09	0.48	bol
16.29	0.0145	-6.78	8071.79	24.83	—	—	—	8048.62	19.19	8071.50	8299.87	0.34	U
15.30	0.0134	-2.52	8084.25	15.21	—	—	—	8063.35	2.51	8071.50	8299.87	5.75	B
14.36	0.0165	-2.70	8064.84	36.03	—	—	—	8055.55	8.30	8071.50	8299.87	4.60	V
15.79	0.0137	-3.09	8084.50	20.21	-2.29	8117.53	8.53	8060.80	3.48	8071.50	8299.87	4.14	R
15.68	0.0136	-2.68	8082.78	18.56	-2.64	8117.12	10.07	8068.19	1.01	8071.50	8299.87	1.59	I
90O													
14.02	0.0162	-2.24	8073.61	11.40	-2.31	8071.98	28.48	8056.64	14.19	8084.69	8206.09	0.11	bol
19.21	0.0127	-2.60	8077.49	16.26	—	—	—	—	—	8076.71	8355.86	0.35	B
18.02	0.0172	-1.47	8078.64	21.09	—	—	—	—	—	8076.71	8383.88	1.45	V
17.41	0.0196	-1.33	8063.50	39.13	—	—	—	—	—	8076.71	8383.88	6.10	R
18.69	0.0139	-2.46	8080.56	2.52	-1.72	8106.07	19.95	—	—	8084.64	8383.88	10.65	I

continued on next page

f_0	γ	g_0	t_0	σ_0	g_1	t_1	σ_1	τ	θ	t_{start}	t_{end}	χ^2	Filter
90T													
13.86	0.0241	-1.10	8095.41	3.80	-0.85	8100.72	10.96	8085.99	3.97	8098.55	8178.55	1.49	bol
20.01	0.0150	-2.30	8089.40	12.37	—	—	—	8043.87	7.70	8098.50	8218.50	0.57	B
18.80	0.0204	-1.26	8090.98	16.68	—	—	—	8039.62	7.33	8098.50	8218.50	1.08	V
17.82	0.0323	-6.16	8092.72	4.91	-2.21	8099.86	10.37	8090.02	6.78	8098.50	8184.56	1.13	R
17.62	0.0358	-2.19	8095.34	5.30	-0.97	8107.44	10.00	8082.11	8.98	8098.50	8178.58	1.10	I
90Y													
13.13	0.0334	-1.02	8123.93	12.88	-0.25	8169.37	4.67	8099.01	8.83	8132.91	8188.71	0.92	bol
20.46	0.0114	-2.11	8123.74	13.78	—	—	—	—	—	8132.90	8218.80	1.78	B
19.84	0.0122	-1.71	8131.18	12.26	-0.71	8162.89	18.00	—	—	8132.90	8218.80	3.90	V
19.93	0.0023	-2.14	8135.21	19.68	-0.84	8169.68	6.10	—	—	8132.90	8188.81	2.15	R
90af													
10.76	0.2624	-0.03	8202.40	0.78	-2.29	8227.29	8.92	8179.49	12.47	8194.56	8218.56	0.12	bol
19.75	0.0461	-1.77	8198.48	9.86	—	—	—	8152.37	5.80	8192.60	8218.63	0.37	B
17.82	0.0919	-0.08	8202.54	0.70	—	—	—	8177.28	5.61	8194.53	8218.63	0.56	V
91S													
13.26	0.0347	-1.23	8355.68	6.76	-0.51	8371.39	6.89	8314.33	13.14	8360.64	8393.54	0.02	bol
20.97	0.0001	-3.10	8350.14	15.10	—	—	—	—	—	8360.58	8393.54	1.02	B
20.66	0.0003	-3.02	8340.28	31.37	—	—	—	—	—	8360.58	8393.54	1.01	V
91T													
12.92	0.0249	-1.18	8377.15	10.04	-0.45	8399.36	14.19	8357.26	2.00	8365.70	8442.39	0.02	bol
13.80	0.0224	-2.53	8375.67	13.64	—	—	—	8340.35	3.94	8365.66	8442.48	10.85	U
13.92	0.0153	-2.21	8377.74	14.53	—	—	—	8357.18	1.89	8363.77	8459.49	5.44	B
12.80	0.0216	-0.17	8381.98	5.30	-1.17	8375.05	25.93	8351.20	5.46	8363.77	8459.49	1.97	V
12.04	0.0299	-0.50	8379.43	6.04	-0.46	8402.07	12.63	8355.21	3.38	8363.77	8459.49	2.47	R
11.64	0.0336	-0.45	8375.61	5.34	-0.62	8408.14	13.38	8325.75	15.78	8365.66	8459.49	4.55	I

continued on next page

f_0	γ	g_0	t_0	σ_0	g_1	t_1	σ_1	τ	θ	t_{start}	t_{end}	χ^2	Filter
91U													
13.04	0.0445	-0.71	8370.00	11.38	-0.02	8381.10	2.45	8319.45	9.86	8366.74	8405.64	5.87	bol
18.05	0.0381	-2.53	8354.29	14.75	—	—	—	8295.93	19.99	8366.73	8405.65	2.08	B
91ag													
13.58	0.0203	-0.29	8414.99	7.57	-2.11	8402.10	27.66	8384.83	10.21	8420.90	8548.10	0.03	bol
16.72	0.0157	-7.04	8402.56	22.13	—	—	—	8391.95	17.73	8419.83	8571.55	2.40	B
15.82	0.0209	-1.54	8407.83	27.34	—	—	—	8310.69	16.67	8419.83	8571.55	2.17	V
15.66	0.0269	-0.86	8425.90	19.74	—	—	—	8349.79	12.41	8420.87	8559.55	1.12	R
15.91	0.0218	-2.48	8397.05	49.99	—	—	—	8387.53	12.30	8420.87	8559.55	3.62	I
91bg													
16.07	0.0261	-2.09	8600.97	11.77	-0.44	8622.80	20.78	8592.44	3.38	8604.01	8734.31	0.05	bol
16.42	0.0220	-3.17	8595.69	11.11	—	—	—	8595.46	2.63	8604.00	8746.60	0.59	B
15.50	0.0302	-1.23	8607.05	6.41	-0.42	8619.68	15.18	8527.83	12.49	8594.28	8746.60	1.04	V
15.49	0.0271	-5.73	8597.45	16.24	-1.08	8634.62	18.52	8580.39	17.79	8604.00	8746.60	1.25	R
16.82	0.0146	-3.33	8592.16	27.64	-1.30	8651.06	48.46	8590.77	3.95	8604.00	8746.60	1.56	I
92A													
14.40	0.0273	-1.58	8642.17	8.83	-0.52	8661.67	7.13	8629.55	1.03	8634.54	8720.34	0.21	bol
15.41	0.0120	-2.81	8640.62	13.73	—	—	—	8627.03	1.89	8633.60	8730.30	2.17	B
13.75	0.0285	-1.18	8644.27	8.56	-0.44	8660.54	5.64	8628.00	1.55	8633.60	8731.30	1.02	V
13.30	0.0341	-0.73	8643.38	5.72	-0.56	8661.07	6.67	8628.74	1.22	8634.50	8720.40	2.49	R
12.27	0.0477	-0.89	8637.66	7.55	-0.69	8663.91	6.72	8597.14	18.50	8634.50	8731.30	4.02	I
92J													
13.15	0.0422	-4.21	8674.04	12.55	-0.17	8707.06	4.98	8660.94	15.13	8687.86	8731.46	0.05	bol
18.62	0.0475	-4.40	8677.78	11.71	—	—	—	8653.43	19.82	8687.77	8731.52	1.91	B
19.13	0.0260	-1.58	8674.23	14.81	—	—	—	8672.65	2.66	8686.78	8731.52	0.69	V

continued on next page

f_0	γ	g_0	t_0	σ_0	g_1	t_1	σ_1	τ	θ	t_{start}	t_{end}	χ^2	Filter
92K													
14.96	0.0299	-2.56	8677.40	12.17	-0.04	8713.47	2.95	8664.02	9.02	8691.74	8767.44	2.06	bol
18.30	0.0216	-1.00	8680.38	7.02	—	—	—	8679.87	1.61	8687.75	8806.59	0.88	B
16.42	0.0295	-2.96	8660.04	18.51	—	—	—	8651.53	7.94	8687.75	8835.57	2.01	V
15.77	0.0388	-1.19	8675.40	14.31	—	—	—	—	—	8691.69	8767.52	2.31	I
92P													
13.04	0.0312	-2.16	8715.23	15.37	-0.11	8739.41	6.37	8678.59	15.90	8720.76	8767.46	0.16	bol
18.75	0.0149	-2.62	8720.24	16.80	—	—	—	8653.99	10.48	8718.67	8793.50	1.77	B
17.18	0.0273	-0.96	8723.82	13.03	—	—	—	8663.18	4.51	8718.67	8793.50	0.44	V
16.54	0.0300	-0.39	8715.00	5.54	—	—	—	—	—	8720.72	8767.56	43.26	I
92ae													
12.61	0.0521	-0.85	8805.96	10.25	-0.34	8825.56	6.18	8775.59	7.63	8807.74	8844.84	0.28	bol
21.01	0.0272	-2.55	8805.01	15.46	—	—	—	8765.52	8.77	8807.67	8844.91	0.86	B
20.40	0.0192	-2.06	8801.77	24.68	—	—	—	8796.80	1.32	8805.83	8844.91	1.30	V
92ag													
12.82	0.0387	-1.15	8800.56	20.23	-0.04	8829.53	3.53	8798.27	1.85	8807.57	8854.47	0.04	bol
20.04	0.0094	-3.53	8804.58	19.52	—	—	—	8758.10	9.37	8806.52	8854.55	8.19	B
17.37	0.0339	-0.76	8813.50	17.02	—	—	—	8799.77	1.02	8806.52	8872.49	1.53	V
18.77	0.0127	-2.15	8819.09	30.26	—	—	—	8788.04	2.51	8807.52	8872.49	1.07	I
92al													
13.56	0.0243	-1.98	8838.05	9.98	-0.50	8861.88	11.80	8814.13	8.08	8840.73	8946.53	0.53	bol
17.20	0.0148	-2.60	8839.73	14.75	—	—	—	8823.31	1.79	8832.87	8955.53	0.36	B
15.16	0.0249	-4.41	8816.30	27.04	—	—	—	8807.11	16.03	8832.87	8955.53	0.38	V
15.19	0.0310	-1.23	8838.74	8.25	-0.48	8864.06	7.64	8816.64	7.59	8840.71	8956.56	0.17	R
14.58	0.0376	-4.16	8834.32	9.04	-0.68	8865.94	11.22	8824.85	10.89	8840.71	8946.59	1.47	I

continued on next page

f_0	γ	g_0	t_0	σ_0	g_1	t_1	σ_1	τ	θ	t_{start}	t_{end}	χ^2	Filter
92aq													
14.33	0.0185	-4.12	8824.97	10.76	-1.01	8845.93	11.97	8822.17	5.97	8840.78	8891.68	0.26	bol
22.34	0.0101	-5.52	8823.67	21.68	—	—	—	8788.80	19.09	8835.88	8891.69	0.69	B
21.79	0.0022	-2.62	8835.28	17.54	—	—	—	8759.91	15.24	8835.88	8891.69	1.00	V
19.82	0.0320	-1.35	8839.11	2.05	—	—	—	8834.16	2.17	8840.75	8891.69	0.93	I
92au													
14.13	0.0275	-4.45	8835.81	10.20	-0.19	8867.65	5.00	8826.04	10.19	8844.95	8885.75	0.04	bol
21.71	0.0005	-5.87	8827.77	15.37	—	—	—	8811.10	11.16	8844.88	8885.84	4.84	B
19.50	0.0328	-1.01	8843.81	6.29	—	—	—	8793.28	12.26	8843.93	8885.84	1.07	V
92bc													
13.58	0.0227	-1.61	8914.53	12.29	-0.42	8944.95	10.35	8895.80	2.20	8904.87	9026.57	0.41	bol
17.71	0.0141	-2.52	8914.14	17.46	—	—	—	8893.63	2.60	8901.71	9026.61	1.16	B
16.14	0.0222	-2.04	8896.86	27.26	-0.15	8942.88	4.32	8886.83	7.35	8901.71	9026.61	0.55	V
15.91	0.0293	-0.65	8916.08	8.74	-0.40	8944.57	8.63	8892.61	3.28	8901.71	9026.61	0.37	R
15.10	0.0377	-1.38	8906.53	10.34	-0.61	8949.37	9.23	8865.31	19.64	8904.84	9026.61	2.25	I
92bg													
13.89	0.0193	-2.29	8906.63	20.67	-0.19	8943.76	6.56	8901.75	2.34	8919.83	8979.73	0.53	bol
20.57	0.0062	-3.33	8912.58	18.75	—	—	—	8909.34	1.80	8919.80	8979.85	1.09	B
20.03	0.0002	-2.79	8912.90	25.37	—	—	—	8899.42	1.88	8919.80	8979.85	0.90	V
17.36	0.0359	-1.58	8919.64	2.24	-0.42	8944.91	5.48	8911.07	3.80	8919.80	8979.77	2.59	I
92bh													
12.83	0.0331	-2.38	8906.29	19.59	-0.10	8949.74	6.10	8897.79	7.87	8919.84	8963.74	0.27	bol
20.23	0.0165	-2.55	8919.91	16.70	—	—	—	8912.11	1.15	8919.83	8963.79	0.37	B
20.00	0.0012	-2.39	8921.17	21.41	—	—	—	8912.80	1.03	8919.83	8963.79	0.82	V
18.15	0.0185	-1.00	8909.43	15.84	-0.59	8950.51	5.65	8885.84	7.91	8919.83	8963.79	1.52	I

continued on next page

f_0	γ	g_0	t_0	σ_0	g_1	t_1	σ_1	τ	θ	t_{start}	t_{end}	χ^2	Filter
92bk													
14.87	0.0297	-1.17	8940.43	7.62	-1.51	8945.77	26.44	8927.81	4.93	8947.79	8979.69	20.35	bol
20.89	0.0078	-6.63	8931.28	18.23	—	—	—	8907.24	18.34	8947.73	8979.69	2.00	B
20.64	0.0007	-2.82	8940.23	17.25	—	—	—	8893.87	13.22	8947.73	8979.69	1.80	V
92bl													
13.96	0.0239	-5.72	8940.66	11.26	-1.62	8962.30	13.17	8930.56	15.26	8954.61	8987.51	15.28	bol
20.40	0.0096	-3.30	8946.31	14.82	—	—	—	8868.26	18.06	8949.56	9012.56	2.31	B
19.09	0.0193	-1.77	8948.89	16.88	—	—	—	8942.66	1.08	8949.56	9012.56	2.00	V
18.77	0.0167	-7.98	8945.00	3.99	-1.04	8970.00	10.00	—	—	8954.56	8987.56	9.32	I
92bo													
14.16	0.0324	-1.43	8988.24	8.35	-0.34	9006.42	6.14	8971.46	1.98	8978.67	9040.47	0.11	bol
18.31	0.0214	-2.45	8987.72	10.65	—	—	—	8972.30	1.53	8978.61	9040.54	1.12	B
17.33	0.0211	-1.86	8983.84	16.86	—	—	—	8963.46	5.77	8978.61	9040.54	0.19	V
16.33	0.0402	-0.56	8989.63	5.75	-0.42	9006.07	4.59	8968.79	3.03	8978.61	9040.54	0.34	R
15.34	0.0465	-1.99	8977.96	10.42	-0.54	9008.35	6.57	8955.25	13.91	8978.61	9040.54	0.72	I
92bp													
13.58	0.0283	-2.90	8978.29	12.94	-0.67	9007.15	9.77	8939.61	18.26	8978.72	9040.52	0.31	bol
20.40	0.0390	-1.77	8983.05	11.76	—	—	—	8965.79	1.72	8978.69	9040.58	1.42	B
21.50	0.0000	-3.18	8976.98	24.75	—	—	—	8947.51	7.15	8978.69	9040.58	1.22	V
20.29	0.0098	-1.86	8981.09	6.96	-1.45	9007.33	10.30	8947.49	7.60	8978.69	9040.58	2.57	I
92br													
14.47	0.0274	-3.07	8981.45	9.57	-0.06	9011.67	3.21	8971.17	6.12	8986.72	9040.52	0.84	bol
18.28	0.0705	-7.16	8979.62	12.53	—	—	—	8966.07	19.99	8986.69	9040.56	1.19	B
21.50	0.0135	-2.61	8982.91	15.16	—	—	—	8945.99	10.53	8986.69	9040.56	0.42	V
92bs													
13.57	0.0263	-1.76	8982.39	15.09	-0.30	9011.39	6.13	8972.21	3.42	8987.76	9037.56	0.19	bol
21.58	0.0014	-4.19	8982.51	18.15	—	—	—	8934.41	17.22	8987.73	9037.65	1.11	B
21.01	0.0003	-3.05	8976.05	28.94	—	—	—	8972.32	2.84	8987.73	9037.65	1.08	V

f_0	γ	g_0	t_0	σ_0	g_1	t_1	σ_1	τ	θ	t_{start}	t_{end}	χ^2	Filter
93B													
13.88	0.0157	-2.63	8995.68	17.79	-0.34	9029.96	10.67	8992.46	2.52	9011.86	9078.76	1.71	bol
22.24	0.0014	-3.97	9001.74	18.70	—	—	—	8926.65	19.88	9007.81	9078.82	0.63	B
20.40	0.0134	-1.82	9006.70	19.77	—	—	—	8936.49	12.56	9007.81	9078.82	2.89	V
20.68	0.0011	-3.72	9004.59	6.21	-2.04	9018.24	22.13	8993.15	8.58	9011.85	9078.82	2.17	I
93H													
14.00	0.0314	-1.97	9063.25	14.42	-0.08	9089.25	4.55	9055.60	3.87	9068.84	9161.44	0.09	bol
19.05	0.0235	-3.49	9066.39	12.18	—	—	—	9031.51	14.68	9068.78	9162.62	1.13	B
18.00	0.0298	-1.31	9072.24	10.52	-0.16	9089.49	4.77	9047.34	4.33	9068.78	9162.62	0.62	V
17.38	0.0368	-0.87	9070.64	15.15	—	—	—	9057.25	2.40	9067.78	9161.53	1.06	R
16.46	0.0463	-0.43	9065.62	6.47	-0.42	9088.65	5.45	9036.51	8.98	9067.78	9162.62	1.28	I
93O													
14.34	0.0159	-2.44	9131.35	14.16	-0.46	9161.56	9.07	9110.66	6.41	9132.52	9187.52	0.08	bol
20.69	0.0101	-4.73	9125.09	19.92	—	—	—	9101.22	12.48	9127.73	9187.54	1.21	B
19.54	0.0160	-1.67	9137.91	13.07	-0.38	9160.34	8.71	9120.12	1.16	9127.73	9187.54	0.37	V
18.76	0.0213	-0.69	9136.66	7.25	-0.72	9163.71	7.84	—	—	9132.47	9187.54	2.24	I
93ae													
14.21	0.0274	-2.30	9299.85	11.59	-0.04	9338.42	7.95	9284.90	8.37	9307.89	9361.69	0.63	bol
17.32	0.0268	-3.47	9292.82	12.59	—	—	—	9256.12	19.75	9302.60	9361.70	0.51	B
17.11	0.0230	-1.55	9297.83	13.06	-0.10	9329.68	5.42	9253.85	11.97	9302.60	9372.60	1.08	V
16.97	0.0298	-0.95	9308.06	9.34	-0.23	9338.32	10.00	9212.42	19.92	9307.80	9372.60	1.08	R
16.69	0.0402	-0.54	9312.98	6.26	-0.11	9327.99	10.00	9294.27	1.88	9302.60	9372.60	0.75	I
93ag													
13.59	0.0252	-2.68	9304.45	18.30	-0.22	9342.58	6.75	9302.13	4.72	9315.94	9428.74	0.19	bol
20.78	0.0158	-3.69	9313.11	16.81	—	—	—	9265.91	17.78	9314.85	9428.77	0.97	B
19.51	0.0235	-1.34	9322.09	15.29	—	—	—	9306.88	1.14	9314.85	9428.77	1.11	V
16.47	0.0523	-7.03	9309.02	12.21	-1.19	9340.85	9.25	9299.99	17.80	9315.85	9428.77	0.18	I

continued on next page

f_0	γ	g_0	t_0	σ_0	g_1	t_1	σ_1	τ	θ	t_{start}	t_{end}	χ^2	Filter
93ah													
13.52	0.0303	-2.13	9303.15	12.74	-0.23	9334.10	5.54	9255.77	18.88	9314.68	9388.48	0.07	bol
17.95	0.0273	-6.75	9299.24	17.17	—	—	—	9282.65	19.58	9314.58	9388.56	0.00	B
17.21	0.0277	-1.28	9296.93	20.31	—	—	—	9295.37	3.52	9314.58	9388.56	0.00	V
94D													
14.41	0.0263	-1.67	9433.27	9.32	-0.47	9453.59	8.05	9415.08	2.68	9421.70	9545.50	1.32	bol
14.29	0.0220	-2.98	9433.16	11.03	—	—	—	9417.35	1.76	9421.66	9545.53	2.48	U
14.52	0.0158	-2.68	9433.38	12.93	—	—	—	9414.24	3.02	9420.90	9545.53	0.38	B
12.85	0.0274	-1.93	9425.10	17.46	-0.11	9452.47	3.35	9409.32	7.80	9420.90	9545.53	0.12	V
12.57	0.0328	-0.98	9431.24	9.57	-0.46	9454.36	5.55	9410.89	5.40	9418.92	9545.53	0.32	R
11.45	0.0439	-2.51	9420.31	11.04	-0.59	9456.15	6.42	9409.43	11.23	9421.58	9545.53	1.06	I
94M													
13.54	0.0313	-1.84	9473.25	10.89	-0.41	9496.93	4.93	9465.80	3.42	9477.81	9542.61	0.11	bol
19.22	0.0119	-2.88	9475.73	14.05	—	—	—	9461.82	2.68	9477.71	9542.67	0.49	B
17.12	0.0295	-2.01	9471.25	13.05	-0.46	9495.94	4.40	9453.22	8.04	9476.76	9546.65	2.05	V
16.51	0.0405	-1.12	9477.61	5.89	-0.51	9496.05	4.51	9450.03	8.97	9477.71	9542.67	3.47	R
15.34	0.0528	-1.99	9472.04	8.91	-0.63	9498.64	5.00	9449.28	15.05	9477.71	9542.67	2.07	I
94Q													
12.68	0.0423	-0.56	9499.51	11.98	-0.02	9528.39	0.75	9476.90	6.78	9507.90	9545.79	14.69	bol
18.67	0.0199	-2.34	9497.07	15.88	—	—	—	9496.69	1.91	9507.80	9545.80	0.43	B
17.81	0.0201	-1.58	9494.02	26.51	—	—	—	—	—	9507.80	9565.70	0.39	V
17.95	0.0025	-1.13	9503.74	5.55	-0.97	9520.66	10.28	—	—	9507.80	9545.80	0.13	R
17.50	0.0275	-0.18	9519.19	2.16	-0.55	9529.29	8.02	—	—	9507.80	9545.80	0.08	I
94S													
12.71	0.0341	-1.31	9516.63	12.45	-0.15	9542.76	3.74	9484.57	10.81	9513.77	9545.67	0.05	bol
15.43	0.0935	-0.31	9527.43	7.20	—	—	—	9498.22	5.55	9513.70	9545.70	3.51	B
15.23	0.0598	-0.29	9525.82	7.45	-0.34	9547.43	7.76	9496.90	5.25	9513.70	9553.70	0.14	V

continued on next page

f_0	γ	g_0	t_0	σ_0	g_1	t_1	σ_1	τ	θ	t_{start}	t_{end}	χ^2	Filter
94T													
16.16	0.0390	-6.13	9507.25	9.97	-3.31	9535.08	13.14	9502.27	6.05	9514.83	9541.63	1.19	bol
9.68	0.2813	-3.65	9510.37	6.52	—	—	—	9505.58	15.01	9514.80	9541.70	0.00	B
18.65	0.0307	-2.01	9506.18	22.82	-0.28	9534.77	3.08	9496.85	3.99	9514.80	9545.70	2.46	V
94ae													
14.05	0.0225	-1.66	9686.61	12.47	-0.45	9715.28	8.97	9665.01	3.39	9673.07	9805.87	0.82	bol
15.82	0.0138	-2.61	9686.05	17.19	—	—	—	9664.69	3.40	9672.97	9843.80	1.66	B
13.99	0.0217	-2.36	9665.75	28.50	-0.11	9712.99	4.15	9660.56	7.78	9672.97	9843.80	0.28	V
13.77	0.0287	-0.76	9688.53	8.43	-0.52	9713.68	8.43	9665.22	3.32	9672.97	9843.80	1.10	R
12.42	0.0371	-3.55	9668.78	16.14	-0.69	9716.57	7.74	9656.28	17.07	9672.97	9805.88	0.64	I
95D													
13.46	0.0238	-1.42	9770.80	11.65	-0.36	9799.33	8.08	9755.41	1.88	9765.77	9851.57	0.12	bol
16.04	0.0122	-2.59	9769.84	16.17	—	—	—	9758.92	1.19	9765.74	9851.63	0.21	B
14.16	0.0250	-1.82	9762.39	18.25	-0.25	9798.23	7.27	9735.17	11.92	9760.10	9861.00	1.00	V
13.89	0.0314	-0.35	9773.50	5.99	-0.34	9798.56	7.18	9753.35	2.09	9760.10	9861.00	1.99	R
13.41	0.0327	-1.13	9763.24	10.27	-0.63	9800.91	8.99	9723.48	17.78	9760.10	9861.00	2.31	I
95E													
12.83	0.0320	-1.18	9776.40	11.42	-0.19	9802.72	5.78	9757.67	3.47	9772.78	9820.68	0.09	bol
19.06	0.0196	-2.23	9776.39	13.96	—	—	—	9692.58	11.66	9772.70	9820.70	1.22	B
17.26	0.0232	-1.15	9778.69	17.49	—	—	—	9763.51	1.88	9772.70	9864.70	0.48	V
16.14	0.0317	-0.67	9778.52	7.35	-0.39	9800.47	6.57	9733.21	8.67	9772.70	9864.70	1.00	R
14.01	0.0471	-2.92	9761.68	13.64	-0.53	9803.55	6.40	9746.04	16.09	9772.70	9864.70	1.68	I
95ac													
12.54	0.0324	-1.14	9994.09	12.01	-0.24	10022.51	5.15	9953.18	10.32	9987.64	10048.64	0.23	bol
20.32	0.0017	-3.10	9992.42	18.06	—	—	—	9928.59	1.89	9987.64	10048.70	4.74	B
17.86	0.0325	-0.41	9996.07	7.86	-0.43	10007.68	10.00	9981.63	1.04	9987.64	10048.70	0.81	V
17.10	0.0402	-0.23	9996.81	4.91	-0.41	10022.32	4.20	9960.09	8.44	9987.64	10048.70	0.52	R
17.78	0.0221	-0.45	9994.55	7.80	-0.69	10022.41	10.52	9953.40	5.88	9987.64	10048.70	0.57	I

continued on next page

f_0	γ	g_0	t_0	σ_0	g_1	t_1	σ_1	τ	θ	t_{start}	t_{end}	χ^2	Filter
95ak													
13.28	0.0292	-3.10	10017.59	7.55	-1.22	10019.50	24.16	10014.73	4.99	10024.80	10091.70	0.85	bol
18.53	0.0232	-2.57	10021.06	15.00	—	—	—	—	—	10024.79	10091.72	0.83	B
17.13	0.0309	-1.00	10027.19	5.14	-0.63	10042.00	6.60	—	—	10024.79	10091.72	0.68	V
16.20	0.0404	-0.37	10025.28	2.83	-0.41	10044.79	5.32	—	—	10024.79	10091.72	3.36	R
16.78	0.0285	-0.48	10025.29	3.42	-1.10	10054.72	11.25	—	—	10024.79	10091.72	0.53	I
95al													
13.71	0.0231	-1.47	10031.65	10.99	-0.41	10057.62	9.57	9982.11	6.38	10025.09	10159.79	1.42	bol
15.85	0.0136	-2.46	10031.18	15.41	—	—	—	9872.62	19.34	10025.00	10161.70	1.61	B
14.24	0.0239	-1.31	10026.81	22.03	—	—	—	10005.60	5.97	10025.00	10161.70	0.48	V
13.69	0.0312	-0.41	10033.26	7.05	-0.39	10057.08	6.80	10020.04	1.08	10025.00	10161.70	0.28	R
12.35	0.0389	-2.94	10015.11	14.83	-0.64	10059.54	7.97	9999.53	17.54	10025.00	10161.70	1.45	I
95bd													
13.35	0.0223	-1.41	10088.23	11.36	-0.46	10117.72	8.53	10068.61	2.66	10077.84	10162.54	0.10	bol
19.74	0.0109	-2.82	10079.84	22.37	—	—	—	10063.14	5.10	10077.80	10182.64	1.54	B
17.43	0.0258	-0.96	10088.59	10.37	-0.37	10112.91	10.00	10064.38	4.11	10077.80	10182.64	0.80	V
16.60	0.0284	-0.52	10091.34	5.96	-0.41	10117.76	6.79	10069.08	2.57	10077.80	10162.64	0.57	R
16.87	0.0187	-0.83	10086.69	10.40	-1.04	10119.42	9.49	10068.28	2.40	10077.80	10162.64	1.78	I
96C													
13.58	0.0243	-1.57	10131.22	10.38	-0.40	10155.72	9.40	10105.81	6.27	10131.97	10216.67	0.58	bol
19.09	0.0146	-2.27	10132.93	13.97	—	—	—	—	—	10131.90	10216.75	5.21	B
17.95	0.0192	-1.54	10126.86	23.57	—	—	—	—	—	10130.94	10216.75	0.77	V
16.87	0.0318	-0.83	10130.65	7.32	-0.41	10156.06	6.01	10107.53	6.17	10131.90	10216.75	0.39	R
16.40	0.0368	-4.82	10123.69	9.52	-0.61	10157.80	10.00	10116.37	9.93	10131.90	10216.75	6.99	I

continued on next page

f_0	γ	g_0	t_0	σ_0	g_1	t_1	σ_1	τ	θ	t_{start}	t_{end}	χ^2	Filter
96X													
13.10	0.0307	-1.41	10192.62	10.48	-0.28	10217.01	6.34	10158.68	7.42	10187.89	10251.58	0.09	bol
15.70	0.0173	-3.18	10190.06	15.33	—	—	—	10134.13	19.67	10187.80	10251.65	0.10	B
14.38	0.0272	-1.11	10195.95	12.67	-0.18	10216.28	4.96	10181.79	1.21	10187.80	10251.65	0.49	V
13.70	0.0368	-0.53	10195.43	5.13	-0.37	10215.47	6.40	10090.78	16.95	10187.80	10251.65	0.21	R
11.41	0.0565	-2.16	10180.28	11.94	-0.39	10218.91	6.54	10160.19	19.81	10187.80	10251.65	2.49	I
96Z													
11.97	0.0425	-2.30	10216.52	9.48	-0.18	10247.60	5.03	10200.90	10.23	10222.62	10280.32	0.07	bol
15.46	0.0468	-0.67	10222.27	6.42	—	—	—	—	—	10222.60	10280.40	0.15	B
15.26	0.0259	-0.98	10222.23	11.05	—	—	—	—	—	10221.60	10280.40	0.01	V
96ab													
14.19	0.0569	-2.36	10221.35	27.14	-0.57	10252.93	7.68	10207.23	3.76	10225.89	10251.79	0.15	bol
27.49	0.0200	-8.00	10219.23	41.55	—	—	—	—	—	10225.80	10251.80	0.77	B
22.69	0.0037	-3.26	10221.49	25.21	—	—	—	—	—	10225.80	10283.70	0.75	V
96ai													
11.57	0.0573	-0.28	10260.47	7.10	-0.10	10272.12	2.88	10220.30	9.05	10254.05	10294.95	3.39	bol
17.65	0.0867	-0.37	10266.31	6.07	—	—	—	10229.12	6.71	10254.00	10295.00	0.97	B
15.85	0.0566	-0.36	10273.08	3.06	—	—	—	10236.95	5.16	10254.00	10295.00	17.10	V
15.11	0.0601	-0.46	10258.88	6.01	-1.37	10288.82	15.28	10231.29	4.83	10254.00	10295.00	1.31	R
14.82	0.0200	-0.89	10252.99	11.52	-0.99	10285.23	10.00	10205.92	8.22	10254.00	10295.00	17.91	I
96bk													
14.57	0.0265	-2.17	10366.90	16.62	-0.24	10387.16	5.88	10354.32	5.10	10373.63	10502.63	0.66	bol
17.12	0.0207	-4.14	10361.99	13.01	—	—	—	10361.55	3.77	10373.60	10521.00	3.58	B
15.93	0.0286	-1.40	10377.98	10.39	—	—	—	—	—	10373.60	10521.00	11.90	V
15.18	0.0395	-0.81	10376.89	10.73	—	—	—	—	—	10373.60	10521.00	0.87	R
15.88	0.0215	-2.22	10385.18	10.88	—	—	—	—	—	10373.60	10521.00	2.86	I

continued on next page

f_0	γ	g_0	t_0	σ_0	g_1	t_1	σ_1	τ	θ	t_{start}	t_{end}	χ^2	Filter
96bl													
13.23	0.0269	-1.36	10377.54	12.09	-0.24	10405.26	5.15	10360.64	3.12	10373.82	10424.52	0.10	bol
20.33	0.0014	-3.46	10374.86	17.56	—	—	—	10349.17	5.80	10373.80	10424.60	1.60	B
19.55	0.0000	-2.62	10373.84	25.53	—	—	—	10365.67	1.60	10373.80	10424.60	4.07	V
17.32	0.0300	-0.46	10381.27	7.54	-0.31	10403.85	5.02	10310.09	12.44	10373.80	10424.60	8.53	R
16.94	0.0300	-1.32	10374.88	8.01	-0.57	10405.73	5.52	10338.85	14.39	10373.80	10424.60	1.34	I
96bo													
13.25	0.0268	-1.34	10388.67	10.38	-0.34	10412.36	5.58	10367.94	3.37	10381.70	10432.60	0.13	bol
18.41	0.0101	-2.24	10387.74	12.23	—	—	—	10374.39	1.27	10381.70	10432.70	3.86	B
17.15	0.0300	-1.34	10391.95	13.06	-0.47	10411.32	4.92	10372.88	2.20	10381.70	10432.70	6.35	V
16.13	0.0300	-0.65	10390.46	7.03	-0.49	10412.71	7.25	10376.89	1.06	10381.70	10432.70	4.82	R
16.11	0.0200	-0.42	10388.16	7.03	-0.61	10412.59	5.93	10344.67	6.42	10381.70	10432.70	14.42	I
96bv													
13.22	0.0178	-2.10	10396.80	20.79	-0.01	10434.09	3.80	10396.75	2.60	10408.90	10451.70	0.09	bol
18.62	0.0069	-2.76	10407.01	15.66	—	—	—	—	—	10408.90	10486.60	10.63	B
16.91	0.0171	-1.49	10404.41	22.29	—	—	—	—	—	10408.90	10486.60	8.53	V
16.58	0.0140	-1.76	10388.00	39.32	—	—	—	—	—	10408.90	10486.60	35.93	R
15.50	0.0200	-7.24	10400.15	10.00	-1.56	10424.57	10.00	10393.50	14.19	10408.90	10451.80	0.10	I
97br													
12.95	0.0266	-2.57	10554.34	14.54	-0.26	10591.08	9.18	10537.73	10.52	10564.97	10623.67	0.14	bol
16.15	0.0163	-2.40	10558.67	14.45	—	—	—	10517.81	10.92	10550.50	10626.70	2.03	B
14.62	0.0264	-0.80	10567.64	10.47	-0.21	10591.20	7.12	10541.21	2.62	10550.50	10626.40	1.19	V
14.65	0.0207	-0.66	10560.92	8.59	-0.80	10584.84	15.47	10541.64	2.25	10550.50	10626.40	1.11	R
13.75	0.0288	-0.22	10558.00	5.85	-0.65	10589.62	14.22	—	—	10564.90	10623.70	0.53	I
97cn													
17.03	0.0316	-3.90	10560.20	22.57	—	—	—	10523.69	11.39	10592.06	10669.45	0.76	V

continued on next page

f_0	γ	g_0	t_0	σ_0	g_1	t_1	σ_1	τ	θ	t_{start}	t_{end}	χ^2	Filter
98bu													
13.36	0.0286	-1.34	10953.90	12.56	-0.24	10979.70	5.93	10932.79	3.66	10947.61	11008.41	0.01	bol
15.17	0.0117	-3.37	10950.34	14.81	-0.30	10967.89	5.29	10912.37	8.43	10947.59	11008.45	1.17	U
14.05	0.0196	-2.19	10941.24	8.84	-3.04	10956.40	13.77	10917.69	18.36	10947.43	11008.45	1.27	B
12.79	0.0300	-0.95	10956.26	10.77	-0.28	10977.32	6.21	10932.37	4.24	10944.68	11008.45	3.56	V
12.18	0.0350	-0.48	10956.80	5.01	-0.39	10978.08	6.17	10939.91	1.53	10944.68	11008.45	1.09	R
9.37	0.0582	-3.84	10936.51	14.39	-0.50	10980.65	6.40	10930.79	17.82	10944.68	11008.45	4.33	I
17.99	0.0000	-6.48	10945.86	26.26	-3.17	10985.44	7.69	10938.92	1.56	10944.80	10984.76	2.94	J
13.90	0.0000	-2.41	10938.16	16.01	-2.04	10978.53	15.21	10935.52	2.37	10944.80	10984.76	5.34	H
13.74	0.0000	-2.70	10937.50	14.98	-1.81	10978.44	17.30	10937.27	2.78	10944.80	10984.76	5.28	K
98de													
15.49	0.0340	-0.15	11027.09	3.81	-1.33	11028.46	11.36	11009.87	3.61	11020.07	11076.77	0.09	bol
19.25	0.0329	-1.75	11026.46	6.93	—	—	—	11009.55	3.22	11018.00	11076.80	0.67	B
18.31	0.0260	-1.75	11026.68	11.21	—	—	—	11005.71	5.25	11018.00	11076.80	0.89	V
16.76	0.0382	-4.66	11015.44	20.38	—	—	—	10996.04	19.57	11020.00	11076.80	1.05	R
17.26	0.0492	-0.52	11037.28	8.64	—	—	—	11009.90	3.91	11020.00	11076.80	1.20	I

A.4 Light Curve Parameters

Table A.2: Light curve parameters.

t_{rise} (days)	t_{max} (JD)	m_{max} (mag)	t_{min} (JD)	m_{min} (mag)	t_{2ndmax} (JD)	m_{2ndmax} (mag)	Δm_{15} (mag)	$t_{-1/2}$ (days)	$t_{+1/2}$ (days)	late slope (mag/day)	Filter
89B											
—	7565.51	12.35	—	—	—	—	0.92	—	12.65	0.0240	bol
—	7563.62	12.40	—	—	—	—	1.55	—	9.72	0.0168	U
—	0.37	0.02	—	—	—	—	0.05	—	0.19	0.0025	
—	7565.07	12.38	—	—	—	—	1.20	—	11.32	0.0129	B
—	0.28	0.01	—	—	—	—	0.03	—	0.17	0.0012	
—	7567.61	12.00	—	—	—	—	0.71	—	15.67	0.0237	V
—	0.49	0.01	—	—	—	—	0.03	—	0.31	0.0015	
—	7565.44	11.84	—	—	—	—	0.47	—	24.46	0.0297	R
—	1.98	0.03	—	—	—	—	0.11	—	1.48	0.0015	
—	—	—	—	—	—	—	—	—	32.45	0.0458	I
—	—	—	—	—	—	—	—	—	18.73	0.0061	
90N											
-25.88	8082.23	11.96	8110.00	13.37	8111.98	13.37	0.82	-9.24	14.16	—	bol
-27.46	8081.70	12.38	—	—	—	—	1.29	-8.14	10.78	—	U
10.42	1.66	0.07	—	—	—	—	0.16	0.63	0.70	—	
-18.84	8083.19	12.77	—	—	—	—	1.05	-10.22	12.27	—	B
0.89	0.15	0.01	—	—	—	—	0.02	0.09	0.11	—	
-25.65	8083.83	12.75	—	—	—	—	0.52	-10.75	19.27	—	V
0.75	0.12	0.01	—	—	—	—	0.01	0.06	0.23	—	
-21.29	8083.45	12.71	8102.91	13.48	8114.52	13.03	0.65	-10.75	17.95	—	R
1.96	0.24	0.06	0.40	0.02	0.62	0.38	0.30	0.36	5.41	—	
-12.66	8081.23	12.99	8099.60	13.56	8114.26	12.94	0.51	-9.60	41.73	—	I
13.03	11.52	0.11	0.53	0.03	11.61	0.27	0.62	0.61	8.84	—	
continued on next page											

t_{rise}	t_{max}	m_{max}	t_{min}	m_{min}	t_{2ndmax}	m_{2ndmax}	Δm_{15}	$t_{-1/2}$	$t_{+1/2}$	late slope	Filter
90O											
—	8076.19	16.60	—	—	—	—	—	—	—	—	B
—	8073.27	16.51	—	—	—	—	—	—	—	—	V
—	—	—	8087.96	17.63	8102.81	17.31	—	—	—	—	I
90T											
—	—	—	—	—	—	—	—	—	—	0.0242	bol
—	—	—	—	—	—	—	—	—	—	0.0150	B
—	—	—	—	—	—	—	—	—	—	0.0209	V
—	—	—	8102.85	18.00	8108.00	17.90	—	-2.55	21.36	0.0319	R
—	—	—	8104.84	18.02	8110.59	17.96	—	-4.92	25.60	0.0348	I
90Y											
—	—	—	8160.20	18.79	8167.33	18.66	—	—	18.47	—	R
90af											
—	—	—	—	—	—	—	—	—	9.64	—	bol
—	8195.96	17.93	—	—	—	—	1.60	—	9.40	—	B
—	0.14	0.00	—	—	—	—	0.03	—	0.03	—	
—	8197.17	17.85	—	—	8202.19	17.93	0.90	—	13.25	—	V
—	0.03	0.00	—	—	3.89	1.35	0.00	—	0.03	—	

t_{rise}	t_{max}	m_{max}	t_{min}	m_{min}	t_{2ndmax}	m_{2ndmax}	Δm_{15}	$t_{-1/2}$	$t_{+1/2}$	late slope	Filter
91T											
-18.25	8376.21	11.60	—	—	—	—	0.85	-11.60	13.71	0.0290	bol
—	8374.05	11.25	—	—	—	—	1.28	—	10.96	0.0225	U
—	0.34	0.01	—	—	—	—	0.04	—	0.19	0.0014	
-18.43	8376.29	11.70	—	—	—	—	1.00	-11.46	12.66	0.0155	B
0.67	0.12	0.00	—	—	—	—	0.01	0.06	0.07	0.0004	
-26.09	8379.04	11.51	—	—	—	—	0.66	-13.60	16.91	0.0265	V
2.01	0.30	0.01	—	—	—	—	0.02	0.06	0.23	0.0006	
-22.05	8378.34	11.44	—	—	—	—	0.61	-13.08	21.53	0.0318	R
0.45	0.12	0.01	—	—	—	—	0.01	0.05	0.44	0.0006	
—	8375.83	11.66	8390.50	12.07	8398.40	12.05	0.41	—	38.12	0.0402	I
—	4.77	0.08	1.25	0.01	4.89	0.09	0.02	—	1.49	0.0008	
—	—	—	—	—	—	—	—	—	—	0.0118	B
—	—	—	—	—	—	—	—	—	—	0.0248	V
—	—	—	—	—	—	—	—	—	24.68	0.0405	I
91bg											
—	8605.80	14.24	—	—	—	—	1.42	—	8.92	0.0303	bol
—	—	—	—	—	—	—	—	-3.28	6.29	0.0220	B
—	—	—	—	—	—	—	—	3.32	0.92	0.0006	
—	8606.66	13.99	—	—	—	—	1.45	-9.52	8.06	0.0310	V
—	5.91	0.23	—	—	—	—	0.41	2.77	2.52	0.0008	
-21.49	8606.93	13.62	—	—	—	—	1.28	—	9.92	0.0399	R
18.20	0.76	0.04	—	—	—	—	0.09	—	0.74	0.0019	
—	8607.10	13.52	—	—	—	—	0.81	—	14.24	0.0316	I
—	1.73	0.15	—	—	—	—	0.23	—	1.46	0.0016	

continued on next page

t_{rise}	t_{max}	m_{max}	t_{min}	m_{min}	t_{2ndmax}	m_{2ndmax}	Δm_{15}	$t_{-1/2}$	$t_{+1/2}$	late slope	Filter
92A											
-11.04	8640.98	12.79	—	—	—	—	1.14	-7.65	10.34	0.0273	bol
-12.49 0.89	8640.24 0.08	12.60 0.01	—	—	—	—	1.38 0.01	-6.90 0.06	10.27 0.08	0.0120 0.0003	B
-14.04 1.14	8642.60 0.15	12.55 0.01	—	—	—	—	0.85 0.01	-9.13 0.07	13.24 0.17	0.0285 0.0002	V
-12.84 7.03	8642.02 0.14	12.53 0.01	—	—	—	—	0.73 0.01	-9.20 1.18	16.93 0.59	0.0341 0.0003	R
-36.81 8.88	8639.21 6.15	12.78 0.10	8652.86 0.17	13.36 0.01	8661.97 6.13	13.16 0.10	0.56 0.14	—	29.90 1.05	0.0452 0.0004	I
92K											
—	—	—	—	—	—	—	—	—	—	0.0216	B
—	—	—	—	—	—	—	—	—	—	0.0295	V
92P											
—	8718.96	16.14	—	—	—	—	0.94	—	13.22	0.0162	B
—	—	—	—	—	—	—	—	—	—	0.0273	V
92ag											
—	—	—	—	—	—	—	—	—	19.19	—	V
—	—	—	—	—	—	—	—	—	26.21	—	I
continued on next page											

t_{rise}	t_{max}	m_{max}	t_{min}	m_{min}	t_{2ndmax}	m_{2ndmax}	Δm_{15}	$t_{-1/2}$	$t_{+1/2}$	late slope	Filter
92al											
—	—	—	—	—	—	—	—	—	—	0.0251	bol
-14.56 28.33	8838.63 0.29	14.60 0.02	— —	— —	— —	— —	1.14 0.03	-8.68 1.56	11.69 0.22	0.0150 0.0005	B
-27.92 6.26	8839.43 0.42	14.63 0.02	— —	— —	— —	— —	0.65 0.03	— —	16.62 0.44	0.0257 0.0005	V
— —	8841.38 1.02	14.65 0.03	— —	— —	— —	— —	0.75 0.04	— —	15.46 3.13	0.0310 0.0008	R
— —	8841.68 0.46	15.01 0.03	8853.57 1.40	15.63 0.02	8864.72 1.32	15.44 0.04	0.57 0.04	— —	33.07 1.01	0.0382 0.0009	I
92aq											
—	8836.02	19.31	—	—	—	—	—	—	14.22	—	V
—	—	—	8845.01	20.13	8845.95	20.12	—	-1.75	22.43	—	I
92au											
—	—	—	8862.69	15.03	8865.37	15.02	—	—	—	—	bol
—	—	—	8881.39	21.77	—	—	—	—	—	—	B
92bc											
-16.12 0.86	8912.71 0.20	11.94 0.01	— —	— —	— —	— —	0.92 0.02	-9.48 0.09	13.07 0.19	0.0249 0.0005	bol
-18.09 2.13	8912.87 0.28	15.18 0.01	— —	— —	— —	— —	0.87 0.03	-9.90 0.10	13.82 0.50	0.0154 0.0008	B
-23.39 -19.54	8912.95 8913.50	15.22 15.23	— —	— —	— —	— —	0.60 0.73	-9.51 -10.51	17.54 15.40	0.0253 0.0301	V
0.81	0.37	0.01	—	—	—	—	0.04	0.10	0.57	0.0005	R
-37.67 7.43	8910.08 0.26	15.52 0.02	8932.91 0.97	16.45 0.03	8945.72 2.30	16.29 0.03	0.76 0.03	— —	14.84 0.74	0.0397 0.0032	I

continued on next page

t_{rise}	t_{max}	m_{max}	t_{min}	m_{min}	t_{2ndmax}	m_{2ndmax}	Δm_{15}	$t_{-1/2}$	$t_{+1/2}$	late slope	Filter	
92bg												
—	—	—	—	—	—	—	—	—	—	—	I	
—	—	—	—	—	—	—	—	—	—	—		
92bh												
—	8919.94	17.69	—	—	—	—	1.08	—	11.90	—	B	
—	8921.59	17.61	—	—	—	—	0.56	—	17.91	—	V	
—	—	—	8940.02	18.47	8949.16	18.27	—	—	—	—	I	
92bl												
—	—	—	—	—	—	—	—	—	—	—	V	
—	—	—	8957.61	18.44	8968.37	18.14	—	—	—	—	I	
92bo												
-14.61	8986.83	12.72	—	—	—	—	1.25	-8.15	9.70	—	bol	
-13.76 4.98	8986.77 0.22	15.84 0.02	—	—	—	—	1.73 0.05	-7.86 0.11	8.75 0.16	—	B	
-21.44 3.99	8987.36 0.25	15.84 0.02	—	—	—	—	0.89 0.03	-8.47 0.12	13.41 0.30	—	V	
-17.69 7.00	8987.74 0.76	15.76 0.03	—	—	—	—	0.73 0.18	-9.43 0.25	16.72 3.51	—	R	
-23.94 9.10	8984.26 0.56	15.95 0.04	8999.40 2.57	16.58 0.07	9005.79 1.74	16.52 0.08	0.62 0.05	-6.79 0.55	27.29 3.29	—	I	
92bp												
—	—	—	—	—	—	—	—	—	—	10.62	—	bol
—	8980.12 0.49	18.57 0.03	—	—	—	—	1.25 0.08	—	11.09 0.29	—	B	
—	8981.41 0.53	18.53 0.02	—	—	—	—	0.65 0.05	—	16.39 0.37	—	V	
—	—	—	8994.70 1.43	19.50 0.06	9006.60 1.12	19.10 0.46	—	—	8.72 8.80	—	I	

continued on next page

t_{rise}	t_{max}	m_{max}	t_{min}	m_{min}	t_{2ndmax}	m_{2ndmax}	Δm_{15}	$t_{-1/2}$	$t_{+1/2}$	late slope	Filter
92br											
—	—	—	—	—	—	—	—	—	—	5.87	—
—	8985.55	19.42	—	—	—	—	1.11	—	—	—	B
92bs											
—	8986.56	18.39	—	—	—	—	—	—	—	—	B
—	8986.95	18.28	—	—	—	—	—	—	—	—	V
93B											
—	—	—	9018.09	19.37	9027.78	19.19	—	—	—	—	I
—	—	—	2.46	0.06	6.45	0.12	—	—	—	—	
93H											
—	9069.69	12.75	—	—	—	—	1.23	—	10.01	0.0314	bol
—	9069.24	17.03	—	—	—	—	1.77	—	8.21	0.0221	B
—	0.45	0.02	—	—	—	—	0.06	—	0.22	0.0009	
—	9071.08	16.73	—	—	—	—	1.01	—	11.89	0.0298	V
—	0.61	0.06	—	—	—	—	0.11	—	0.56	0.0014	
—	9069.96	16.57	—	—	—	—	0.78	—	14.58	0.0369	R
—	0.45	0.02	—	—	—	—	0.04	—	0.39	0.0018	
—	—	—	9081.34	17.11	9085.16	17.09	—	—	—	0.0462	I
—	—	—	1.35	0.03	2.09	0.14	—	—	—	0.0014	
93O											
—	9134.23	12.30	—	—	—	—	1.07	—	11.39	—	bol
-26.95	9133.82	17.79	—	—	—	—	1.24	-7.92	10.84	—	B
8.18	0.43	0.02	—	—	—	—	0.05	0.51	0.23	—	
-15.86	9136.55	17.85	—	—	—	—	0.71	-11.59	15.61	—	V
21.75	0.65	0.02	—	—	—	—	0.05	2.57	0.36	—	
—	9135.03	18.05	9151.79	18.78	9161.75	18.60	0.71	—	32.91	—	I
—	0.97	0.02	0.46	0.02	0.77	0.03	0.04	—	7.50	—	

continued on next page

t_{rise}	t_{max}	m_{max}	t_{min}	m_{min}	t_{2ndmax}	m_{2ndmax}	Δm_{15}	$t_{-1/2}$	$t_{+1/2}$	late slope	Filter
93ae											
—	—	—	—	—	—	—	—	—	—	0.0228	V
—	9310.25	16.06	—	—	—	—	—	-10.05	12.44	—	I
93ag											
—	9317.28	12.31	—	—	—	—	1.09	—	10.97	0.0254	bol
—	9316.54	18.28	—	—	—	—	1.25	—	10.86	0.0144	B
—	0.53	0.03	—	—	—	—	0.10	—	0.37	0.0015	
—	9318.00	18.13	—	—	—	—	0.61	—	17.00	0.0239	V
—	0.59	0.03	—	—	—	—	0.05	—	0.56	0.0009	
—	—	—	9330.50	18.85	9341.08	18.57	—	-4.40	11.14	0.0405	I
—	—	—	1.46	0.08	1.75	0.24	—	1.29	10.77	0.0036	
94D											
-16.42	9432.54	12.72	—	—	—	—	1.18	-7.92	10.29	0.0263	bol
-14.31	9432.31	11.30	—	—	—	—	1.99	-7.55	8.14	0.0220	U
0.49	0.19	0.02	—	—	—	—	0.05	0.13	0.13	0.0010	
-17.51	9432.90	11.86	—	—	—	—	1.46	-8.08	9.88	0.0158	B
0.69	0.18	0.02	—	—	—	—	0.03	0.11	0.16	0.0008	
-21.35	9433.06	11.90	—	—	—	—	0.81	-8.24	14.07	0.0275	V
1.77	0.36	0.07	—	—	—	—	0.08	0.17	0.61	0.0009	
-19.50	9432.17	11.86	—	—	—	—	0.81	-7.73	13.40	0.0328	R
1.02	0.23	0.02	—	—	—	—	0.03	0.12	0.75	0.0009	
-17.44	9429.62	12.10	9445.30	12.73	9453.97	12.59	0.63	-6.14	30.57	0.0434	I
0.43	0.05	0.00	0.19	0.01	0.15	0.01	0.01	0.03	0.11	0.0003	

t_{rise}	t_{max}	m_{max}	t_{min}	m_{min}	t_{2ndmax}	m_{2ndmax}	Δm_{15}	$t_{-1/2}$	$t_{+1/2}$	late slope	Filter
94ae											
-19.13	9685.40	12.40	—	—	—	—	0.95	-9.30	12.68	0.0232	bol
-19.42 0.43	9685.47 0.16	13.23 0.01	— —	— —	— —	— —	0.95 0.01	-9.47 0.08	13.04 0.15	0.0149 0.0004	B
-22.65 2.15	9685.65 1.06	13.09 0.06	— —	— —	— —	— —	0.62 0.08	-9.34 0.34	17.34 0.90	0.0251 0.0013	V
-20.06 0.35	9686.50 0.40	12.99 0.01	— —	— —	— —	— —	0.73 0.03	-10.76 0.10	15.50 0.53	0.0290 0.0006	R
-22.29 2.83	9682.55 0.32	13.33 0.03	9702.88 1.05	14.08 0.03	9714.64 1.67	13.84 0.08	0.65 0.03	-7.68 0.16	19.84 9.69	0.0339 0.0052	I
95D											
-12.90	9768.96	12.03	—	—	—	—	0.94	—	12.80	0.0242	bol
— —	9768.87 0.36	13.45 0.02	— —	— —	— —	— —	0.99 0.04	— —	12.76 0.24	0.0128 0.0013	B
-30.39 7.58	9769.72 0.22	13.40 0.01	— —	— —	— —	— —	0.63 0.01	-10.40 0.36	17.33 0.19	0.0250 0.0013	V
-15.80 1.33	9769.91 0.32	13.49 0.01	— —	— —	— —	— —	0.64 0.01	-10.59 0.21	22.50 1.94	0.0315 0.0009	R
— —	9766.70 0.24	13.65 0.01	9786.02 0.29	14.32 0.01	9797.98 0.26	14.15 0.01	0.61 0.01	-9.39 0.60	39.34 0.22	0.0326 0.0010	I

continued on next page

t_{rise}	t_{max}	m_{max}	t_{min}	m_{min}	t_{2ndmax}	m_{2ndmax}	Δm_{15}	$t_{-1/2}$	$t_{+1/2}$	late slope	Filter
95E											
—	9775.24	11.69	—	—	—	—	1.00	—	12.25	—	bol
—	9774.78	16.83	—	—	—	—	1.09	—	12.02	—	B
—	0.59	0.03	—	—	—	—	0.12	—	0.39	—	
—	9775.79	16.08	—	—	—	—	0.55	—	18.25	0.0241	V
—	0.66	0.02	—	—	—	—	0.05	—	0.62	0.0029	
—	9776.91	15.54	—	—	—	—	0.76	—	14.87	0.0317	R
—	4.73	0.04	—	—	—	—	0.18	—	2.15	0.0023	
—	9773.40	15.35	9792.13	16.01	9801.55	15.85	0.61	—	34.46	0.0437	I
—	1.50	0.04	1.45	0.04	1.23	0.04	0.07	—	4.44	0.0021	
95ac											
—	9992.99	11.61	—	—	—	—	0.85	—	13.82	—	bol
—	9992.24	17.23	—	—	—	—	0.91	—	13.42	—	B
—	0.27	0.02	—	—	—	—	0.03	—	0.19	—	
—	9994.83	17.22	—	—	—	—	0.57	-9.75	17.91	—	V
—	2.61	0.10	—	—	—	—	0.16	5.46	0.80	—	
—	9995.67	17.09	10014.97	17.77	10020.51	17.69	0.60	—	28.56	—	R
—	1.31	0.05	1.07	0.03	1.21	0.19	0.08	—	3.62	—	
—	9992.42	17.31	10009.85	17.71	10018.29	17.66	0.39	—	38.12	—	I
—	5.92	0.05	1.07	0.02	2.50	0.05	0.12	—	0.92	—	

continued on next page

t_{rise}	t_{max}	m_{max}	t_{min}	m_{min}	t_{2ndmax}	m_{2ndmax}	Δm_{15}	$t_{-1/2}$	$t_{+1/2}$	late slope	Filter
95ak											
—	—	—	—	—	—	—	—	—	—	8.18	0.0363
—	—	—	—	—	—	—	—	—	—	0.0237	B
—	—	—	—	—	—	—	—	—	—	0.0025	
—	—	—	—	—	—	—	—	—	11.31	0.0309	V
—	—	—	—	—	—	—	—	—	2.71	0.0017	
—	—	—	—	—	10041.35	16.52	—	—	—	0.0404	R
—	—	—	—	—	1.26	0.15	—	—	—	0.0015	
—	—	—	—	—	10051.27	16.48	—	—	—	—	I
—	—	—	—	—	1.87	0.04	—	—	—	—	
95al											
—	10029.98	12.22	—	—	—	—	0.92	—	12.89	0.0236	bol
—	10029.89	13.39	—	—	—	—	1.00	—	12.72	0.0139	
—	0.38	0.02	—	—	—	—	0.04	—	0.27	0.0006	
—	10030.57	13.24	—	—	—	—	0.55	—	18.50	0.0259	V
—	0.90	0.03	—	—	—	—	0.04	—	0.59	0.0006	
—	10029.20	13.22	—	—	—	—	0.63	-5.99	23.95	0.0312	R
—	3.77	0.05	—	—	—	—	0.14	4.36	4.34	0.0010	
—	10027.53	13.49	10045.60	14.06	10057.53	13.84	0.53	—	39.34	0.0354	I
—	0.57	0.04	1.04	0.03	1.91	0.09	0.05	—	1.26	0.0016	

continued on next page

t_{rise}	t_{max}	m_{max}	t_{min}	m_{min}	t_{2ndmax}	m_{2ndmax}	Δm_{15}	$t_{-1/2}$	$t_{+1/2}$	late slope	Filter
95bd											
-17.09	10086.66	11.93	—	—	—	—	0.94	-9.28	12.76	—	bol
-20.08 2.34	10085.54 0.17	17.29 0.01	—	—	—	—	0.85 0.02	-8.26 0.13	13.80 0.23	—	B
-21.46 7.52	10087.68 0.47	16.49 0.02	—	—	—	—	0.70 0.03	-9.85 0.16	15.95 0.47	0.0264 0.0015	V
-19.29 1.98	10089.46 0.63	16.06 0.02	10108.40 2.29	16.91 0.08	10114.06 2.58	16.89 1.53	0.81 0.03	-11.99 0.19	13.46 0.55	—	R
-15.78 7.73	10085.11 0.52	16.03 0.03	10104.54 0.90	16.71 0.02	10117.51 0.98	16.42 0.07	0.60 0.04	-8.87 0.56	40.84 0.80	—	I
96C											
—	—	—	—	—	—	—	—	—	—	0.0244	bol
—	—	—	—	—	—	—	—	—	—	0.0147	B
—	—	—	—	—	—	—	—	—	—	0.0006	
—	—	—	10149.17	17.24	10152.46	17.23	—	—	12.82	0.0318	R
—	—	—	0.98	0.04	1.50	0.04	—	—	3.13	0.0020	
—	—	—	10144.59	17.51	10156.12	17.30	—	—	33.55	—	I
—	—	—	0.75	0.02	6.61	0.11	—	—	1.85	—	
96X											
—	10191.67	11.80	—	—	—	—	1.10	—	11.27	—	bol
—	10191.49 0.22	13.28 0.02	—	—	—	—	1.29 0.04	—	10.73 0.21	—	B
—	10192.17 0.50	13.22 0.01	—	—	—	—	0.69 0.04	-6.68 3.33	16.01 0.34	—	V
—	10193.62 8.43	13.16 0.06	—	—	—	—	0.81 0.33	—	12.36 3.06	—	R
—	10189.00 4.35	13.37 0.03	10207.46 1.77	13.99 0.02	10216.40 0.94	13.88 0.04	0.58 0.06	—	34.49 1.62	—	I

continued on next page

t_{rise}	t_{max}	m_{max}	t_{min}	m_{min}	t_{2ndmax}	m_{2ndmax}	Δm_{15}	$t_{-1/2}$	$t_{+1/2}$	late slope	Filter
96ai											
—	—	—	—	—	10271.52	15.46	—	—	20.37	—	V
—	—	—	—	—	—	—	—	—	23.70	—	R
—	—	—	10271.59	14.56	10282.32	14.42	—	—	—	—	I
96bk											
—	—	—	—	—	—	—	—	—	11.47	—	V
—	—	—	—	—	—	—	—	-10.72	9.47	—	I
96bl											
—	—	—	—	—	—	—	—	—	12.12	—	bol
—	—	—	—	—	—	—	—	—	11.39	—	B
—	—	—	—	—	—	—	—	—	18.77	—	V
—	—	—	10394.28	17.76	10404.75	17.45	—	—	12.71	—	I
96bo											
—	10387.39	11.92	—	—	—	—	1.06	—	11.45	—	bol
—	10387.10	16.16	—	—	—	—	1.26	-7.83	10.74	—	B
—	0.22	0.01	—	—	—	—	0.03	1.27	0.13	—	
—	10388.72	15.76	—	—	—	—	0.70	-8.58	16.12	—	V
—	0.22	0.01	—	—	—	—	0.02	0.41	0.36	—	
—	10388.13	15.44	—	—	—	—	0.74	-7.75	15.73	—	R
—	0.21	0.01	—	—	—	—	0.01	1.01	0.48	—	
—	10386.18	15.69	10401.96	16.20	10411.36	15.97	0.51	—	33.51	—	I
—	5.30	0.02	0.18	0.01	0.43	0.02	0.14	—	1.06	—	
96bv											
—	—	—	10417.99	15.97	10426.50	15.81	—	—	—	—	I

t_{rise}	t_{max}	m_{max}	t_{min}	m_{min}	t_{2ndmax}	m_{2ndmax}	Δm_{15}	$t_{-1/2}$	$t_{+1/2}$	late slope	Filter
97br											
-37.15 12.62	10559.67 0.17	14.07 0.02	— —	— —	— —	— —	— —	-10.01 0.31	11.62 0.23	0.0163 0.0011	B
-21.71 2.99	10563.92 0.60	13.78 0.02	— —	— —	— —	— —	0.65 0.04	-14.19 0.29	16.76 0.37	0.0269 0.0017	V
-18.99 8.78	10561.51 0.51	13.75 0.02	— —	— —	— —	— —	0.41 0.03	-11.92 0.40	28.70 0.69	— —	R
98bu											
-18.30	10952.37	12.04	—	—	—	—	0.92	—	13.04	—	bol
— —	10950.62 0.17	11.92 0.01	— —	— —	— —	— —	1.19 0.03	— —	11.15 0.16	— —	U
-27.97 10.83	10952.51 0.16	12.21 0.00	— —	— —	— —	— —	1.01 0.02	-7.89 0.54	12.72 0.07	— —	B
-20.65 7.58	10954.46 0.09	11.86 0.00	— —	— —	— —	— —	0.75 0.01	-9.86 0.39	15.12 0.08	— —	V
-14.44 1.01	10954.85 0.15	11.67 0.01	10971.91 0.32	12.47 0.00	10973.10 0.39	12.47 0.00	0.79 0.01	-10.53 0.42	12.86 0.29	— —	R
-16.94 2.94	10950.23 0.09	11.65 0.01	10968.57 0.17	12.31 0.01	10978.71 0.12	12.12 0.01	0.62 0.01	-6.45 0.31	35.11 0.11	— —	I
— — —	10948.10 — 10948.98	11.57 — 11.47	10971.73 10960.61	13.36 11.98	10982.90 10976.03	12.60 11.74	1.15 —	— —	— —	— —	J H K

continued on next page

t_{rise}	t_{max}	m_{max}	t_{min}	m_{min}	t_{2ndmax}	m_{2ndmax}	Δm_{15}	$t_{-1/2}$	$t_{+1/2}$	late slope	Filter
98de											
-16.24	11027.55	14.14	—	—	—	—	1.26	-6.72	10.09	—	bol
-15.22 7.44	11026.37 0.15	17.60 0.01	— —	— —	— —	— —	1.97 0.04	-5.49 0.20	6.57 0.17	— —	B
-19.93 3.57	11028.08 0.12	16.85 0.01	— —	— —	— —	— —	1.30 0.02	-7.17 0.09	10.00 0.17	— —	V
-26.68 3.40	11028.81 0.14	16.63 0.01	— —	— —	— —	— —	0.98 0.02	-8.10 0.09	12.44 0.18	— —	R
-19.92 1.34	11031.47 0.55	16.63 0.01	— —	— —	— —	— —	0.79 0.06	-10.43 0.13	14.54 0.29	— —	I

A.5 *UBVRI* Light Curves

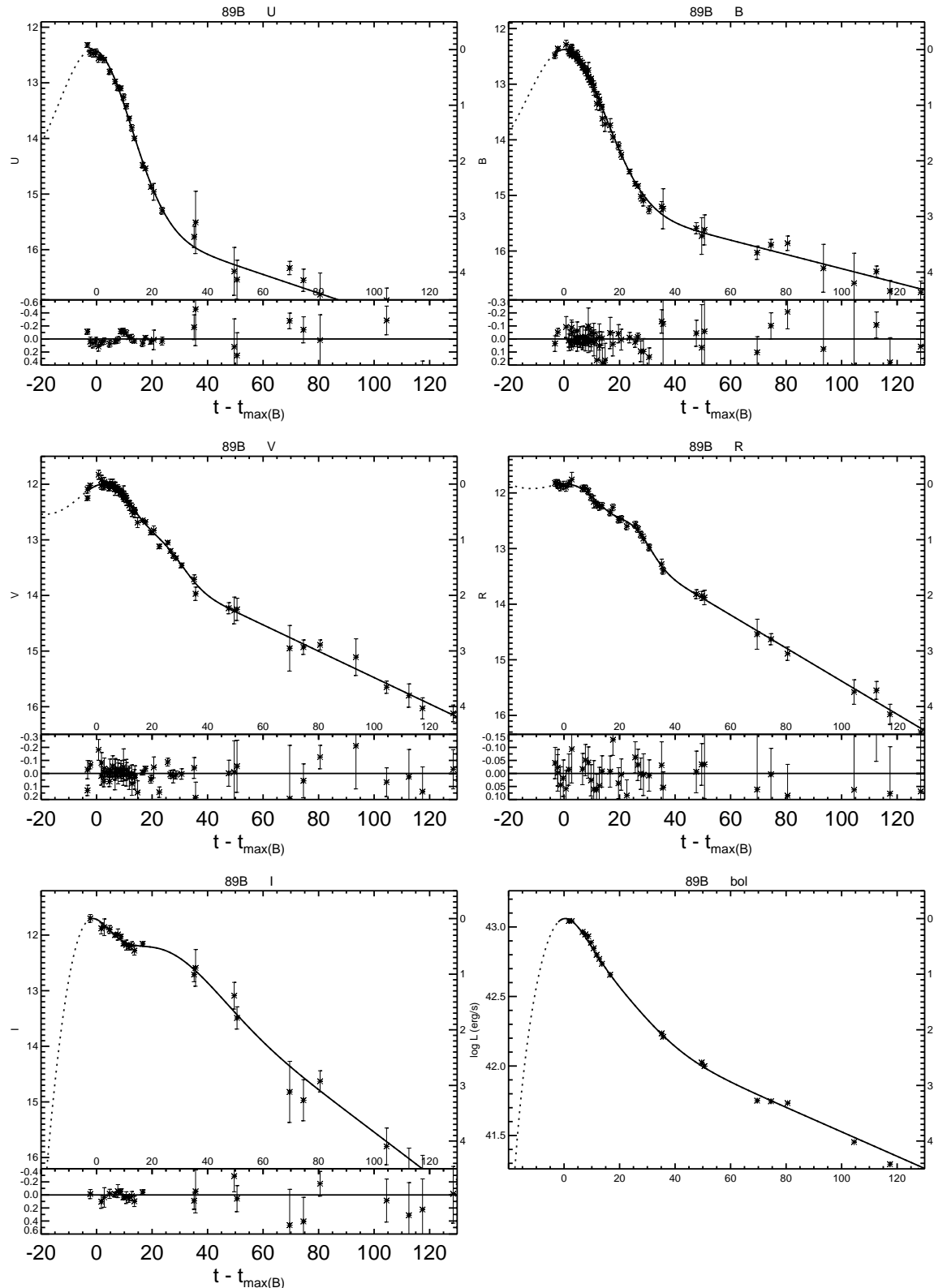


Figure A.1: *UBVRI* light curves of SN 1989B.

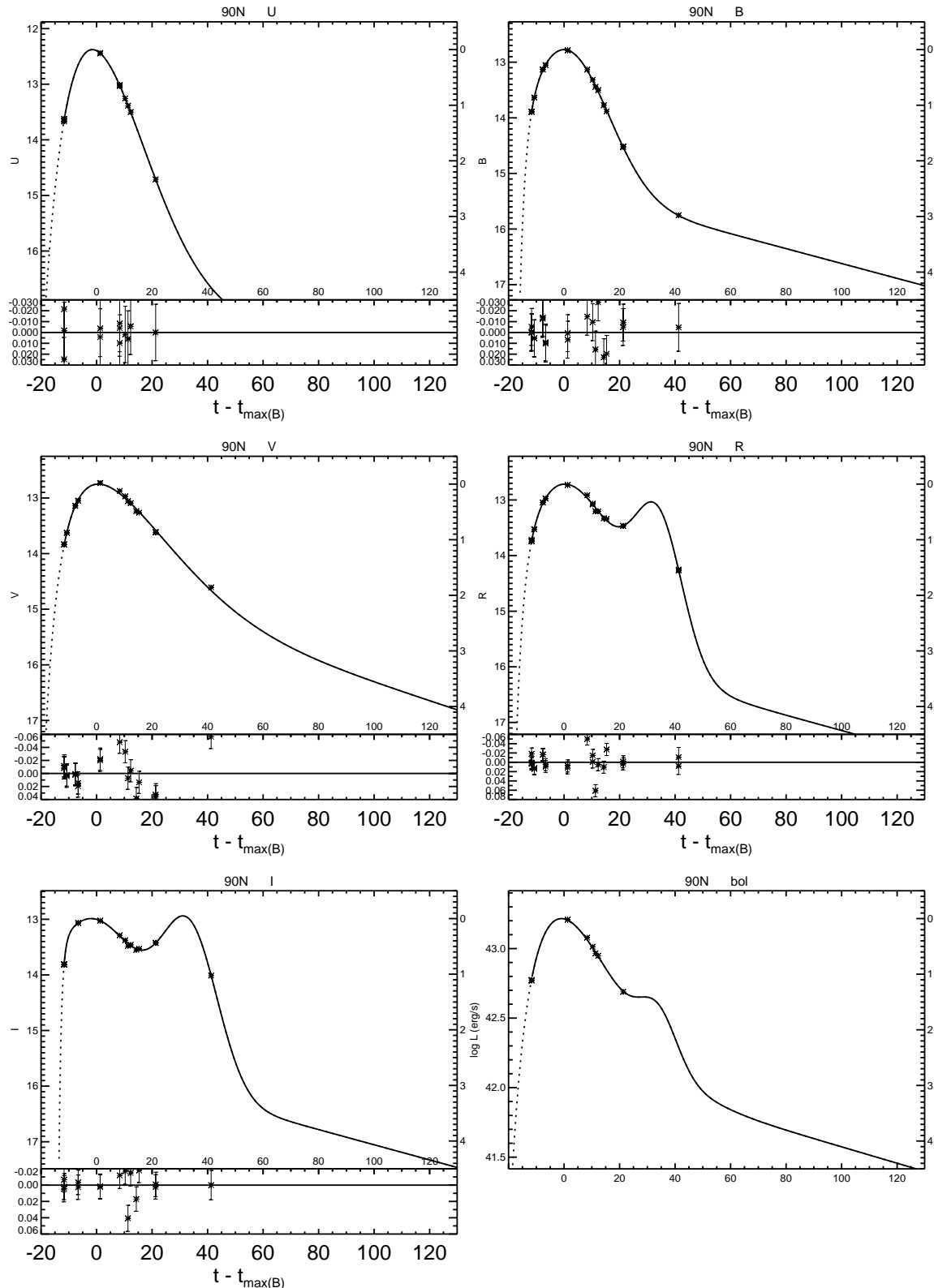


Figure A.2: *UBVRI* light curves of SN 1990N.

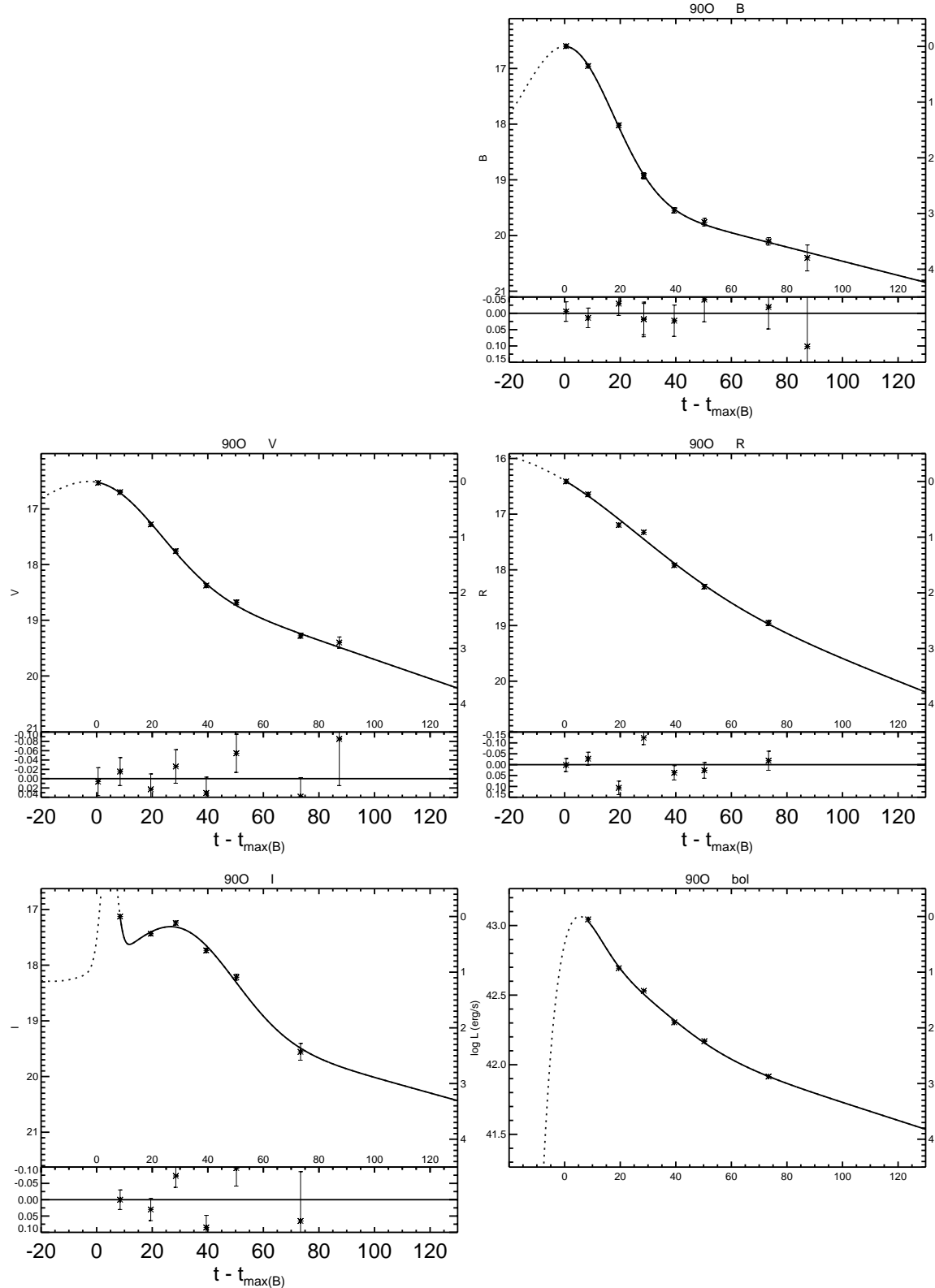


Figure A.3: *UBVRI* light curves of SN 1990O.

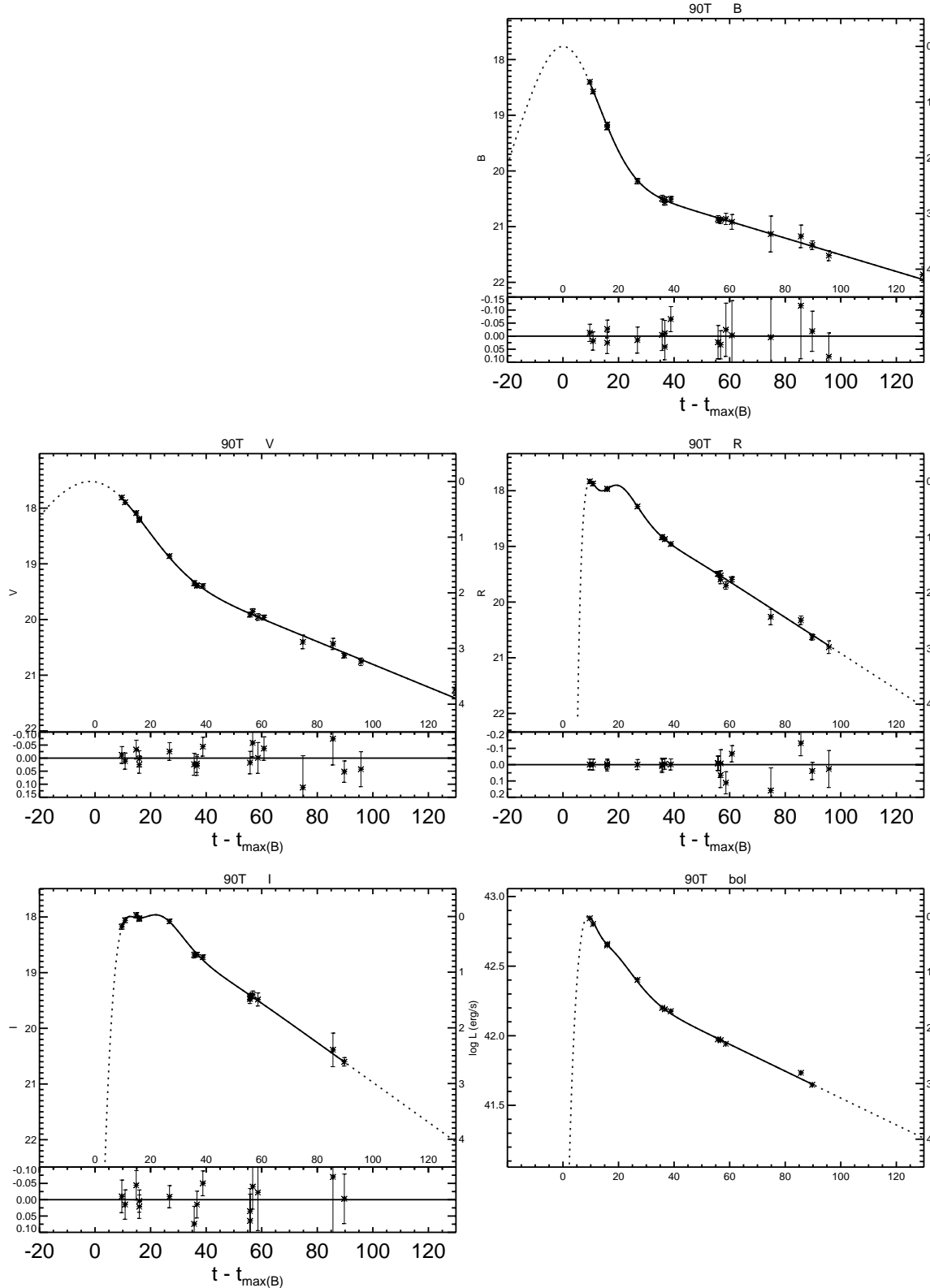


Figure A.4: *UBVRI* light curves of SN 1990T.

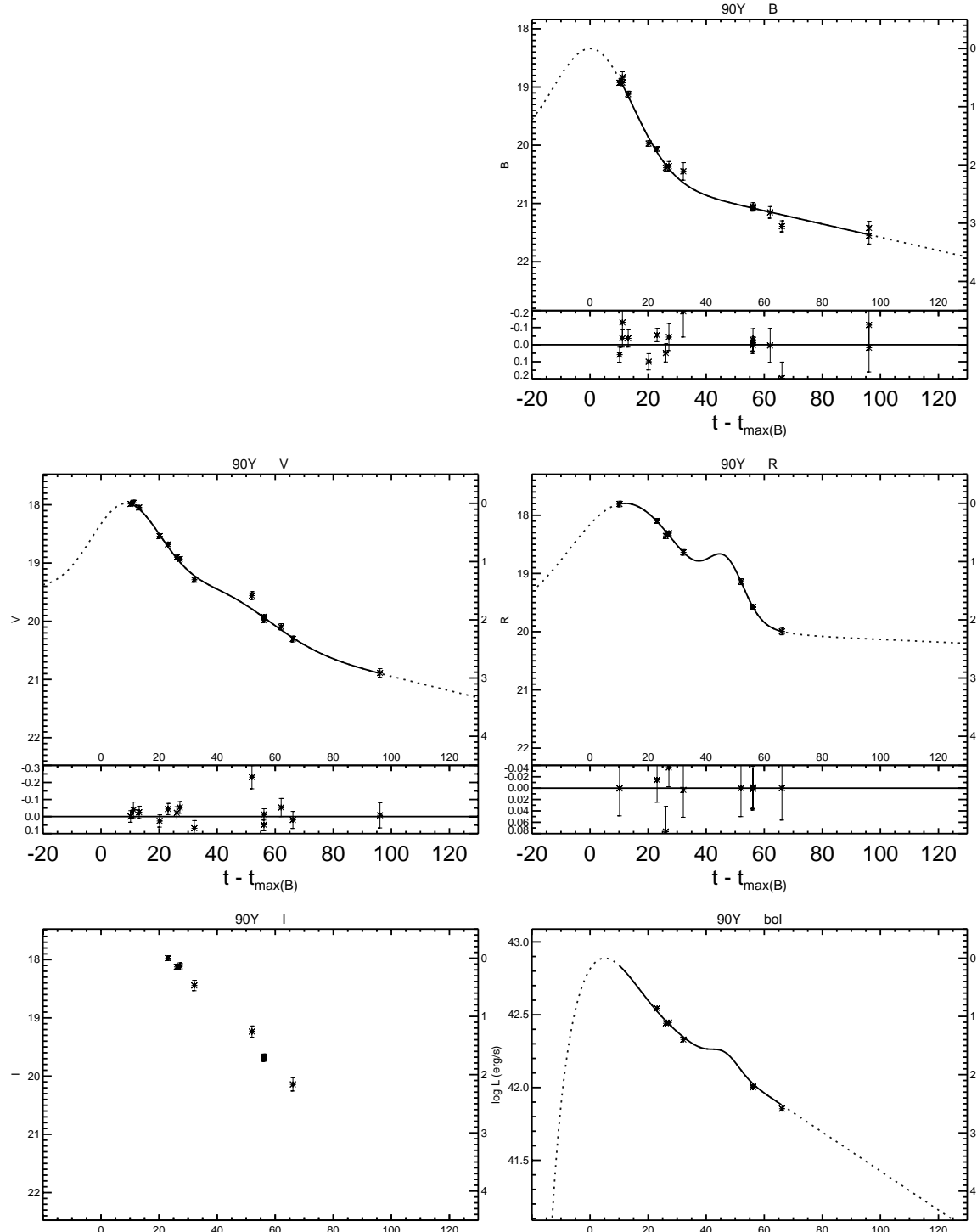


Figure A.5: *UBVRI* light curves of SN 1990Y.

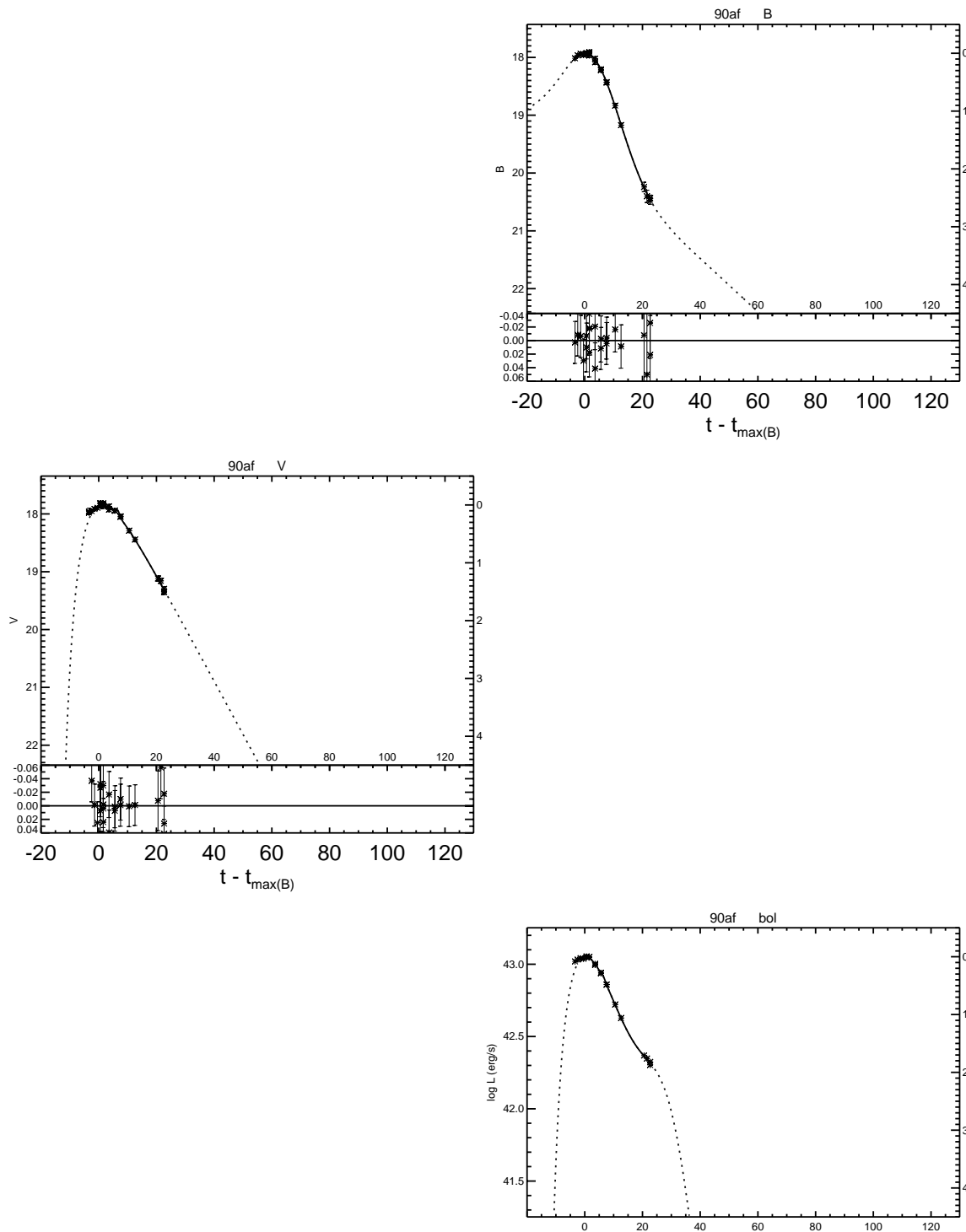


Figure A.6: $UBVRI$ light curves of SN 1990af.

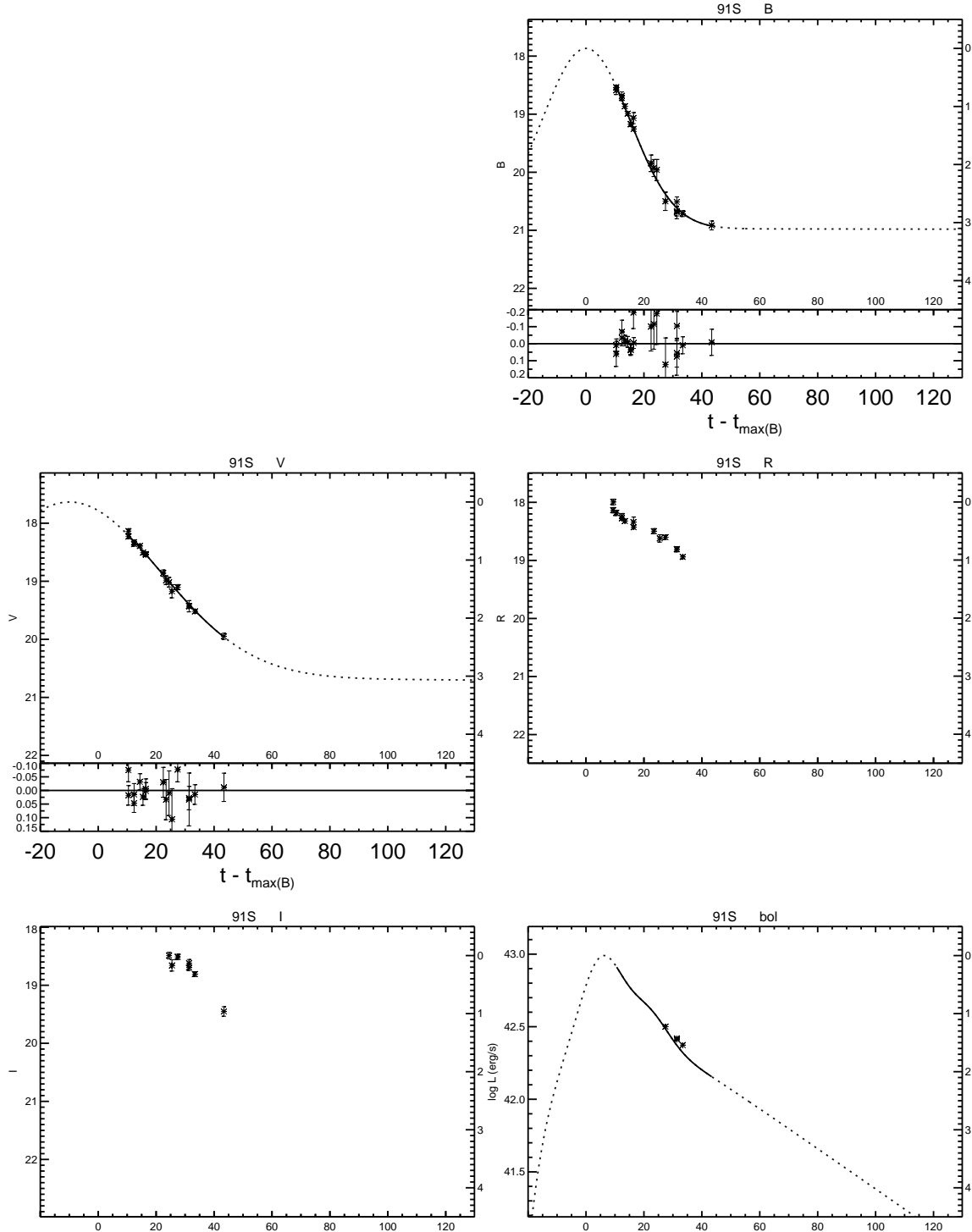


Figure A.7: *UBVRI* light curves of SN 1991S.

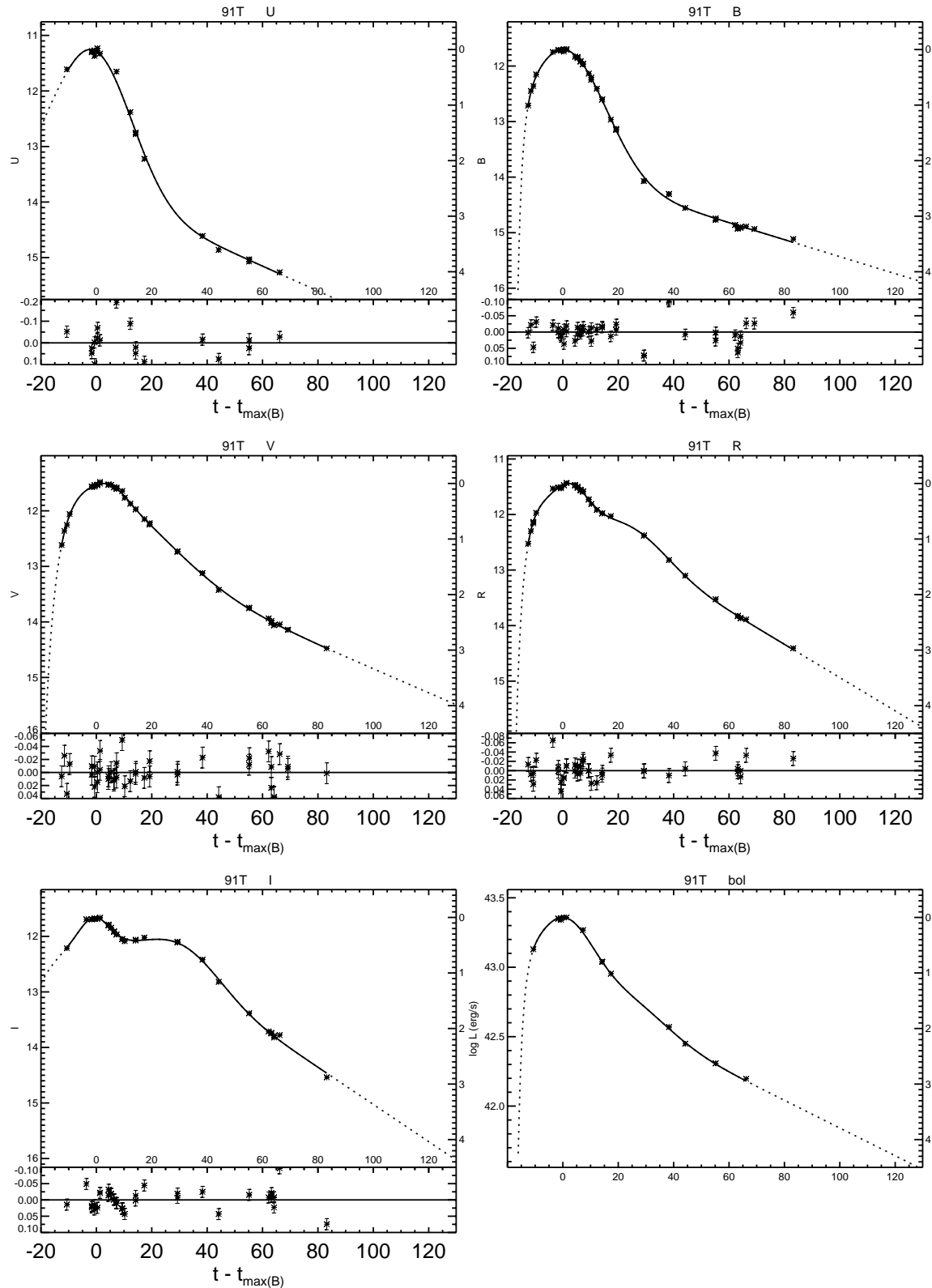


Figure A.8: *UBVRI* light curves of SN 1991T.

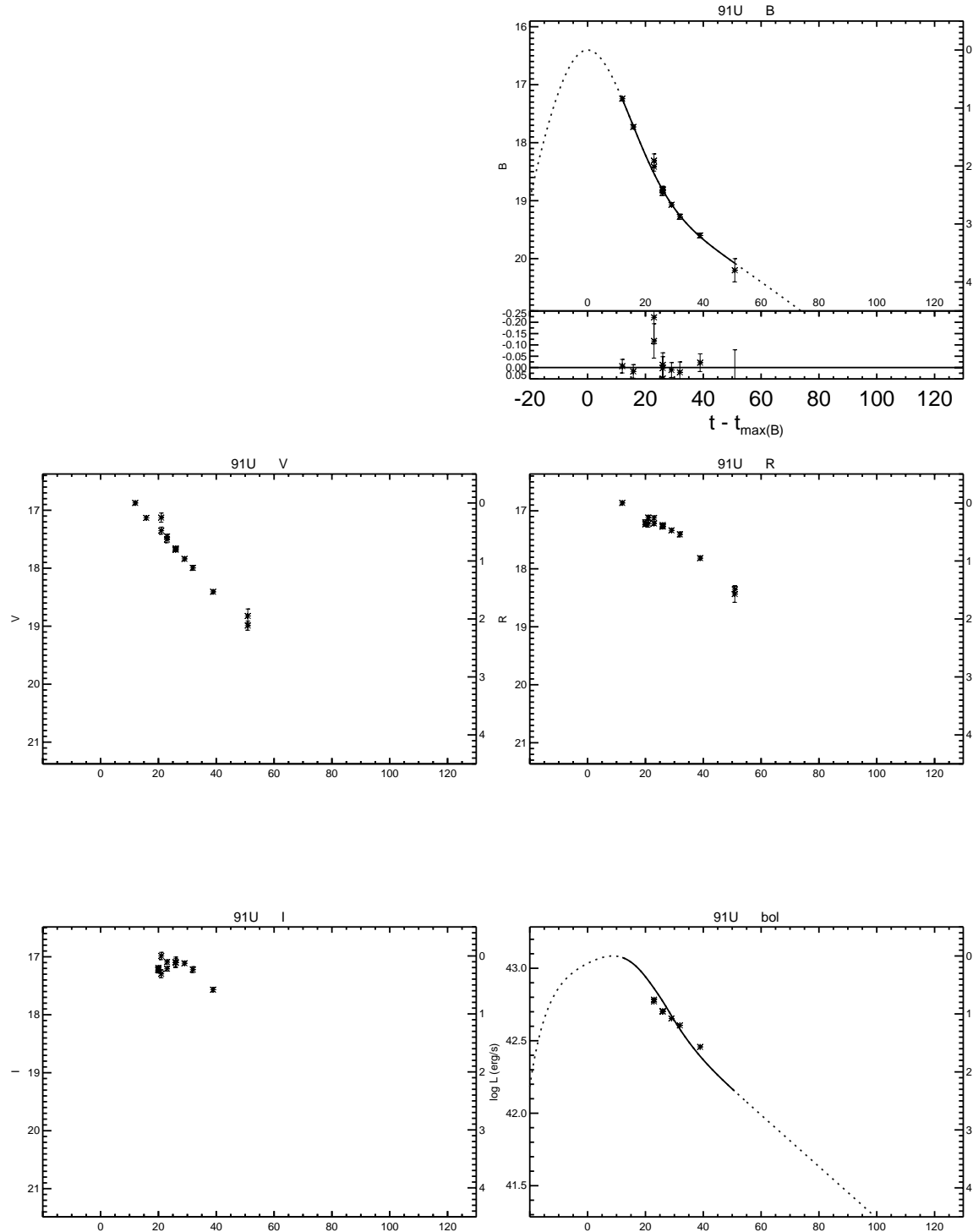


Figure A.9: *UBVRI* light curves of SN 1991U.

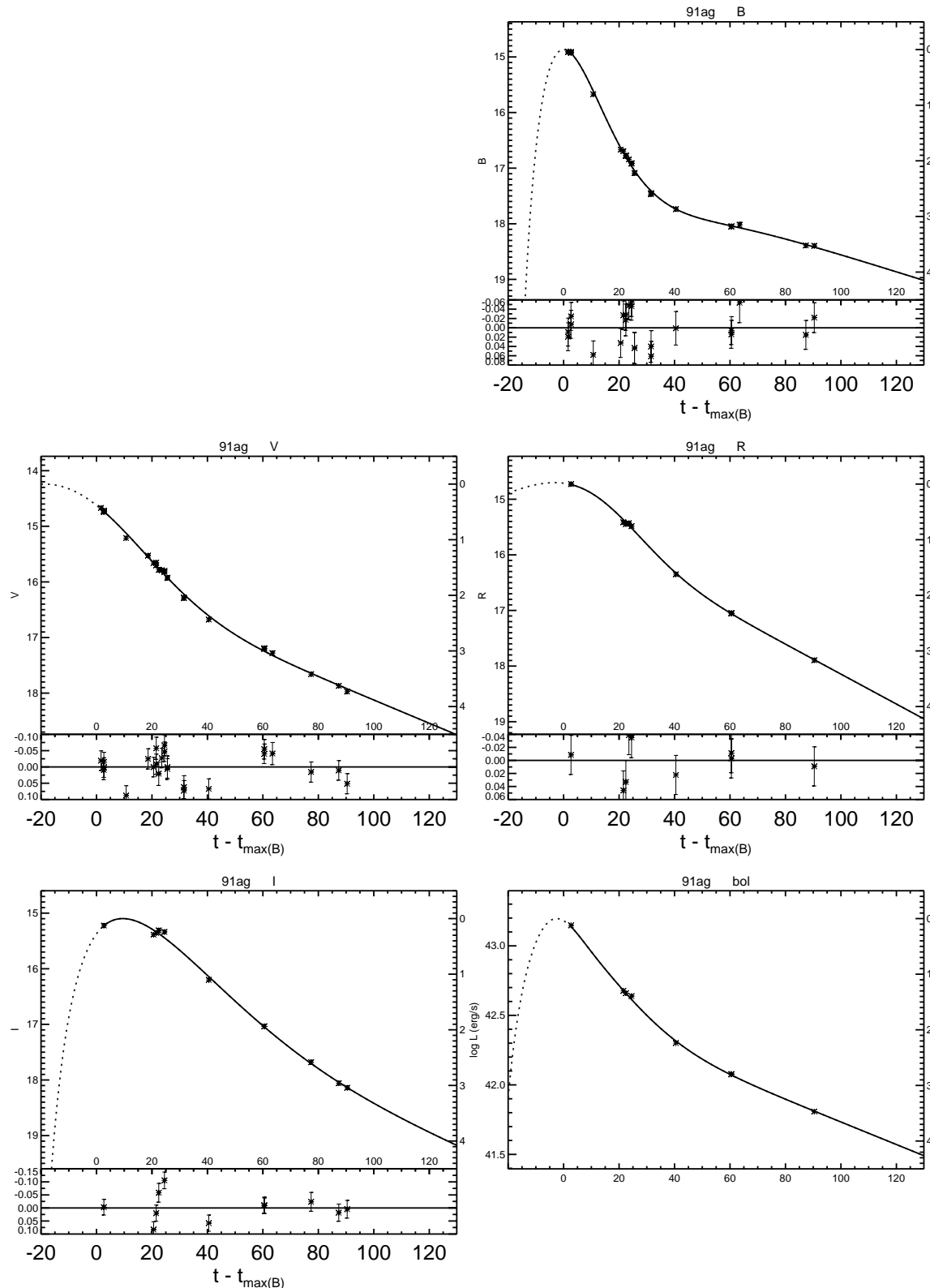


Figure A.10: $UBVRI$ light curves of SN 1991ag.

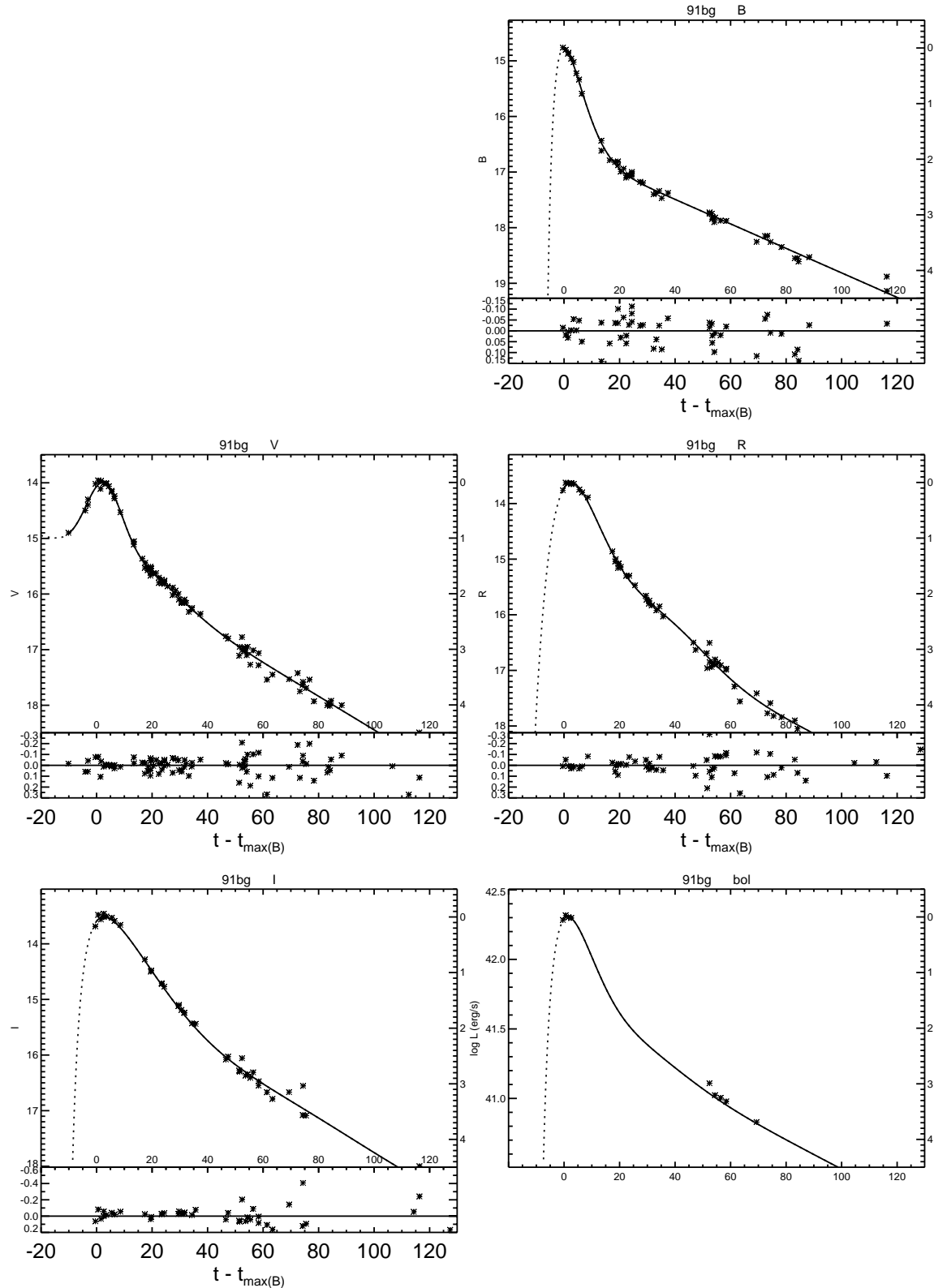


Figure A.11: *UBVRI* light curves of SN 1991bg.

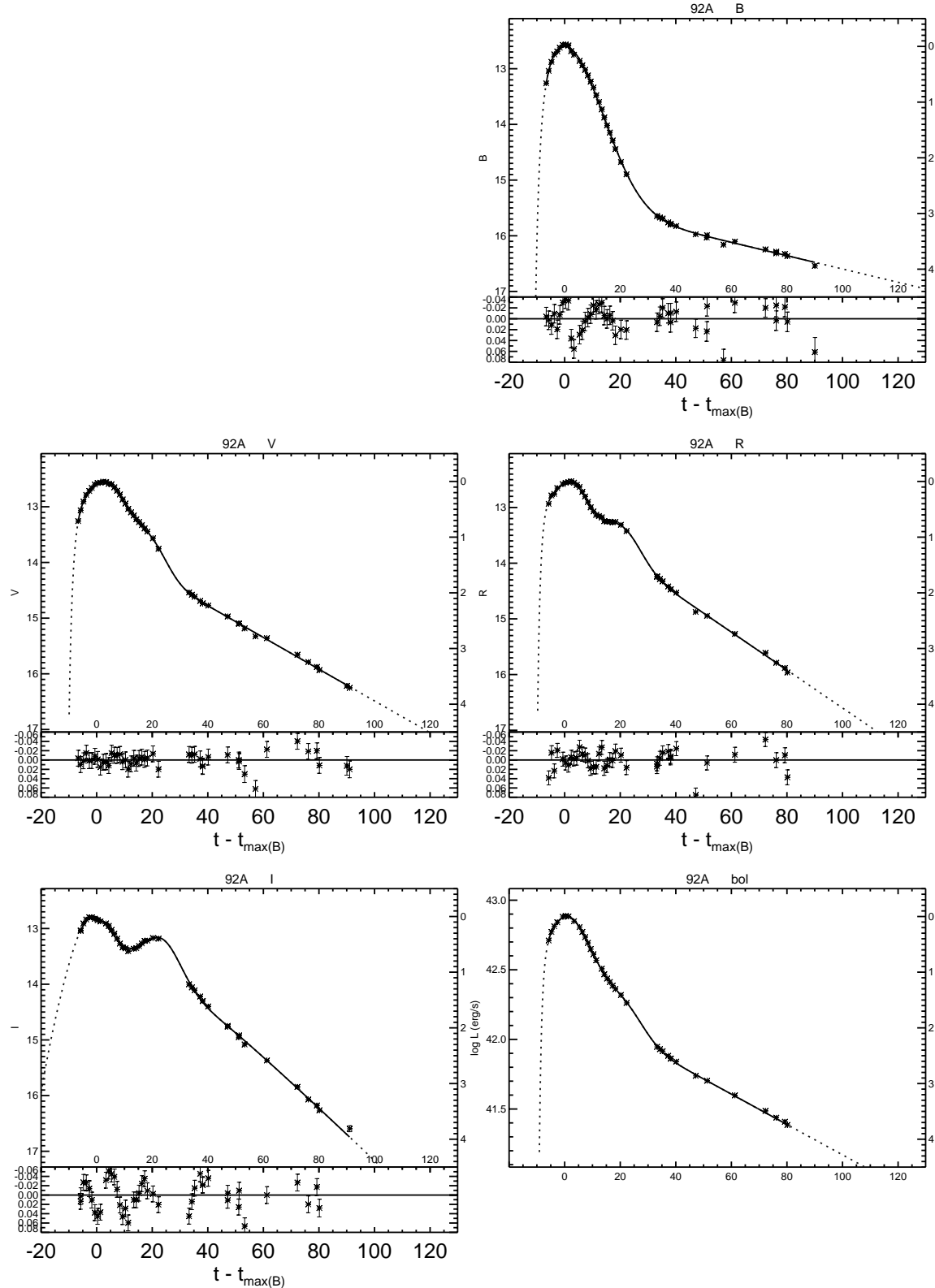


Figure A.12: *UBVRI* light curves of SN 1992A.

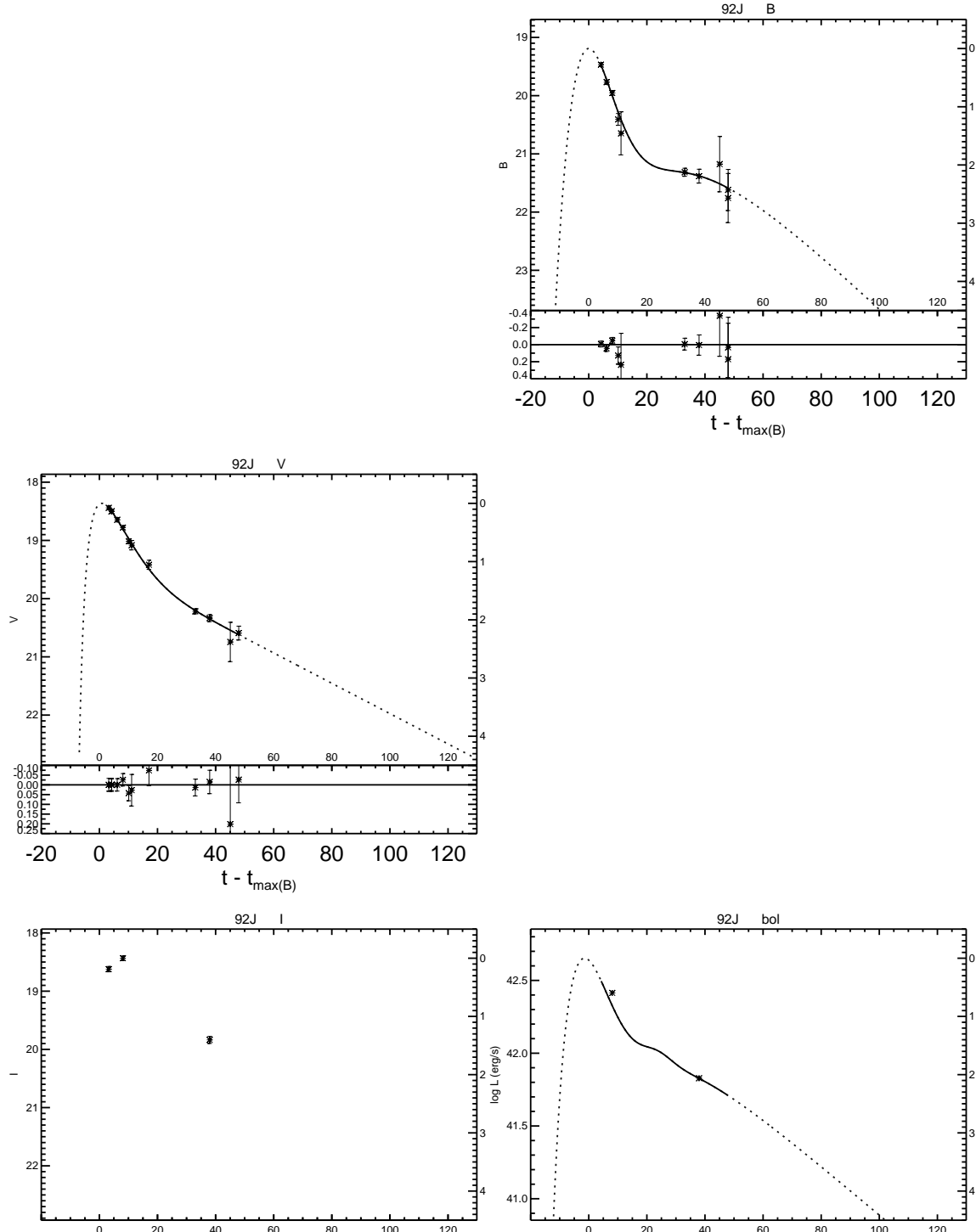


Figure A.13: *UBVRI* light curves of SN 1992J.

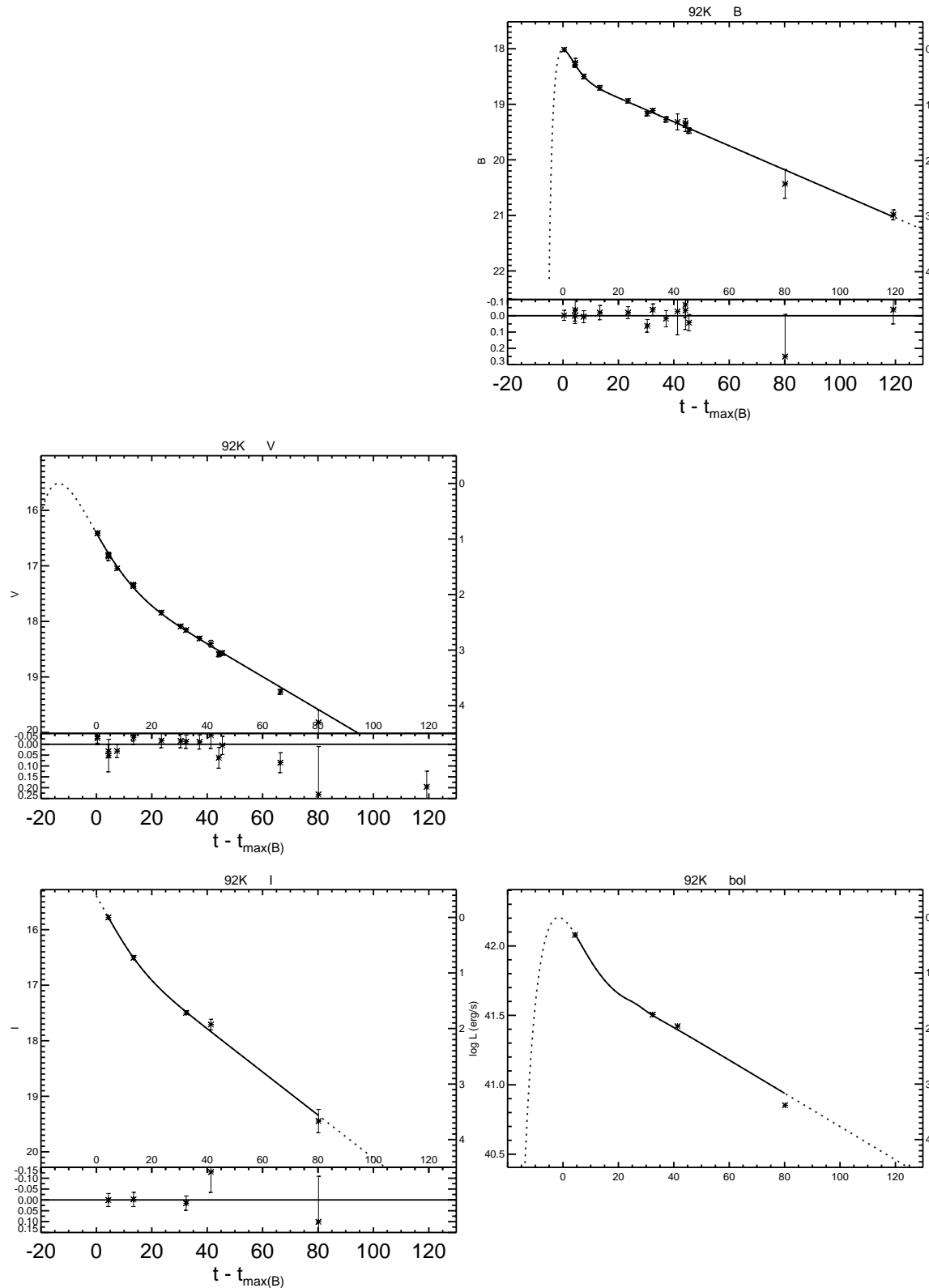


Figure A.14: *UBVRI* light curves of SN 1992K.

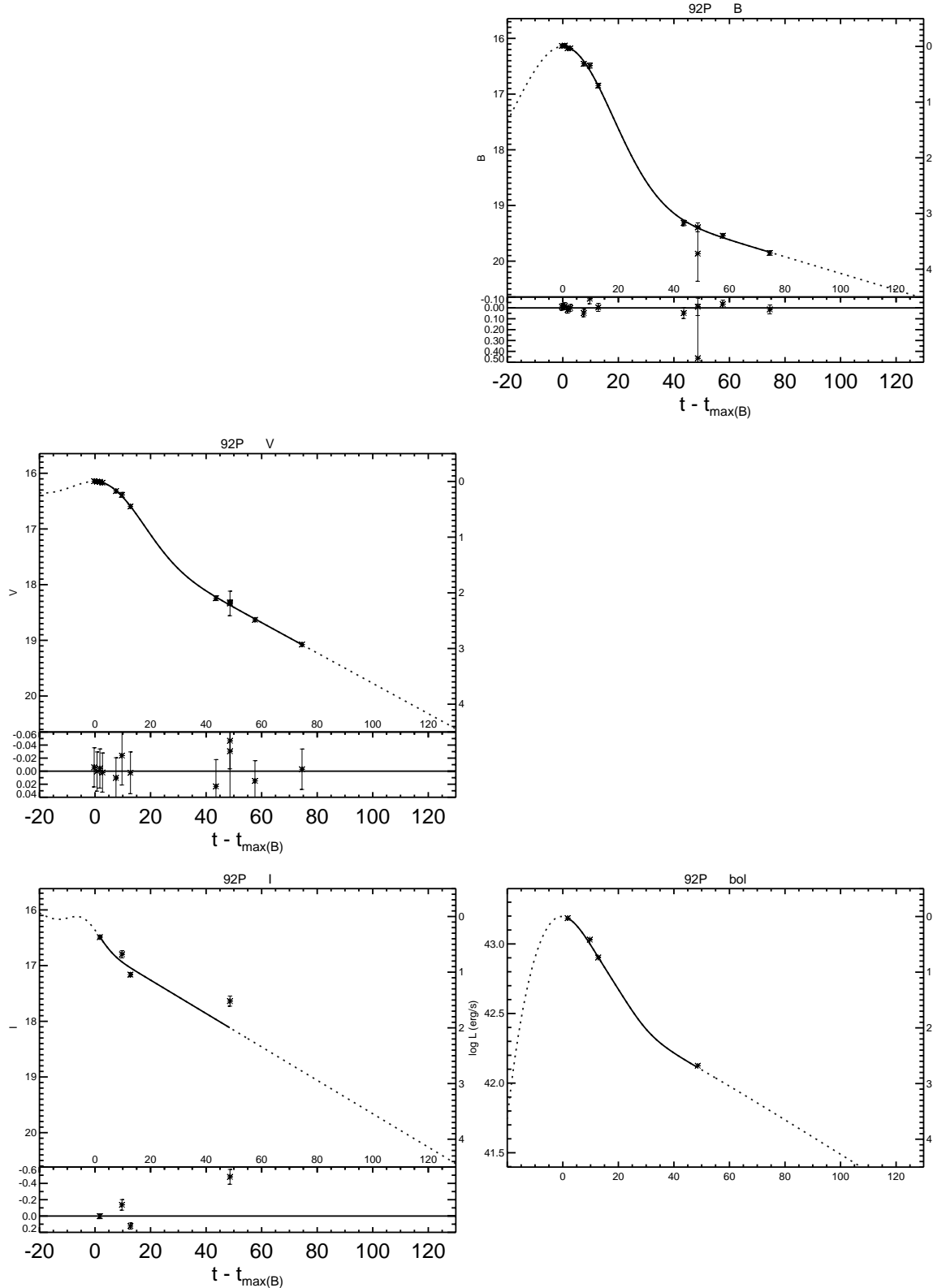


Figure A.15: *UBVRI* light curves of SN 1992P.

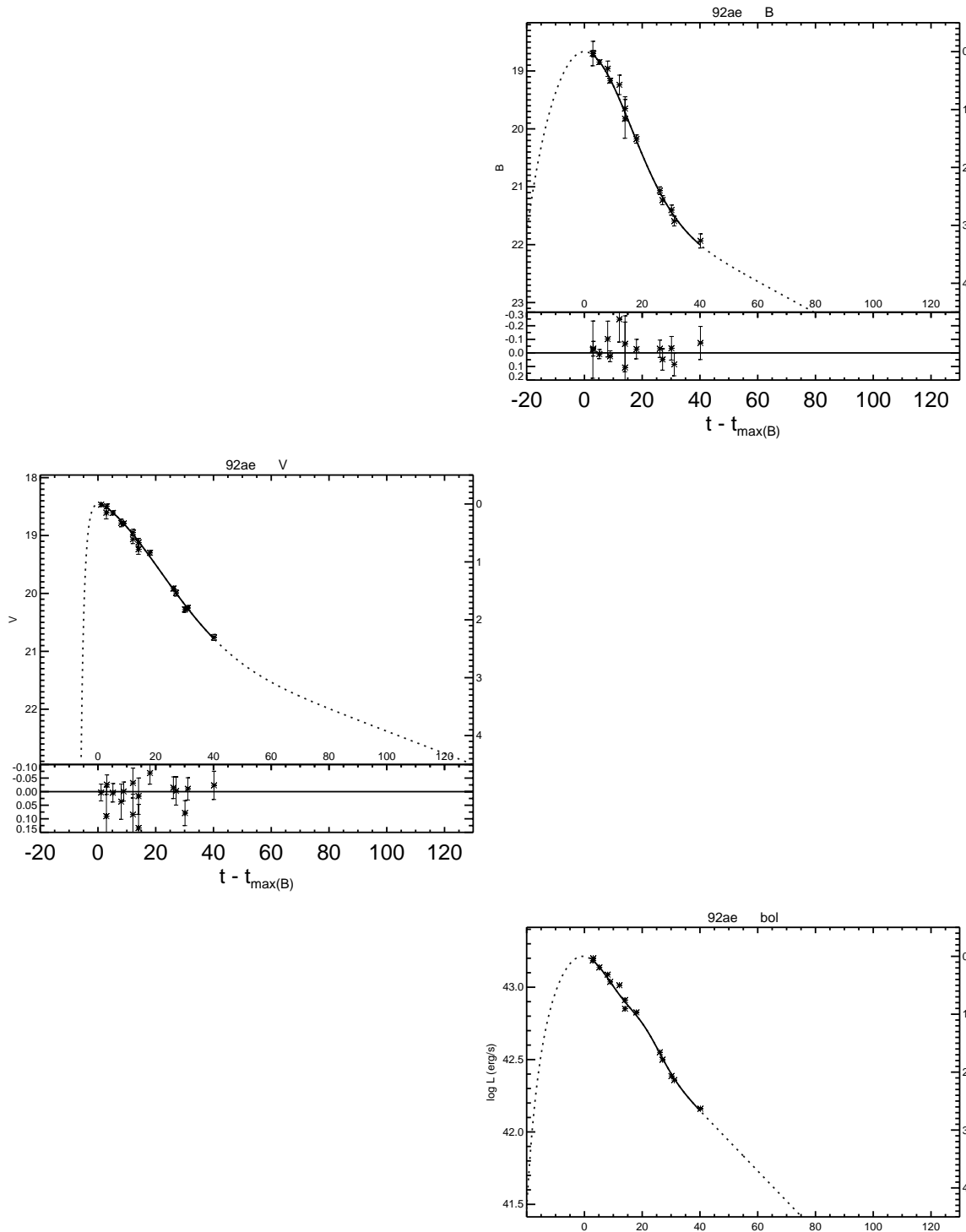


Figure A.16: $UBVRI$ light curves of SN 1992ae.

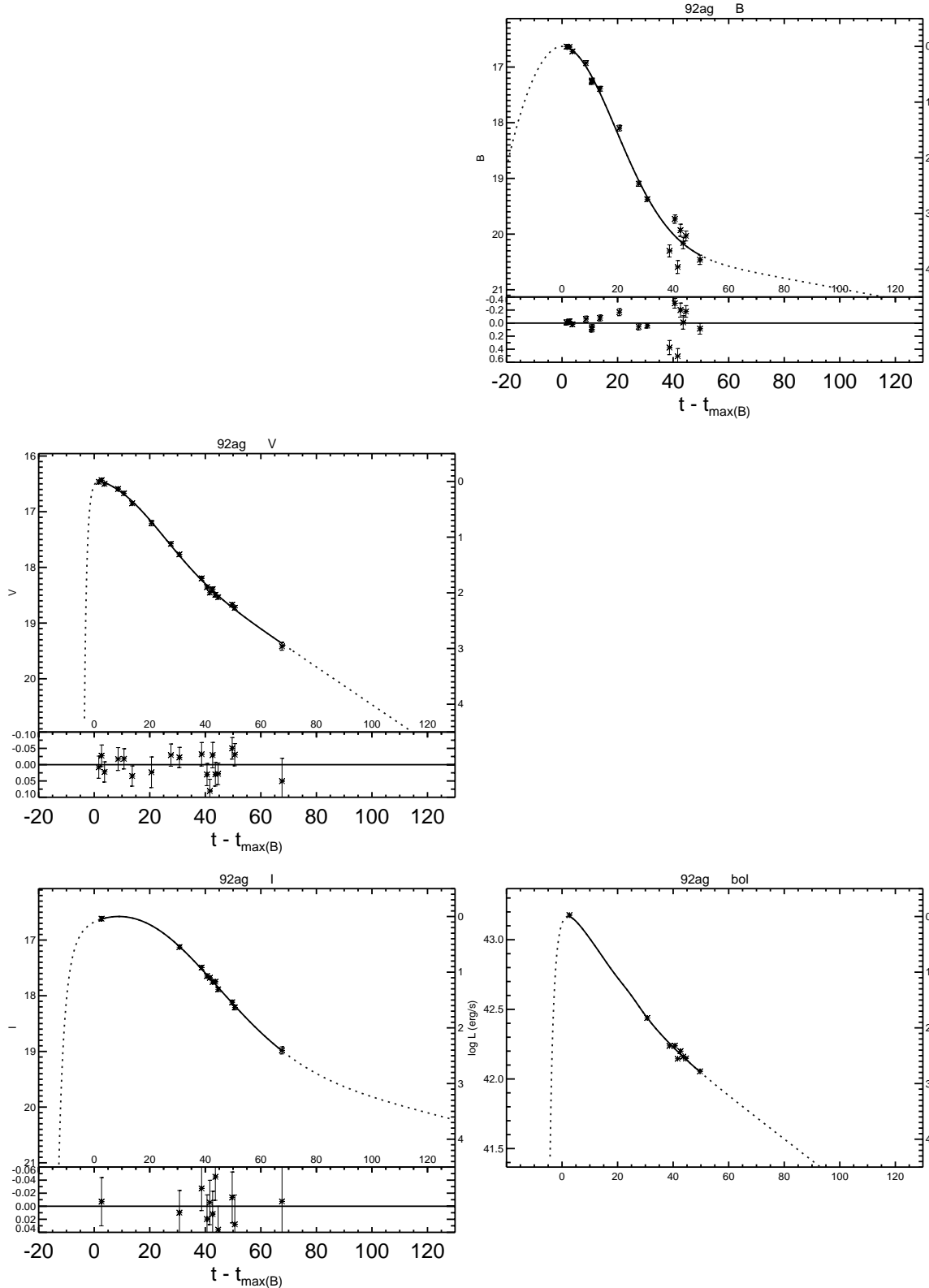


Figure A.17: *UBVRI* light curves of SN 1992ag.

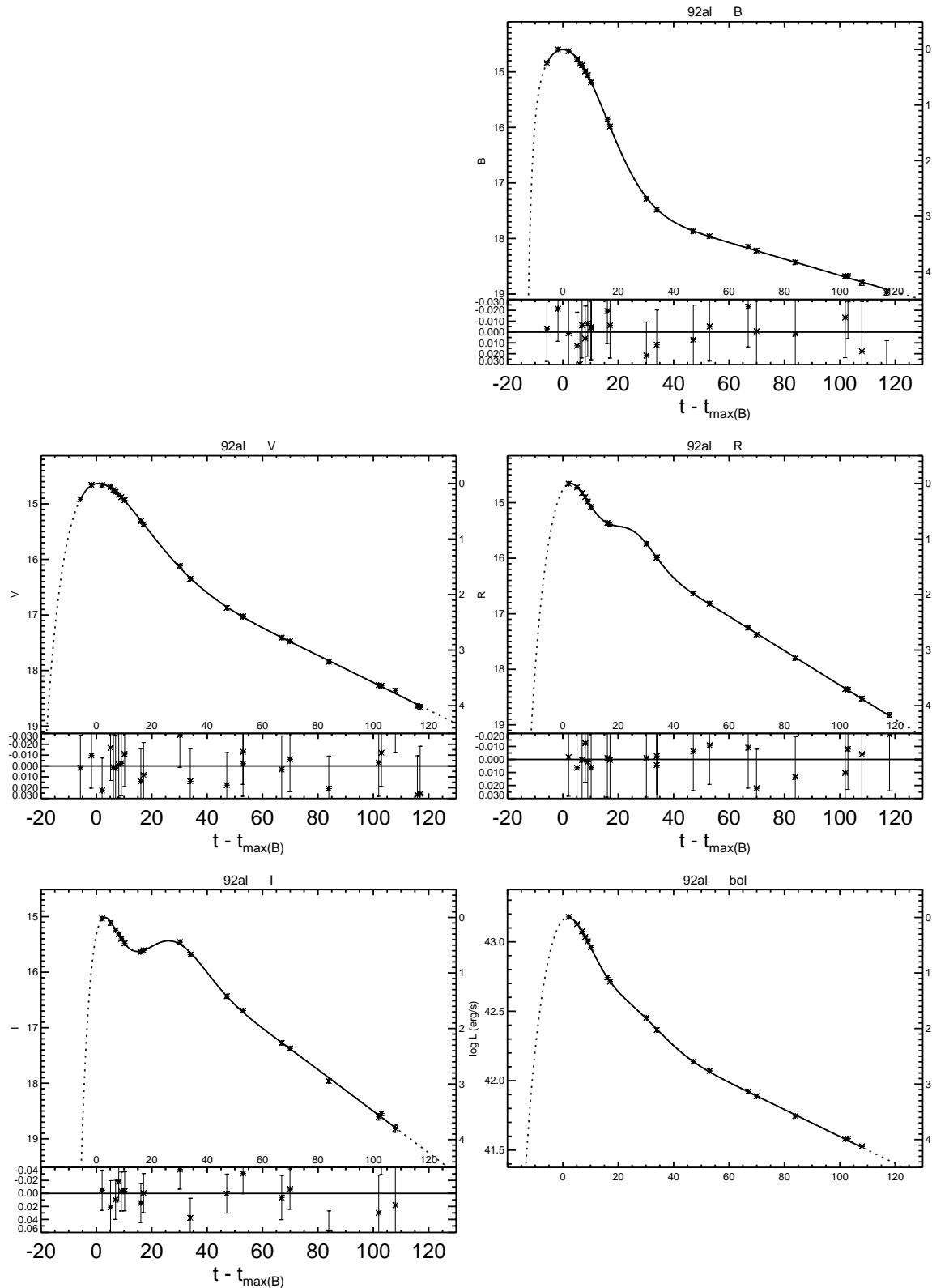


Figure A.18: *UBVRI* light curves of SN 1992al.

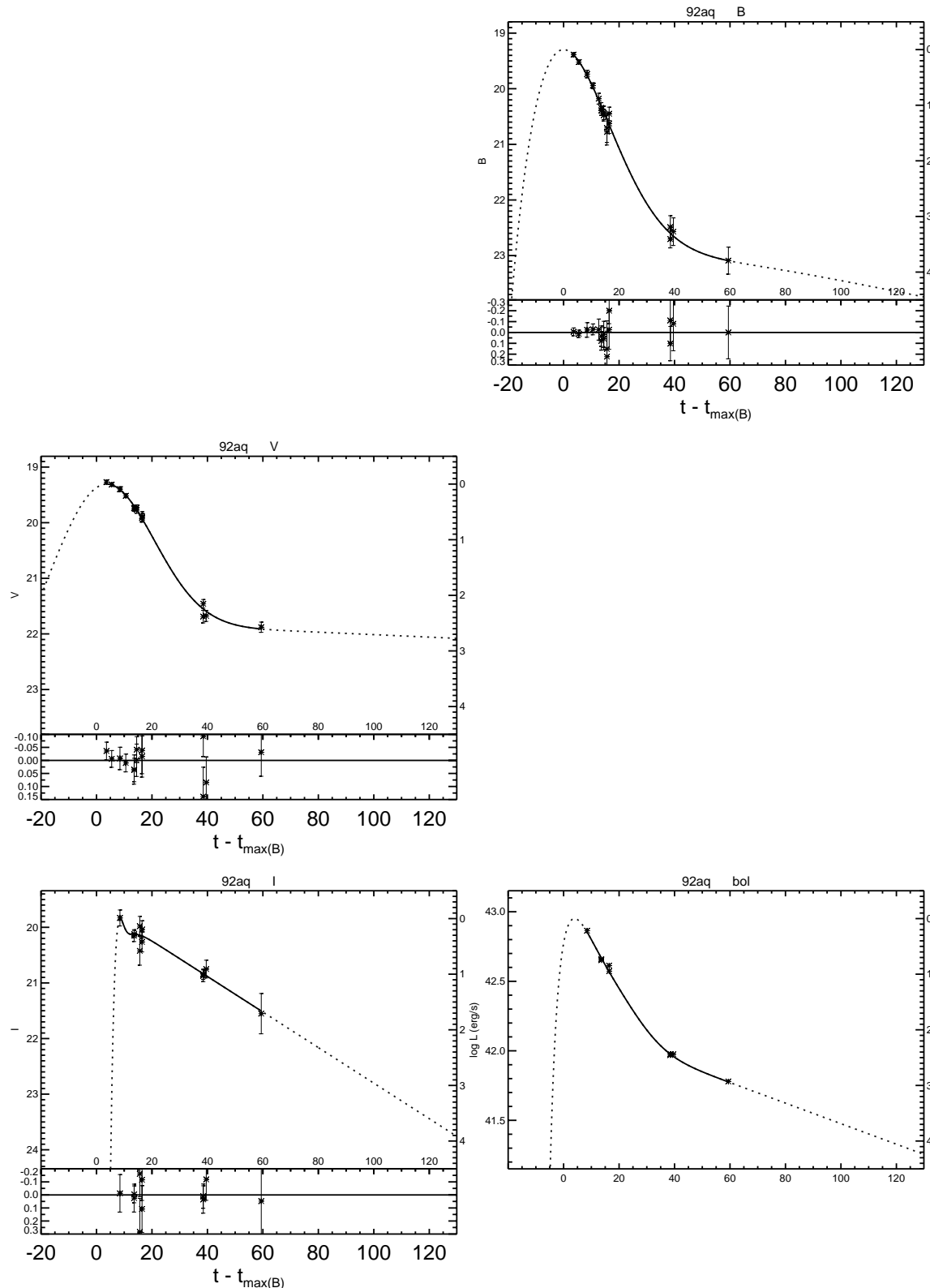


Figure A.19: *UBVRI* light curves of SN 1992aq.

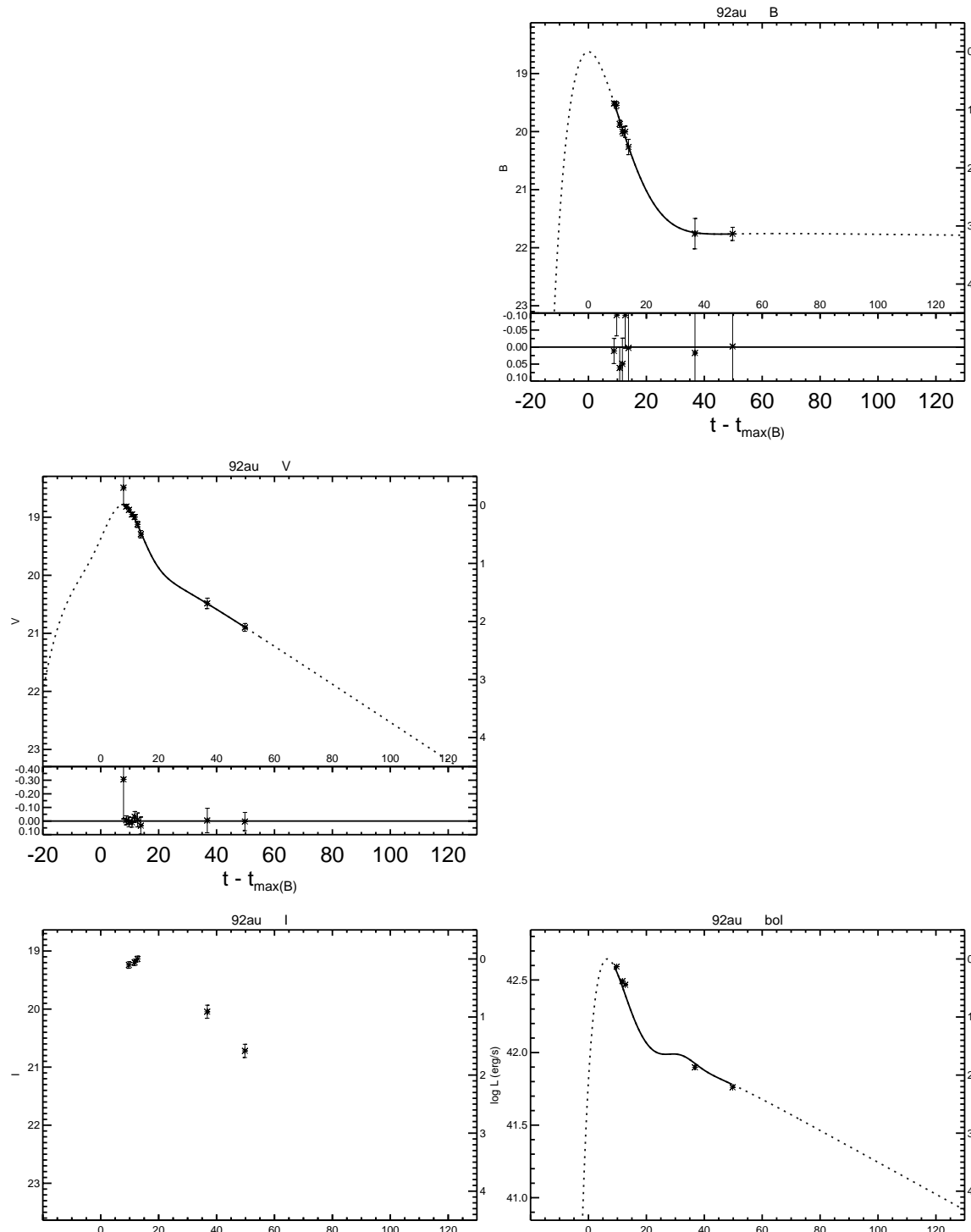


Figure A.20: $UBVRI$ light curves of SN 1992au.

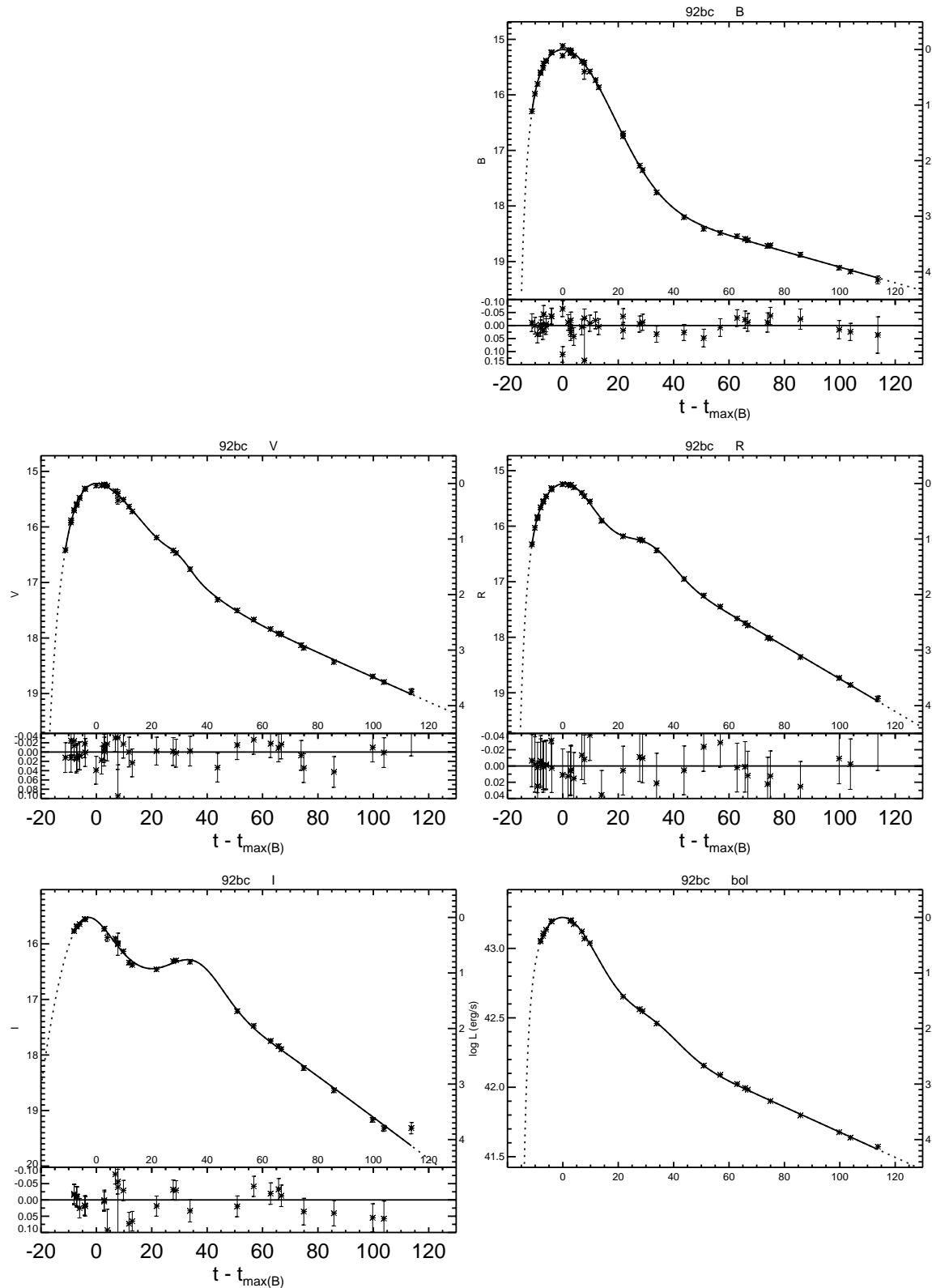


Figure A.21: *UBVRI* light curves of SN 1992bc.

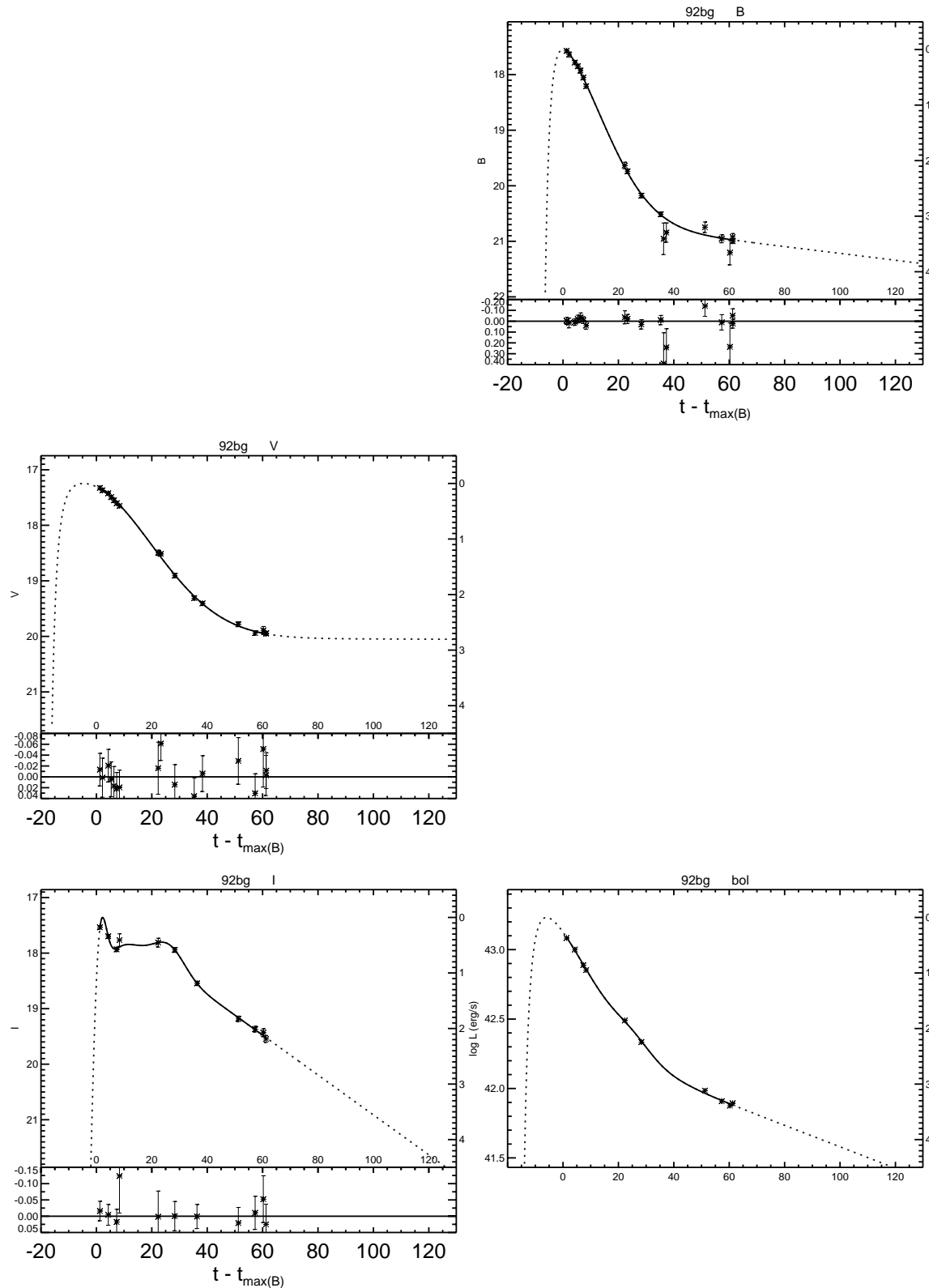


Figure A.22: $UBVRI$ light curves of SN 1992bg.

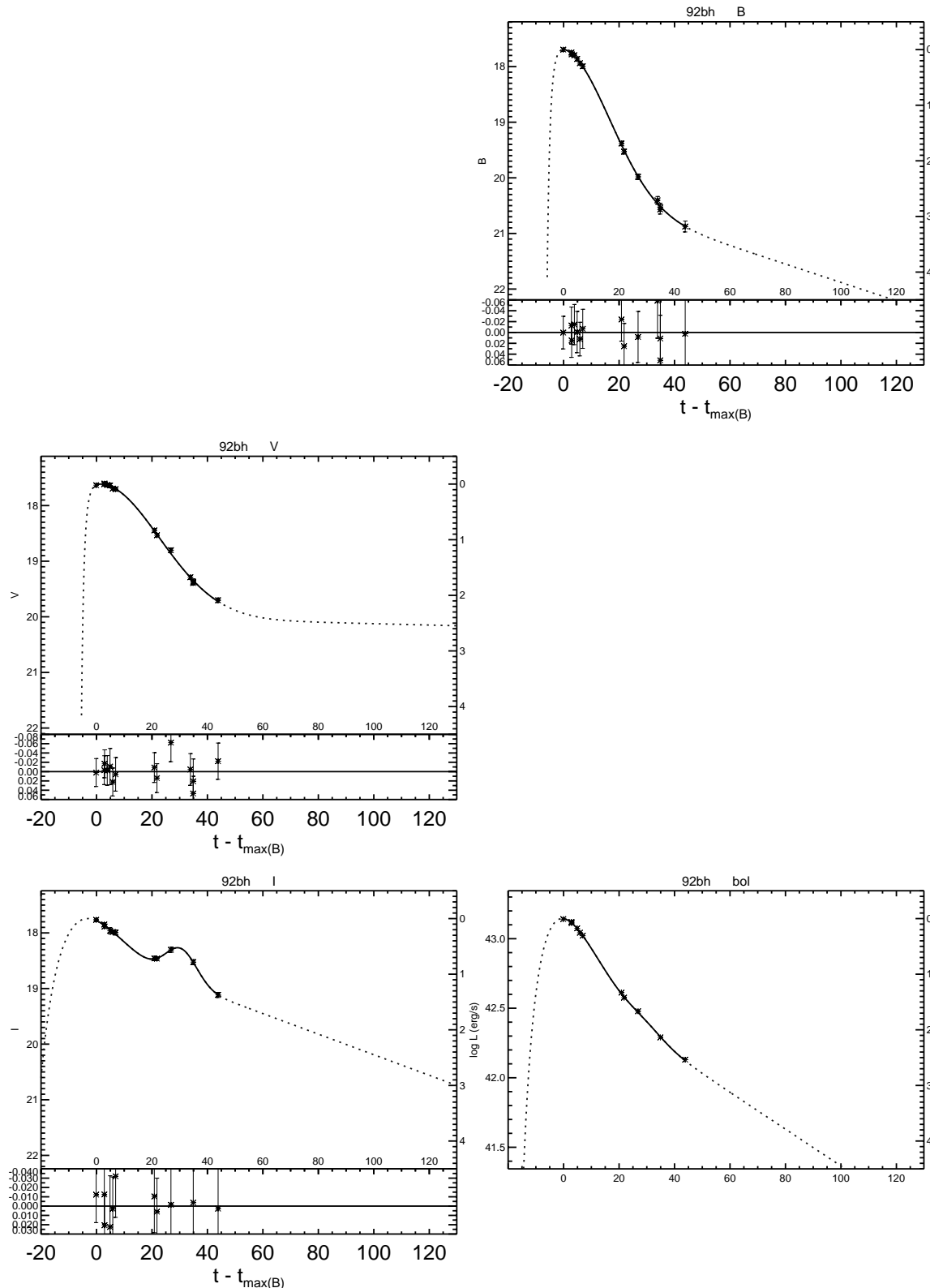


Figure A.23: *UBVRI* light curves of SN 1992bh.

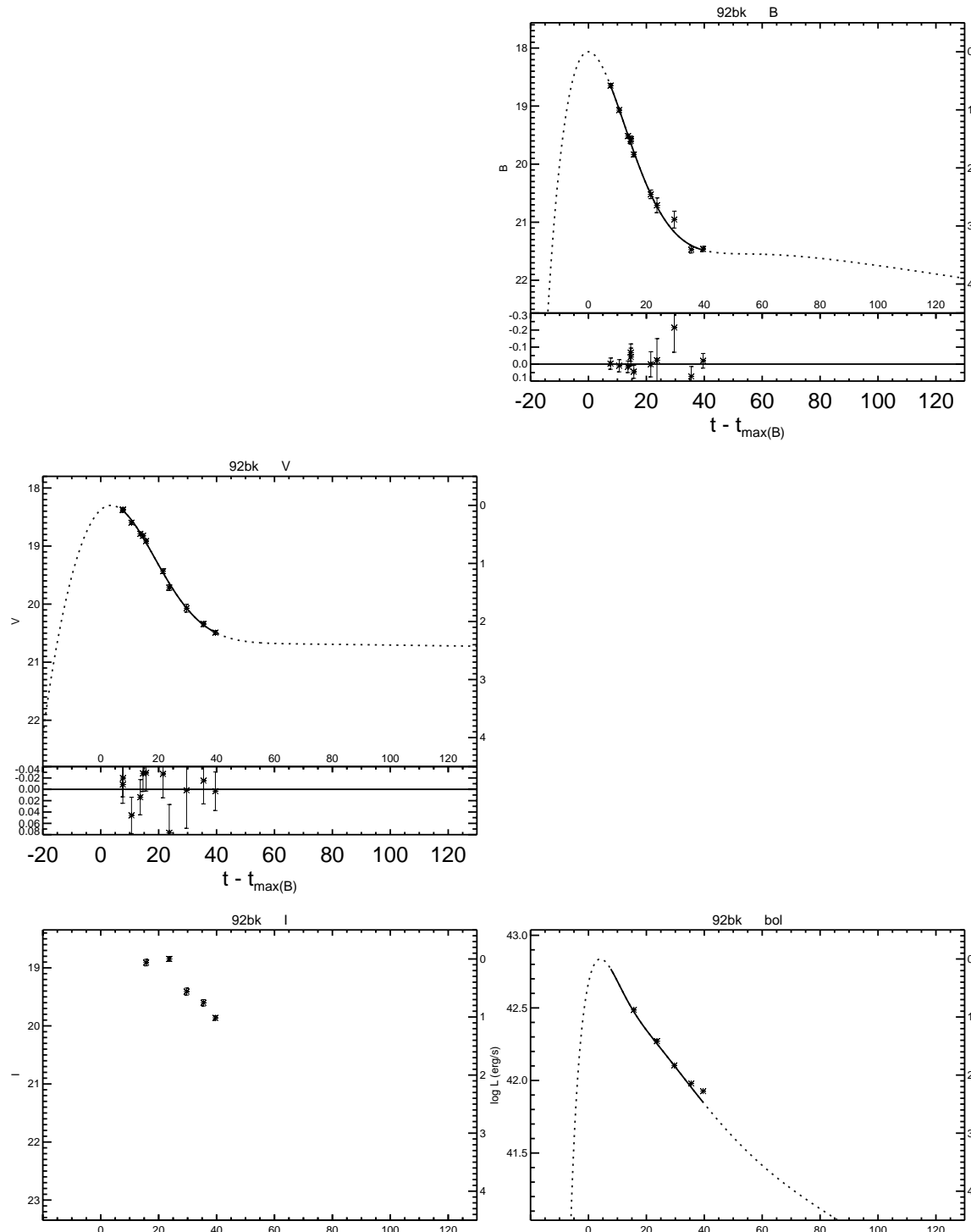


Figure A.24: *UBVRI* light curves of SN 1992bk.

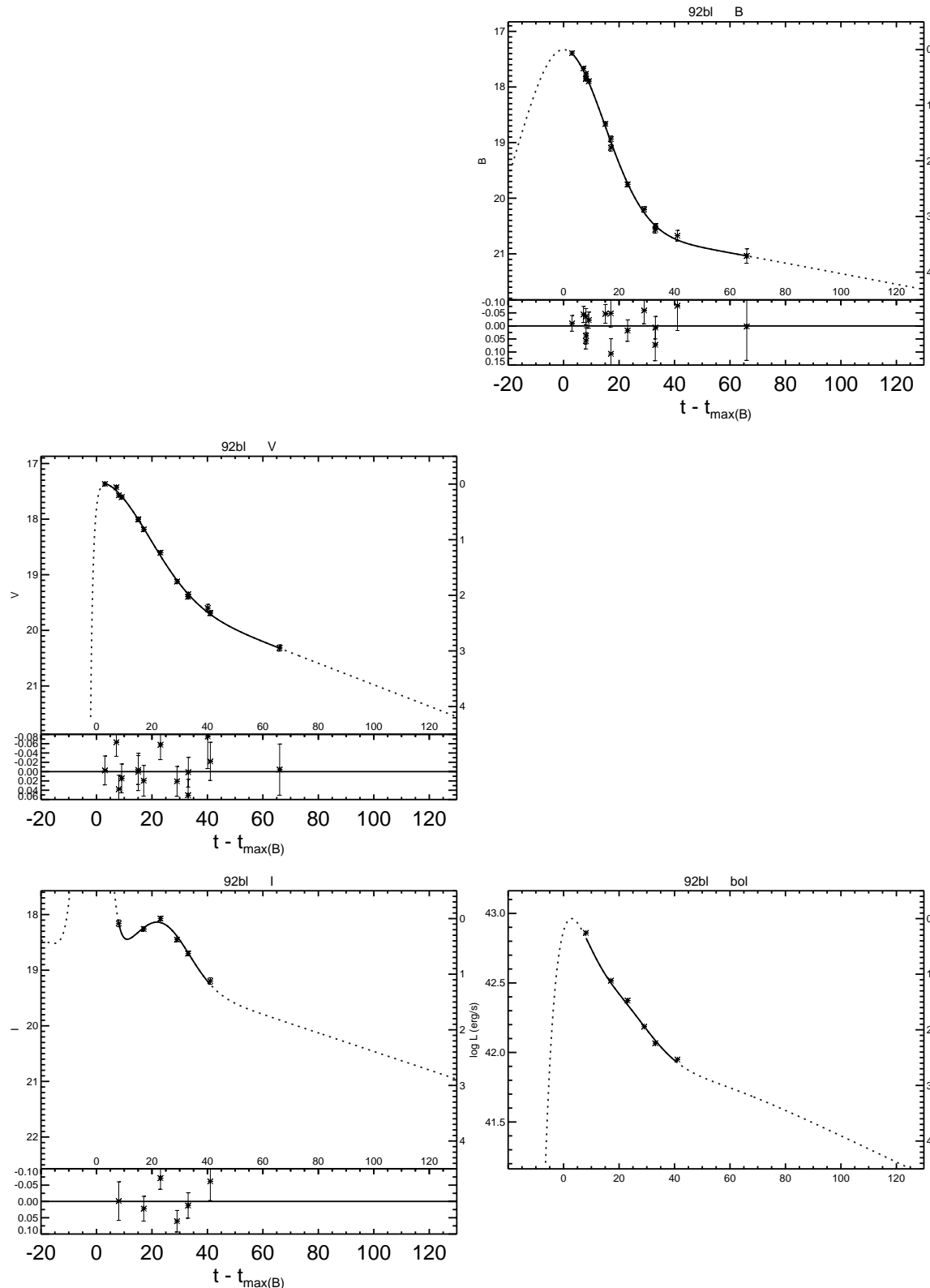


Figure A.25: *UBVRI* light curves of SN 1992bl.

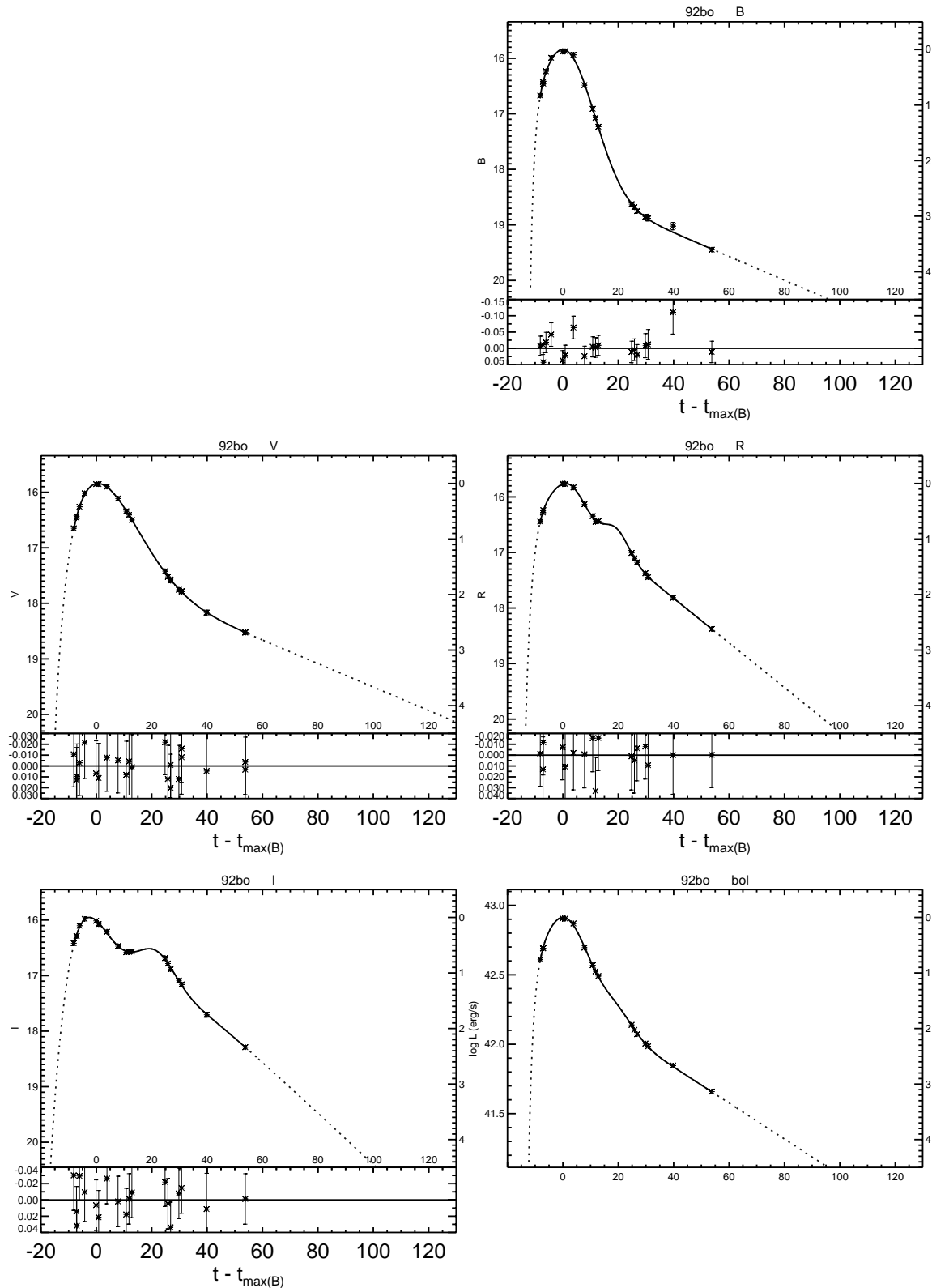


Figure A.26: *UBVRI* light curves of SN 1992bo.

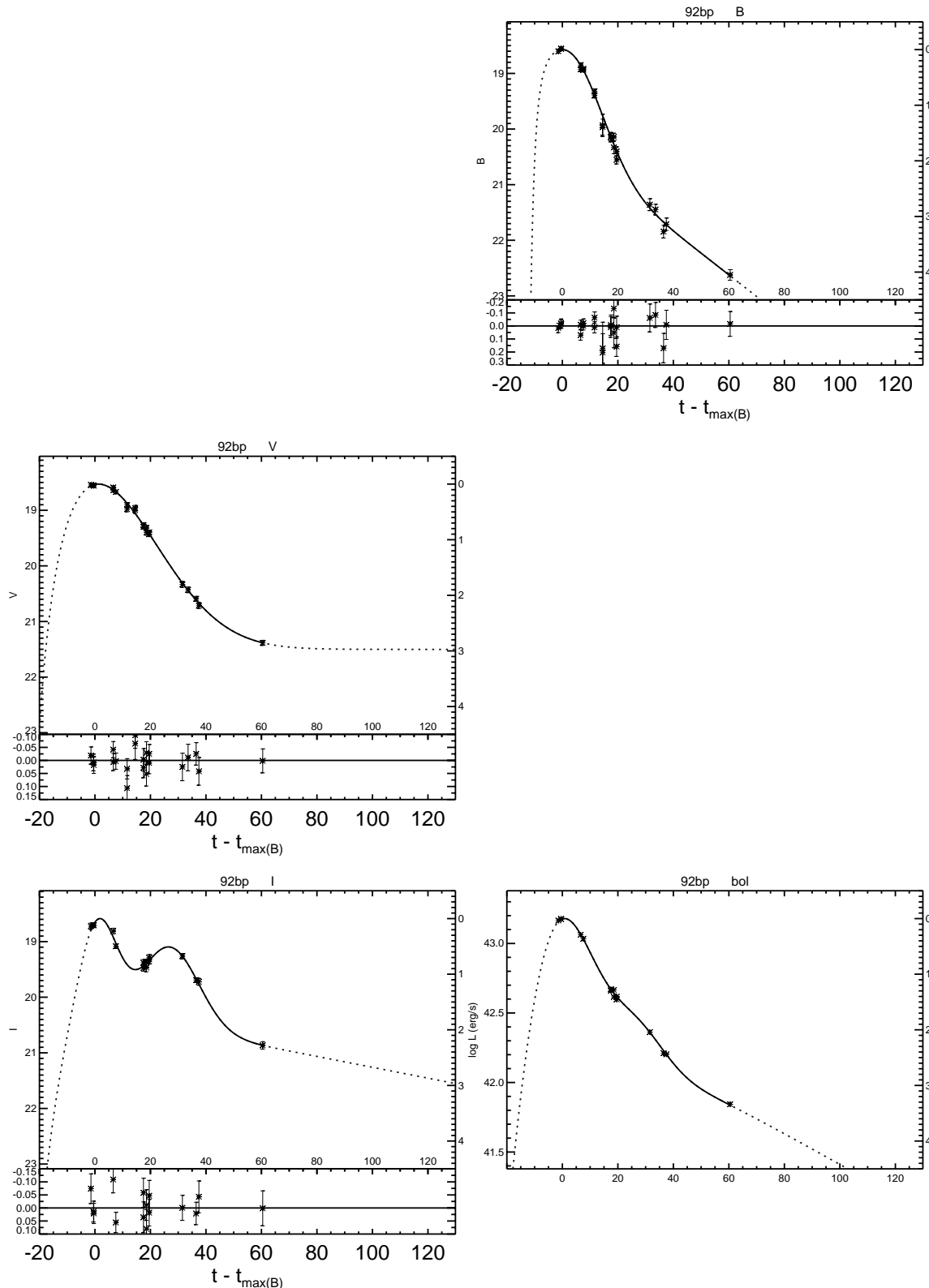


Figure A.27: *UBVRI* light curves of SN 1992bp.

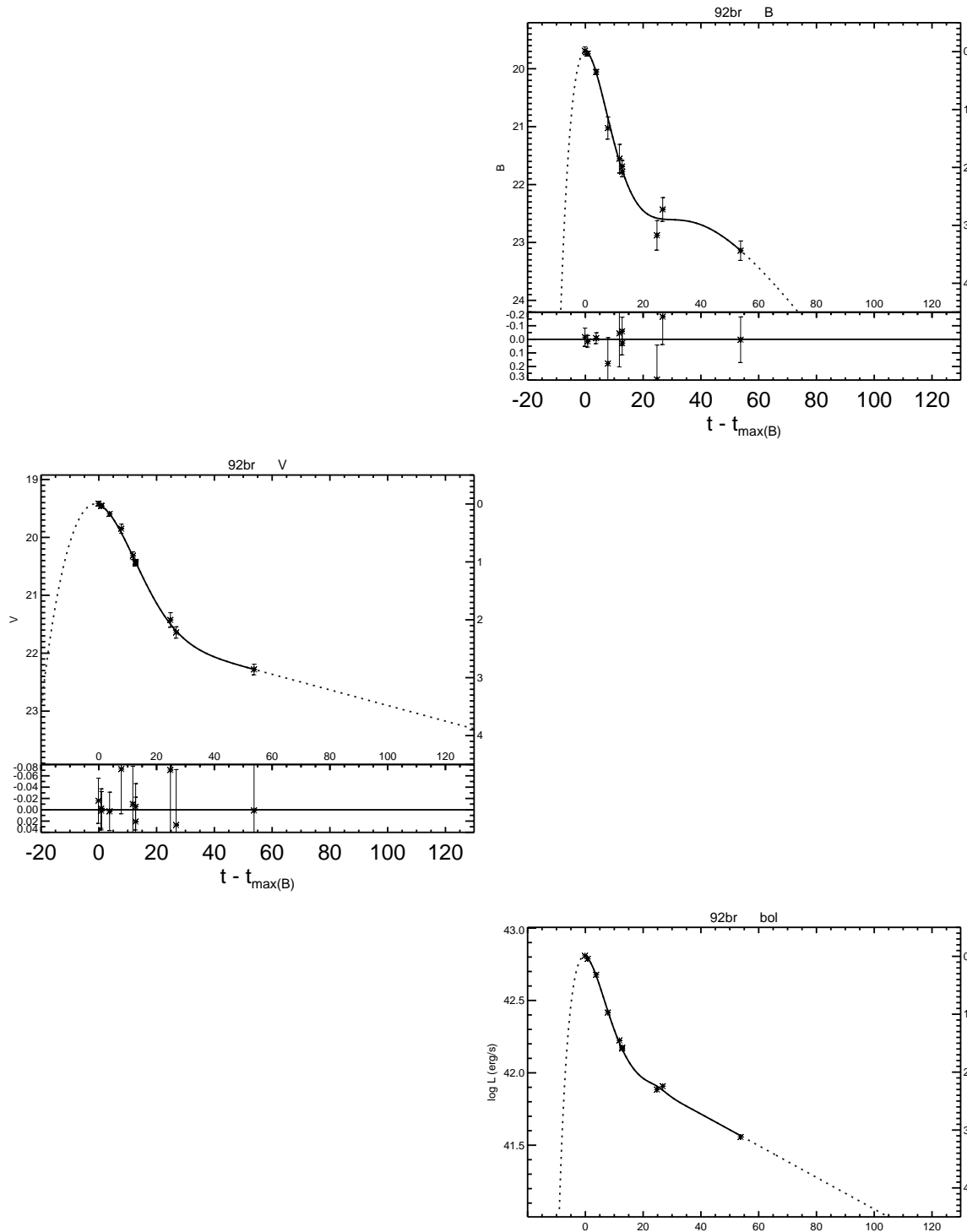


Figure A.28: *UBVRI* light curves of SN 1992br.

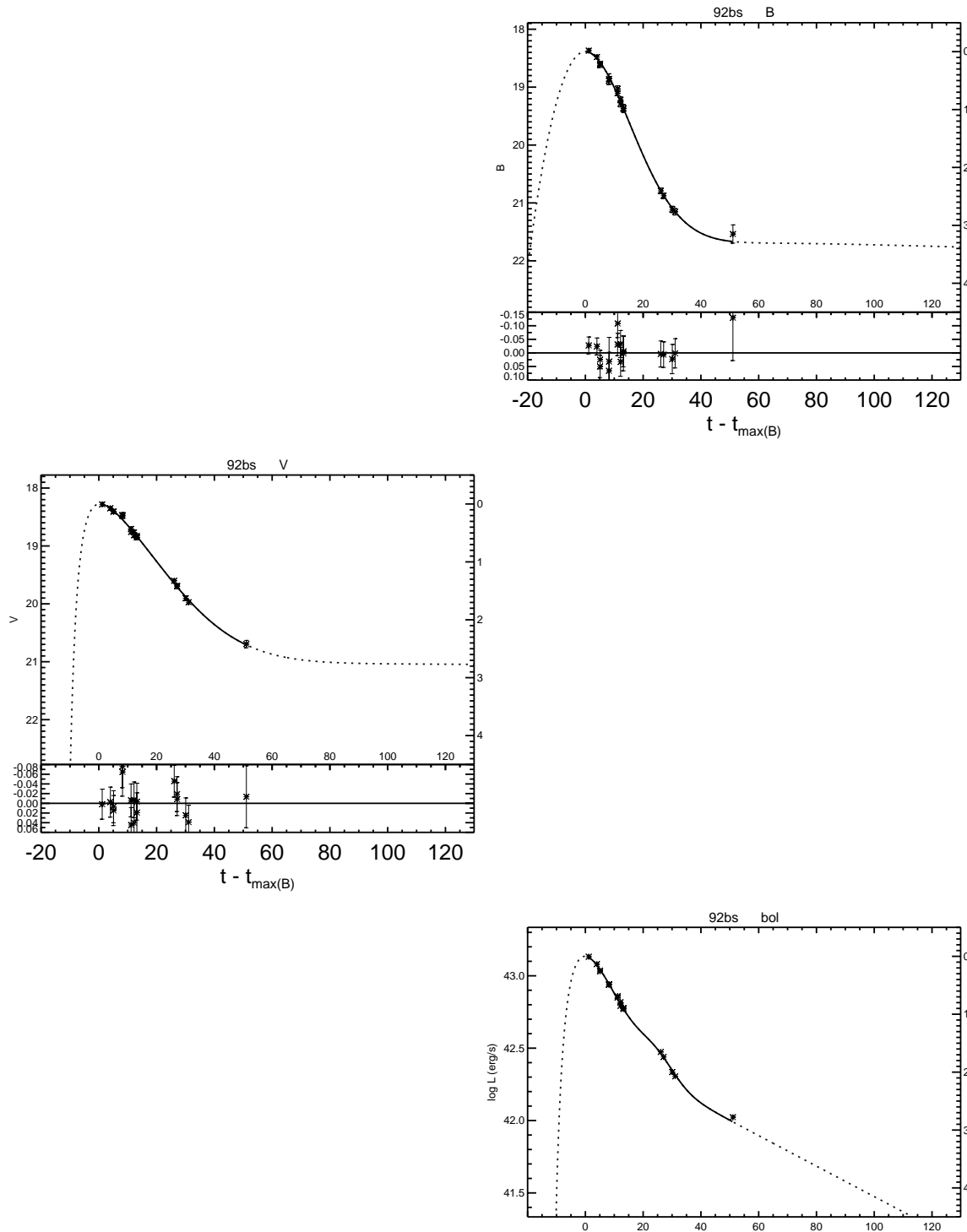


Figure A.29: *UBVRI* light curves of SN 1992bs.

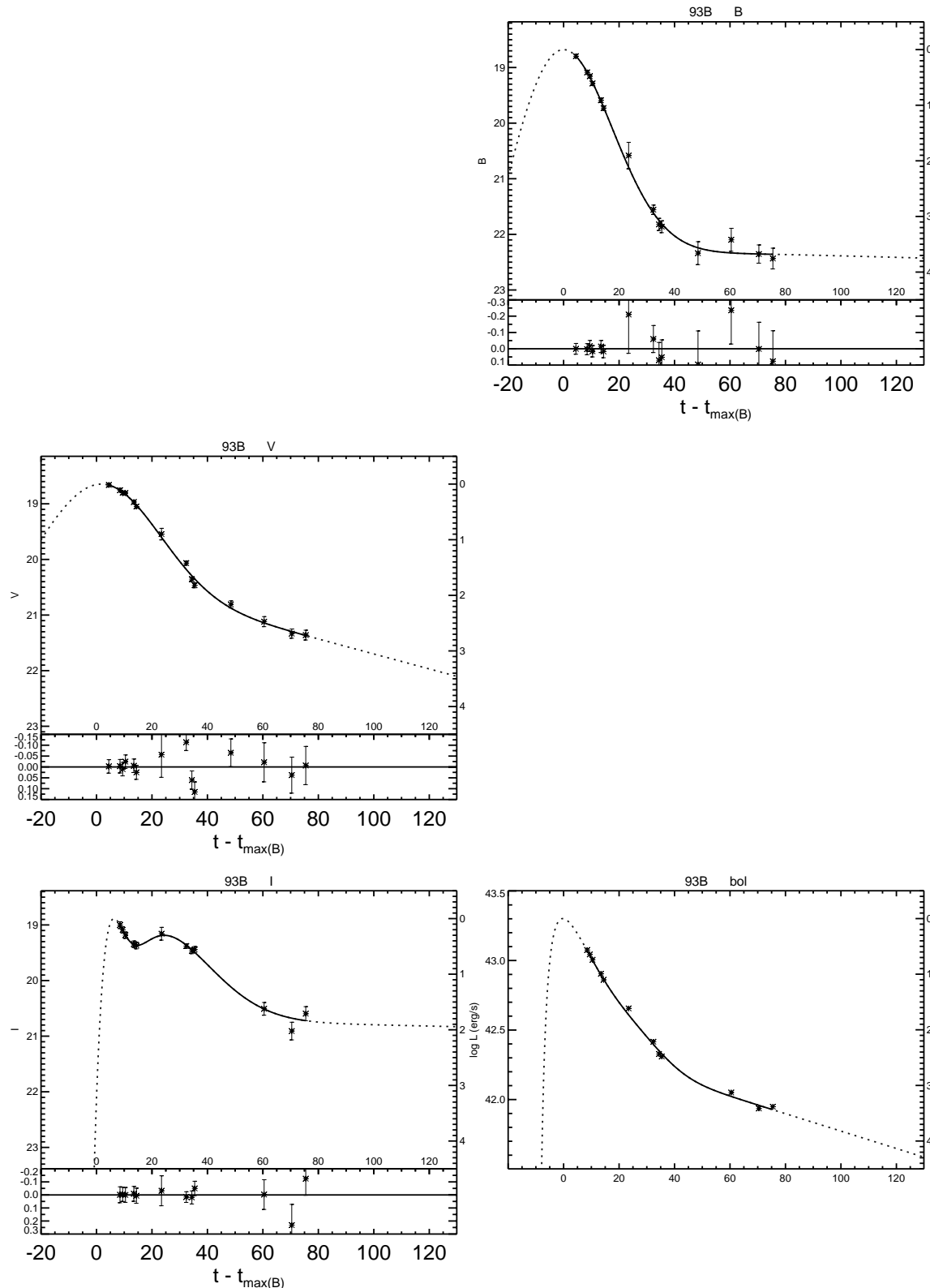


Figure A.30: $UBVRI$ light curves of SN 1993B.

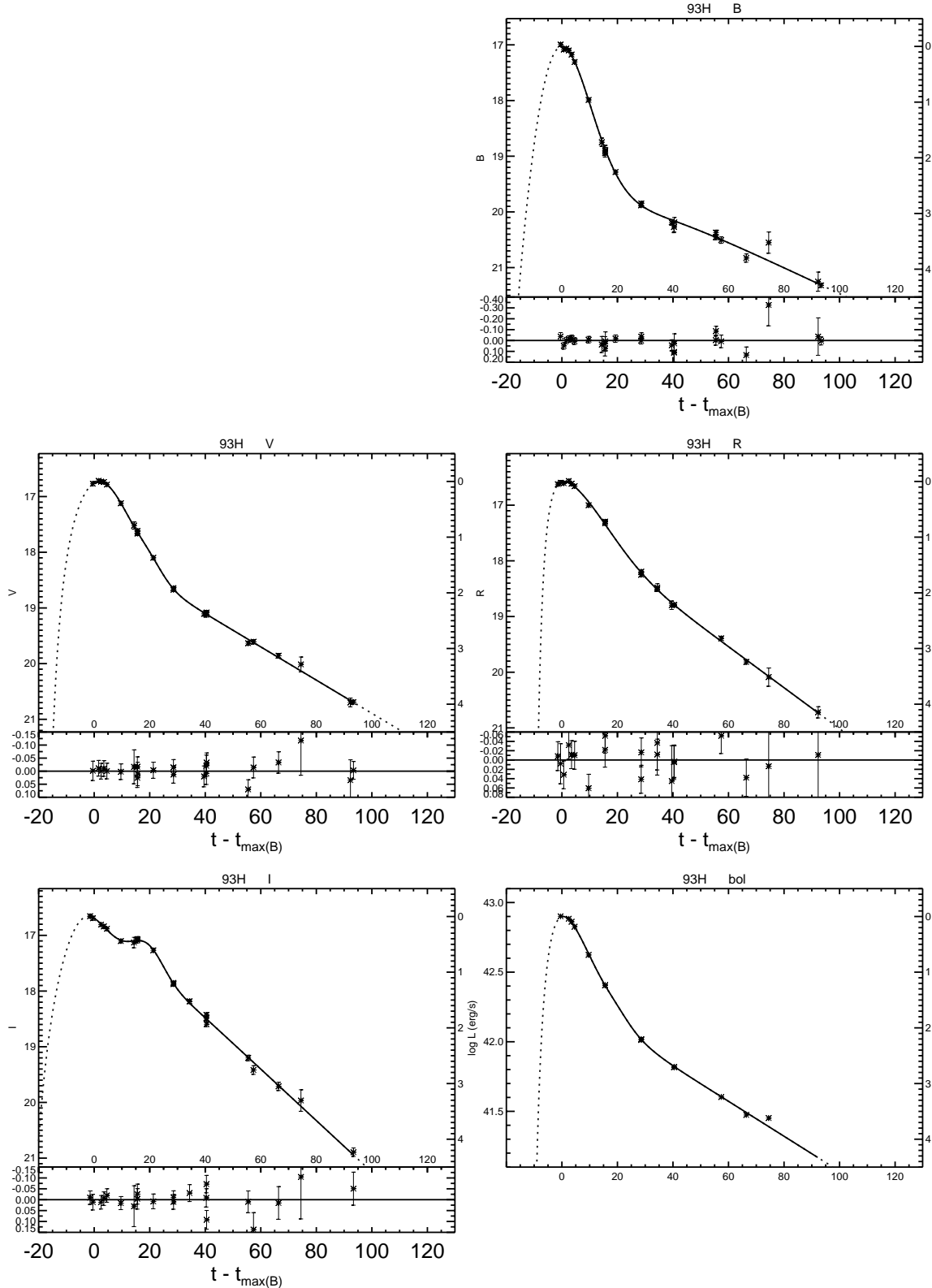


Figure A.31: *UBVRI* light curves of SN 1993H.

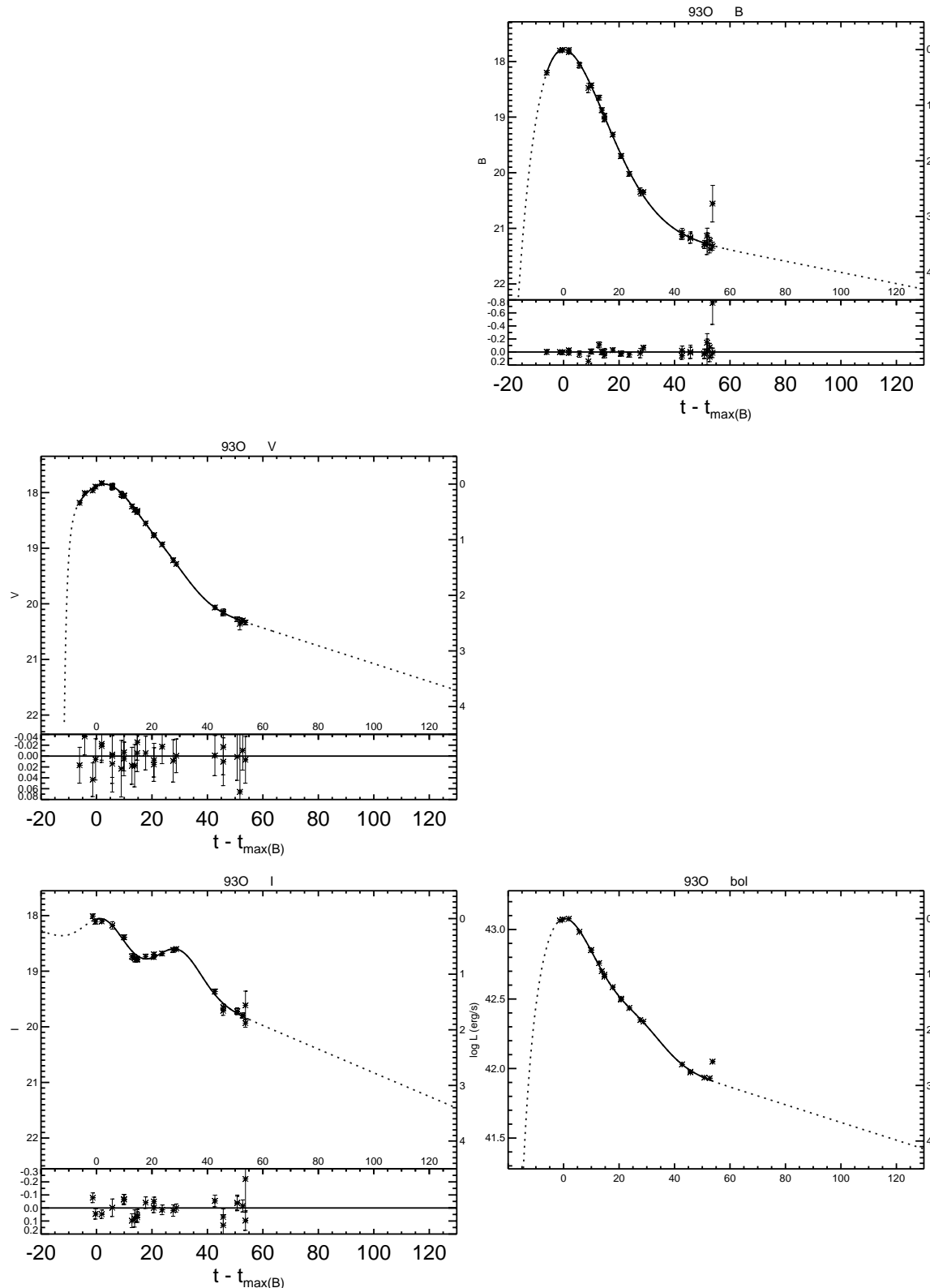


Figure A.32: $UBVRI$ light curves of SN 1993O.

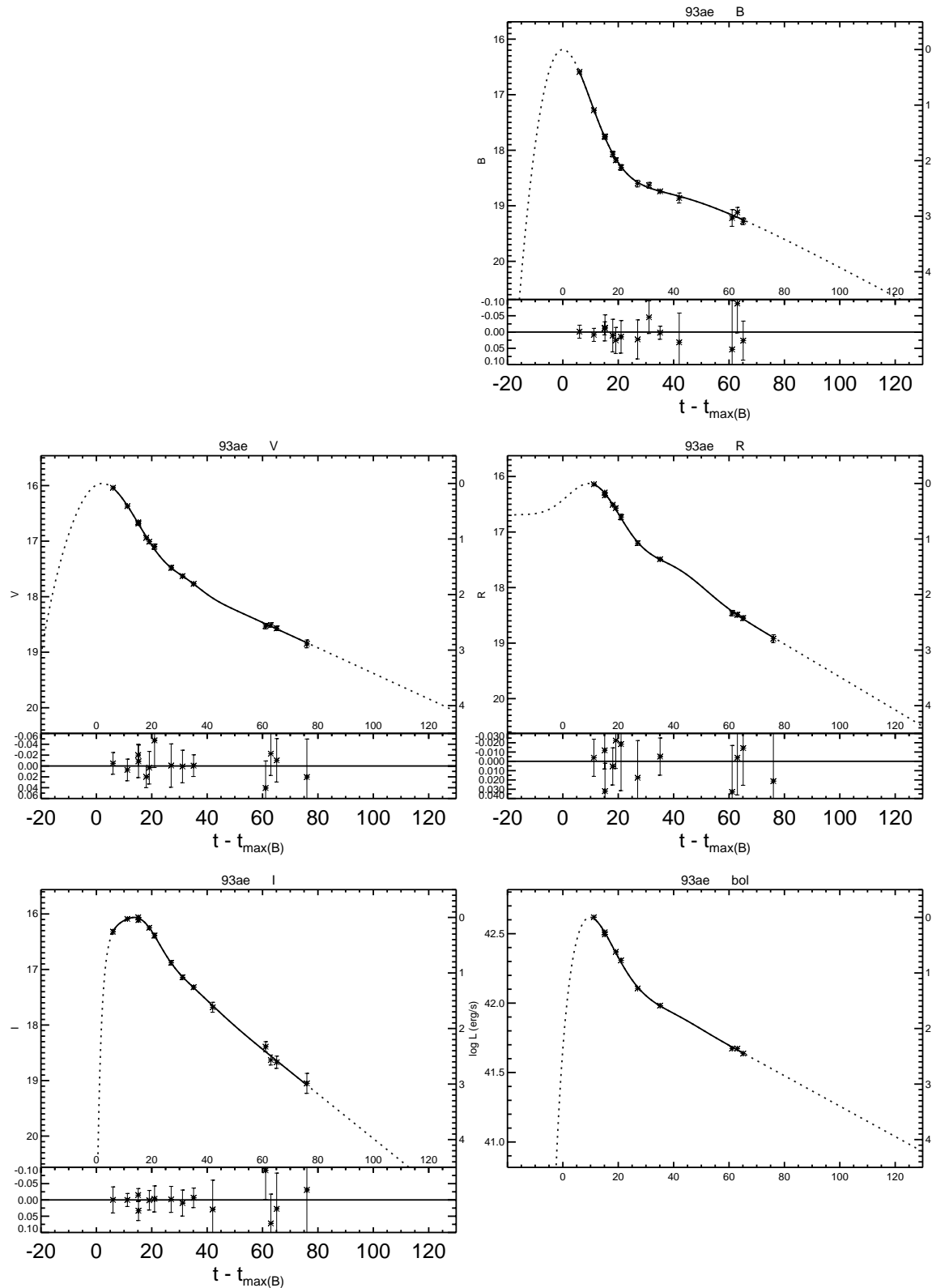


Figure A.33: *UBVRI* light curves of SN 1993ae.

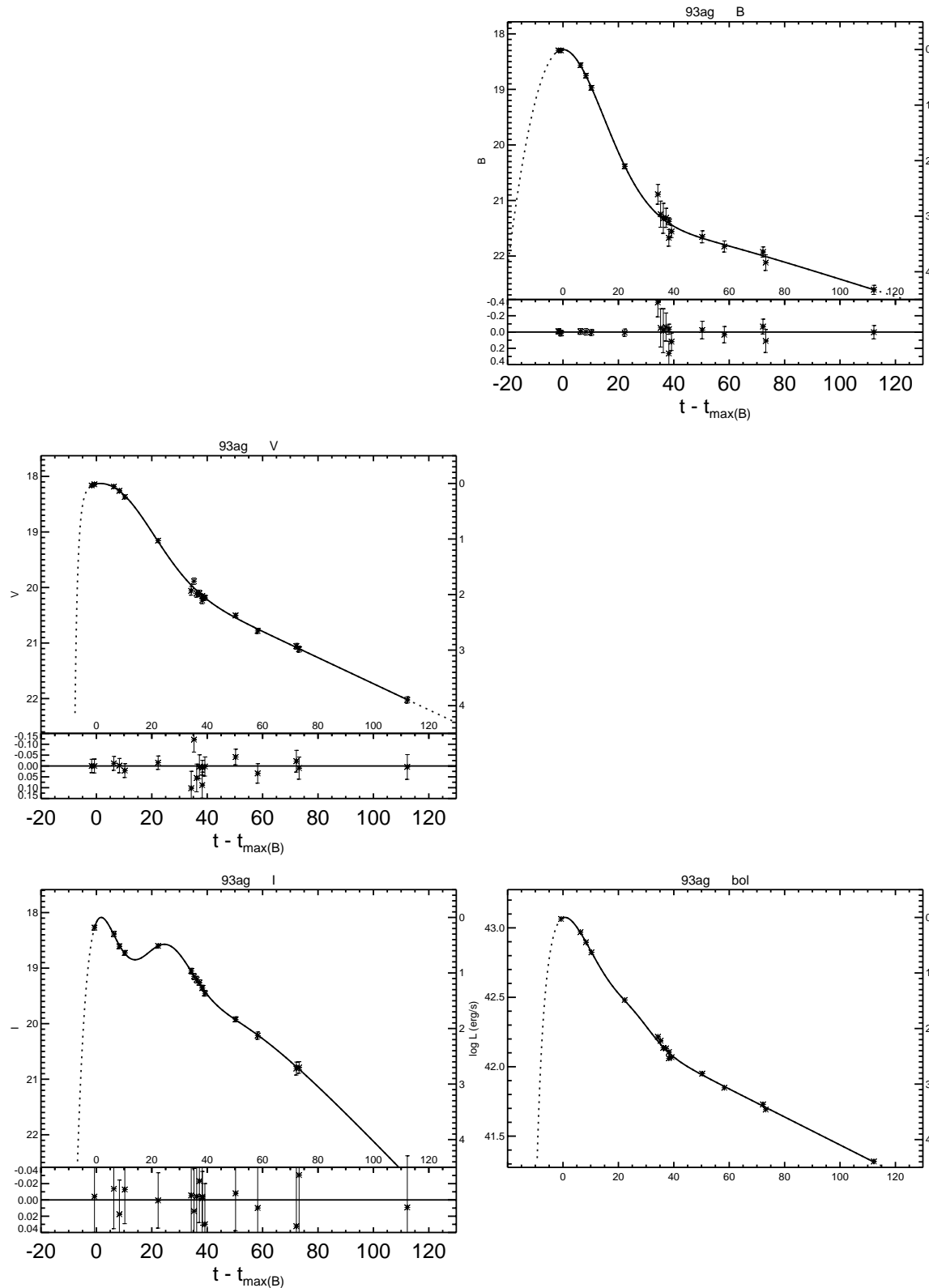


Figure A.34: $UBVRI$ light curves of SN 1993ag.

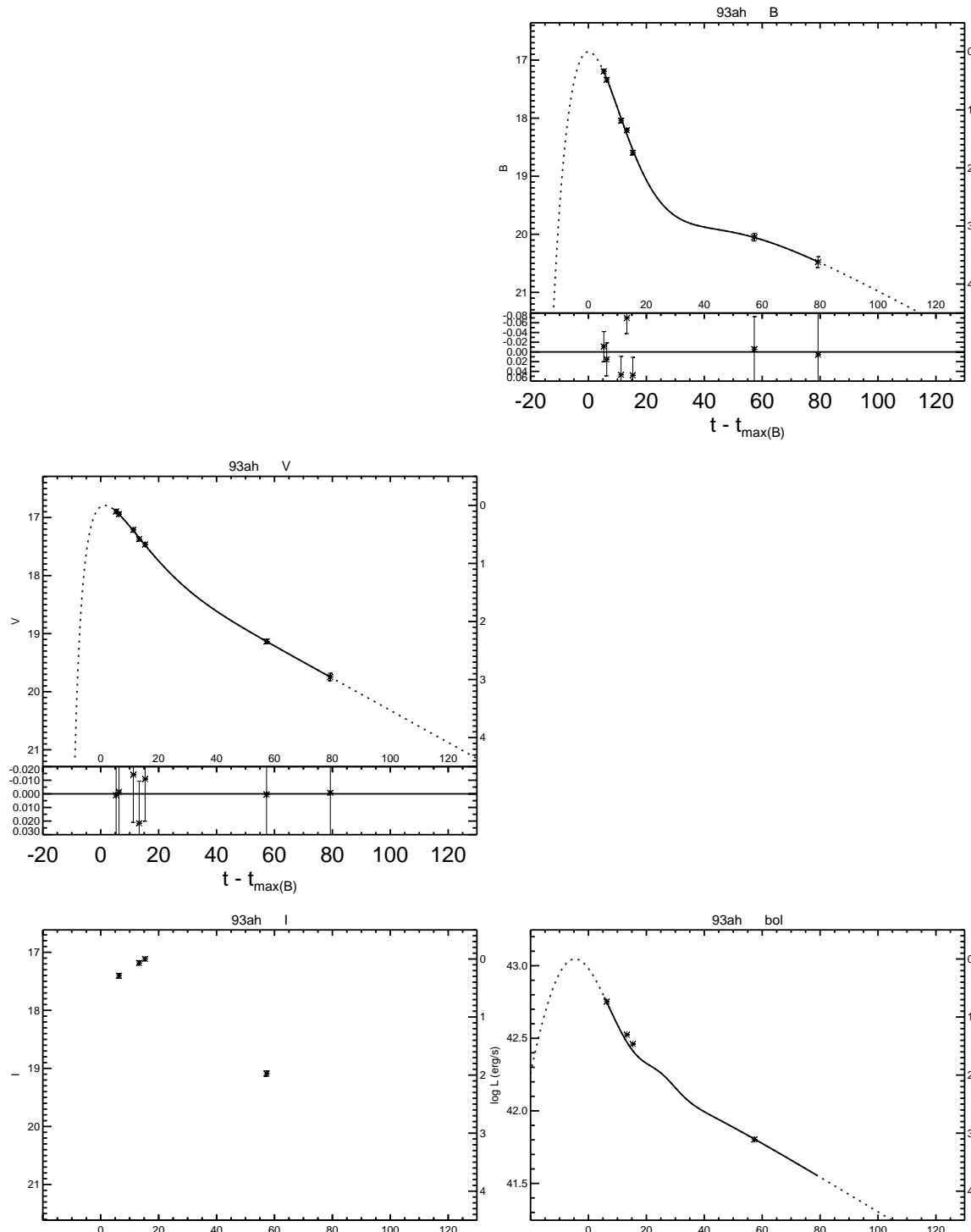


Figure A.35: *UBVRI* light curves of SN 1993ah.

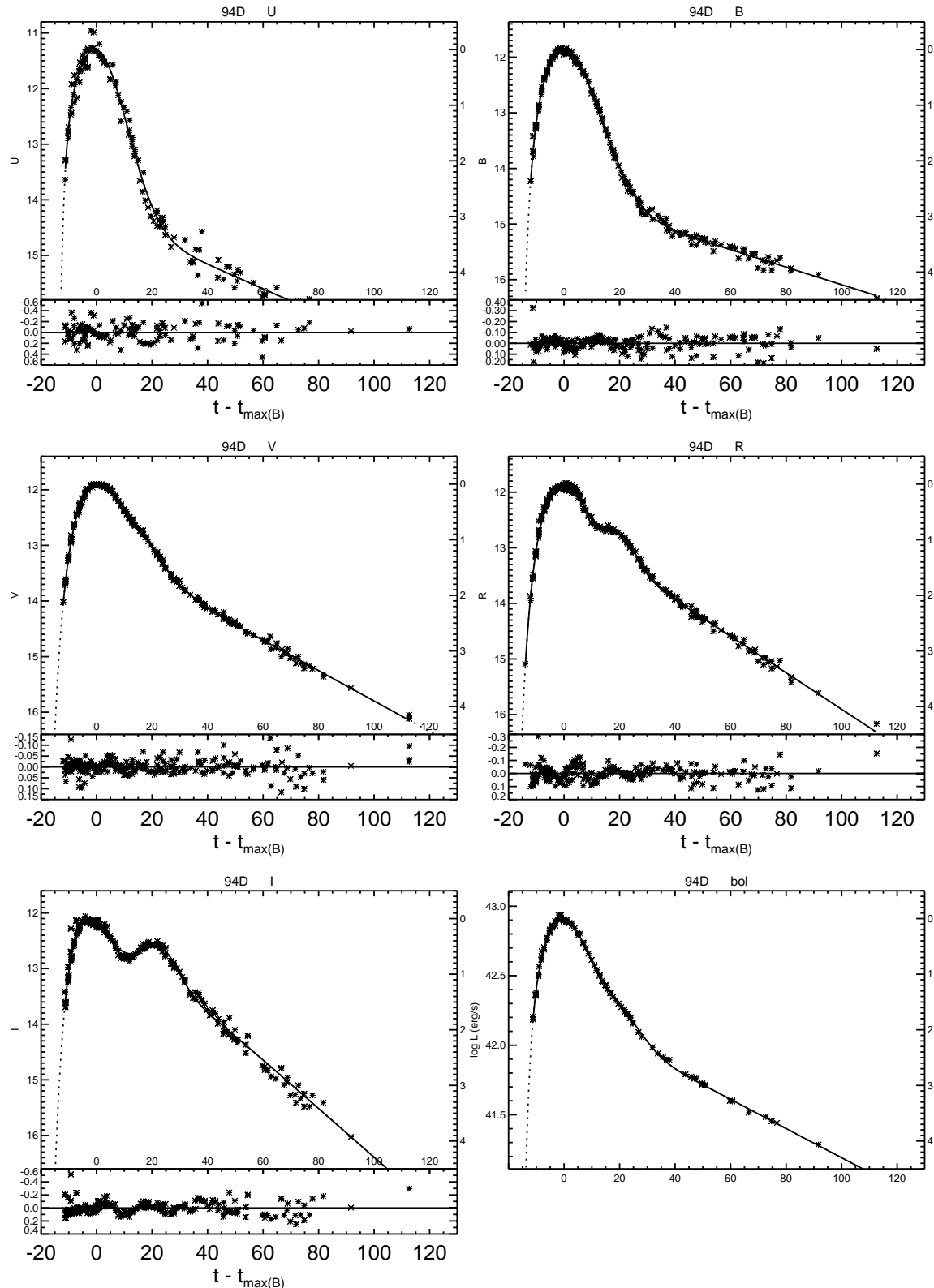


Figure A.36: $UBVR$ I light curves of SN 1994D.

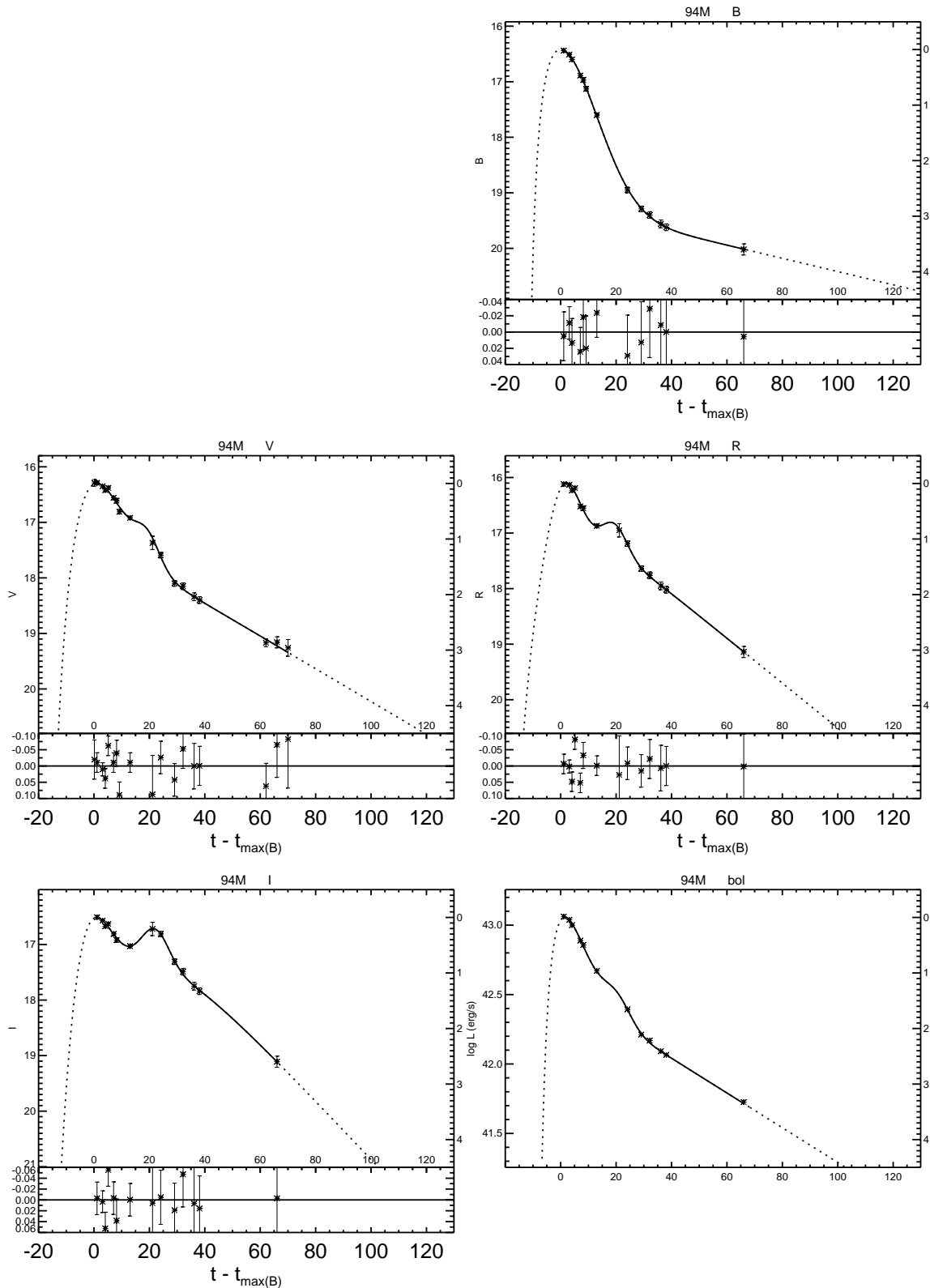


Figure A.37: *UBVRI* light curves of SN 1994M.

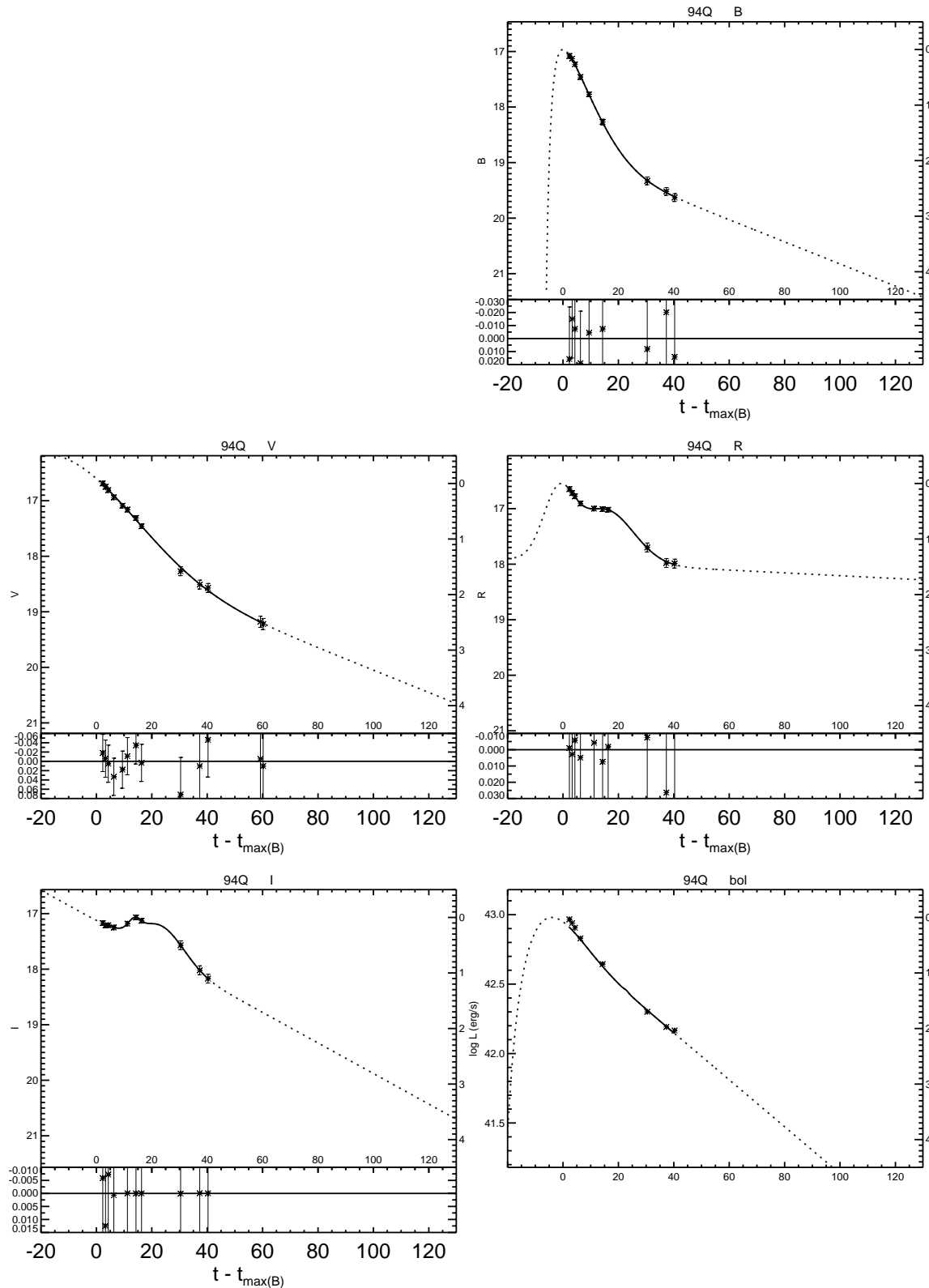


Figure A.38: *UBVRI* light curves of SN 1994Q.

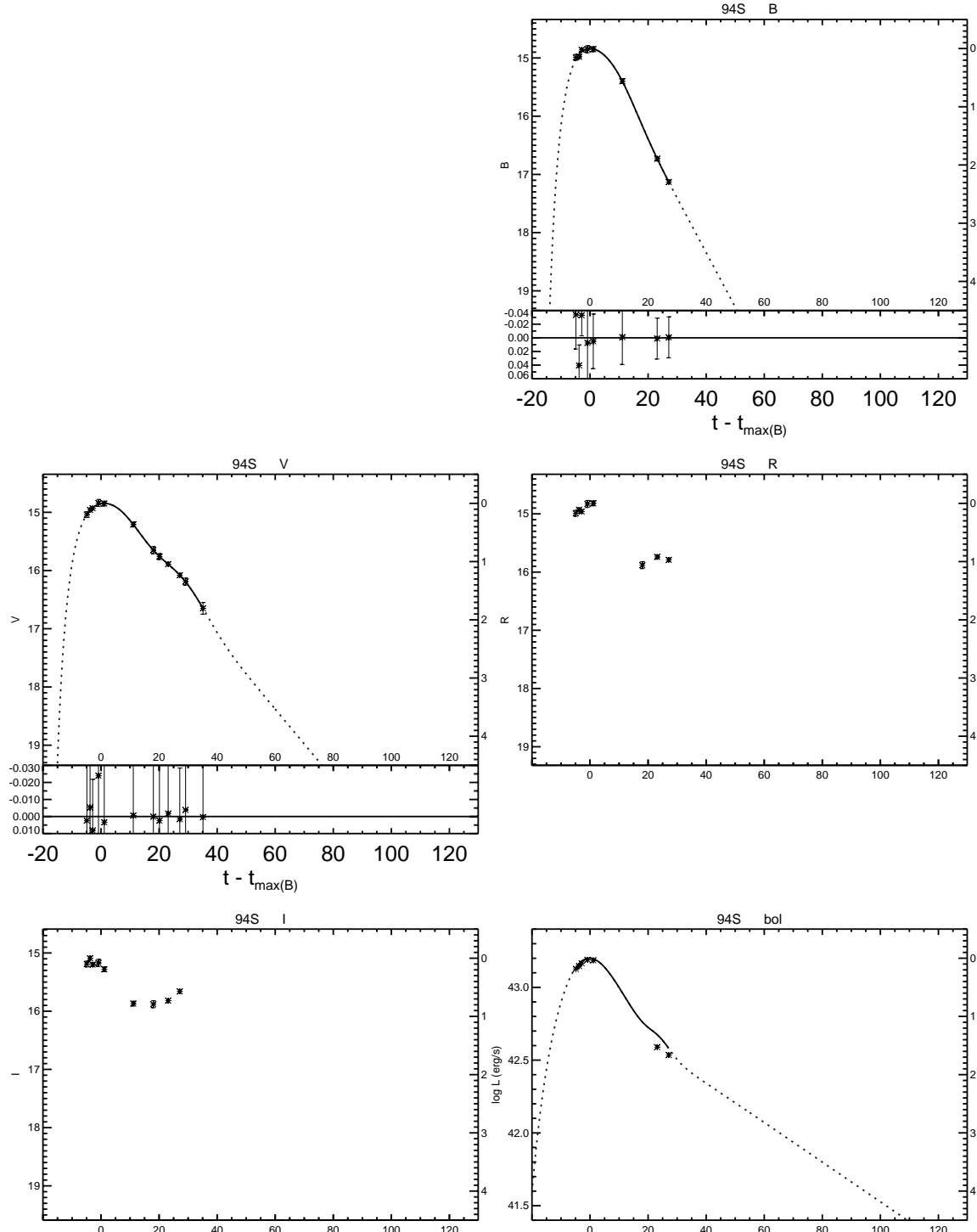


Figure A.39: *UBVRI* light curves of SN 1994S.

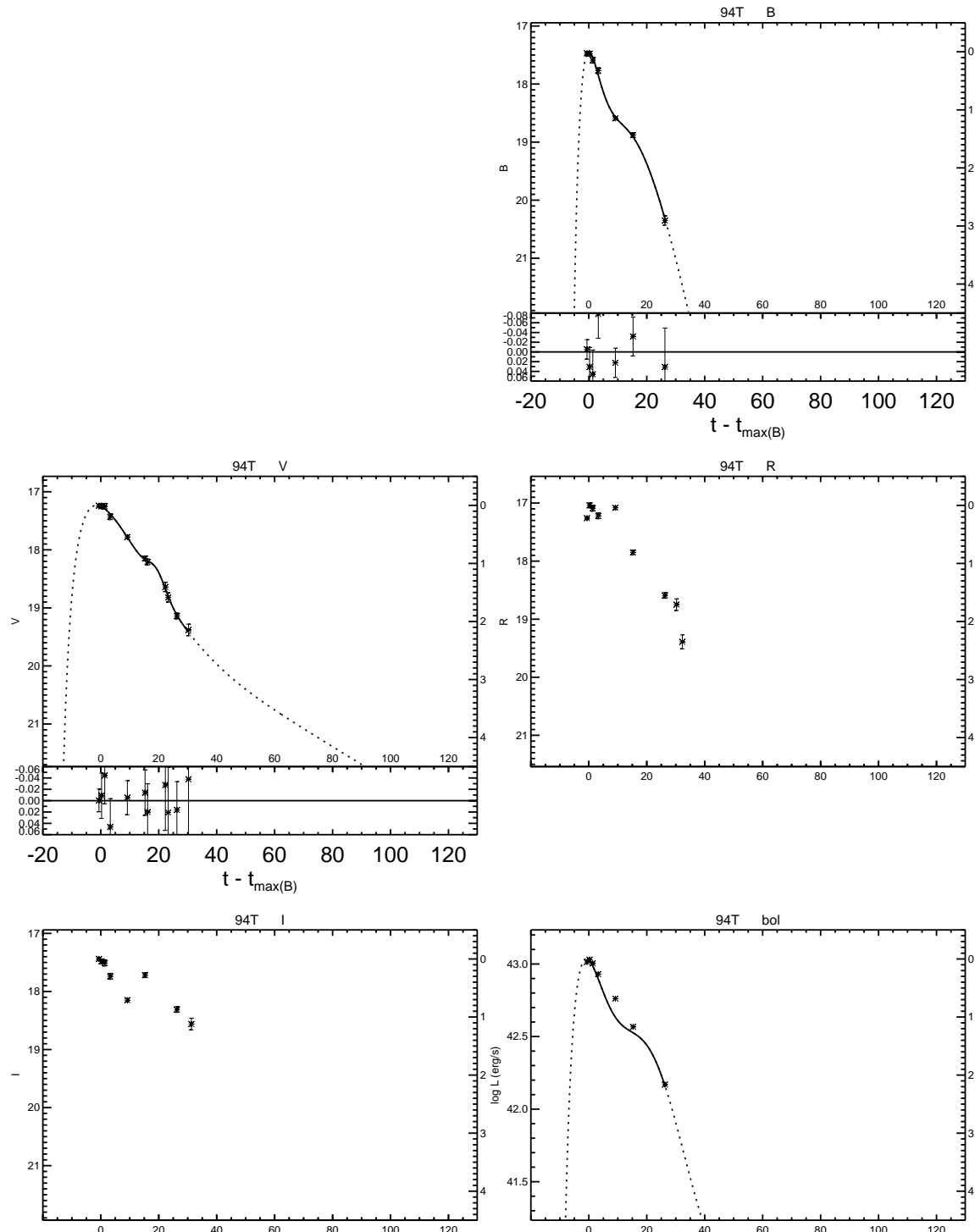


Figure A.40: *UBVRI* light curves of SN 1994T.

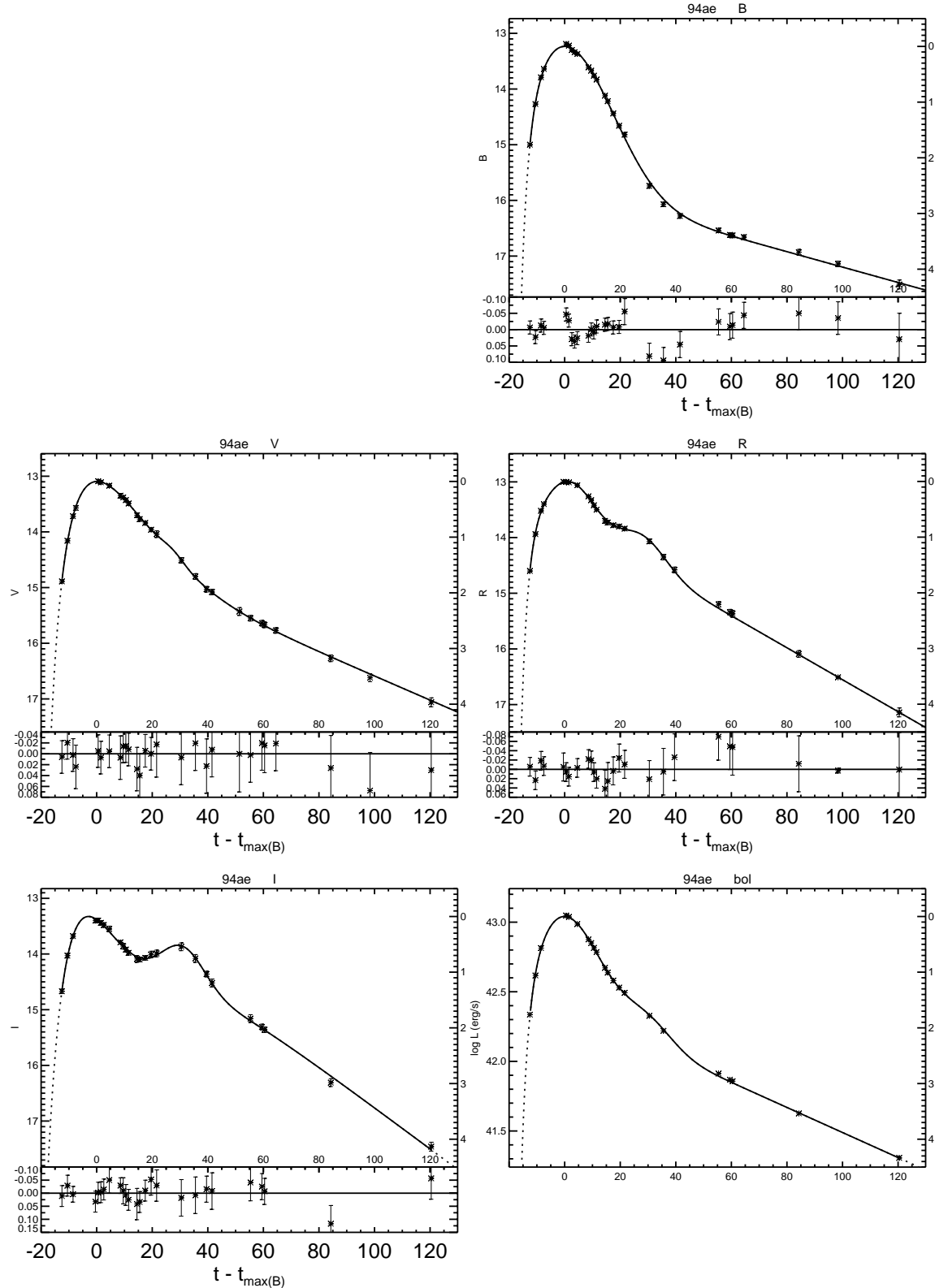


Figure A.41: *UBVRI* light curves of SN 1994ae.

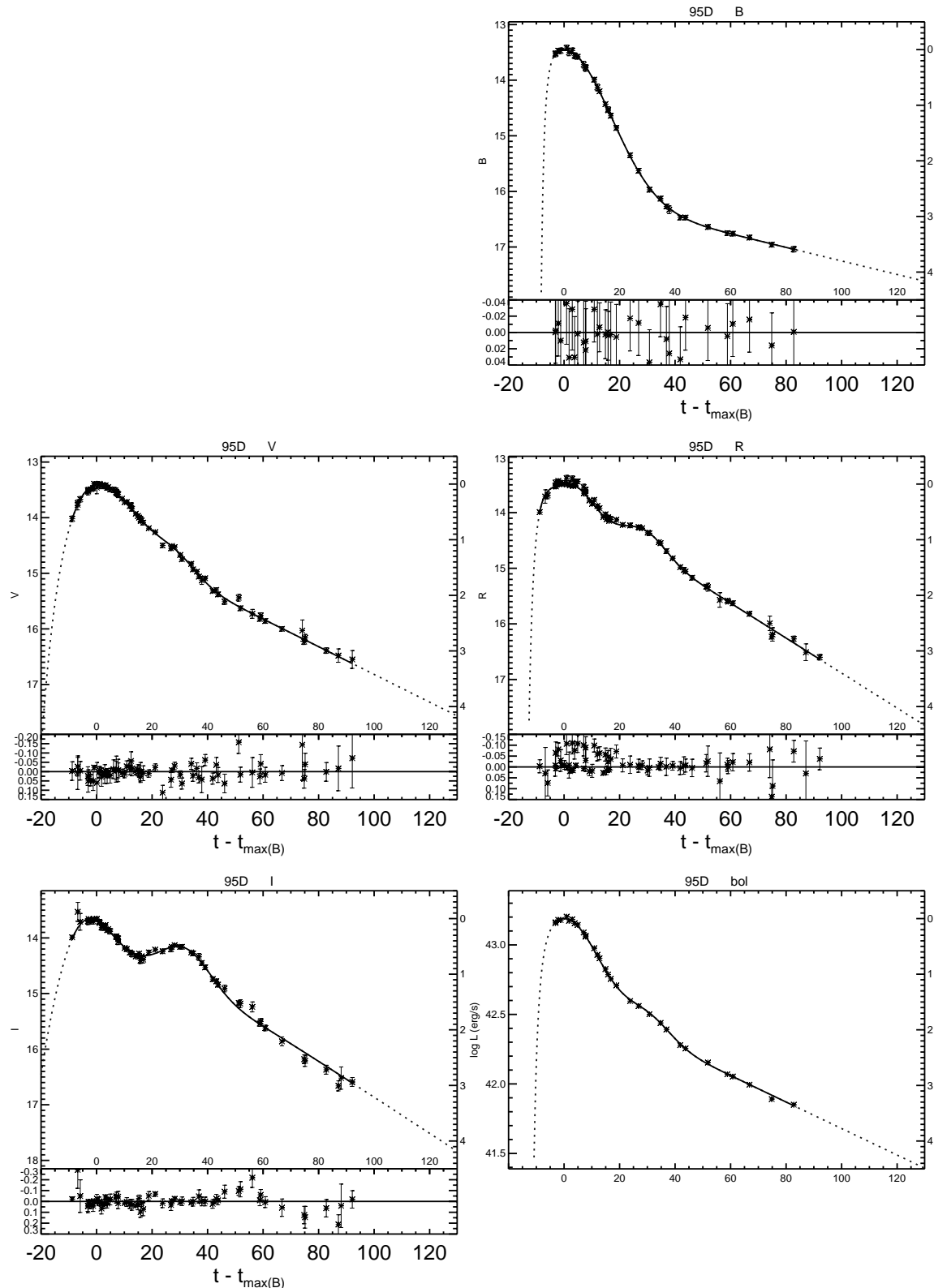


Figure A.42: *UBVRI* light curves of SN 1995D.

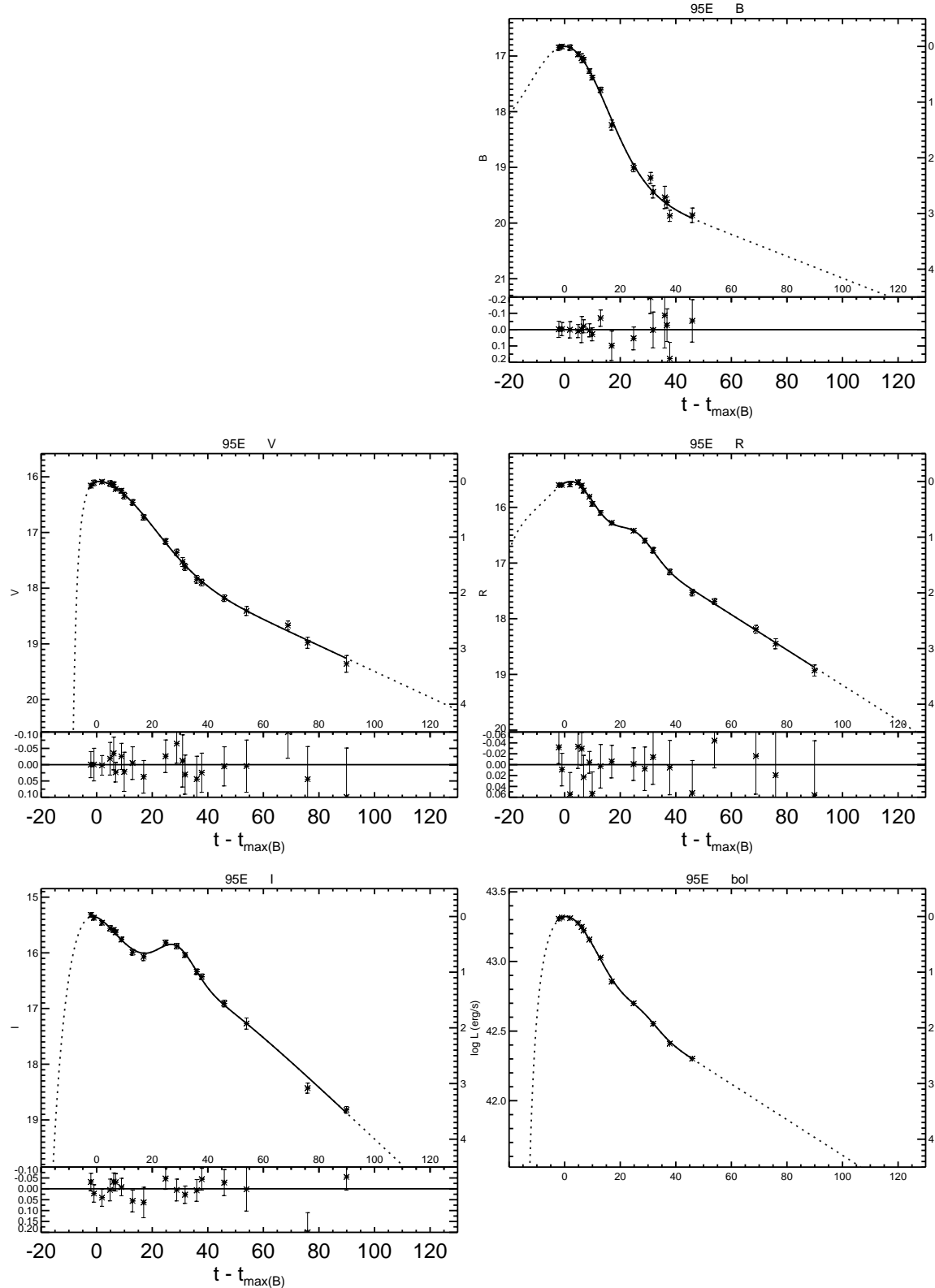


Figure A.43: *UBVRI* light curves of SN 1995E.

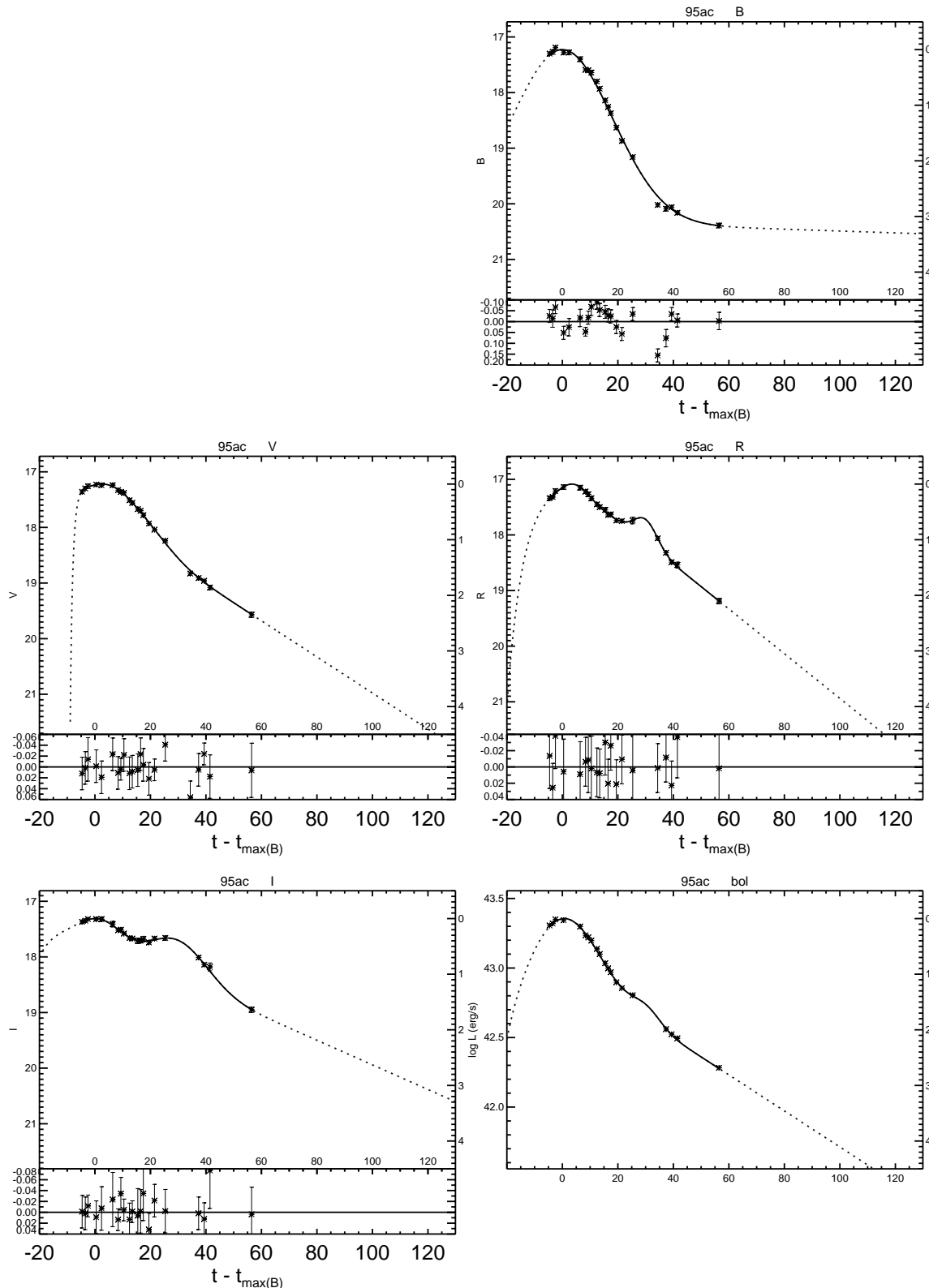


Figure A.44: *UBVRI* light curves of SN 1995ac.

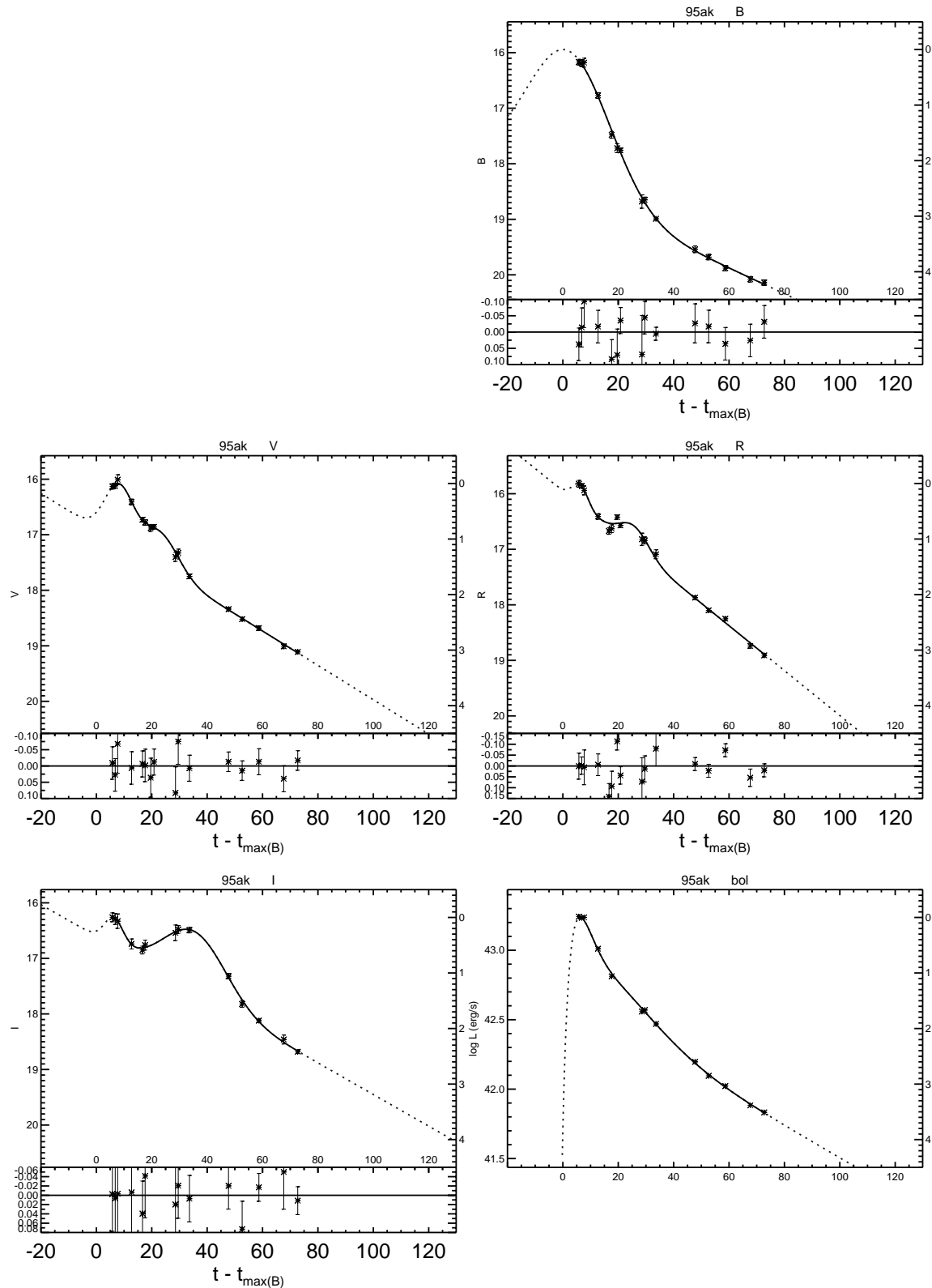


Figure A.45: *UBVRI* light curves of SN 1995ak.

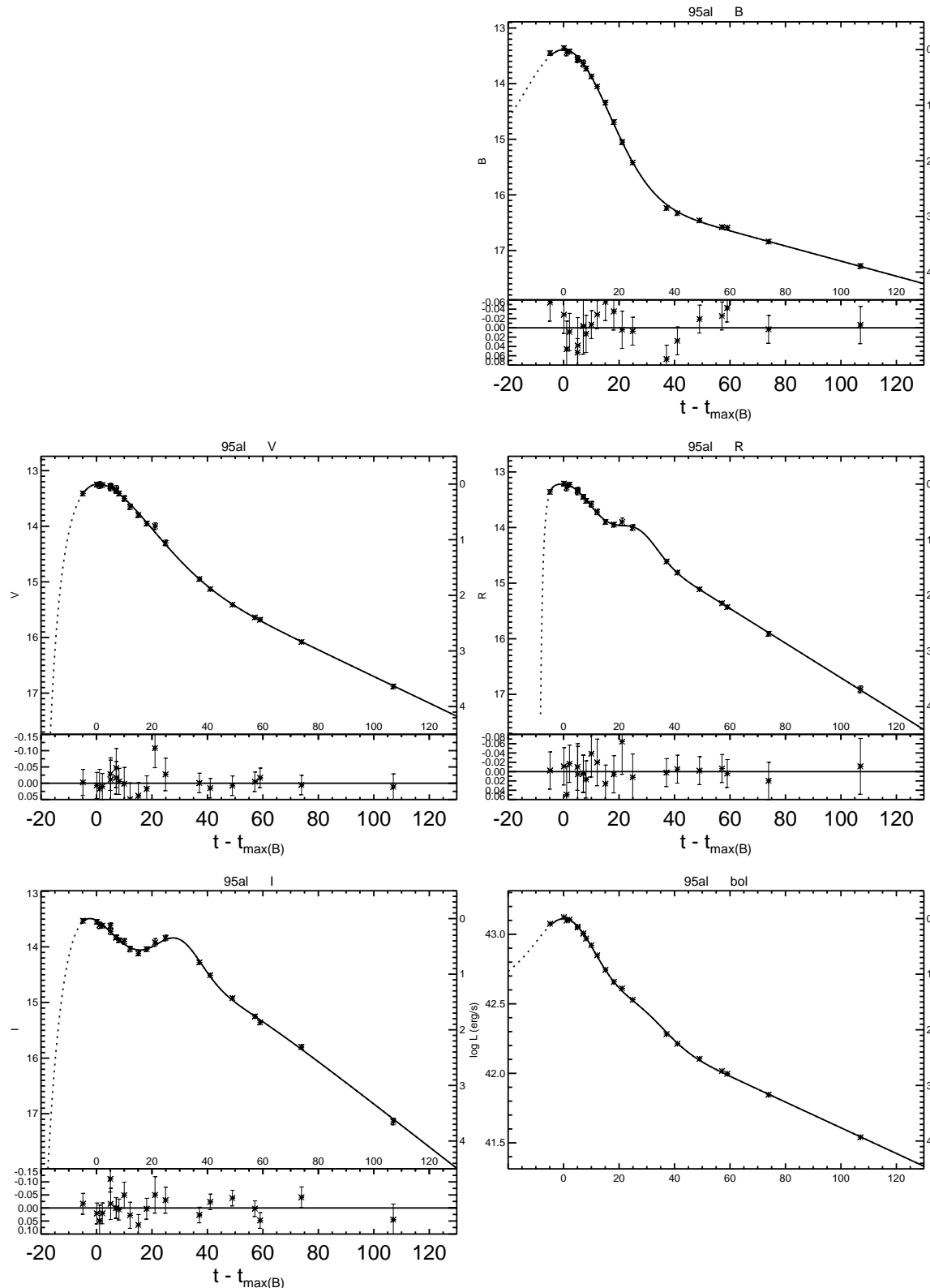


Figure A.46: *UBVR* light curves of SN 1995al.

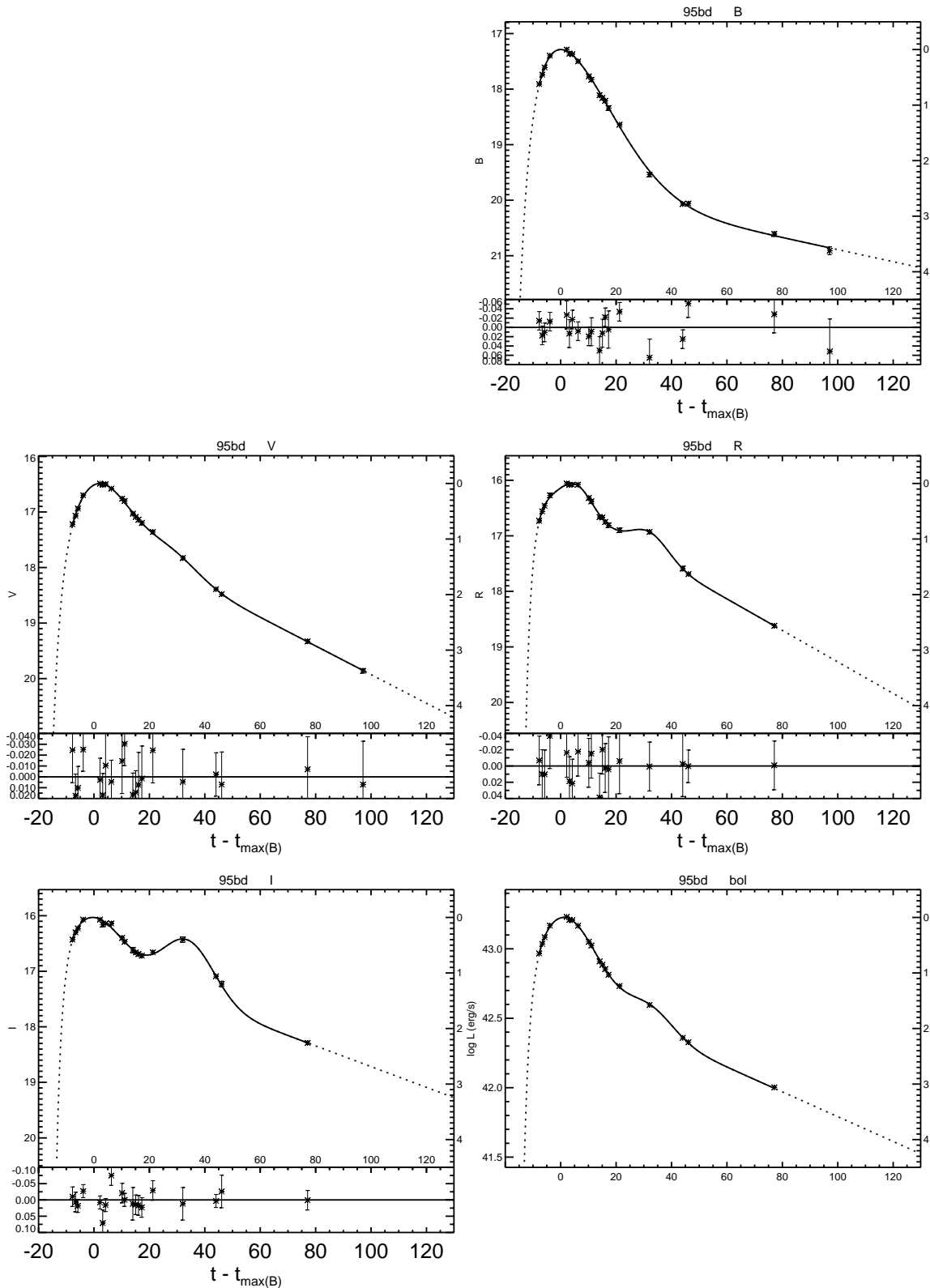


Figure A.47: *UBVRI* light curves of SN 1995bd.

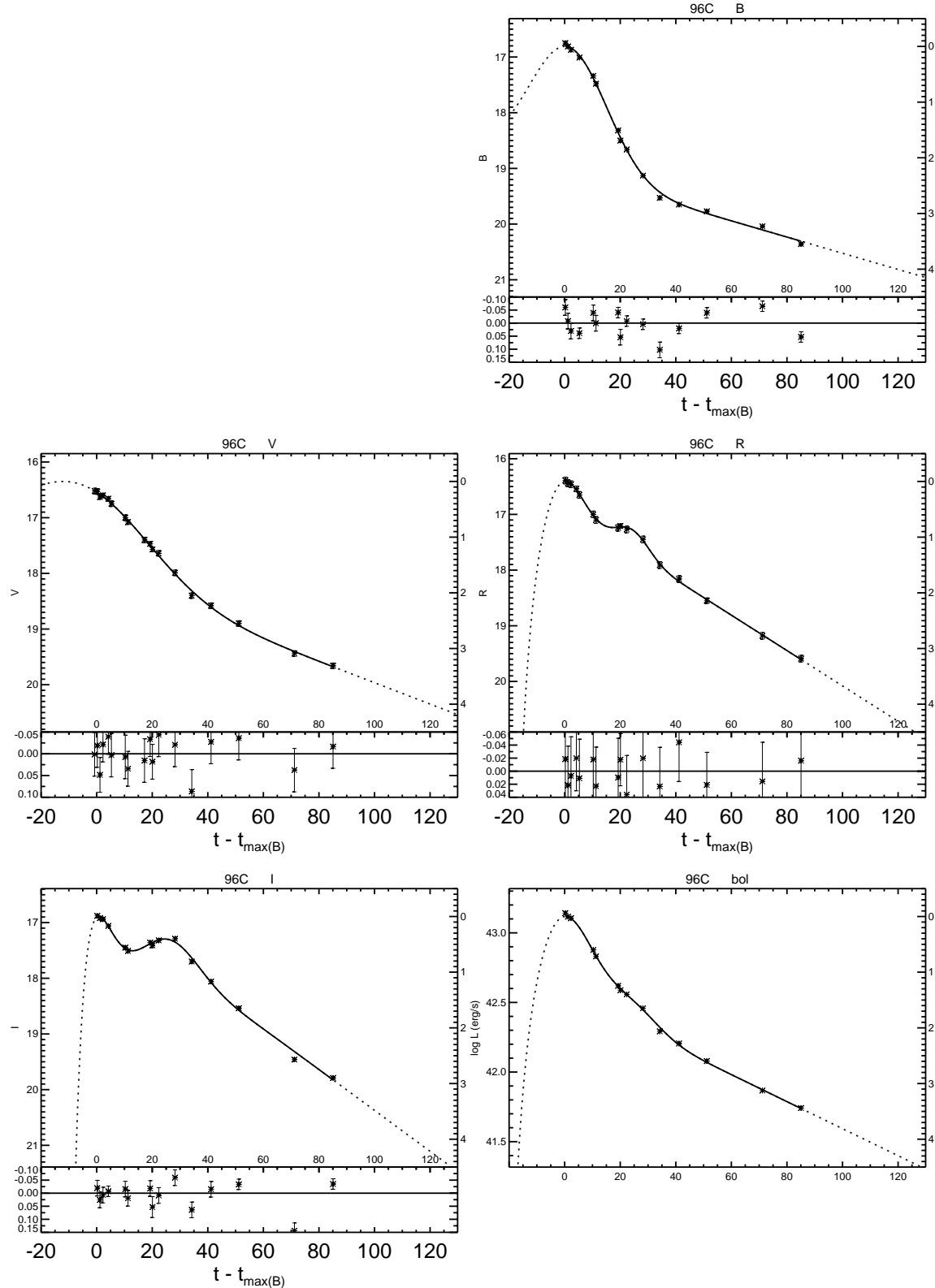


Figure A.48: *UBVRI* light curves of SN 1996C.

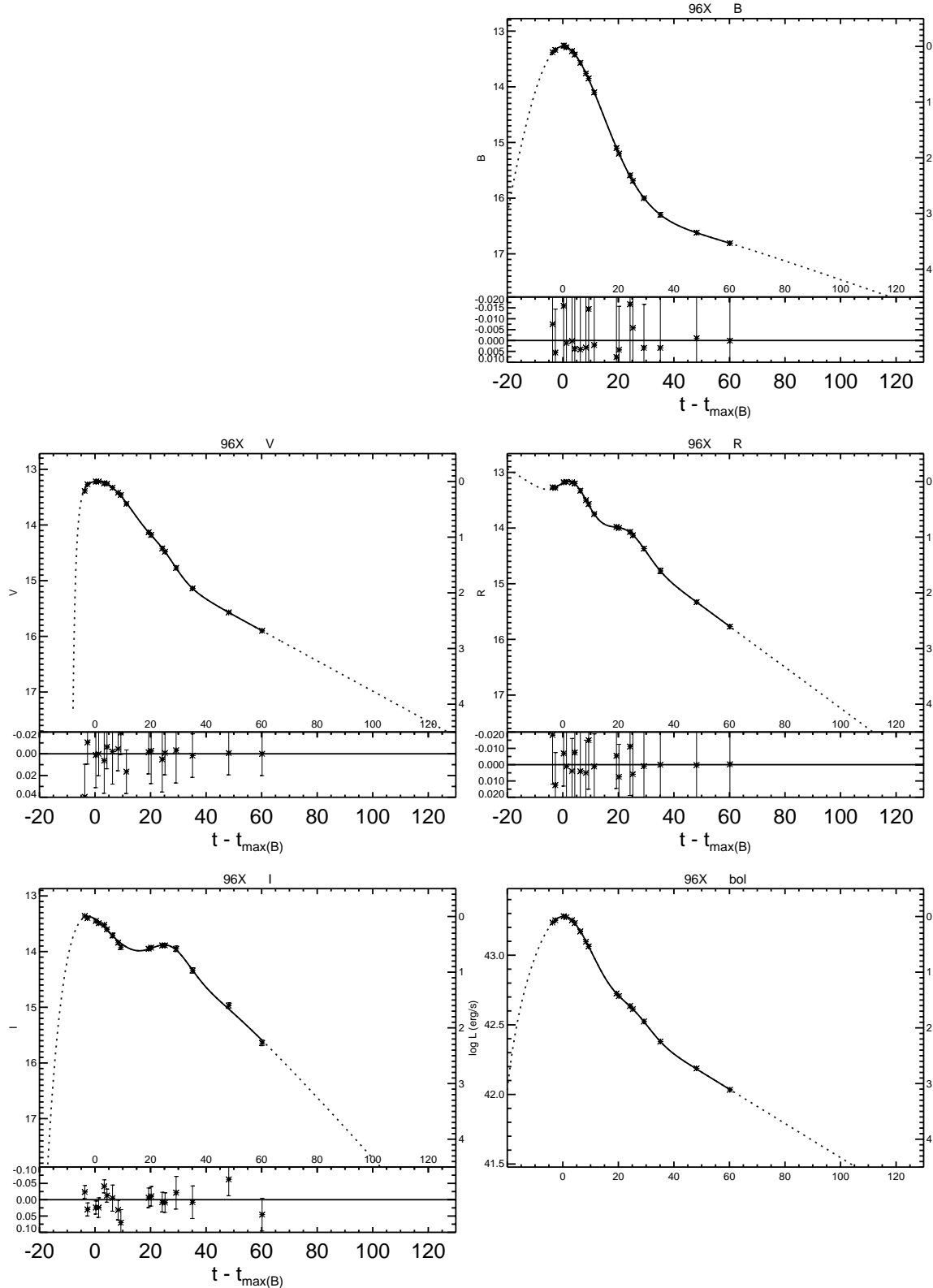


Figure A.49: *UBVRI* light curves of SN 1996X.

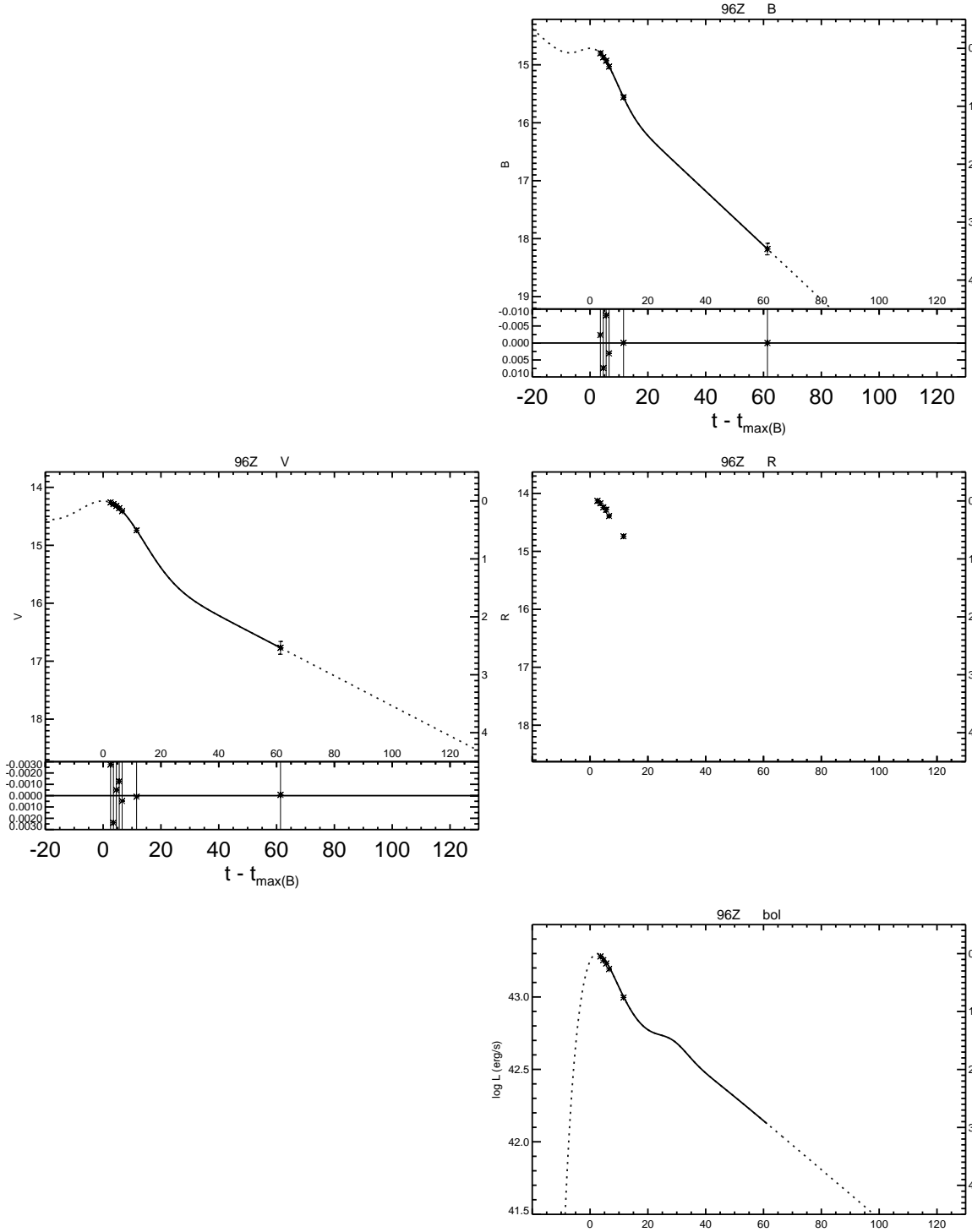


Figure A.50: *UBVRI* light curves of SN 1996Z.

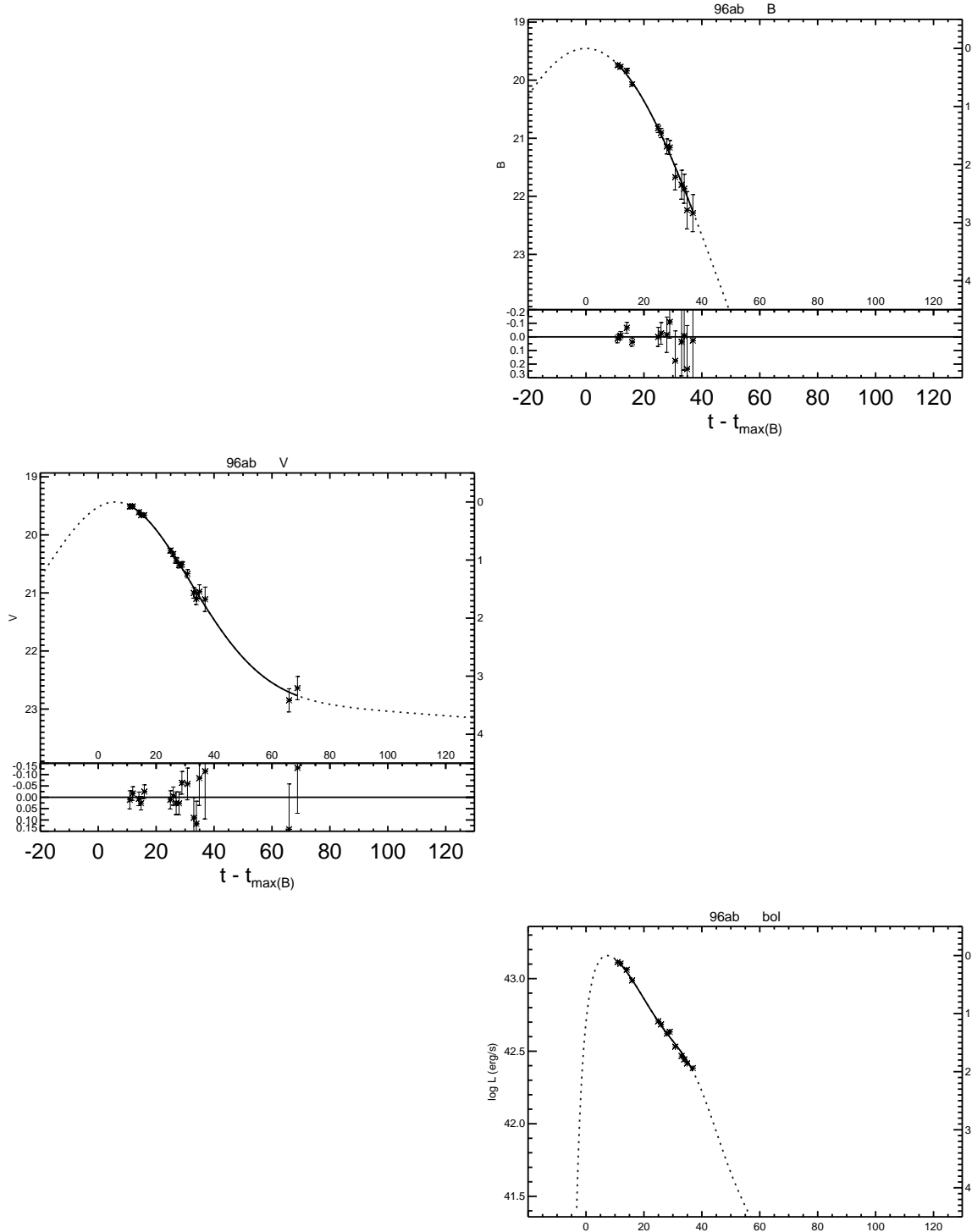


Figure A.51: *UBVRI* light curves of SN 1996ab.

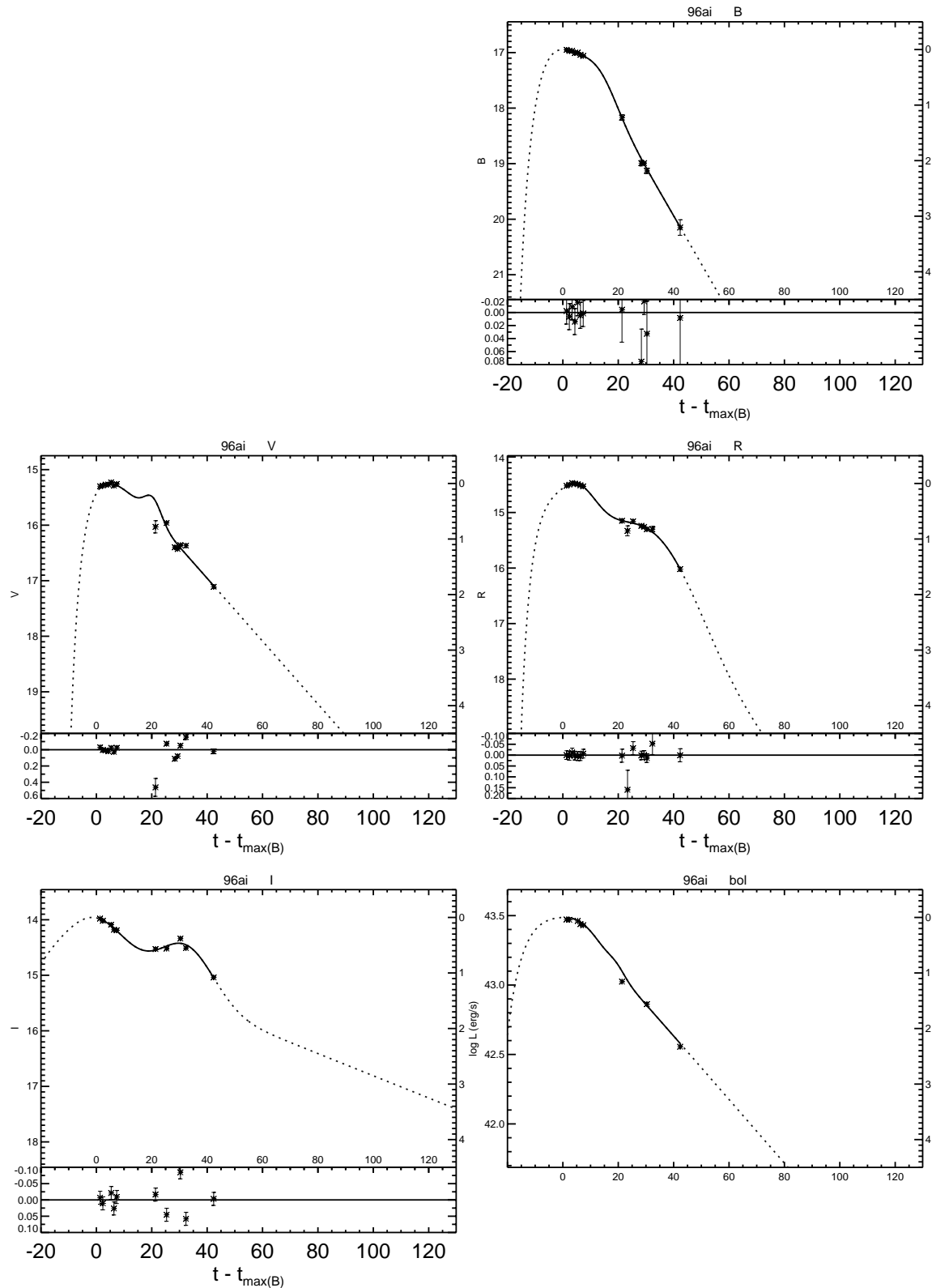


Figure A.52: $UBVRI$ light curves of SN 1996ai.

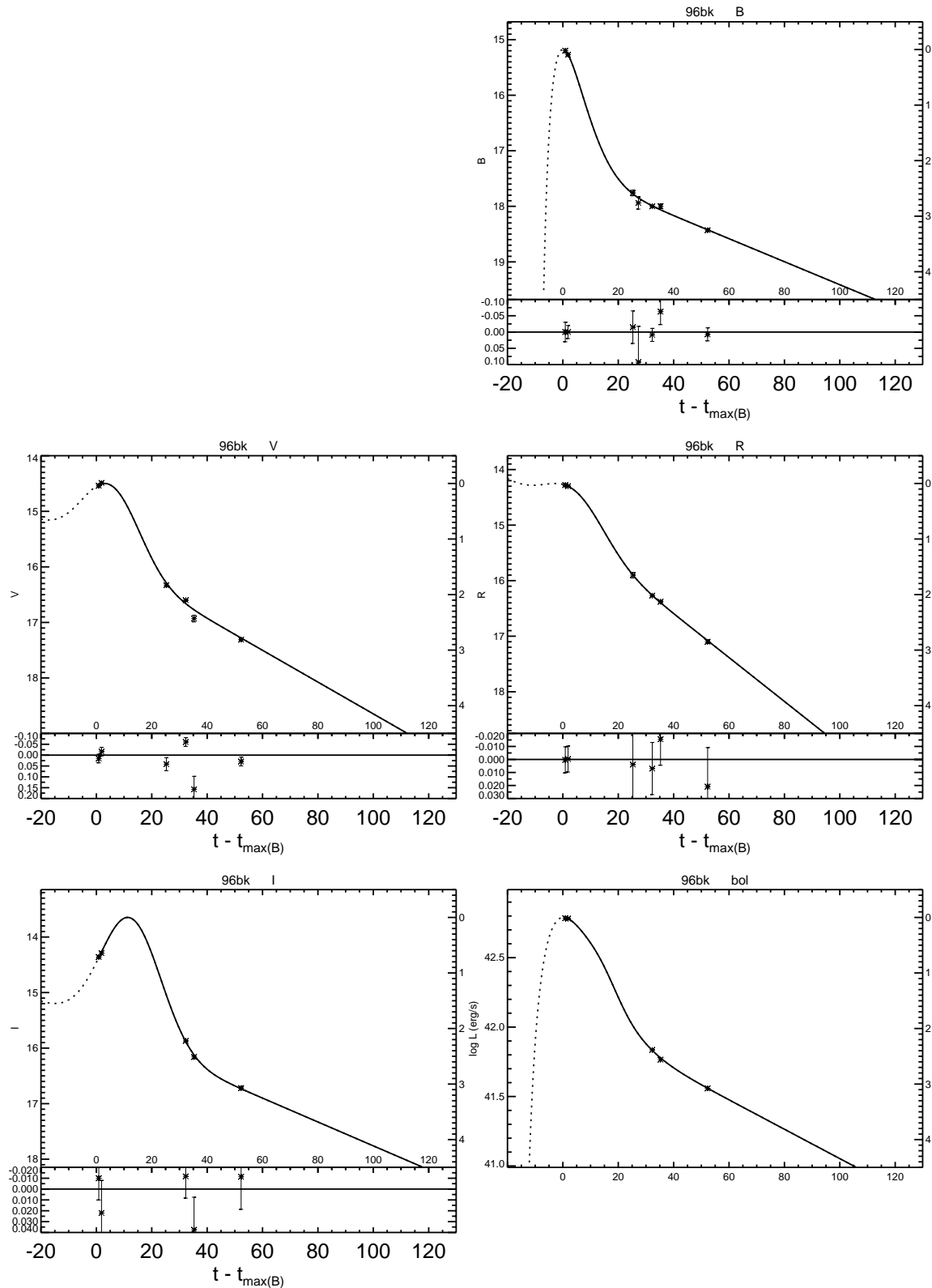


Figure A.53: *UBVRI* light curves of SN 1996bk.

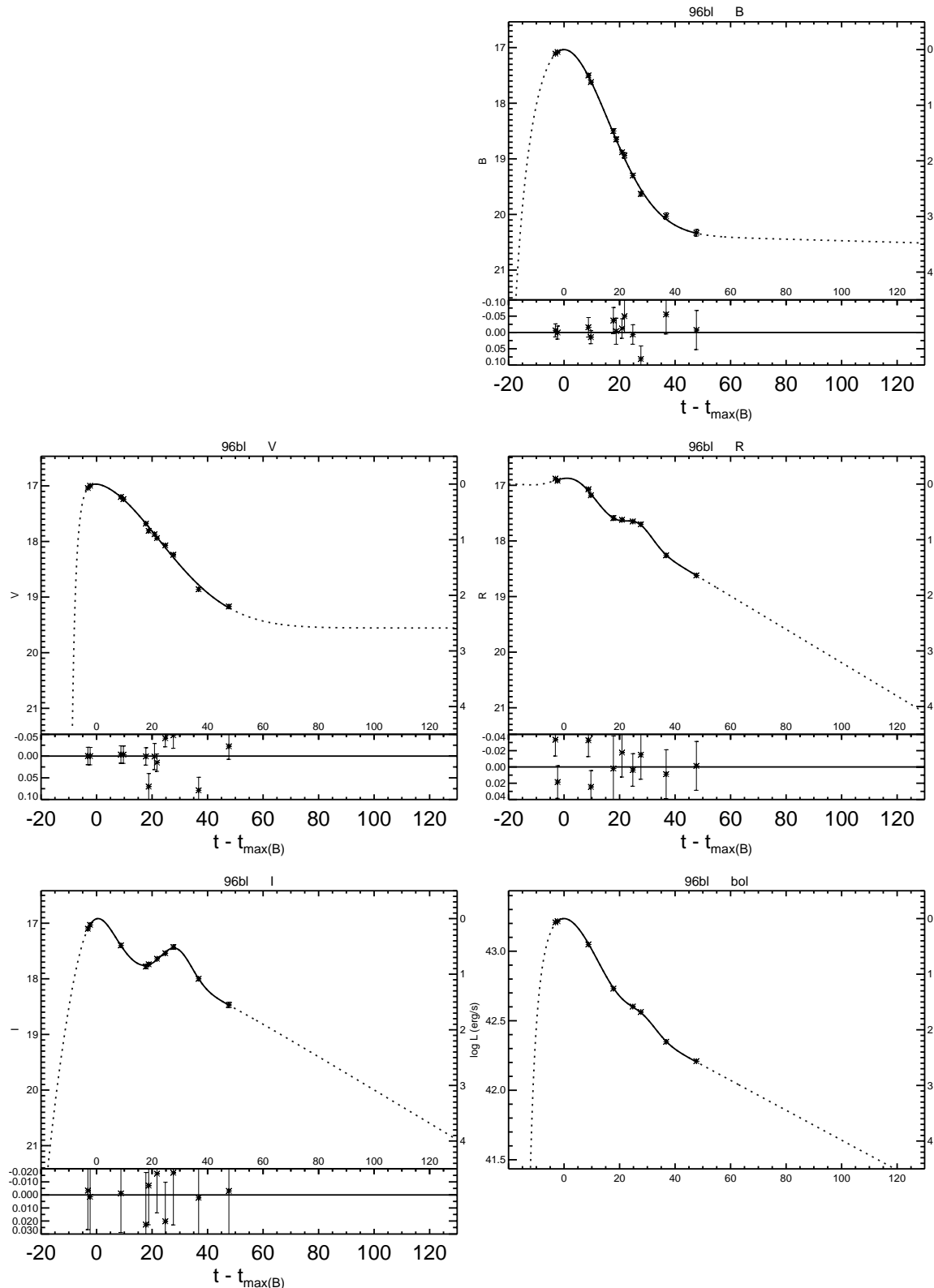


Figure A.54: *UBVR* light curves of SN 1996bl.

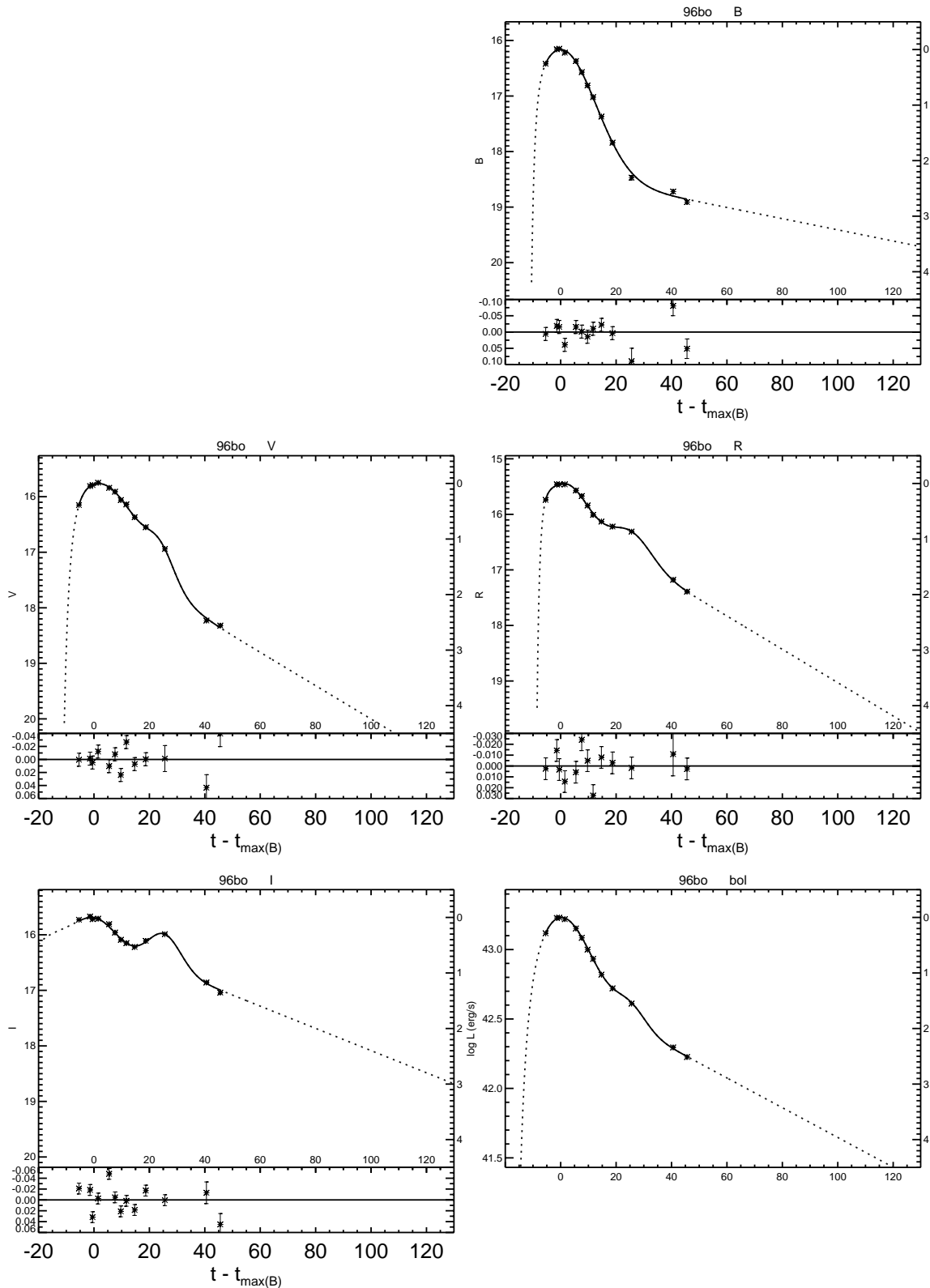


Figure A.55: *UBVRI* light curves of SN 1996bo.

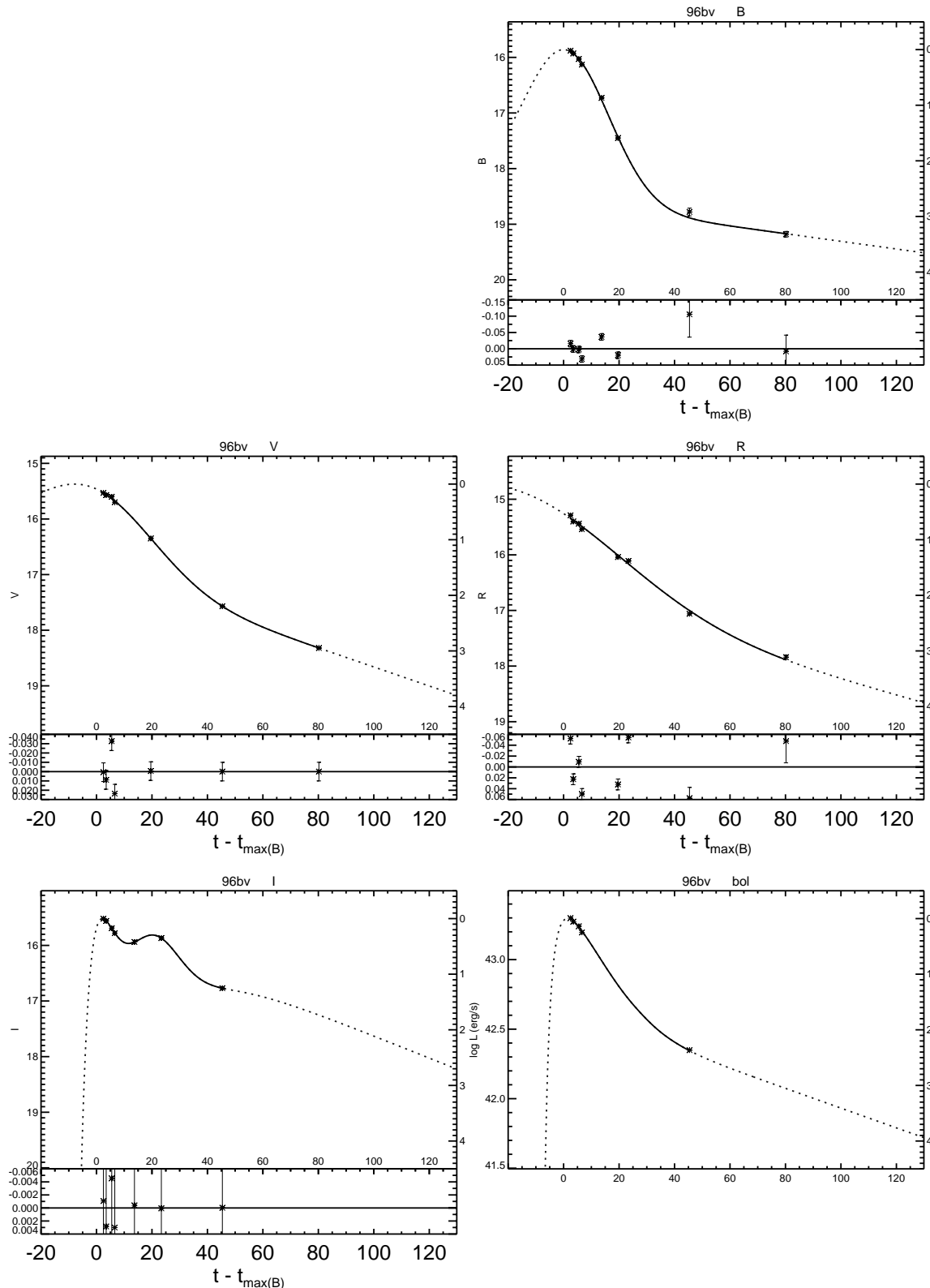


Figure A.56: $UBVRI$ light curves of SN 1996bv.

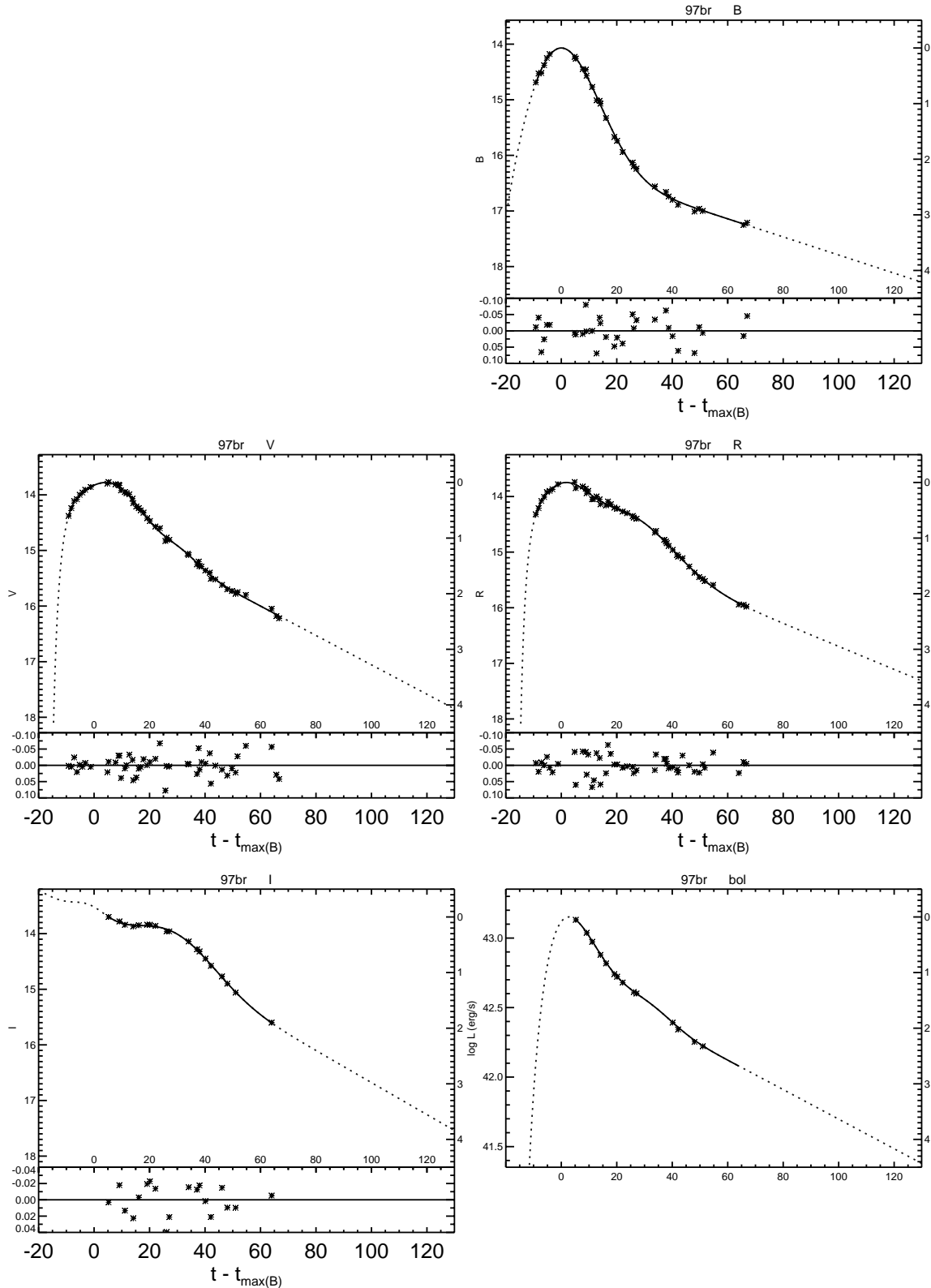


Figure A.57: *UBVRI* light curves of SN 1997br.

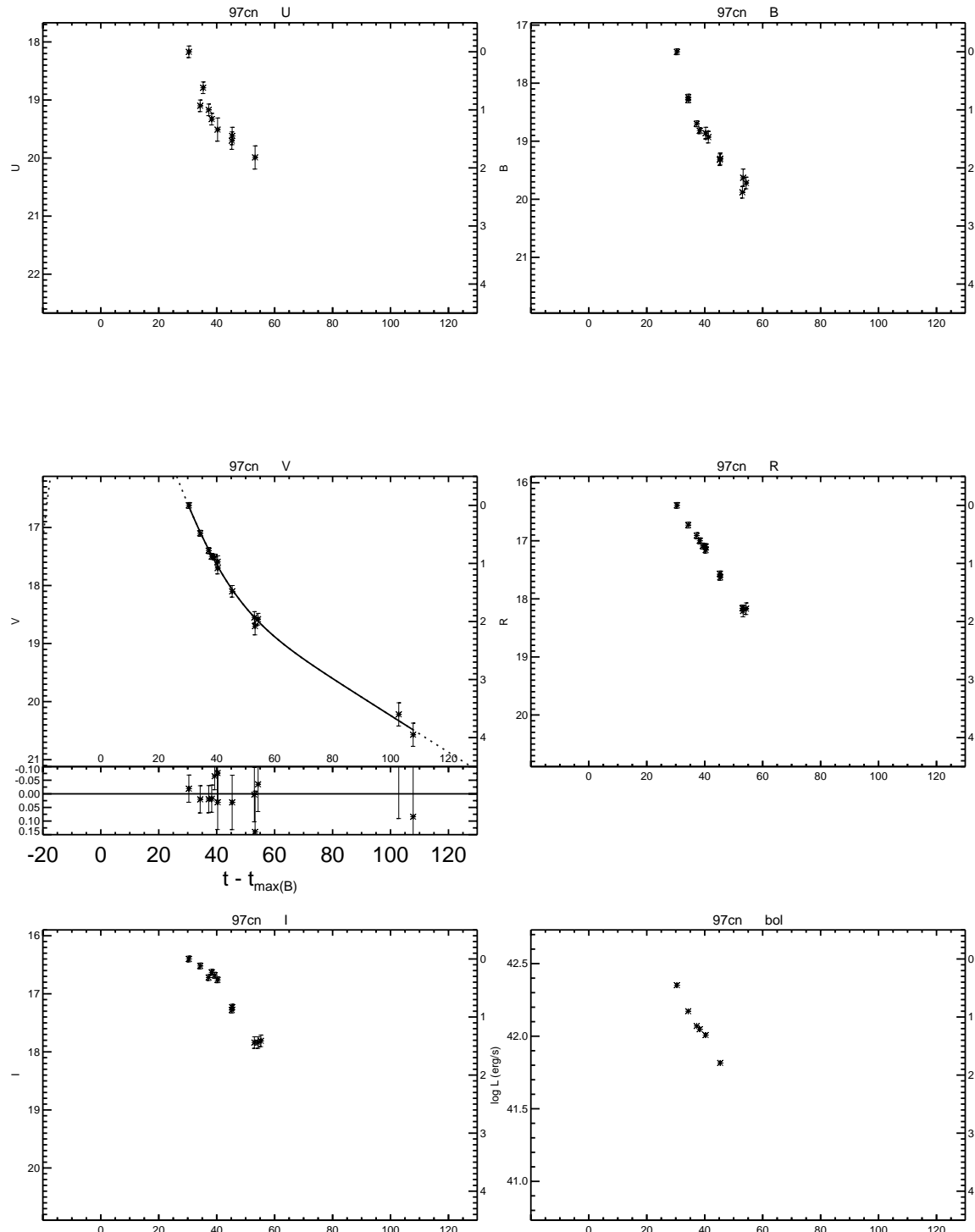


Figure A.58: *UBVRI* light curves of SN 1997cn.

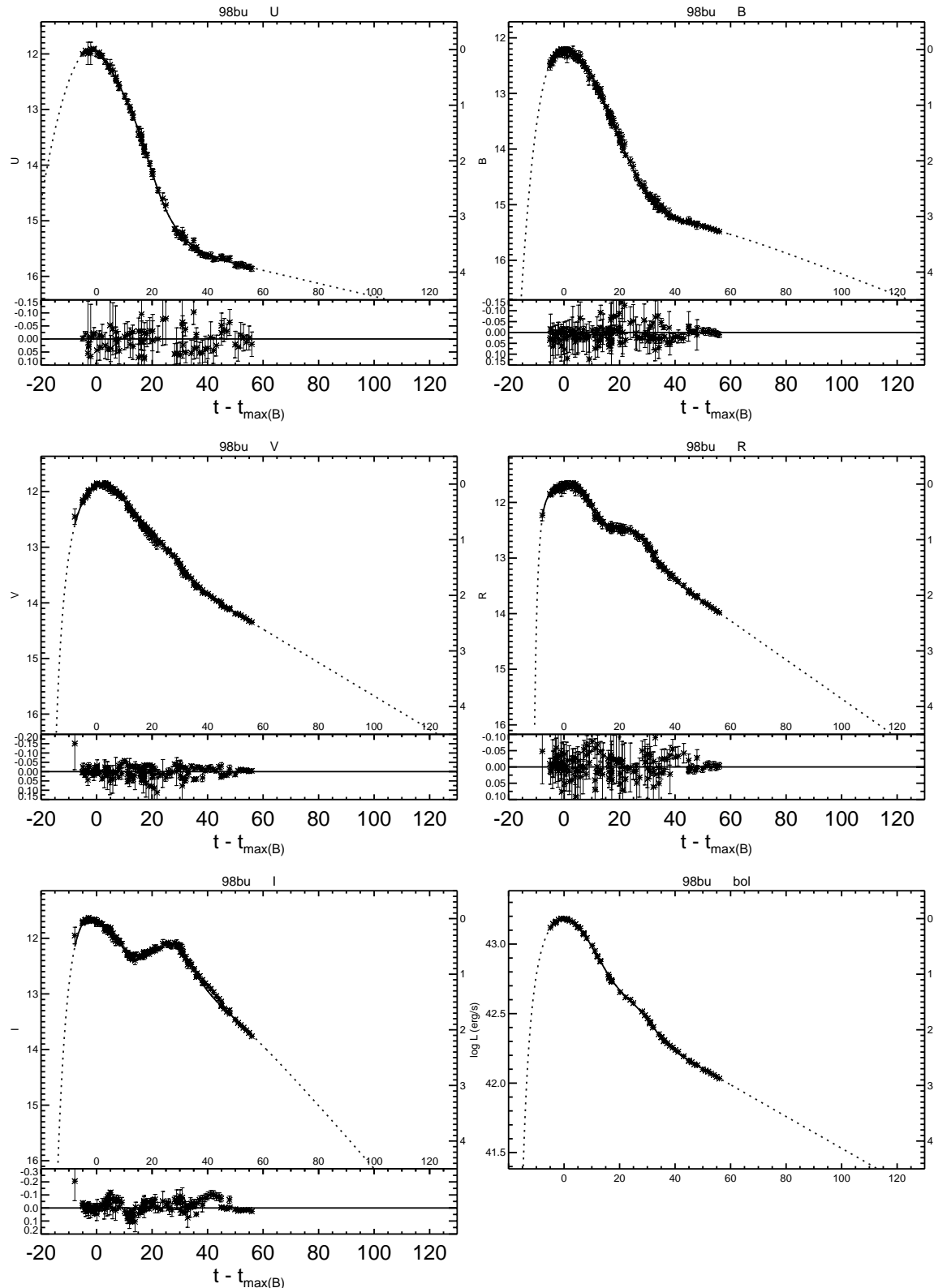


Figure A.59: *UBVRI* light curves of SN 1998bu.

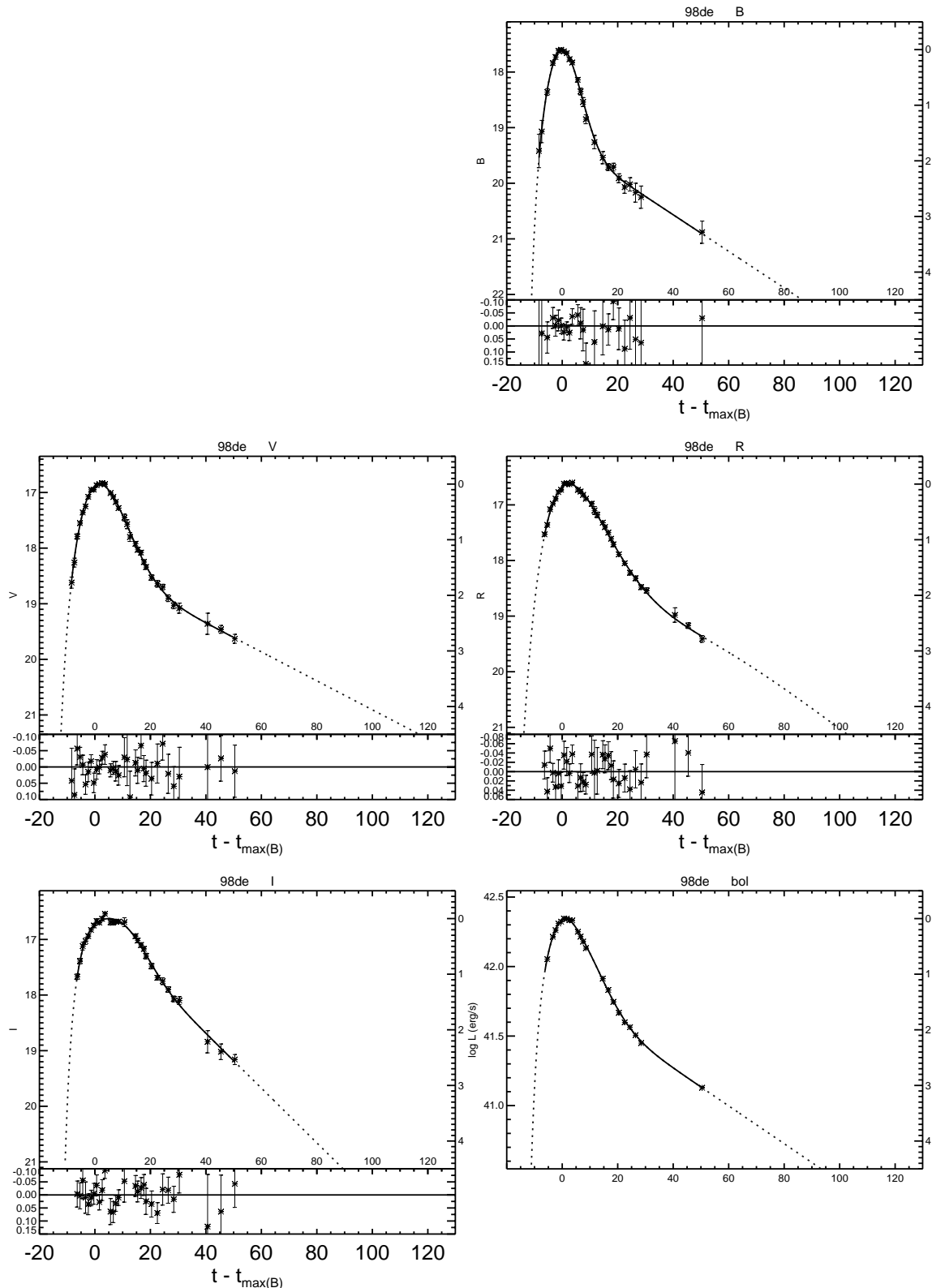


Figure A.60: $UBVRI$ light curves of SN 1998de.

Bibliography

- Aldering G., Knop R., Nugent P. (2000). “The Rise Times of High- and Low-Redshift Type Ia Supernovae Are Consistent.” *AJ*, **119**, 2110.
- Arnett W.D. (1982). “Type I Supernovae. I - Analytic Solutions for the Early Part of the Light Curve.” *ApJ*, **253**, 785.
- Arnett W.D., Branch D., Wheeler J.C. (1985). “Hubble’s Constant and Exploding Carbon-Oxygen White Dwarf Models for Type I Supernovae.” *Nature*, **314**, 337.
- Bessell M.S. (1990). “UBVRI passbands.” *PASP*, **102**, 1181.
- Bevington P.R., Robinson D.K. (1992). *Data Reduction and Error Analysis for the Physical Sciences*. McGraw-Hill, New York, second edition.
- Bouchet P., Phillips M.M., Suntzeff N.B., et al. (1991). “The Bolometric Lightcurve of Supernova 1987A. II. Results from Visible and Infrared Spectrophotometry.” *A&A*, **245**, 490.
- Bowers E.J.C., Meikle W.P.S., Geballe T.R., et al. (1997). “Infrared and Optical Spectroscopy of Type Ia Supernovae in the Nebular Phase.” *MNRAS*, **290**, 663.
- Branch D., Tammann G.A. (1992). “Type Ia Supernovae as Standard Candles.” *ARA&A*, **30**, 359.
- Cappellaro E., Mazzali P.A., Benetti S., et al. (1997). “SN Ia Light Curves and Radioactive Decay.” *A&A*, **328**, 203.
- Contardo G., Leibundgut B., Vacca W.D. (2000). “Epochs of Maximum Light and Bolometric Light Curves of Type Ia Supernovae.” *A&A*, **359**, 876.
- Davis P. (1993). “Levenberg-Marquardt Methods and Nonlinear Estimation.” *SIAM News*, **26**(6).
- Della Valle M., Kissler-Patig M., Danziger J., et al. (1998). “Globular Cluster Calibration of the Peak Brightness of the Type Ia Supernova 1992A and the Value of H_0 .” *MNRAS*, **299**, 267.
- Drenkhahn G., Richtler T. (1999). “SN 1994D in NGC 4526: a Normally Bright Type Ia Supernova.” *A&A*, **349**, 877.
- Elias J.H., Frogel J.A., Hackwell J.A., et al. (1981). “Infrared Light Curves of Type I Supernovae.” *ApJ*, **251**, L13.

- Elias J.H., Matthews K., Neugebauer G., et al. (1985). "Type I Supernovae in the Infrared and Their Use as Distance Indicators." *ApJ*, **296**, 379.
- Filippenko A.V., Richmond M.W., Branch D., et al. (1992). "The Subluminous, Spectroscopically Peculiar Type Ia Supernova 1991bg in the Elliptical Galaxy NGC 4374." *AJ*, **104**, 1543.
- Fillipenko A.V. (1997). "Optical Spectra of Supernovae." *ARA&A*, **35**, 309.
- Fisher A., Branch D., Hatano K., et al. (1999). "On the Spectrum and Nature of the Peculiar Type Ia Supernova 1991T." *MNRAS*, **304**, 67.
- Garnavich P.M., Kirshner R.P., Challis P., et al. (1998). "Constraints on Cosmological Models from Hubble Space Telescope Observations of High-z Supernovae." *ApJ*, **493**, L53.
- Hamuy M., Phillips M.M., Maza J., et al. (1991). "The Optical Light Curves of SN 1980N and SN 1981D in NGS 1316 (Fornax A)." *AJ*, **102**, 208.
- Hamuy M., Phillips M.M., Suntzeff N.B., et al. (1996a). "BVRI Light Curves for 29 Type Ia Supernovae." *AJ*, **112**, 2408.
- Hamuy M., Phillips M.M., Suntzeff N.B., et al. (1996b). "The Absolute Luminosities of the Calan/Tololo Type Ia Supernovae." *AJ*, **112**, 2391.
- Hamuy M., Phillips M.M., Suntzeff N.B., et al. (1996c). "The Hubble Diagram of the Calan/Tololo Type Ia Supernovae and the Value of H_0 ." *AJ*, **112**, 2398.
- Hamuy M., Phillips M.M., Suntzeff N.B., et al. (1996d). "The Morphology of Type Ia Supernovae Light Curves." *AJ*, **112**, 2438.
- Hernandez M., Meikle W.P.S., Aparicio A., et al. (2000). "An early-time infrared and optical study of the Type Ia Supernova 1998bu in M96." *MNRAS*, **319**, 223.
- Hillebrandt W., Niemeyer J.C. (2000). "Type Ia Supernova Explosion Models." *ARA&A*, **38**, 191.
- Höflich P., Wheeler J.C., Thielemann F.K. (1998). "Type Ia Supernovae: Influence of the Initial Composition on the Nucleosynthesis, Light Curves, and Spectra and Consequences for the Determination of Ω_M and Λ ." *ApJ*, **495**, 617.
- Jacoby G.H., Branch D., Clardullo R., et al. (1992). "A Critical Review of Selected Techniques for Measuring Extragalactic Distances." *PASP*, **104**, 599.
- Jeffery D.J. (2001). "Radioactive Decay Energy Deposition in Supernovae and the Exponential/Quasi-Exponential Behavior of Late-Time Supernova Light Curves." arXiv:astro-ph/9907015.
- Jeffery D.J., Leibundgut B., Kirshner R.P., et al. (1992). "Analysis of the Photospheric Epoch Spectra of Type Ia Supernovae SN 1990N and SN 1991T." *ApJ*, **397**, 304.
- Jha S., Garnavich P.M., Kirshner R.P., et al. (1999). "The Type Ia Supernova 1998bu in M96 and the Hubble Constant." *ApJS*, **125**, 73.

- Jha S., the High-Z Supernova Search Team (2001). "Testing Cosmic Acceleration with Type Ia Supernovae." In A. Lasenby, A. Wilkinson (eds.), *New Cosmological Data and the Values of the Fundamental Parameters*, volume 201 of *IAU Symposium*. arXiv:astro-ph/0101521.
- Kirshner R.P., Jeffery D.J., Leibundgut B., et al. (1993). "SN 1992A: Ultraviolet and Optical Studies Based on HST, IUE, and CTIO Observations." *ApJ*, **415**, 589.
- Kuchner M.J., Kirshner R.P., Pinto P.A., et al. (1994). "Evidence for $^{56}\text{Ni} \rightarrow ^{56}\text{Co} \rightarrow ^{56}\text{Fe}$ Decay in Type Ia Supernovae." *ApJ*, **426**, L89.
- Leibundgut B. (1988). *Light Curves of Supernovae Type I*. Ph.D. thesis, Universität Basel.
- Leibundgut B. (2000). "Type Ia Supernovae." *A&A Rev.*, **10**, 179.
- Leibundgut B., Kirshner R.P., Filippenko A.V., et al. (1991). "Premaximum Observations of the Type Ia SN 1990N." *ApJ*, **371**, L23.
- Leibundgut B., Kirshner R.P., Phillips M.M., et al. (1993). "SN 1991bg - A Type Ia Supernova with a Difference." *AJ*, **105**, 301.
- Li W.D., Qiu Y.L., Qiao Q.Y., et al. (1999). "The Type Ia Supernova 1997br in ESO 576-G40." *AJ*, **117**, 2709.
- Lira P., Suntzeff N.B., Phillips M.M., et al. (1998). "Optical Light Curves of the Type Ia Supernovae SN 1990N and SN 1991T." *AJ*, **115**, 234.
- Mazzali P.A., Cappellaro E., Danziger I.J., et al. (1998). "Nebular Velocities in Type Ia Supernovae and Their Relationship to Light Curves." *ApJ*, **499**, L49.
- Meikle P., Hernandez M. (2000). "Infrared and Optical Study of the Type Ia SN 1998bu in M96." *Mem. Soc. Astron. Italiana*, **71**(2), 299.
- Meikle W.P.S. (2000). "The Absolute Infrared Magnitudes of Type Ia Supernovae." *MNRAS*, **314**, 782.
- Meikle W.P.S., Cumming R.J., Geballe T.R., et al. (1996). "An Early-Time Infrared and Optical Study of the Type Ia Supernovae SN 1994D and 1991T." *MNRAS*, **281**, 263.
- Milne P.A., The L.S., Leising M.D. (1999). "Positron Escape from Type Ia Supernovae." *ApJS*, **124**, 503.
- Minkowski R. (1941). "Spectra of Supernovae." *PASP*, **53**, 224.
- Modjaz M., Li W., Filippenko A.V., et al. (2001). "The Subluminous Type Ia Supernova 1998de in NGC 252." *PASP*. submitted, arXiv:astro-ph/0008012.
- Munari U., Barbon R., Tomasella L., et al. (1998). "Supernova 1998bu in NGC 3368." *IAU Circ.*, **6902**, 1.
- Nadyozhin D.K. (1994). "The Properties of Ni \rightarrow Co \rightarrow Fe decay." *ApJS*, **92**, 527.
- Patat F., Benetti S., Cappellaro E., et al. (1996). "The Type Ia Supernova 1994D in NGC 4526: The Early Phases." *MNRAS*, **278**, 111.

- Perlmutter S., Aldering G., Goldhaber G., et al. (1999). "Measurements of Ω and Λ from 42 High-Redshift Supernovae." *ApJ*, **517**, 565.
- Perlmutter S., Gabi S., Goldhaber G., et al. (1997). "Measurements of the Cosmological Parameters Ω and Λ from the First Seven Supernovae at $z \geq 0.35$." *ApJ*, **483**, 565.
- Phillips M.M. (1993). "The Absolute Magnitudes of Type Ia Supernovae." *ApJ*, **413**, L105.
- Phillips M.M., Lira P., Suntzeff N.B., et al. (1999). "The Reddening-Free Decline Rate versus Luminosity Relationship for Type Ia Supernovae." *AJ*, **118**, 1766.
- Pinto P.A., Eastman R.G. (2000). "The Physics of Type Ia Supernova Light Curves. I. Analytic Results and Time Dependence." *ApJ*, **530**, 744.
- Pinto P.A., Eastman R.G. (2001). "The Type Ia Supernova Width-Luminosity Relation." *ApJ*, submitted, astro-ph/0006171.
- Press W.H., Teukolsky S.A., Vetterling W.T., et al. (1992). *Numerical Recipes in C: The Art of Scientific Computing*. Cambridge University Press, second edition.
- Richmond M.W., Treffers R.R., Filippenko A.V., et al. (1995). "UBVRI Photometry of the Type Ia SN 1994D in NGC 4526." *AJ*, **109**, 2121.
- Riess A.G. (2000). "The Case for an Accelerating Universe from Supernovae." *PASP*, **112**, 1284.
- Riess A.G. (2001). private communication.
- Riess A.G., Filippenko A.V., Challis P., et al. (1998). "Observational Evidence from Supernovae for an Accelerating Universe and a Cosmological Constant." *AJ*, **116**, 1009.
- Riess A.G., Filippenko A.V., Li W., et al. (1999a). "Is there an Indication of Evolution of Type Ia Supernovae from Their Rise Times?" *AJ*, **118**, 2668.
- Riess A.G., Filippenko A.V., Li W., et al. (1999b). "The Rise Time of Nearby Type Ia Supernovae." *AJ*, **118**, 2675.
- Riess A.G., Kirshner R.P., Schmidt B.P., et al. (1999c). "BVRI Light Curves for 22 Type Ia Supernovae." *AJ*, **117**, 707.
- Riess A.G., Press W.H., Kirshner R.P. (1996a). "Is the Dust Obscuring Supernovae in Distant Galaxies the Same as Dust in the Milky Way?" *ApJ*, **473**, 588.
- Riess A.G., Press W.H., Kirshner R.P. (1996b). "A Precise Distance Indicator: Type Ia Supernova Multicolor Light-Curve Shapes." *ApJ*, **473**, 88.
- Ruiz-Lapuente P., Spruit H.C. (1998). "Bolometric Light Curves of Supernovae and Postexplosion Magnetic Fields." *ApJ*, **500**, 360.
- Sadakane K., Yokoo T., Arimoto J.I., et al. (1996). "Type Ia Supernova SN 1995D in NGC 2962: Optical *V*, *R*, and *I* Band Photometry and Spectra." *PASJ*, **48**, 51.
- Saha A., Sandage A., Labhardt L., et al. (1997). "Cepheid Calibration of the Peak Brightness of Type Ia Supernovae. VIII. SN 1990N in NGC 4639." *ApJ*, **486**, 1.

- Saha A., Sandage A., Tammann G.A., et al. (1999). "Cepheid Calibration of the Peak Brightness of Type Ia Supernovae. IX. SN 1989B in NGC 3627." *ApJ*, **522**, 802.
- Savage B.D., Mathis J.S. (1979). "Observed Properties of Interstellar Dust." *ARA&A*, **17**, 73.
- Schlegel D.J., Finkbeiner D.P., Davis M. (1998). "Maps of Dust Infrared Emission for Use in Estimation of Reddening and Cosmic Microwave Background Radiation Foregrounds." *ApJ*, **500**, 525.
- Schmid-Kaler T. (1982). "Physical Parameters of the Stars." In K. Schaifer, H. Voigt (eds.), *Landolt-Börnstein*, volume VI/2b, chapter 4.1.1.6. Springer, Berlin.
- Silbermann N.A., Harding P., Ferrarese L., et al. (1999). "The Hubble Space Telescope Key Project on the Extragalactic Distance Scale. XIV. The Cepheids in NGC 1365." *ApJ*, **515**, 1.
- Smith R., et al. (2000). "SN 1994D Photometry from CTIO and CfA." private communication.
- Spyromilio J., Meikle W.P.S., Allen D.A., et al. (1992). "A Large Mass of Iron in Supernova 1991T." *MNRAS*, **258**, 53P.
- Suntzeff N.B. (1996). "Observations of Type Ia Supernovae." In R. McCray, Z. Wang (eds.), *Supernovae and Supernova Remnants*, volume 145 of *IAU Colloquium*, page 41, Cambridge. Cambridge University Press.
- Suntzeff N.B., Bouchet P. (1990). "The Bolometric Light Curve of SN 1987A. I. Results from ESO and CTIO U to Q0 Photometry." *AJ*, **99**, 650.
- Suntzeff N.B., Phillips M.M., Covarrubias R., et al. (1999). "Optical Light Curve of the Type Ia Supernova 1998bu in M96 and the Supernova Calibration of the Hubble Constant." *AJ*, **117**, 1175.
- Tanvir N.R., Shanks T., Ferguson H.C., et al. (1995). "Determination of the Hubble Constant from Observations of Cepheid Variables in the Galaxy M96." *Nature*, **377**, 27.
- Tonry J. (1997). In M. Livio, M. Donahue, N. Panagia (eds.), *The Extragalactic Distance Scale*, volume 10 of *Space Telescope Science Institute Symposium Series*. Cambridge University Press.
- Turatto M., Benetti S., Cappellaro E., et al. (1996). "The Properties of the Peculiar Type Ia Supernova 1991bg. I. Analysis and Discussion of Two Years of Observations." *MNRAS*, **283**, 1.
- Turatto M., Piemonte A., Benetti S., et al. (1998). "A New Faint Type Ia Supernova: SN 1997cn in NGC 5490." *AJ*, **116**, 2431.
- Vacca W.D., Leibundgut B. (1996). "The Rise Times and Bolometric Light Curve of SN 1994D: Constraints on Models of Type Ia Supernovae." *ApJ*, **471**, L37.
- Wells L.A., Phillips M.M., Suntzeff B., et al. (1994). "The Type Ia Supernova 1989B in NGC 3627 (M66)." *AJ*, **108**, 2233.

Abstract

Light curves of Type Ia Supernovae have been analyzed using an analytic model. This model is ideally suited to objectively evaluate the variety among individual Type Ia Supernova light curve parameters, because it provides a continuous representation of the observational data and avoids a-priori assumptions commonly made. The filter light curves also can be used to construct bolometric light curves. They form an important link between theoretical models and observations. A number of physical parameters of the supernovae are derived directly from the bolometric light curves, e.g. the amount of ^{56}Ni synthesized during the explosion and the γ -ray transport.

Zusammenfassung

Lichtkurven von Typ Ia Supernovae wurden mittels einer analytischen Methode untersucht. Deren kontinuierliche Form ermöglicht eine gründliche Analyse und eine unabhängige Parameterstudie. Exemplarisch wurden zwei Parameter – die Epochen der maximalen Helligkeit in Filtern und die Ansteigzeit – eingehend untersucht. Die Filterlichtkurven eignen sich auch zur Konstruktion von bolometrischen Lichtkurven. Diese Größe lässt einen Vergleich mit theoretischen Modellen zu. Auch die Menge des während der Explosion synthetisierten ^{56}Ni wurde berechnet und Aussagen über die Absorption der γ -Strahlung in den Ejekta gemacht.

Danksagung

An erster Stelle möchte ich mich bei meinem Betreuer Dr. Bruno Leibundgut dafür bedanken, dass er mich die gesamte Zeit hindurch mit Ausdauer begleitet und unterstützt hat.

Dr. Bruno Leibundgut, Dr. habil. Ewald Müller und Prof. Dr. Wolfgang Hillebrandt danke ich dafür, dass sie mein Interesse auf das spannende Gebiet der Typ Ia Supernovae gelenkt haben und dass sie die Finanzierung meiner Arbeit ermöglichten.

Mein Dank gilt auch meinen Zimmerkollegen Andreas, Jana, Henrik, Georg, Martin und Bernhard für die durchwegs angenehme, entspannte Atmosphäre und die vielen lehrreichen Diskussionen und Episoden.

Allen Mitarbeitern am Max-Planck-Institut für Astrophysik und des European Southern Observatory danke ich für die freundliche Atmosphäre und Hilfsbereitschaft, insbesondere den System Administratoren, Sekretärinnen und Bibliothekaren. Von den unzähligen netten Kollegen am MPA und der ESO möchte ich neben meinen Zimmerkollegen einige nennen: Jan, Volker, Micha, Conrad, Andreas H., Andreas K., Daniel, Felix, Nathalie, Marc, Patrick, Martino und Elena. Für das Korrekturlesen möchte ich Jürgen, Jan und Volker danken, insbesondere dem Latex-Spezialisten Jan. Auch ohne so manche Tasse Kaffee von Karsten wäre diese Arbeit wohl nicht fertig geworden.

Insbesondere Dank gebührt den Menschen, die mich auf dem letzten Stück begleitet haben, zu denen auch meine neuen Kollegen gehören, die mich tagsüber so prächtig unterhalten haben, dass ich abends erfrischt an meine Doktorarbeit gehen konnte: Csaba für's Vorsingen längst vergessen geglaubter Ohrwürmer, Herrn Dipl. Ing. Oliver H. für's ständige Gekabbele, Brigitte für den Ausgleich im Büro und Peter für viele gute Gespräche und Auffmunterungen.

Olaf gab mir den letzten Anstoß. Danke.

Meinen Eltern und meiner Schwester möchte ich dafür danken, dass sie mich immer voll und ganz unterstützt haben. Sie haben es mir ermöglicht, mich auf meine Arbeit zu konzentrieren und waren immer für mich da.

Curriculum Vitae

Name: Gertrud Contardo

Geburtsdatum: 25. April 1970

Geburtsort: Mühldorf am Inn

Staatsangehörigkeit: deutsch

Familienstand: ledig

Bildungsweg:

1989 Abitur am Gymnasium Dorfen

1989 - 1996 Studium der Physik an der Technischen Universität München

Diplomarbeit
“Spektrale Entwicklung von Galaxien in kosmologischen Szenarien” am Max-Planck-Institut für Astrophysik in Garching

1996 – 1997 Promotionsstipendium am Max-Planck-Institut für Astrophysik

1997 – 1999 Studentship am European Southern Observatory in Garching

1999 – 2000 Promotionsstipendium am Max-Planck-Institut für Astrophysik